NTNU

Norwegian University of
Science and Technology

Time Domain Simulation of Jack-Up in Second Order Irregular Seas

Michael Binsar Lubis

Marine Technology
Submission date: June 2016
Supervisor: Jørgen Amdahl, IMT
Co-supervisor: Sverre Haver, IMT

Norwegian University of Science and Technology
Department of Marine Technology

NTNU - Trondheim
Norwegian University of
Science and Technology

Time Domain Simulation of Jack-Up in Second Order Irregular Seas

Michael Binsar Lubis

Marine Technology

Submission date : June 2016

Supervisor : Jørgen Amdahl, IMT

Co-supervisor : Sverre Kristian Haver, IMT

Norwegian University of Science and Technology

Departement of Marine Tchnology

NTNU
Norges teknisk-naturvitenskapelige universitet
Institutt for marin teknikk

MASTER WORK 2016

for

Stud. Techn. Michael Lubis

Time-domain simulation of marine structures in irregular seas

Tidsplananalyse av marine konstruksjoner i iregulær sjø

For dynamically sensitive marine structures or marine structures subjected to large displacements the extreme response is often determined on the basis of short-term time domain simulation of extreme sea states using the environmental contour line method.
A challenge with time-domain analysis is the representation of the sea spectrum. For linear analysis and small displacements is common to use fast Fourier transform (FFT) of the sea spectrum. In order to avoid repetition of the wave history several thousand of uniformly spaced wave components may be needed. For nonlinear time domain simulations the computational requirements of FFT will become prohibitive. An alternative to FFT is to use a few wave components based on equal area principle. This implies that emphasis is placed on the energy rich parts of the wave spectrum. The accuracy of this method must be demonstrated. Using the computer program USFOS it was shown in a previous master thesis work that this method is quite good for floating structures with eigenperiods far away from the energy rich periods of the wave spectrum, but less accurate for structures with eigenperiods in the range of 4-5 seconds. The results depend also on whether the wave forces are mass dominated or drag dominated. It has been suggested that the accuracy may be improved by increasing the subdivision of the wave spectrum in the vicinity of the structure eigenperiod(s).

In USFOS the built-in algorithm for realisation of irregular seas states is based upon linear wave theory and extrapolation of wave kinematics to the instantaneous sea surface (Wheeler stretching). Improved accuracy is obtained by using 2^{nd} order wave theory for surface elevation Wheeler stretching of linear wave kinematics to the surface, and the user may specify the frequency components of the discretised wave spectrum in the input. Most correct is to base wave kinematics completely on 2^{nd} order theory. Eivind Bækkedal implemented this in a previous master thesis work. Rigorous calculation according to 2^{nd} order theory are very time consuming and methods to reduce computation time are highly requested An alternative to perform calculations "on the fly" is to represent pre-calculated wave kinematics on a relatively coarse 3D grid and interpolation to actual structure coordinates. The grid may be particularly coarse at large depth. Another alternative may be to use 2^{nd} order theory only close to sea surface or for a few members. The purpose of the project and master thesis work is to investigate various options to save CPU consumption in time domain simulations in nonlinear, irregular seas.

The following topics should be addressed:

1. Verify the second order simulation of the surface by comparing the empirical distribution of global crest heights (global crest height = largest crest between zero-up-crossings) with the crest height distribution suggested by Forristall (2000).

Validate the simulation of second order kinematics by comparing with the work of others in the literature. Do also compare the calculated vertical profile of the horizontal particle speed under wave crests by the results of Stokes 5th wave profile with the same crest height and wave period as the simulated wave.

2. Perform static and dynamic time domain analysis of a jack-up platform. Select a severe sea state (for the further analysis, it is convenient if the worst sea state along the 100-year contour is selected) and compare the quasi-static results obtained by a full second order analysis with the corresponding quasi-static results obtained using a Stokes 5th profile for some selected waves of the simulation.

3. Carry out a sufficient number of second order analyses for establishing the distribution function for the 3-hour maximum quasi-static responses with some confidence. Assume that the 100-year quasi-static responses can be estimated by the 90-95% value of the 3-hour extreme value distribution.

   Estimate the 100-year crest height and the associated mean period, and estimate the 100-year quasi-static response using the Stokes 5th profile. Compare the results with those obtained from second order simulation.

4. Conduct a full dynamic second order analysis for the same sea state as above. Is it possible in practice to perform 30 full 3-hour analysis for the purpose of obtaining a reasonable sample of 3-hour dynamic extremes, either as full 3-hour simulations or by representing a 3-hour simulation by six 30-minutes simulations?

5. The rest of the thesis is devoted to discussing and testing various approximate ways for doing a second order analysis of the selected jack-up. The following approaches should be considered:

   I. 2nd order theory in upper layers - linear theory below a certain depth (which is to be varied)
   II. Linear theory to some point before the worst wave groups.
   III. Spool to extreme wave groups – the time before group maximum crest height to be varied.
   IV. Use of pre-calculated wave kinematics on a grid

   The accuracy and time consumption shall be presented for the various methods.

6. Conclusions and recommendation for further work

Literature studies of specific topics relevant to the thesis work may be included.

The work scope may prove to be larger than initially anticipated. Subject to approval from the supervisors, topics may be deleted from the list above or may be reduced in extent if the work becomes more extensive than anticipated.

In the thesis the candidate shall present his personal contribution to the resolution of problems within the scope of the thesis work.

Theories and conclusions should be based on mathematical derivations and/or logic reasoning identifying the various steps in the deduction.

The candidate should utilise the existing possibilities for obtaining relevant literature.

Thesis format
The thesis should be organised in a rational manner to give a clear exposition of results, assessments, and conclusions. The text should be brief and to the point, with a clear language. Telegraphic language should be avoided.

The thesis shall contain the following elements: A text defining the scope, preface, list of contents, summary, main body of thesis, conclusions with recommendations for further work, list of symbols and acronyms, references and (optional) appendices. All figures, tables and equations shall be numerated.

The supervisors may require that the candidate, in an early stage of the work, presents a written plan for the completion of the work. The plan should include a budget for the use of computer and laboratory resources, which will be charged to the department. Overruns shall be reported to the supervisors.

The original contribution of the candidate and material taken from other sources shall be clearly defined. Work from other sources shall be properly referenced using an acknowledged referencing system.

The report shall be submitted in two copies:
- Signed by the candidate
- The text defining the scope included
- In bound volume(s)
- Drawings and/or computer prints which cannot be bound should be organised in a separate folder.
- The report shall also be submitted in pdf format along with essential input files for computer analysis, spreadsheets, MATLAB files etc in digital format.

Ownership
NTNU has according to the present rules the ownership of the thesis. Any use of the thesis has to be approved by NTNU (or external partner when this applies). The department has the right to use the thesis as if the work was carried out by a NTNU employee, if nothing else has been agreed in advance.

Thesis supervisors:
Prof. Jørgen Amdahl
Prof. II Sverre Haver

Deadline: June 10 2016

Trondheim, February 8th, 2016

Jørgen Amdahl

Preface

This report is the result of a master thesis work conducted at the Department of Marine Technology at the Norwegian University of Science and Technology. The scope of work was formulated by Prof. Jørgen Amdahl and Prof. Sverre Haver.

This report deals with time domain simulation of a jack-up paltform exposed to second order irregular waves. The main focus is to observe the effect of second order irregular waves on jack-up paltform and investigate the alternative methods to reduce computational time. The validity of second order model is checked by comparing the surface and kinematics to theoretical value and previous work. In this work, a Matlab program also is built to establish both surface elevation and particle kinematics of second order irregular waves. In addition, the sea surface and wave kinematics are transferred as grid file from MATLAB to USFOS to calculate the jack-up response.

I would like to thank Professor Jørgen Amdahl and Professor Sverre Haver for their great help and guidance during the thesis work. I also would like to thank Mr. Bjørn Tore Bach for allowing me to use multiple computers to run the analysis.

Trondheim, June 8, 2016

Michael Binsar Lubis

Abstract

For dynamically sensitive structures or marine structure sujected to large displacements (such as jack-up paltform) the extreme response is often determined on the basis of short term time domain simulation of extreme sea states using environmental contour line method. A challenge with time-domain simulation is the representation of the sea spectrum. For first order wave (Gaussian seas), there is no big obstacle to performs a complete 3-hour simulation. However, the computational requirements becomes prohibitive for second order irregular waves. The purpose of this report is to observe the effect of second order irregular waves on jack-up platform and also contribute to developement and verification of strategies on decreasing the computational time for time domain analysis.

This report mainly consists of seven parts. First part consists of the review about wave theory, the probabilistic model of ocean waves, methods of establishing kinematics, methods for simulating a sea spectrum and method for calculating response of structure. In addition, some strategies for reducing computational time also presented.

The second part consists of explanation about the numerical. In the third part, a verification study is performed. The second order model is compared with theoretical wave distribution and 5^{th} Stokes wave. At the end of third part, the static analysis of second order irregular seas on single vertical cylinder with small diameter is performed. The four part deals with strategies to reduce time for calculating time for second order wave while the fourth part contains the metocean analysis. The last part presents the effect of second order irregular wave on jack-up platform.

From the study, it is found that for second order wave, Wheeler method gives underestimation for wave horizontal velocity below the sea surface. Compared to 5^{th} Stokes, linear extrapolation produces greater surface horizontal velocity though it produces smaller horizontal velocity below mean sea surface. For jack-up case and Ultimate Limit State purposes, the largest static baseshear could come from wave which has crest smaller than 100-year wave crest but has comparable wave length to distance between jack-up leg. However, the largest static overturning moment tend to occurs from wave with crest close to the 100-year wave crest. In addition, dynamic analysis of the observed jack-up produces 20% larger baseshear and 90% larger oveturning moment than static anaysis.

Contents

List of Figures

List of Tables

Nomenclature

$a_{x,1}$, $a_{y,1}$, $a_{z,1}$	First order particle wave acceleration in *x*, *y* and *z*-direction
$a_{x,2}$, $a_{y,2}$, $a_{z,2}$	Second order particle wave acceleration in *x*, *y* and *z*-direction
B	Coefficient for stream function
BC_{FS}	Free surface boundary condition
BC_{SB}	Sea bottom boundary condition
C_M	Added mass coefficient
C_D	Drag coefficient
$\boldsymbol{C}$	Global damping matrix
c	Wave crest
$\overline{c_{cr,i}}$	Critical damping for eigenmode *i*
c_l	Largest crest (largest maximum surface elevation)
c_1, c_2	First and second order wave celerity
$D(\theta)$	Spreading function
D_s	Arbitrary reference level for stream function
d	Water depth
dF	Morrison force in strip element
dF_a	Added mass in strip element
E	Modulus Young
E_n	Total wave energy per wave length
$E[\mathrm{x}]$	Expected value of x
erfc( )	Complimentary error function
$F_{\boldsymbol{X20M}}(X)$	Cumulative distribution of 20-minute largest value
$F_{\boldsymbol{X3H}}(X)$	Cumulative distribution of 3-hour largest value
$F_{\boldsymbol{C}}(C)$	Cumulative distribution of wave crest
$F_{C_{3h}}(c)$	Cumulative distribution function of 3-hour crest
$F_{\boldsymbol{H}}(H)$	Cumulative distribution of wave height
$F_{H_s}(h_s)$	Cumulative distribution function of significant wave height
F_{X_N}	Cumulative distribution of largest maxima out of N number of maxima
$F_{\boldsymbol{\zeta_m}}(\zeta_m)$	Cumulative distribution function of maximum surface elevation
$F_{\boldsymbol{\zeta_{lm}}}(\zeta_{lm})$	Cumulative distribution function of largest maximum surface elevation

$f(\zeta)$	Probability density function of surface elevation
$f_{\zeta_m}(\zeta_m)$	Probability density function of maximum surface elevation
$f_{\zeta_{lm}}(\zeta_{lm})$	Probability density function of largest maximum surface elevation
$f_{H_s}(H_s)$	Probability density function of significant wave height
$f_{H_s,T_p}(H_s, T_p)$	Join probability density function of significant wave height and peak period
g	Gravity acceleration
H	Wave height
H_b	Wave height limit for breaking waves
H_s	Significant wave height
$H_{0.01}$	Wave height with 100-year return peeriod
I	Moment inertia of cylinder
i, j	Component/order number
$\boldsymbol{K}$	Global stiffness matrix
K_v	Normalized coefficient for spreading function
k	Wave number
k_e	Element stiffness
k_{m01}	Wave number from mean period (T_{m01})
k_p	Wave number of spectral peak period (T_p)
k_1, k_2	First and second order regular wave number
L	Length of element
$\boldsymbol{M}$	Global mass matrix
M_e	External moment
M_i	Internal moment
m_e	mass of element
m_n	*n-th* moment of wave spectrum
m_X	Sample mean
N	Number of component/sample
N_{EA}	Number of equal area component
$N_{p,outside}$	Number of measurement data (for scatter plot) outside the contour line
$N_{p,total}$	Total number of measurement data (for scatter plot)
N_{peak}	Number of peaked component
N_s	Shape function for displacement ($s= w$) or rotation ($s= \theta$)

N_x	Axial force
$\vec{n}$	Normal vector
n_y	Return period
p_o	Atmospheric pressure
p_1, p_2	First and second order hydrodynamic pressure
Q	Shear force
Q_v	Volume flow per unit span under wave in moving frame reference
$\boldsymbol{R}$	Force matrix
$R(\tau)$	Autocorelation function of surface elevation
$\boldsymbol{r}, \dot{\boldsymbol{r}}, \ddot{\boldsymbol{r}}$	Displacement, velocity and acceleration of response
S_X	Sample variance
S_1	Steepness parameter
$s(\omega)$	Wave spectrum
$s_1(\omega)$	One-side spectrum
$s_2(\omega)$	Two-side spectrum
T	Wave period
T_f	Duration of simulation (fundamentel period)
T_{ULS}	Wave period for Ultimate Limit State analysis
T_{m24}	Mean period between maxima
T_p	Peak period
T_1 or T_{m01}	Wave mean period
T_2 or T_{m02}	Mean zero-crossing period
t	Time instance
U_r	Ursell number
u_x, u_y, u_z	Wave particle velocity in *x*, *y* and *z*-direction
$u_{x,1}$, $u_{y,1}$, $u_{z,1}$	First order particle wave velocity in *x*, *y* and *z*-direction
$u_{x,2}$, $u_{y,2}$, $u_{z,2}$	Second order particle wave velocity in *x*, *y* and *z*-direction
$\vec{V}$	Vector of wave particle velocity
v	Spreading power
w	Lateral displacement
X, Z	Coordinate in moving frame reference
x, y, z	Coordinate in fixed frame reference

z_{old} , z_{new}	z-coordinate before and after Wheeler stretching
α_w	Scale parameter of weibull distribution
α_1	Rayleigh damping coefficient (mass)
α_2	Rayleigh damping coefficient (stiffness)
β_r	Radius of contour line in Gaussian space
β_w	Shape parameter of weibull distribution
$\Gamma( )$	Gamma function
γ_e	Euler constant ≈ 0.5772
γ_1	Skewness coefficient
$\hat{\gamma}_1$	Sample skewness coefficient
γ_2	Kurtosis
$\hat{\gamma}_2$	Sample kurtosis
Δt	Time interval
$\Delta\theta$	Wave direction interval
$\Delta\omega$	Angular frequency interval
ε	Wave phase angle
ϵ	Small parameter of potential velocity/surface elevation power series
ζ	Surface elevation
ζ_a	Amplitude of surface elevation (mainly equal to ζ_{a1})
ζ_{a1}	Amplitude of first order surface elevation
$\zeta_i{}'$	Coefficient of Stokes wave surface elevation of *i*-th order
ζ_{lm}	Largest maximum surface elevation
ζ_m	Maximum surface elevation
ζ_1, ζ_2	First and second order surface elevation
$\bar{\zeta}$	Surface elevation in frequency domain
η	Standardized variable of Rice distribution
θ	Direction of wave propagation
λ	Wave length
λ_c	Damping ratio
λ_w	Location parameter of weibull distribution
λ_1, λ_2	First and second order regular wave length
μ_{HL}	Mean of largest waave height

$\mu_{T_p\|H_s}$	Mean of spectral period for given significant wave height
$\mu_X{}^{(n)}$	*n*-th statistical moment for x as variable
$\overline{\mu_X}^{(n)}$	*n*-th statistical central moment for x as variable
μ_{X_N}	Mean of largest maxima
μ_ζ	Mean of surface elevation
ξ	Bandwith parameter for Rice distribution
ξ_F	Natural coordinate
ρ	Density of seawater
ρ_e	Structure element mass per unit
$\sigma_{T_p\|H_s}$	Standard deviation of spectral period for given significant wave height
$\sigma_x{}^2$	Variance of x
σ_{X_N}	Standard deviation of largest maxima
σ_ζ	Standard deviation of surface elevation
σ_θ	Standard deviation of wave direction
τ	Time difference
$\Phi( )$	Standard Gauss cumulative distribution function
$\boldsymbol{\phi}$	Eigenmode of structure
ϕ	Velocity potential
$\phi_i{}'$	Coefficient of Stokes wave potential velocity of *i*-th order
ϕ_1, ϕ_2	First and second order velocity potential
ψ_s	Stream function
ω	Wave angular frequency
ω_{cut}	Cut-off angular frequency
ω_n	Natural frequency of structure (lowest eigenfrequency)
ω_{nyq}	Nyquist angular frequency
ω_p	Peak angular frequency
ω_1, ω_2	First and second order regular wave angular frequency

Abbreviations

CDF	Cumulative Distribution Function
CPU	Central Processing Unit
FFT	Fast Fourier Transform
JONSWAP	Joint North Sea Wave Project
NPD	Norwegian Petroleum Directorate
PDF	Probability Density Function
PM	Pierson-Moskowitz
ULS	Ultimate Limit State

1. Introduction

The sea surface is a random phenomenom. It is irregular and always changes in time. Finding the mathematical expression to represent the exact condition of sea surface is very difficult and cumbersome. In practice, the condition of certain sea is usually represented by a set of significant wave height and spectral peak period. For ultimate limit state purposes, the extreme sea condition and its return period can be predicted from probabilistic model by utilizing the set of significant wave height and spectral peak period. Knowing the extreme sea condition, the corresponding wave load can be calculated by a certain wave theory to find the responses of a marine structure.

For quasi-static method, the static responses of structure can be determined by finding the wave load corresponding to the most probable highest wave in certain return period. However, in reality, the responses of structure are also affected by the period of load which is based on the wave period for wave load case. When the largest natural period of structure is located close the most energetic wave period, it is not enough to only analyze the static response of the structure. The dynamic responses of the structure should be analyzed in time-domain where the equation of motion is solved each time step.

A main challenge with time-domain analysis is the representation of the sea spectrum. A sea spectrum is characterized by a combination of significant wave height and spectral peak period. One combination of significant wave height and spectral peak period can be assumed valid for 3-hour. Therefore, a complete 3-hour history of sea surface elevation is required to find the highest surface elevation. For linear representation of wave, it is common to use inverse *Fast Fourier Transform* (FFT) of the sea spectrum. In order to avoid repetition of 3-hour wave history, several thousand of uniformly spaced wave components may be needed. Each time step will include N wave components to compute the wave kinematic. For simulations of second order sea with the associated kinematics, the computational time requirements become prohibitive as it needs to include N^2 wave components in each time step.

At previous master project by Lubis [27] and master thesis by Bækkedal [6], it is shown that by utilizing various alternative methods such as randomize the representation of wave frequency in

certain frequency interval or using equal are method can decrease the required wave components. As a result, the computational time reduces significantly. However, it is found that the simulation time is still rigorous. In his project, Lubis [27] showed that some alternatives can be applied to reduce the computational time in extent for single vertical cylinder case. This method should be tested for real structure.

This report addresses the the static and dynamic responses of the jack-up platform when the second order irregular wave is applied to the structure. However, a verification study is performed for single vertical cylinder. The result from single vertical cylinder is compared to another analysis of second order wave by Evardsen [12]. In addition, a revisit and verification of previous work by Bækkedal [6] and Lubis [27] to reduce the required number of harmonic component are also performed and the tested into jack-up. The result of various alternatives to reduce the computational time in extent for jack-up platform is presented. In the end, 3-hour simulations of jack-up in second order irregular seas are performed. A *MATLAB* algorithm to calculate second order surface and kinematics in irregular sea is created and utilized in this work while *USFOS* is used to calculate the response of the jack-up platform.

2. Ocean Wave Theories

This section reviews the existing theories for establishing the wave particle kinematics both in regular and irregular sea condition. In regular sea condition, the wave is modeled by a single harmonic component with certain amplitude and frequency while irregular sea condition means combination of number hamonic component with various amplitudes and frequencies. When the wave length is much larger than the structure dimensions, the forces can be calculated directly from the wave particle kinematic of undisturbed wave field. In this case, the quality of wave particle kinematics determines the accuracy of the applied load in the structure.

In this section, the governing equation and method to find its solution is presented first. Afterwards, the linear wave theory (first order wave) in regular and irregular condition is presented. The next part consists of second order wave theory on regular and irregular wave field. The rest of this section reviews higher order wave theories and methods to find the wave particle kinematic from mean surface level to the exact surface.

2.1. Governing Equations

The seawater is assumed incompressible and inviscid. The fluid velocity vector $\vec{V}(x, y, z, t) = (u_x, u_y, u_z)$ at time t and at coordinate x, y, and z can be described by gradient of a velocity potential ϕ. This means that:

$$(u_x, u_y, u_z) = \left(\frac{\partial \phi}{\partial x}, \frac{\partial \phi}{\partial y}, \frac{\partial \phi}{\partial z}\right) \tag{2.1}$$

The velocity potential is introduced because of mathematical purposes and does not have any physical meaning. To satisfy the irrotational condition, $\nabla \times \vec{V}$ is equal to zero in every location of the fluid. In addition, since the water is incompressible then $\nabla . \vec{V}$ is also equal to zero in every location in the fluid. As consequence, the velocity potential has to satisfy Laplace equation:

$$\nabla . \vec{V} = \frac{\partial^2 \phi}{\partial x^2} + \frac{\partial^2 \phi}{\partial y^2} + \frac{\partial^2 \phi}{\partial z^2} = \nabla^2 \phi = 0 \tag{2.2}$$

Where: seabed ($-d$) $\leq z \leq$ surface elevation (ζ); and $-\infty \leq x, y \leq \infty$.

By introducing some boundary conditions, the velocity potential can be found. Figure 2.1 describes the boundary condition, coordinate system and some used parameters.

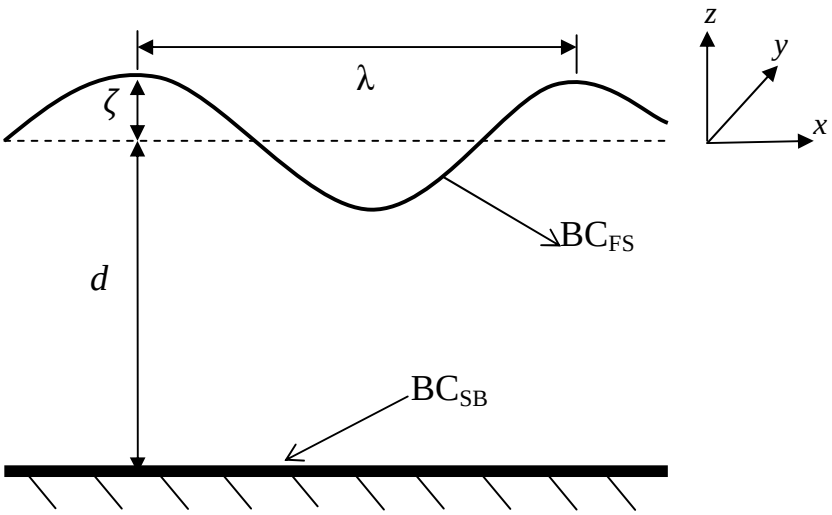

Figure 2.1 Coordinate System

2.1.1. Bottom boundary condition (BC_{SB})

To satisfy the impermeability condition of seabed, boundary condition at seabed (z = - d) states that the velocity normal to the boundary must be equal to zero. Therefore, $\nabla\phi.\vec{n} = 0$. This implies that for flat surface:

$$\frac{\partial\phi}{\partial z} = 0; \quad z = -d \tag{2.3}$$

2.1.2. Dynamic free-surface boundary condition

The water pressure at the free surface is equal to the atmospheric pressure (p_o), then the dynamic free-surface boundary conditon for two-dimentional wave:

$$g\zeta + \frac{\partial\phi}{\partial t} + \frac{1}{2}\underbrace{\left(\left(\frac{\partial\phi}{\partial x}\right)^2 + \left(\frac{\partial\phi}{\partial y}\right)^2 + \left(\frac{\partial\phi}{\partial z}\right)^2\right)}_{non-linear} + p_o = p_o \; ; \; z = \zeta(x,y,t) \tag{2.4}$$

2.1.3. Kinematic free-surface boundary condition

Based on the fact that the particles of water on free surface have to stay on the free surface, the vertical particle velocity has to be equal to the rate of change of water surface elevations.

$$\frac{\partial\zeta}{\partial t} + \underbrace{u_x\frac{\partial\zeta}{\partial x} + u_y\frac{\partial\zeta}{\partial y}}_{non-linear} = u_z; z = \zeta(x,y,t) \tag{2.5}$$

2.1.4. Combined free surface boundary condition (BCFS)

The combination of dynamic and kinematic boundary condition gives [36]:

$$\frac{\partial^2\phi}{\partial t^2} + g\,u_z + \underbrace{\frac{1}{2}\left(\frac{\partial}{\partial t} + u_x\frac{\partial}{\partial x} + u_y\frac{\partial}{\partial y}\right)\left|\vec{\nabla}\phi\right|^2 + \left(u_x\frac{\partial^2\phi}{\partial x\partial t} + u_y\frac{\partial^2\phi}{\partial y\partial t}\right)}_{non-linear} = 0; \quad z = \zeta(x,y,t) \tag{2.6}$$

2.2. Method of Solution

To solve the boundary value problem, the perturbation scheme method is applied. This method assumes potential velocity (ϕ) and water surface elevation (ζ) as a convergent power series with small parameter (ϵ), such as the wave steepness (H/λ). In this way, the velocity potential and surface elevation can be expressed as [19], [36]:

$$\begin{aligned}\phi(x,y,z,t;\epsilon) &= \widetilde{\phi_1}(x,y,z,t)\,\epsilon + \widetilde{\phi_2}(x,y,z,t)\,\epsilon^2 + \widetilde{\phi_3}(x,y,z,t)\,\epsilon^3 \ldots O\left(\epsilon^{i+1}\right)\\ &= \phi_1(x,y,z,t;\epsilon) + \phi_2(x,y,z,t;\epsilon) + \phi_3(x,y,z,t;\epsilon) \ldots O(\phi_{i+1})\end{aligned} \tag{2.7}$$

$$\begin{aligned}\zeta(x,y,t;\epsilon) &= \widetilde{\zeta_1}(x,y,t)\,\epsilon + \widetilde{\zeta_2}(x,y,t)\,\epsilon^2 + \widetilde{\zeta_3}(x,y,t)\,\epsilon^3 \ldots O\left(\epsilon^{i+1}\right)\\ &= \zeta_1(x,y,t;\epsilon) + \zeta_2(x,y,t;\epsilon) + \zeta_3(x,y,t;\epsilon) \ldots O(\zeta_{i+1})\end{aligned} \tag{2.8}$$

Where λ and *H* are wavelength and wave height respectively. In equation 2.7 and 2.8, ϕ_i and ζ_i respectively refer to the *i*-th order of potential velocity and water surface elevation. Substituting equation 2.7 to equation 2.2 gives:

$$\nabla^2\phi = \nabla^2\phi_1 + \nabla^2\phi_2 + \nabla^2\phi_3 + \cdots \tag{2.9}$$

In addition, introducing equation (2.7) to equation (2.3) gives:

$$\frac{\partial\phi_1}{\partial z} = 0, \frac{\partial\phi_2}{\partial z} = 0, \ldots \;; at\; z = -d \tag{2.10}$$

The combined free surface boundary condition is expressed as a Maclaurin series of the mean water level condition. As the consequence, the velocity potential at free surface is expressed as Maclaurin series:

$$\phi(x,y,\zeta,t) = \phi(x,y,0,t) + \zeta\frac{\partial\phi(x,y,0,t)}{\partial z} + \frac{\zeta^2}{2}\frac{\partial^2\phi(x,y,0,t)}{\partial z^2} + \cdots \tag{2.11}$$

2.3. First-Order Pertubation (Linear Wave Theory)

The parameter ϵ in equation 2.7 and 2.8 can be related to wave steepness (H/λ). When wave steepness is small enough, the linear wave theory is valid. In this case, the first order error of water surface elevation and velocity potential is neglected. The velocity potential is only described by the first term of its power series. In addition, the non-linear term from equation 2.4 until 2.6 is neglected. Laplace equation, bottom boundary condition, dynamic free-surface boundary condition and combined free-surface boundary condition equation respectively becomes [36]:

$$\nabla^2\phi_1 = 0 \;\; ; -\mathrm{d} \leq z \leq 0, y \leq \infty \tag{2.12}$$

$$\frac{\partial\phi_1}{\partial z} = 0; \quad z = -d \tag{2.13}$$

$$g\zeta_1 + \frac{\partial\phi_1}{\partial t} = 0; \quad z = 0 \tag{2.14}$$

$$\frac{\partial^2\phi_1}{\partial t^2} + g\frac{\partial\phi_1}{\partial z} = 0; \quad z = 0 \tag{2.15}$$

The equations 2.12 until 2.15 are solved in regular wave condition. However, the result can be used to describe the irregular wave condition.

2.3.1. First order solution for regular wave conditon

The first order solution is acquired by assuming a horizontal sea bottom and free surface of infinite horizontal extent. This solution is known as linear wave theory and sometimes called Airy theory since it was first presented by Airy in 1841 [14]. The velocity potential is assumed as a product of several functions which each function only depends on one independent variable. The assumed velocity potential form is [19]:

$$\phi_1 = f(z)\, sin\,(k(x\, cos(\theta) + y\, sin(\theta)) - \omega t) \tag{2.16}$$

Where ω is angular frequency [rad/s] and equal to $2\pi/T$, k is wave number and equal to $2\pi/\lambda$, and θ is the wave propagation direction relative to x-axis. T is the wave period. If the wave is assumed as two-dimentional wave which is valid for long-crested wave, and the assumed velocity potential is assigned into the boundary condition, the form of velocity potential that satisfies Laplace equation [36]:

$$\phi_1 = g\,\zeta_a \frac{cosh\,(k(z+d))}{\omega\,cosh\,(kd)} sin\,(kx-\omega t) \tag{2.17}$$

ζ_a is the amplitude of water surface elevation. The form of first order water surface elevation:

$$\zeta\,(t) = \zeta_{a1}\,cos\,(kx-\omega t) \tag{2.18}$$

From equation 2.16, the velocity potential oscilates with angular frequency (ω). As a consequence, equation 2.14 can be rewritten as:

$$-\omega^2\phi_1 + g\frac{\partial\phi}{\partial z} = 0; \quad z = 0 \tag{2.19}$$

From equation 2.18, it is shown that there is connection between wave number (k) and angular frequency (ω). This connection is presented in dipersion relation [14]:

$$\omega^2 = gk\,\tanh\,(kd) \tag{2.20}$$

For large water depth, $lim_{d\to\infty}\,tanh(kd) = 1$ then the dispersion relation becomes $\omega^2 = g\,k$. The first order particle wave kinematics can be calculated from velocity potential as mentioned in equation 2.1:

$$u_{x,1} = \frac{\partial\phi_1}{\partial x} = gk\zeta_{a1}\frac{cosh\,(k(z+d))}{\omega\,cosh\,(kd)}cos\,(kx-\omega t) \tag{2.21}$$

$$u_{z,1} = \frac{\partial\phi_1}{\partial z} = gk\zeta_{a1}\frac{sinh\,(k(z+d))}{\omega\,cosh\,(kd)}sin\,(kx-\omega t) \tag{2.22}$$

$$a_{x,1} = \frac{\partial^2\phi_1}{\partial x dt} = gk\zeta_{a1}\frac{cosh\,(k(z+d))}{cosh\,(kd)}sin\,(kx-\omega t) \tag{2.23}$$

$$a_{z,1} = \frac{\partial^2\phi_1}{\partial z dt} = -gk\zeta_{a1}\frac{sinh\,(k(z+d))}{cosh\,(kd)}cos(kx-\omega t) \tag{2.24}$$

Where $u_{x,1}$, $u_{z,1}$, $a_{x,1}$ and $a_{z,1}$ are particle velocities in x and z-direction, and acceleraton in x and z-direction respectively. The phase different between particle velocity and aceleration in certain direction is $\pi/2$. Therefore, when $u_{x,1}$ has maximum value, $a_{x,1}$ is equal to zero and likewise. The first order hydrodynamic pressure p_1 is:

$$p_1 = -\rho \frac{\partial \phi_1}{\partial t} = \rho g \zeta_{a1} \frac{cosh\,(k(z+d))}{cosh\,(kd)} cos(kx - \omega t) \quad (2.25)$$

For three-dimention wave which is valid for short crested wave, the first order particle kinematic becomes:

$$u_{x,1} = \frac{\partial \phi_1}{\partial x} = gk\,cos(\theta)\,\zeta_{a1} \frac{cosh\,(k(z+d))}{\omega\,cosh\,(kd)} cos(k(x\,cos(\theta) + y\,sin(\theta)) - \omega t) \quad (2.26)$$

$$u_{y,1} = \frac{\partial \phi_1}{\partial y} = gk\,cos(\theta)\,\zeta_{a1} \frac{cosh\,(k(z+d))}{\omega\,cosh\,(kd)} cos(k(x\,cos(\theta) + y\,sin(\theta)) - \omega t) \quad (2.27)$$

$$u_{z,1} = \frac{\partial \phi_1}{\partial z} = gk\zeta_{a1} \frac{sinh\,(k(z+d))}{\omega\,cosh\,(kd)} sin(k(x\,cos(\theta) + y\,sin(\theta)) - \omega t) \quad (2.28)$$

$$a_{x,1} = \frac{\partial^2 \phi_1}{\partial x dt} = gk\,cos(\theta)\,\zeta_{a1} \frac{cosh\,(k(z+d))}{cosh\,(kd)} sin(k(x\,cos(\theta) + y\,sin(\theta)) - \omega t) \quad (2.29)$$

$$a_{y,1} = \frac{\partial^2 \phi_1}{\partial y dt} = gk\,cos(\theta)\,\zeta_{a1} \frac{cosh\,(k(z+d))}{cosh\,(kd)} sin(k(x\,cos(\theta) + y\,sin(\theta)) - \omega t) \quad (2.30)$$

$$a_{z,1} = \frac{\partial^2 \phi_1}{\partial z dt} = -gk\zeta_{a1} \frac{sinh\,(k(z+d))}{cosh\,(kd)} cos(k(x\,cos(\theta) + y\,sin(\theta)) - \omega t) \quad (2.31)$$

2.3.2. First order solution for irregular wave conditon

In reality, the shape of wave is irregular. Since the first order solution for regular wave is a linear system then the solution for irregular wave can be found by superpositioning regular wave solution. The superposition start by introducing phase angle (ε) for each regular wave component. Therefore, the velocity potential and surface elevation for two-dimension linear irregeular wave [36]:

$$\phi_1 = \phi_{1,1} + \phi_{1,2} + \phi_{1,3} + \cdots = \sum_i^N \phi_{1,i} \quad (2.32)$$

$$\zeta_1(t) = \zeta_{1,1} + \zeta_{1,2} + \zeta_{1,3} + \cdots = \sum_i^N \zeta_{1,i} = \sum_i^N \zeta_{a1,i} \cos\,(k_i x - \omega_i t + \varepsilon_i) \quad (2.33)$$

Where i is the number of first order regular wave component. Each $\zeta_{1,i}$ has its own amplitude ($\zeta_{a1,i}$), wave number (k_i), wave frequency (ω_i) and phase angle (ε_i). Similar to velocity potential, the particle kinematics for linear irregular wave are also expressed as superposition of regular linear potential velocity. For two-dimension wave:

$$u_{x,1} = \sum_i^N \frac{\partial \phi_{1,i}}{\partial x} = \sum_i^N g k_i \zeta_{a1,i} \frac{cosh\,(k_i(z+d))}{\omega_i cosh\,(k_i d)} cos\,(k_i x - \omega_i t + \varepsilon_i) \quad (2.34)$$

$$u_{z,1} = \sum_i^N \frac{\partial \phi_{1,i}}{\partial z} = \sum_i^N g k_i \zeta_{a1,i} \frac{sinh\,(k_i(z+d))}{\omega_i\, cosh\,(k_i d)} sin\,(k_i x - \omega_i t + \varepsilon_i) \quad (2.35)$$

$$a_{x,1} = \sum_i^N \frac{\partial^2 \phi_{1,i}}{\partial x \partial t} = \sum_i^N g k_i \zeta_{a1,i} \frac{cosh\,(k_i(z+d))}{cosh\,(k_i d)} sin\,(k_i x - \omega_i t + \varepsilon_i) \quad (2.36)$$

$$a_{z,1} = \sum_i^N \frac{\partial^2 \phi_{1,i}}{\partial z \partial t} = -\sum_i^N g k_i \zeta_{a1,i} \frac{sinh\,(k_i(z+d))}{cosh\,(k_i d)} cos\;(k_i x - \omega_i t + \varepsilon_i) \quad (2.37)$$

A wave spectrum represents the irregular wave condition. The linear wave components can be calculated from wave spectrum. The method of calculating linear wave component from spectrum is presented in section 4.2. For three dimension wave, the linear irregular wave kinematics:

$$u_{x,1} = \sum_i^N \frac{g k_i\, cos(\theta_i)\, \zeta_{a1,i}\, cosh\big(k_i(z+d)\big)}{\omega_i\, cosh(k_i d)} cos(k_i(x\, cos(\theta_i) + y\, sin(\theta_i)) - \omega_i t + \varepsilon_i) \quad (2.38)$$

$$u_{y,1} = \sum_i^N \frac{g k_i\, sin(\theta_i)\, \zeta_{a1,i}\, cosh\big(k_i(z+d)\big)}{\omega_i\, cosh(k_i d)} cos(k_i(x\, cos(\theta_i) + y\, sin(\theta_i)) - \omega_i t + \varepsilon_i) \quad (2.39)$$

$$u_{z,1} = \sum_i^N \frac{g k_i\, \zeta_{a1,i}\, sinh\Big(k_j(z+d)\Big)}{\omega_i\, cosh(k_i d)} sin(k_i(x\, cos(\theta_i) + y\, sin(\theta_i)) - \omega_i t + \varepsilon_i) \quad (2.40)$$

$$a_{x,1} = \sum_i^N \frac{g k_i\, cos(\theta_i)\, \zeta_{a1,i}\, cosh\big(k_i(z+d)\big)}{cosh(k_i d)} sin(k_i(x\, cos(\theta_i) + y\, sin(\theta_i)) - \omega_i t + \varepsilon_i) \quad (2.41)$$

$$a_{y,1} = \sum_i^N \frac{g k_i\, sin(\theta_i)\, \zeta_{a1,i}\, cosh\big(k_i(z+d)\big)}{cosh(k_i d)} sin(k_i(x\, cos(\theta_i) + y\, sin(\theta_i)) - \omega_i t + \varepsilon_i) \quad (2.42)$$

$$a_{z,1} = -\sum_i^N \frac{g k_i\, \zeta_{a1,i}\, sinh\big(k_i(z+d)\big)}{cosh(k_i d)} cos(k_i(x\, cos(\theta_i) + y\, sin(\theta_i)) - \omega_i t + \varepsilon_i) \quad (2.43)$$

When realizing linear wave component from wave spectrum, there is an issue to determine first order kinematics above mean water surface. Johannessen [23] shows that unless the amplitudes of harmonic component in the upper part decay exponentially, the horizontal velocity from first

order component is not defined above mean water level. In this case, some approximation method is used. The approximation method is presented in section 2.5.

2.4. Second Order Perturbation

Equation 2.4, 2.5 and 2.6 contain non-linear term. First order pertubation scheme neglects these terms with assumption that the wave stepness is small (the surface elevation is smaller than the wavelength). When the wave stepness is sufficiently large, the second order pertubation scheme should be used. In this scheme, to find the velocity potential and surface elevation, the non-linear term in equation 2.4, 2.5 and 2.6 has to be included. Moreover, the second order term in velocity potential power series have to be included. The solution of second order perturbation problem becomes the correction term of first order perturbation result. The second order perturbation problem is presented as [36]:

$$\nabla^2\phi_2 = 0; \qquad -d \le z \le 0, y \le \infty \tag{2.44}$$

$$\frac{\partial\phi_2}{\partial z} = 0; \quad z = -d \tag{2.45}$$

$$g\zeta_2 + \frac{\partial\phi_2}{\partial t} + \frac{1}{2}\left|\vec{\nabla}\phi_1\right|^2 + \zeta_1\frac{\partial^2\phi_1}{\partial z\partial t} = 0; \quad z = 0 \tag{2.46}$$

$$\frac{\partial^2\phi_2}{\partial t^2} + g\frac{\partial\phi_2}{\partial z} + \frac{\partial}{\partial t}\left|\vec{\nabla}\phi_1\right|^2 + \zeta_1\frac{\partial}{\partial z}\left[\frac{\partial^2\phi_1}{\partial t^2} + g\frac{\partial\phi_1}{\partial z}\right] = 0; \quad z = 0 \tag{2.47}$$

Similar to first order perturbation, the solution of second order pertubation can be solved in regular and irregular sea.

2.4.1. Second order solution in regular wave condition

In 1847, Stokes presented a theoretical formula for first and second order perturbation problem specifically for a single (regular) wave. This theory is commonly referred as Stokes second order theory. The solution for velocity potential ($\phi = \phi_1 + \phi_2$) and water surface elevation ($\zeta = \zeta_1 + \zeta_2$) contain first order and second order solution [6].

$$\zeta\,(t) = \zeta_{a1}\left\{\underbrace{cos(kx - \omega t)}_{linear} + \underbrace{k\zeta_{a1}\frac{3 - tanh^2(kd)}{4tanh^3(kd)}cos\,(2(kx - \omega t))}_{second-order}\right\} + O\left(\left(\frac{\zeta_{a1}}{\lambda}\right)^3\right) \tag{2.48}$$

$$\phi = \frac{g\zeta_{a1}cosh\big(k(z+d)\big)}{\omega\, cosh(kd)}\left\{\underbrace{sin(kx-\omega t)}_{linear} + \underbrace{k\zeta_{a1}\frac{3\,cosh\big(2k(z+d)\big)}{8sinh^3(kd)}sin\big(2(kx-\omega t)\big)}_{sum-frequency}\right\} \quad (2.49)$$
$$\underbrace{-(k\zeta_{a1})^2\frac{1}{2sinh\,(2kd)}\frac{gt}{k}}_{mean-drift} + O\left(\left(\frac{\zeta_{a1}}{\lambda}\right)^3\right)$$

From equation 2.49, it can be observed that there is mean-drift term. This term is linearly dependent on time. In this case, the mean of particle velocity and acceleration changes with time. For large water depth, since $lim_{d\to\infty}\, sinh\,(2kd) = \infty$, the mean drift term can be neglected. Beside mean-drift, the sum-frequency term appears in the formula. This term shows that there is another oscilation frequency which is higher than frequency of linear component. This is very crucial for structure with low eigenperiod (high eigenfrequency) such as heave, pitch and roll eigenperiod of of TLP [14] where large dynamic response can be excited by the sum-frequency term. Nevertheless, similar to mean-drift term, for large water depth, the sum-frequency can be neglected. The other term is different-frequency term, which is contained in the third order part. The different-frequency term is critical for structure with high eigenperiod (low eigenfrequency) such as eigenperiod of moored barge [14]. Equation 2.48 and 2.49 show that there is no phase different between linear and second order term. This indicates that the regularity in wave shape is maintained. The second order dispersion relation is equal to first order dispersion relation, which implies that the phase speed of second order component is equal to phase speed of first order component. Equation 2.50 shows the equation of wave phase speed:

$$c_2 = \frac{\lambda_2}{T_2} = \frac{\omega_2}{k_2} = \frac{2\omega_1}{2k_1} = c_1 \quad (2.50)$$

Where c_2 and c_1 are second first order phase speed respectively. For large water depth, second order surface elevation term converges to $k{\zeta_{a1}}^2/2$. Therefore, the only correction on second order wave theory for infinite water depth is the correction of water surface elevation while the kinematics value is same as first order particle kinematics. Figure 2.2 illustrates the surface elevation from second order stokes theory for d = 500 m, ζ_a = 10 m, T = 12 s.

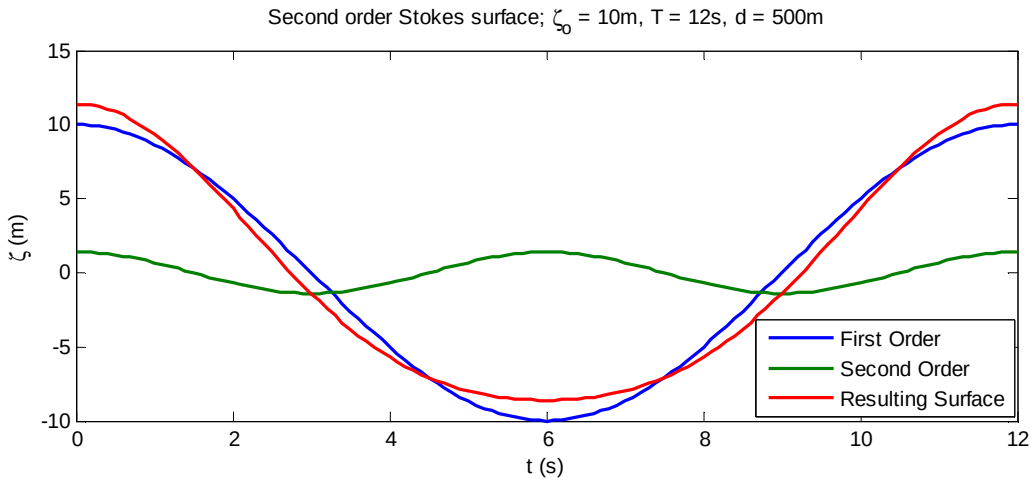

Figure 2.2 Second Order Stokes Water Surface

By utilizing the second order stokes velocity potential for finite depth, the second order correction of particle kinematics for two-dimensional wave [6]:

$$u_{x,2} = \frac{\partial \phi_2}{\partial x} = \frac{3g(k\zeta_{a1})^2}{8\omega}\left(2\frac{cosh\,(k(z+d))}{cosh\,(kd)}\right)\left(\frac{cosh\,(2k(z+d))}{sinh^3(kd)}\right)cos\,(2(kx-\omega t)) \quad (2.51)$$

$$u_{z,2} = \frac{\partial \phi_2}{\partial z} = \frac{3g(k\zeta_{a1})^2}{8\omega}\left(\frac{sinh\,(k(z+d)) + 3sinh\,(3k(z+d))}{2\cosh(kd)\,sinh^3\,(kd)}\right)sin\,(2(kx-\omega t)) \quad (2.52)$$

$$a_{x,2} = \frac{\partial^2 \phi_2}{\partial x dt} = \frac{3g(k\zeta_{a1})^2}{8}\left(4\frac{cosh\,(k(z+d))}{cosh\,(kd)}\right)\left(\frac{cosh\,(2k(z+d))}{sinh^3(kd)}\right)sin\,(2(kx-\omega t)) \quad (2.53)$$

$$a_{z,2} = \frac{\partial^2 \phi_2}{\partial z dt} = -\frac{3g(k\zeta_{a1})^2}{8}\left(\frac{sinh(k(z+d)) + 3sinh\,(3k(z+d))}{2cos\,h(kd)\,sinh^3(kd)}\right)\cos\,(2(kx-\omega t)) \quad (2.54)$$

Equations 2.51 to 2.54 are correction term to first order problem and should be added to first order solution presented in equation 2.21 to 2.24 respectively. Similar to first order velocity potential, second order velocity potential is also valid only up to mean water surface level. Therefore, an approximation method (explained at section 2.5) should be used to find kinematics at free surface. The, correction term for hydrodynamic pressure (p_2):

$$p_2 = -\rho\frac{\partial \phi_2}{\partial t} = \rho g k {\zeta_{a1}}^2\left[\frac{1}{2sinh\,(2kd)} + 2\left(\frac{cosh\,(k(z+d))}{cosh\,(kd)}\right)\frac{3cosh\,(2k(z+d))}{8sinh^3\,(kd)}cos(2(kx-\omega t))\right] \quad (2.55)$$

2.4.2. Second order solution in irregular wave condition

In 1981, Sharma and Dean [36] proposed a method to calculate the water surface elevation and particle kinematics for nonlinear wave in irregular sea. The formulation is based on the pertubation scheme and also accounts the stream function that is demonstrated by Dean (presented in section 2.6.2). Similar to stokes second order, the method utilizes the solution of first order perturbation scheme (ϕ_1) then includes the second order correction term (ϕ_2). The second order term considers the interaction between each wave component. As a consequence, the formulation contains the diferent-frequency term and sum-frequency term. The second order correction term for velocity potential of irregular two-dimention wave is [36]:

$$\phi_2 = \overbrace{\frac{1}{4}\sum_{i=1}^{N}\sum_{j=1}^{N}\frac{g^2\zeta_{a1,i}\zeta_{a1,j}}{\omega_i\omega_j}\frac{cosh\left(k_{ij}^{-}(z+d)\right)}{cosh\left(k_{ij}^{-}d\right)}\frac{D_{ij}^{-}}{\omega_i-\omega_j}\sin\left(\psi_i-\psi_j\right)}^{different-frequency} + \underbrace{\frac{1}{4}\sum_{i=1}^{N}\sum_{j=1}^{N}\frac{g^2\zeta_{a1,i}\zeta_{a1,j}}{\omega_i\omega_j}\frac{cosh\left(k_{ij}^{+}(z+d)\right)}{cosh\left(k_{ij}^{+}d\right)}\frac{D_{ij}^{+}}{\omega_i+\omega_j}sin\left(\psi_i+\psi_j\right)}_{sum-frequency} \tag{2.56}$$

Where:

$k_{ij}^{-} = |k_i - k_j|$

$k_{ij}^{+} = |k_i + k_j|$

$\psi_i = k_i x - \omega_i t + \varepsilon_i$

$R_i = k_i tanh\,(k_i d)$

$$D_{ij}^{-} = \frac{\left(\sqrt{R_i}-\sqrt{R_j}\right)\left[\sqrt{R_j}(k_i^2-R_i^2)-\sqrt{R_i}\left(k_j^2-R_j^2\right)\right]+2\left(\sqrt{R_i}-\sqrt{R_j}\right)^2\left(k_ik_j+R_iR_j\right)}{\left(\sqrt{R_i}-\sqrt{R_j}\right)^2-k_{ij}^{-}\,tanh\left(k_{ij}^{-}d\right)}$$

$$D_{ij}^{+} = \frac{\left(\sqrt{R_i}+\sqrt{R_j}\right)\left[\sqrt{R_j}(k_i^2-R_i^2)+\sqrt{R_i}\left(k_j^2-R_j^2\right)\right]+2\left(\sqrt{R_i}+\sqrt{R_j}\right)^2\left(k_ik_j-R_iR_j\right)}{\left(\sqrt{R_i}+\sqrt{R_j}\right)^2-k_{ij}^{+}\,tanh\left(k_{ij}^{+}d\right)}$$

It should be noticed that k_{ij}^{-} and k_{ij}^{+} is the magnitude of difference-frequency and sum-frequncy wave number. In three dimention (short wave approximation), k_{ij}^{-} and k_{ij}^{+} refer to the magnitude of difference-frequency and sum-frequency wave number vector, $\left|\overrightarrow{k_\iota}-\overrightarrow{k_J}\right|$ and $|\overrightarrow{k_\iota}+\overrightarrow{k_J}|$. The second order contribution to the water surface elevation:

$$\zeta_2 = \overbrace{\frac{1}{4}\sum_{i=1}^{N}\sum_{j=i}^{N}\zeta_{a1,i}\zeta_{a1,j}\left(\frac{D_{ij}^{-}-\left(k_ik_j+R_iR_j\right)}{\sqrt{R_iR_j}}+\left(R_i+R_j\right)\right)cos\left(\psi_i-\psi_j\right)}^{different-frequency} + \underbrace{\frac{1}{4}\sum_{i=1}^{N}\sum_{j=i}^{N}\zeta_{a1,i}\zeta_{a1,j}\left(\frac{D_{ij}^{+}-\left(k_ik_j-R_iR_j\right)}{\sqrt{R_iR_j}}+\left(R_i+R_j\right)\right)cos\left(\psi_i+\psi_j\right)}_{sum-frequency} \tag{2.57}$$

This equation is valid for small and large water depth, with assumption there is no wave break phenomenom. However, when it comes to large water depth, $lim_{d\to\infty}\, tanh(kd) = 1$ and $lim_{d\to\infty}\frac{cosh(k(z+d))}{cosh(kd)} = e^{kz}$. As a result, D_{ij}^{+} is equal to zero indicating that the sum-frequency term can be negelcted for large water depth. The second order correction term can be simplified into equation 2.58 and 2.59 [23]:

$$\phi_2 = -\sum_{i=1}^{N}\sum_{j=i+1}^{N}\zeta_{a1,i}\zeta_{a1,j}\,\omega_i exp\left((k_i-\,k_j)z\right)sin\left(\psi_i-\psi_j\right) \tag{2.58}$$

$$\zeta_2 = \frac{1}{2}\sum_{i=1}^{N}{\zeta_{a1,i}}^2 k_i cos(2\psi_i) + \frac{1}{2}\sum_{i=1}^{N}\sum_{j=i+1}^{N}\zeta_{a1,i}\zeta_{a1,j}\left(\left(k_i+k_j\right)cos\left(\psi_i+\psi_j\right)-\left(k_i-k_j\right)cos\left(\psi_i-\psi_j\right)\right) \tag{2.59}$$

This expression is valid to use for continous spectrum. From equation 2.56 and 2.57, to calculate the correction term of surface elevation and velocity potential, N^2 wave components should be included. Because of that, the computational time and also the required memory are significantly increased since the velocity potential and surface elevation are updated on each time step.

The interaction between wave components with very different frequency produces another issue. The derivatives of velocity potential and surface elevation are not defined if the spectrum is summed up to high frequency. To resolve this problem, a cut-off frequency can be used [23]. With cut-off frequency, the highest frequency in the spectrum is limited. The other way to account for this problem is by limiting the interaction between waves with very different frequency.

Similar to first order regular wave problem, the particle kinematics is not defined above the mean surface level. Therefore an approximation method should be used.

2.5. Approximation of Particles Kinematics above Mean Surface

The first order and second order pertubation are solved at mean water surface elevation. Therefore, if the particle kinematics at true surface wants to be established, some approximation schemes must be utilized.

2.5.1. Constant stretching (extrapolation of Airy theory)

This method utilitizes the result from Airy wave theory, which is a solution for first order pertubation scheme. Therefore, this method should be used only for first order wave. In this method, the wave particle kinematics is calculated up to the surface elevation in wave trough by Airy wave theory. At wave crest, the wave particle kinematics is calculated until mean water surface elevation ($z = 0$) then it is assumed uniform for $0 \leq z \leq \zeta$, where $z = 0$ refers to mean water surface elevation. Figure 2.3 illutrates this method.

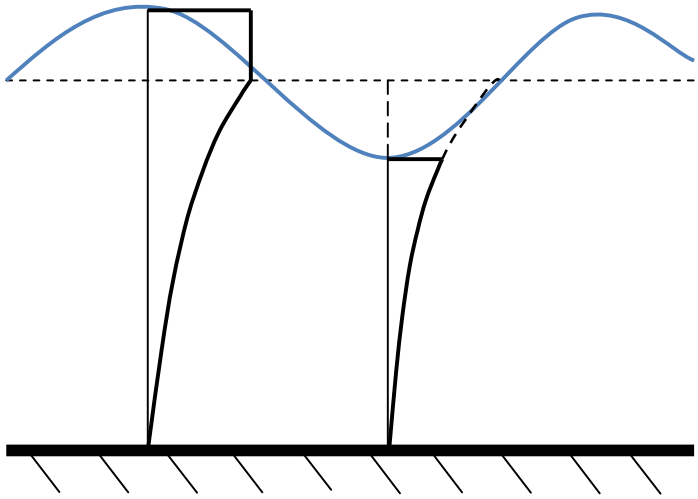

Figure 2.3 Extrapolation of Airy theory

2.5.2. Wheeler stretching

The popular approximation method to calculate wave particle kinematics at real surface is the method proposed by Wheeler. In this method, the water surface (the second order or the first order water surface) is assumed as Gaussian process then the linear theory (first order solution) is applied to calculate the wave particle kinematics. By applying this approach, it is observed that the calculated wave particle kinematics at $z=0$ refer to the measured free surface kinematics.

Therefore, the vertical coordinate (*z*-coordinate) is stretched such that the wave particle kinematics at free surface after stretching are equal to wave particle kinematics at *z*=0 before stretching process. The new vertical coordinate (z_{new}) follows equation 2.60. Figure 2.4 describes the wheeler stretching method.

$$z_{new} = \frac{z_{old} - \zeta}{1 + \frac{\zeta}{d}} \tag{2.60}$$

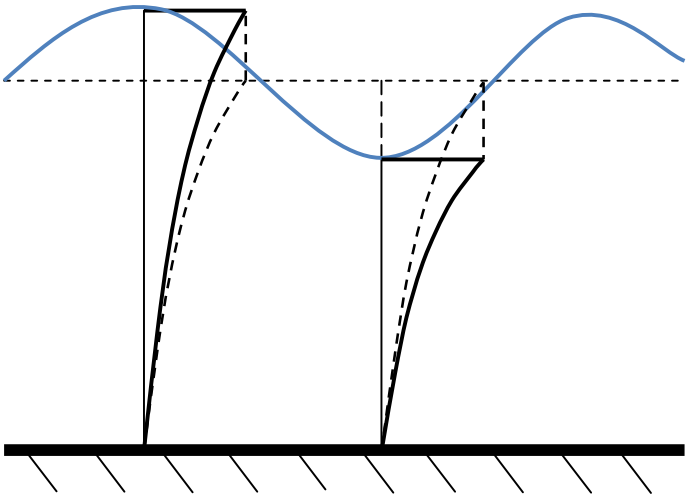

Figure 2.4 Wheeler Stretching

For irregular sea, there is an issue regarding high frequency components. For steep wave case, the wavenumber of high frequency component from dispersion relation is higher than the actual wavenumber. In reality, steep wave with high frequency components contain significant bound wave which has lower frequency. As a result, the first order wave overestimates the contribution of short wave component for particle wave kinematics. This issue is discussed by Johannessen [23]. To avoid this issue, a cut-off frequency (ω_{cut}) is intoduced where the suggested value is $\omega_{cut} = 4\omega_p$.

Wheeler streching can be applied directly for first order wave, either in regular or irregular condition. However, for second order wave, water surface elevation from combination of first order surface and second order correction should be linearized. The linearization can be done by assuming the second order irregular surface as Gaussian process. By using Fourier transform, the combination of first and second order wave surface is represented by a new set of harmonic component. Utilizing these new component set, the wave particle kinematics can be calculated by first order wave theory. As a consequence, the simulation will based on *N* wave component or

at least significantly less than N^2 component. In this way, the memory and computational time can be decreased.

Wheeler stretching is relatively good if applied to second order surface than first order surface (for first order surface, Wheeler stretching underestimate the wave particle kinematics). However there is an issue regarding the underestimated wave particle kinematics below free surface level.

2.5.3. Linear extrapolation

Linear extrapolation can be used to determine the wave particle kinematics for $z > 0$. In this method, the wave particle kinematics are calculated until mean surface ($z = 0$) then extrapolated by MacLaurin series up to the free surface. Velocity potential for $z > 0$ can be written as:

$$\phi(x,z,t) = \phi_1(x,0,t) + \phi_2(x,0,t) + z\frac{\partial \phi_1}{\partial z}(x,0,t) \tag{2.61}$$

Removing the second order velocity potential (ϕ_2), equation 2.61 represents linear interpolation for first order wave. By its definition, the particle wave kinematics are exponential from seabed to mean water surface but linear above the mean water surface. The wave particle kinematics for $z > 0$ becomes:

$$u_x(x,z,t) = \frac{\partial \phi_1}{\partial x}(x,0,t) + \frac{\partial \phi_2}{\partial x}(x,0,t) + z\frac{\partial^2 \phi_1}{\partial z \partial x}(x,0,t)\,; \quad z > 0 \tag{2.62}$$

$$u_z(x,z,t) = \frac{\partial \phi_1}{\partial z}(x,0,t) + \frac{\partial \phi_2}{\partial z}(x,0,t) + z\frac{\partial^2 \phi_1}{\partial^2 z}(x,0,t)\,; \quad z > 0 \tag{2.63}$$

$$a_x(x,z,t) = \frac{\partial^2 \phi_1}{\partial x \partial t}(x,0,t) + \frac{\partial^2 \phi_2}{\partial x \partial t}(x,0,t) + z\frac{\partial^3 \phi_1}{\partial z \partial x \partial t}(x,0,t)\,; \quad z > 0 \tag{2.64}$$

$$a_z(x,z,t) = \frac{\partial^2 \phi_1}{\partial z \partial t}(x,0,t) + \frac{\partial^2 \phi_2}{\partial z \partial t}(x,0,t) + z\frac{\partial^3 \phi_1}{\partial^2 z \partial t}(x,0,t)\,; \quad z > 0 \tag{2.65}$$

To apply equations 2.62 until 2.65 into a continuous spectrum (for irregular wave condition), a cut-off frequency is introduced. Stansberg [39] proposes that the cut-off frequency is equal to:

$$\omega_{cut} = \sqrt{\frac{2g}{H_s}} \tag{2.66}$$

This cut-off frequency is discussed further in section 4.3.2. Since the profile of wave particle kinematics above mean water level is linear, it marginally underestimates the surface velocity at crest when compared to experiment result [40]. The linear extrapolation method is illustrated by figure 2.5.

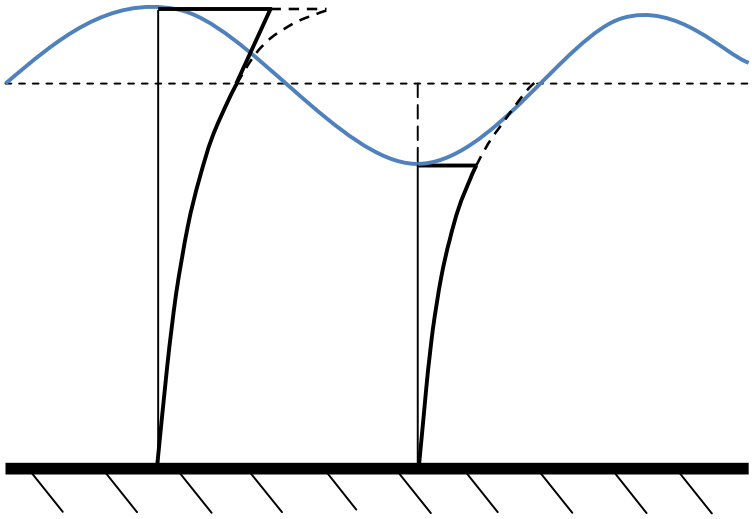

Figure 2.5 Linear Extrapolation

2.6. Others Regular Wave Theory

When dealing with regular wave condition, it is possible to solve perturbation scheme in higher order than second order, for example the 5th Stokes wave theory. In addition, the particle kinematics can be calculated from stream function instead of potential velocity.

2.6.1. Stokes wave

It is presented before that Stokes wave theory can solve pertubation scheme up to second order term. In general, Stokes wave theory can be used to solve pertubation scheme up to higher order term. The Stokes wave theory basically is sumation of potential velocity from different order. The formulation of Stokes wave theory up to N-th order:

$$\phi = \sum_{i=1}^{N} \phi_i' cosh\{k(z+d)\} cos(\omega t - kx) \tag{2.67}$$

$$\zeta = \sum_{i=1}^{N} \zeta_i' \frac{sin\big(i(\omega t - kx)\big)}{k} \tag{2.68}$$

$\phi_i'$and ζ_i' are the coefficient of potential velocity and surface elevation of *i-th* order, respectively. These coefficients are determined from iteration process and proportional to wave stepness (H/λ). Since the potensial is a product of summation process, then the particle kinematics are [37]:

$$u_x = \frac{\partial \phi}{\partial x} = \sum_{i=1}^{N} i \frac{\omega}{k} \phi_i' cosh\{k(z+d)\} sin(\omega t - kx) \tag{2.69}$$

$$u_z = \frac{\partial \phi}{\partial z} = \sum_{i=1}^{N} \frac{\omega}{k} \phi_i' sinh\{k(z+d)\} cos(\omega t - kx) \tag{2.70}$$

$$a_x = \frac{\partial^2 \phi}{\partial x dt} = \sum_{i=1}^{N} i \frac{\omega^2}{k} \phi_i' cosh\{k(z+d)\} cos(\omega t - kx) \tag{2.71}$$

$$a_z = \frac{\partial^2 \phi}{\partial z dt} = -\sum_{i=1}^{N} \frac{\omega^2}{k} \phi_i' sinh\{k(z+d)\} sin(\omega t - kx) \tag{2.72}$$

Stokes 5th wave is able to represent more accurate wave shape. In addition, it is able to produce more accureate particle wave kinematics which means more accurate load and response. However, this theory is relatively complex to do. In addition, wave will break when $2\zeta_a/\lambda$ less than 1/7 and Stokes wave theory is not valid for breaking wave. Nevertheless, for design wave method (presented in section 3.4), Stokes 5th wave is normally used.

2.6.2. Stream function (Dean stream function)

In shallow water, the pertubation scheme will fail. The shape contains many local maxima and does not represent the ocean wave. Therefore, another theory should be applied. Dean [9] presented another approach than pertubation shceme to define the velocity potential. Instead from potential velocity, the particle kinematics is found from stream functions. The stream function (ψ_s):

$$\frac{\partial \psi_s}{\partial X} = -u_z \;;\; \frac{\partial \psi_s}{\partial Z} = u_x \tag{2.73}$$

If (*x, z*) is fixed frame reference, (*X, Z*) is frame reference which moves with the waves at phase speed *c*. In this case, $x = X + ct$, t = time and z = Z. The fluid is still assumed as irrotational and incompressible, similar to pertubation scheme. The stream function also should fulfill [9], [16]:

Laplace equation: $$\frac{\partial^2 \psi_s}{\partial X^2} + \frac{\partial^2 \psi_s}{\partial Z^2} = 0 \quad (2.74)$$

Bottom boundary condition: $$\psi_s(X, 0) = 0 \quad (2.75)$$

Kinematic free surface condition: $$\psi_s\big(X, \zeta(X)\big) = -Q_v \quad (2.76)$$

Dynamic free surface condition: $$\frac{1}{2}\left[\left(\frac{\partial \psi_s}{\partial X}\right)^2 + \left(\frac{\partial \psi_s}{\partial Z}\right)^2\right] + g\,\zeta(X) = R_s;\ Z = \zeta(X) \quad (2.77)$$

Where Q_v is the volume flow per unit span under the wave in (X, Z) frame and R_s is positive constant [16]. The equation 2.74 and 2.75 are satisfied by a stream function [35]:

$$\psi_s(X, Z) = B_0 Z + \sum_{j=1}^{N} B_j \frac{sinh\,(j\,k\,Z)}{cosh\,(j\,k\,D_s)} cos\,(j\,k\,X) \quad (2.78)$$

Where k is the wave number and N is the order of stream function. D_s is arbritrary reference level. B_j and k are determined in such way that equation 2.73 satisfies equation 2.75 and 2.76. In addition, it should be noted that all equation in this particular section is based on normalized parameter. Further explanation can be found at Reinecker and Fenton's paper [35].

High number of N will improve the accuracy of solution. For deep water, N=3 is satisfactory while for shallow water N can be up to 30. The stream function theory does not need truncation as pertubation scheme. In addition, when the wave height/depth is less than 0.5, the difference between 5th order Stokes and stream function is neglegible.

2.7. Breaking Waves

For particular water depth, there is an upper limit of wave height. When the wave steepness is high enough, the wave become unstable and break. The wave height limit (H_b) is expressed as function of wave length (λ) depth (d). For shallow water, the wave height limit is expressed as [8]:

$$H_b = 0.142\,\lambda\,tanh\,(kd) \quad (2.79)$$

Figure 2.6 shows the normalized wave height limit (H_b/λ) as function of normalized water depth (d/λ). It can be observed, when the water depth is suficiently depth enough, the H_b/λ converges

to 0.142. Therefore, for depth water (when $tan\,h(kd) \rightarrow 1$), the wave height limit can be determined by:

$$H_b = 0.142\,\lambda \tag{2.80}$$

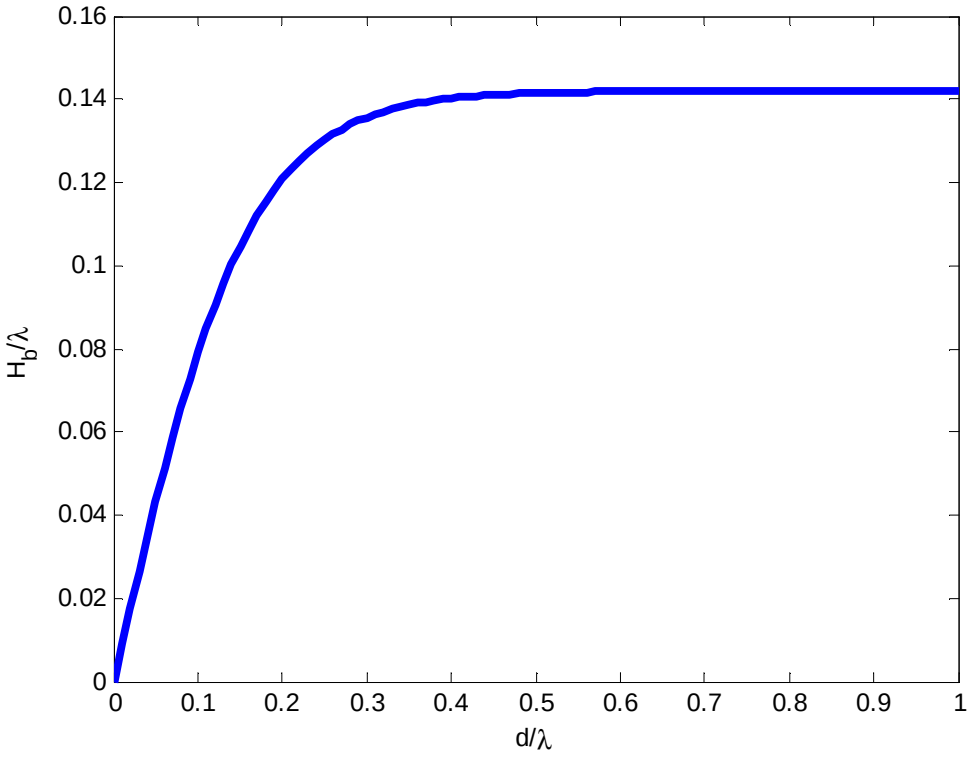

Figure 2.6 Wave Height Limit for Breaking Wave

3. Ocean Wave Statistics

Ocean wave is a random process which continously changes with time. Because of that, it is convenient to fit a probabilistic model into particular ocean location for further analysis. The problem is how to determine the parameters of the probabilistic model of ocean wave as they also changes in time. However, these parameters change slower than the ocen surface itself. Therefore, the ocean wave can be observed for certain duration where the process is assumed as a stationary process. The typical duration is 3-4 hours [30]. This analysis is known as short-term analysis of sea surface. To analyze the wave condition for longer duration, e.g. for 100 year duration, the long-term analyze is applied.

3.1. Method of Moment

The parameters of certain probabilistic model can be acquired by method of moment or maximum likelihood method. Since method of moment is relatively simpler compared to the other method, method of moment is the only approach that is described and used in this report. The method of moment based on principle that the probabilistic model moment is equal to the sample moment.The statistical moment and central moment of probability model for x as variable are [26]:

Moment: $$\mu_{\mathrm{X}}^{(n)} = \int_{-\infty}^{\infty} \mathrm{x}^n \, f_{\mathbf{X}}(\mathrm{x}) \, dx \tag{3.1}$$

Central moment $$\bar{\mu}_{\mathrm{X}}^{(n)} = \int_{-\infty}^{\infty} (\mathrm{x} - \mu_{\mathrm{X}})^n \, f_{\mathbf{X}}(\mathrm{x}) \, dx \tag{3.2}$$

Where $\mu_{\mathrm{X}} = \mu_{\mathrm{X}}^{(1)}$. These moment and central moment are fitted to the moment from sample.

3.1.1. Expected value

The expected value is equal to the first moment:

$$E[\mathrm{x}] = \mu_{\mathrm{X}} = \mu_{\mathrm{X}}^{(1)} = \int_{-\infty}^{\infty} \mathrm{x} \, f_{\mathbf{X}}(\mathrm{x}) \, d\mathrm{x} \tag{3.3}$$

For standard Gaussian distribution, $E[\mathrm{x}]$ is equal to zero. The expected value from sample ($m_X = m_X^{(1)}$) is:

$$m_{\mathrm{X}} = m_{\mathrm{X}}^{(1)} = \frac{1}{N}\sum_{i=1}^{N} \mathrm{x}_i \tag{3.4}$$

N is the number of sample x.

3.1.2. Variance

The variance is equal to second central moment:

$$\sigma_{\mathrm{X}}{}^2 = Var[\mathrm{x}] = \bar{\mu}_{\mathrm{X}}^{(2)} = E[(\mathrm{x} - E[\mathrm{x}])^2] = \int_{-\infty}^{\infty} (\mathrm{x} - \mu_{\mathrm{X}})^2 \, f_{\mathbf{X}}(\mathrm{x}) \, d\mathrm{x} \tag{3.5}$$

If μ_X is equal to zero, the variance is equal to second moment. The standard deviation (σ_X) is equal to square root of variance. The variance of sample ($S_X{}^2$) is:

$$S_X{}^2 = \frac{1}{N-1}\sum_{i=1}^{N} (\mathrm{x}_i - m_X)^2 \tag{3.6}$$

3.1.3. Skewness

Skewness of a distribution function can be determined from the third and second central moment. The skewness describes the symetry of probality density function. For symetry probability density function, skewness coefficient is equal to zero. Skewness is represented by a skewness coefficient (γ_1) which is:

$$\gamma_1 = \frac{\bar{\mu}_X^{(3)}}{\left(\bar{\mu}_X^{(2)}\right)^{3/2}} = \frac{\bar{\mu}_X^{(3)}}{{\sigma_X}^3} \tag{3.7}$$

Since standard Gaussian model is a symetry probability density function, γ_1 is equal to zero. In reality, sea surface have slightly positive skewness which imply it contains of higher peak than through. For the measurement, the skewness coefficeint of sample ($\hat{\gamma}_1$) is:

$$\hat{\gamma}_1 = \frac{\frac{1}{N}\sum_{i=1}^{N}(\mathrm{x}_i - m_X)^3}{{S_X}^3} \tag{3.8}$$

3.1.4. Kurtosis

Kurtosis, also known as flatness coefficient, describes the peakedness of the distribution. It is calculated from:

$$\gamma_2 = \frac{\bar{\mu}_X^{(4)}}{\left(\bar{\mu}_X^{(2)}\right)^2} = \frac{\bar{\mu}_X^{(4)}}{{\sigma_X}^4} \tag{3.9}$$

For standard Gaussian distribution, γ_2 is equal to 3. The kurtosis of sample is:

$$\hat{\gamma}_2 = \frac{\frac{1}{N}\sum_{i=1}^{N}(\mathrm{x}_i - m_X)^4}{{S_X}^4} \tag{3.10}$$

3.2. Short Term Analysis of Sea Surface

As mentioned before, the sea surface (ocean wave) can be assumed as a stationary process for certain duration (3-4 hours). In this condition, the mean and standard deviation are assumed independent of time which means they are constant. The sea surface (ζ) can be assumed as a Gaussian process. Therefore, Gauss probability density function is used to express the distribution of sea surface. The formula for Gauss (normal) probability density function [26] with ζ as parameter:

$$f(\zeta) = \frac{1}{\sqrt{2\pi}\,\sigma_\zeta} exp\left(-\frac{1}{2}\left(\frac{\zeta - \mu_\zeta}{\sigma_\zeta}\right)^2\right) \tag{3.11}$$

Where μ_ζ and σ_ζ are mean and standard deviation of sea surface respectively. It is possible to set the mean of sea surface equal to zero which gives σ_ζ is the only unknown parameter and can be calculated from second central moment (presented in equation 4.20) or by method of moment (utilizing equation 3.6).

3.2.1. Distribution of maximum for linear surface elevation

A local maximum for water surface elevation is defined by $\partial\zeta/\partial t = 0$ and $\partial^2\zeta/\partial t^2 < 0$. In the other hand, global maximum is the maximum of water surface elevation from a zero crossing wave. The magnitude of local maximum could be less than zero (mean sea surface elevation) while the the global maximum is always positive. In general, the ocean surface is a broadband process, where the number for local maximum is larger (different) than global maximum. For narrowband process, number of local maxima is close or similar to number of global maxima. In addition, the period of each zero croessing wave component is relatively constant while it is not constant in broadband process. The narrowband and broadband process of sea surface is illustrated in figure 3.1.

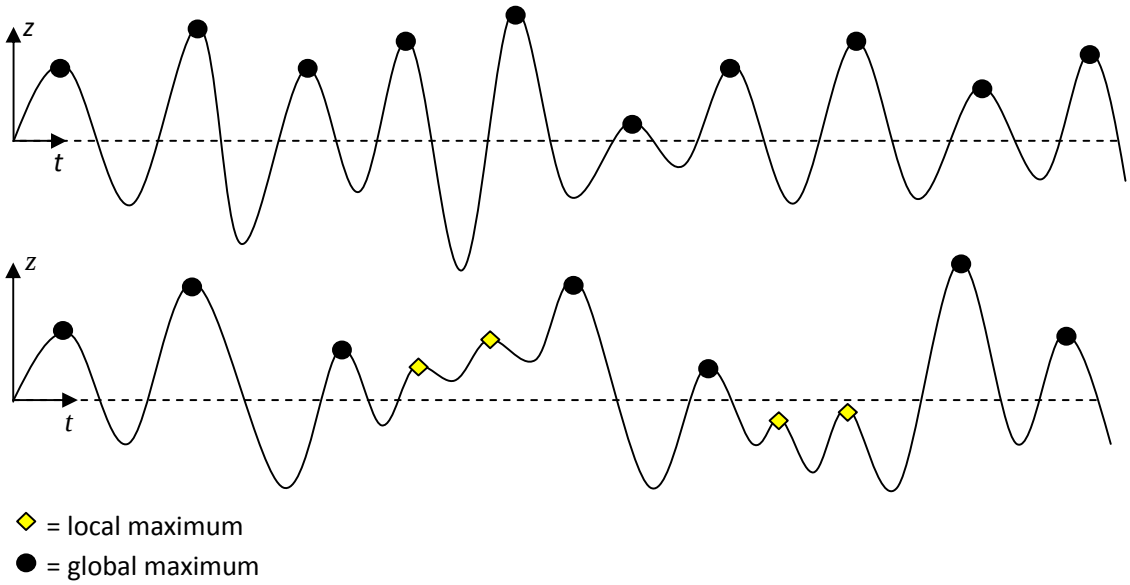

Figure 3.1 Illustration of narrowband and broadband process
Up: Narrowbad; Down: Broadband

3.2.1.1. Rayleigh distribution for narrowband sea surface

If the sea surface is assumed as narrowband and Gaussian process, the distribution of sea surface maximum (ζ_m) follows Rayleigh distribution. The probability density function (PDF) and cummulative distribution function (CDF) of Rayleigh distribution is presented in equation 3.12 and 3.13 respectively [26].

$$f_{\boldsymbol{\zeta_m}}(\zeta_m) = \frac{\zeta_m}{{\sigma_\zeta}^2} exp\left(-\frac{1}{2}\left(\frac{\zeta_m}{\sigma_\zeta}\right)^2\right) \tag{3.12}$$

$$F_{\boldsymbol{\zeta_m}}(\zeta_m) = 1 - exp\left(-\frac{1}{2}\left(\frac{\zeta_m}{\sigma_\zeta}\right)^2\right) \tag{3.13}$$

3.2.1.2. Rice distribution for broadband sea surface

For broadband process and assuming the sea surface is a Gaussian process, the probability density function $f_{\boldsymbol{\eta}}(\eta)$ and cumulative distribution function $F_{\boldsymbol{\eta}}(\eta)$ of normalized maximum (η), accounting both local and global maxima, is formulated in Rice distribution [7].

$$f_{\boldsymbol{\eta}}(\eta) = \frac{1}{\sqrt{2\pi}}\xi\, exp\left(-\frac{1}{2}\left(\frac{\eta}{\xi}\right)^2\right) + \eta\sqrt{1-\xi^2}\, exp\left(-\frac{1}{2}\eta^2\right)\, \Phi\left(\frac{\eta}{\xi}\sqrt{1-\xi^2}\right) \tag{3.14}$$

$$F_{\boldsymbol{\eta}}(\eta) = 1 - \frac{1}{2} erfc\left(\frac{\eta}{\sqrt{2}\,\xi}\right) - \sqrt{1-\xi^2}\; exp\left(-\frac{1}{2}\eta^2\right) \Phi\left(\frac{\eta}{\xi}\sqrt{1-\xi^2}\right) \tag{3.15}$$

$$\eta = \frac{\zeta_m}{\sigma_\zeta};\ \xi^2 = 1 - \frac{m_2^2}{m_0 m_4}, 0 \le \xi \le 1\ \ ;\ \ erfc(x) = \frac{2}{\sqrt{\pi}} \int_x^\infty exp(-t^2)dt$$

η is a standardized variable of Rice distribution. ξ is a bandwith parameter that contains information about the condition of number of peaks in one zero-crosing wave. If $\xi = 0$, the Rice distribution becomes Rayleigh distribution (equation 3.12 and 3.13) while when $\xi = 1$, Rice distribution becomes Gauss distribution. Φ is the standard Gauss cumulative distribution. m_n is the *n-th* moment of the wave spectrum which is presented in equation 4.20. Mean and variance of η is expressed in equation 3.16.

$$\mu_\eta = \sqrt{\frac{\pi}{2}(1-\xi^2)}\ ;\ {\sigma_\eta}^2 = 1 - \left(\frac{\pi}{2} - 1\right)(1-\xi^2) \tag{3.16}$$

3.2.1.3. Distribution of largest maximum

To find the largest maximum (ζ_{lm}), each maximum is assumed statistically independent and identically distributed. This assumption is slighlty conservative but acceptable for practical purpose. The cumulative distribution of largest maxima from *N* maxima:

$$F_{\boldsymbol{\zeta_{lm}}}(\zeta_{lm}) = \left(P(\zeta_{m,i} \le \zeta_{lm})\right)^N = \left(F_{\boldsymbol{\zeta_m}}(\zeta_{lm})\right)^N \tag{3.17}$$

For broadband process, the number of maxima (*N*) is equal to T_f / T_{m24}. When $N \rightarrow \infty$, the distribution of largest maxima asymptotically goes to Gumbel distribution [26].The expected value, standard deviation and the mode for the largest maxima for broadbanded process [7]:

$$mode = \sqrt{2\ ln\ \left(N\sqrt{1-\xi^2}\right)} \tag{3.18}$$

$$\mu_{\eta_{lm}} = \sqrt{2}\left(\sqrt{ln\ \left(N\sqrt{1-\xi^2}\right)} + \frac{\gamma_e}{2\sqrt{ln\left(N\sqrt{1-\xi^2}\right)}}\right) \tag{3.19}$$

$$\sigma_{\eta_{lm}} = \frac{\pi}{\sqrt{6}} \frac{1}{\sqrt{2\ ln\left(N\sqrt{1-\xi^2}\right)}} \tag{3.20}$$

Where γ_e is Euler constant and aprroximately equal to *0.5772*. The error of expectation value of largest maxima is in the order $O\left(\left(ln\left(N\sqrt{1-\xi^2}\right)\right)^{-3/2}\right)$.

For narrowbanded process (Rayleigh distribution), the expectation value, standard deviation and the mode of largest maxima can be found from equation 3.18 until 3.20 by setting $\xi = 0$ and multiply the result with σ_ζ. The result is presented in equation 3.21 to 3.23.

$$mode = \sigma_\zeta \sqrt{2\ ln\ (N)} \tag{3.21}$$

$$\mu_{\zeta_{lm}} = \sigma_\zeta \sqrt{2}\left(\sqrt{ln\ (N)} + \frac{\gamma_e}{2\sqrt{ln(N)}}\right) \tag{3.22}$$

$$\sigma_{\zeta_{lm}} = \sigma_\zeta \frac{\pi}{\sqrt{6}} \frac{1}{\sqrt{2\ ln(N)}} \tag{3.23}$$

Number of maxima (N) in narrowbanded process is equal to T_f / T_{m02}. Due to its simplicity, Rayleigh model is more commonly used than Rice distribution. The short term distribution of extreme surface elevation depends on H_s and T_p when the process is assumed Gaussian.

3.2.1.4. Distribution of wave height

To find the distribution of wave height (H), first it is assumed that $H = 2\zeta_m$. It assumed that the wave height also follows the Rayleigh distribution. Then the cummulative distribution of wave height $F_{\boldsymbol{H}}(H)$ is expresed in equation 3.24.

$$F_{\boldsymbol{H}}(H) = 1 - exp\left(-\frac{1}{8}\left(\frac{H}{\sigma_\zeta}\right)^2\right) \tag{3.24}$$

Furthermore, the expected value of largest wave height, $\mu_{HL} = 2\mu_{\zeta_{lm}}$. In reality, the wave height is not necessarily twice the peak of surface elevation from mean water level (as it is shown in figure 2.2 at section 2.4.1). By including the second order term, the crest will be higher than through for regular wave case. Therefore, this approximation is also conservative. The others distribution function should be used, especially when accounting the nonlinearity in water surface elevation.

3.2.2. Distribution of maxima for higher order surface elevation

In reality, the distance between crest and mean surface level is larger than the distance between trough and mean surface level. This implies that the water surface elevation does not exactly follow Gaussian distribution as well as water surface maxima does not follow Rayleigh distribution. Since the largest magnitude of wave particle velocity is located at the crest, it is important to determine the accurate value of crest. Therefore, another distribution which includes the nonlinearity is used.

3.2.2.1. Forristall Distribution

Forristall distribution agrees well with the second order process of surface elevation. The model is a 2-parameter weibull for particular H_s and T_{m01}. The cumulative distribution functions of wave height (H) and wave crest (c), respectively, are [17], [18]:

$$F_{\boldsymbol{H}}(H) = 1 - exp\left(-2.263\left(\frac{H^2}{H_s}\right)^{2.126}\right) \tag{3.25}$$

$$F_{\boldsymbol{C}}(c) = 1 - exp\left(-\left(\frac{c}{\alpha_f H_s}\right)^{\beta_f}\right) \tag{3.26}$$

Forristall wave height distribution (equation 3.25) is actually fitted to data of 116-hours huricane-generated waves in Gulf Mexico. Therefore, it is more appropriate to call equation 3.25 as an empirical distribution of wave height instead of distibution of higher order surface elevation. On the other hand, equation 3.26 is based on second order wave model which makes it is appropriate to call it as distibution of higher order surface elevation. α_f and β_f are found from fitting the distribution function to experiment results. The fits are forced to match the Rayleigh distribution with $\alpha_f = 1/\sqrt{8}$ and $\beta_f = 2$ when stepness (S_1) and Ursell number (U_r) are equal to zero. For 2-dimensional wave, the best fit comes when [18]:

$$\begin{aligned} \alpha_f &= 0.3536 + 0.2892\, S_1 + 0.1060\, U_r \\ \beta_f &= 2 - 2.1597\, S_1 + 0.0968\, U_r^2 \end{aligned} \tag{3.27}$$

In the other hand, the best fit for 3-dimensional wave simulation are [18]:

$$\alpha_f = 0.3536 + 0.2568\, S_1 + 0.0800\, U_r$$
$$\beta_f = 2 - 1.7912\, S_1 + 0.5302\, U_r + 0.284\, U_r^2 \tag{3.28}$$

The wave steepness parameter (S_1) and Ursell number (U_r) with assumption large water depth:

$$S_1 = \frac{2\pi}{g}\frac{H_s}{{T_{mo1}}^2}; \quad U_r = \frac{H_s}{d^3 k_{mo1}^2} \tag{3.29}$$

k_{mo1} is the wave number from mean period (T_{m01}, described in section 4.1.2) and d is the water depth. Forisstall distribution is larger crest height than the result from Rayleigh or Rice. It can be concluded that the Rayleigh and Rice is not conservative regarding the wave crest. There is no Forisstall distribution for wave trough but it can be assumed that Rayleigh and Rice give overestimate value of wave trough. The mode of Forristal crest distribution (wave crest which is only exceeded once in certain duration) can be found by equation 3.30.

$$F_C(c) = 1 - exp\left(-\left(\frac{c_l}{\alpha_f H_s}\right)^{\beta_f}\right) = 1 - \frac{1}{N} \;\rightarrow\; c_l = H_s\, \alpha_f \big(ln(N)\big)^{1/\beta_f} \tag{3.30}$$

Similar to Rayleigh and Rice, Forisstall distribution also converges to Gumbel distribution for very large N. Therefore, the the mean and standar deviation for the largest crest from Forisstall distribution can be expressed as mean and standard deviation of Gumbel distribution with Weibull as its initial distribution [26]. This is expressed in equation 3.31 and 3.32 [6].

$$\mu_{c_l} = \alpha_f H_s \left(\big(ln(N)\big)^{1/\beta_f} + \frac{\gamma_e}{\beta_f \big(ln(N)\big)^{\frac{\beta_f - 1}{\beta_f}}} \right) \tag{3.31}$$

$$\sigma_{c_l} = \frac{\pi}{\sqrt{6}} \frac{\alpha_f H_s}{\beta_f \big(ln(N)\big)^{\frac{\beta_f - 1}{\beta_f}}} \tag{3.32}$$

3.2.2.2. Modified Rayleigh

Another way to present the distribution of higer order surface elevation is by modifying Rayleigh distribution. This method is presented by Stansberg [38]. The modification is based on the increased steepness. The correction term is determined by considering second order regular wave. The expected largest crest (largest maxima) for certain duration from Rayleigh model

is $\mu_{\zeta_{lm}}$. This value is modified as presented in equation 3.33. k_p is first order wavenumber of spectral peak period (T_p).

$$\mu_{c_l} = \mu_{\zeta_{lm}}\left(1 + \frac{1}{2\,k_p\mu_{\zeta_{lm}}}\right) \tag{3.33}$$

3.2.3. Gumbel Distribution

As presented in previous sections, the extreme distribution of any distribution with exponential type (including Rayleigh, Rice and Forristall) converges to Gumbel distribution when $N\rightarrow\infty$. The cummulative distribution of Gumbel for largest value of x out of N-number of x (x_N) as parameter:

$$F_{\boldsymbol{X_N}}(\mathrm{x}_N) = exp\left(-exp\left(-\frac{(\mathrm{x}_N - \alpha_G)}{\beta_G}\right)\right)$$
$$\alpha_G = \mu_{x_N} - 0.5772\beta_G; \quad \beta_G = \frac{\sigma_{\mathrm{x}_N}\sqrt{6}}{\pi} \tag{3.34}$$

Where μ_{X_N} and σ_{X_N} are expected value and standard deviation of x_N respectively. Moreover, Gumbel distribution is usually used for extreme value of sample when the distribution model is still unknown. From sample, after the sample is sorted from the smallest to the highest, the cumulative distribution can be found by:

$$F_i = \frac{i}{N+1}; \quad i = 1,2,3,\dots,N; \;\; N = total\ number\ of\ sample \tag{3.35}$$

To check if the sample follows Gumbel distribution or not, the Gumbell paper can be used. If the sample cummulative distribution tends to construct straight line, then it can be concluded that the sample follows Gumbel model.

3.3. Long Term Analysis of Sea Surface

In structural analysis, it is important to find the extreme value (e.g. extreme crest) for duration more than 3-4 hours, e.g. for 100 or 10000 year. In this case, the assumption that sea surface is a stationary process is not valid anymore. Since the condition of short-term analysis is depend on certain H_s and T_p (H_s and T_p are assumed constant in short-term analysis), the variation of H_s and T_P should be considered for long-term analysis.

3.3.1. Full long-term of sea surface

In full long-term method, the wave crest is modelled by joint probability function of wave crest short-term distribution of and seastate (H_s and T_p) long-term variation. The full long-term cummulative distribution for 3-hour wave crest is expressed in equation 3.35 [20].

$$F_{C_{3h}}(c) = \int_{H_s}\int_{T_p} \underbrace{F_{C_{3h}|H_s,T_p}(c|H_s,T_p)}_{\substack{Short-term\\ distribution}} \underbrace{f_{H_s,T_p}(H_s,T_p)}_{\substack{variation\ in\\ H_s and\ T_p}}\, dh_s\, dt_p \tag{3.36}$$

$f_{H_s,T_p}(H_s,T_p)$ is the joint probability density function of H_s and T_p and determined empirically from the scatter diagram of H_s and T_p. It is considered that:

$$f_{H_s,T_p}(H_s,T_p) = f_{H_s}(H_s)\, f_{T_p|H_s}(T_p|H_s) \tag{3.37}$$

Where $f_{H_s}(H_s)$ is the marginal distribution of H_s while $f_{T_P|H_s}(T_p|H_s)$ is the conditional distribution of T_p for given H_s. A 3-paremeter Weibull distribution can be used as $f_{H_s}(H_s)$. The cummulative distribution for 3-parameter Weibull of $F_{H_s}(H_s)$ [21]:

$$F_{H_s}(H_s) = 1 - exp\left(-\left(\frac{H_s-\lambda_w}{\alpha_w}\right)^{\beta_w}\right); \qquad h_s \geq \lambda_w \tag{3.38}$$

Where λ_w, α_w, and β_w are the location, scale and shape parameter of 3-parameter Weibull model respectively. These parameters can be determined by method of moment. The final realtionships between model parameters and sample moment are presented from equation 3.39 to 3.41 [21].

$$m_\zeta = \lambda_w + \alpha_w\, \Gamma\left(1+\frac{1}{\beta_w}\right) \tag{3.39}$$

$$S_X{}^2 = \alpha_w{}^2\left[\Gamma\left(1+\frac{2}{\beta_w}\right) - \Gamma^2\left(1+\frac{1}{\beta_w}\right)\right] \tag{3.40}$$

$$\hat{\gamma}_1 = \frac{\Gamma\left(1+\frac{3}{\beta_w}\right) - 3\Gamma\left(1+\frac{1}{\beta_w}\right)\Gamma\left(1+\frac{2}{\beta_w}\right) + 2\Gamma^3\left(1+\frac{1}{\beta_w}\right)}{\left[\Gamma\left(1+\frac{2}{\beta_w}\right) - \Gamma^2\left(1+\frac{1}{\beta_w}\right)\right]^{3/2}} \tag{3.41}$$

m_ζ, $S_X{}^2$, and $\hat{\gamma}_1$ are respectively mean, variance and kurtosis of sea surface sample which is presented in section 3.1. $\Gamma(\ \ )$ is gamma function.

There is a limitation for this model since $H_s \geq \lambda_w$. The model is not good for small H_s where it is usually important for fatigue analysis. However, for extreme analysis, 3-parameter Weibull is adequate to use. Another distribution for $f_{\boldsymbol{H_s}}(H_s)$ is a hybrid model where $f_{\boldsymbol{H_s}}(H_s)$ is modelled as log-normal distribution below a particular value and as 2-parameter Weibull at the upper tail. This model gives no limitation for small H_s though it is more complicated than 3-parameter Weibull model.

$f_{\boldsymbol{Tp|H_s}}(T_p|H_s)$can be modelled by log-normal model. The log-normal probability density function and cumulative distribution function of T_p is presented from equation 3.42 to 3.43 [21].

$$f_{\boldsymbol{Tp|H_s}}(T_p|H_s) = \frac{1}{T_p\sqrt{2\pi}\,\sigma_{ln\,(T_p|H_s)}} exp\left(-\frac{1}{2}\left(\frac{ln(T_p) - \mu_{ln\,(T_p|H_s)}}{\sigma_{ln\,(T_p|H_s)}}\right)^2\right) \tag{3.42}$$

$$F_{\boldsymbol{Tp|H_s}}(T_p|H_s) = \Phi\left(\frac{ln(T_p) - \mu_{ln\,(T_p|H_s)}}{\sigma_{ln\,(T_p|H_s)}}\right) \tag{3.43}$$

$\Phi(\quad)$ indicates the Gauss (normal) cumulative distributution function. $\mu_{ln\,(T_p|H_s)}$and $\sigma_{ln\,(T_p|H_s)}$ are mean and standard deviation of $ln\,(T_p)$ for particular H_s. These parameter can be determined from mean ($\mu_{T_p|H_s}$) and standard deviation ($\sigma_{T_p|H_s}$) of spectral peak period for particular H_s value by equation (3.44) and (3.45) [26].

$$\mu_{ln\,(T_p|H_s)} = ln\left(\frac{{\mu_{T_p|H_s}}^2}{\sqrt{{\mu_{T_p|H_s}}^2 + {\sigma_{T_p|H_s}}^2}}\right) \tag{3.44}$$

$${\sigma_{ln\,(T_p|H_s)}}^2 = ln\left(\frac{{\mu_{T_p|H_s}}^2 + {\sigma_{T_p|H_s}}^2}{{\mu_{T_p|H_s}}^2}\right) \tag{3.45}$$

In addition, the largest wave crest with return period n_y year (n_y-year wave crest) corresponds to probability:

$$1 - F_{\boldsymbol{C_{3h}}}(c) = \frac{3}{n_y \times 365 \times 24} \tag{3.46}$$

This analysis also can be applied for wave height case.

3.3.2. Contour line method

In some cases, the short-term distribution function is hard to define. For example is when the relation of the structure response and water surface elevation is nonlinear. Finding a proper short-term distribution can be a time consuming process. To save time, the contour line method can be used.

In contour line method, the contours of environmental parameter (in this case H_s and T_p) for specific extreme fractiles are determined. These contours are independent of the structure behaviour. In this case, H_s and T_p are transformed to standard Gaussian variables, ($H_s \rightarrow U_1$ and $T_p \rightarrow U_2$) by Rosenblatt transformation [20]. The Rosenblatt transformation states that:

$$H_s = F_{\boldsymbol{H_s}}^{-1}\big(\Phi(U_1)\big); \quad T_p = F_{\boldsymbol{T_p|H_s}}^{-1}\big(\Phi(U_2)\big) \tag{3.47}$$

Where Φ is a Gauss (normal) cummulative distribution function. Then the contour line can be created by calculating U_1 and U_2 along a circle with radius $\beta_r = \sqrt{U_1^2 + U_2^2}$. For environmental contour line refers to n_y year return period, β_r can be determined by equation 3.48.

$$\beta_r = \Phi^{-1}\left(1 - \frac{3}{365 \times 24 \times n_y}\right) \tag{3.48}$$

The contour is representing the combination of H_s and T_p that gives the same probability of excedence. One can chose the most critical combination as an input to short-term extreme value distribution.

3.4. Design Wave Method

It is important to analyze the structure responses from the extreme wave condition with certain return period. By performing the longterm analysis, the extreme wave crest can be determined. Assigning this value to proper wave theory, the particle kinematics of the wave can be calculated. It is common to use 5th Stokes wave for suficiently deep water or dean stream for shallow water. From particle kinematics, the load from wave is determined and the structure responses are calculated.

The value that is assigned in wave theory, e.g. 5th Stokes, should be the wave crest and period. For ultimate limit state analysis, the worst wave crest in 100 year and its period should be

utilized. It will be shown in section 9.4 that assigning 100 year wave height (for example the 100-year wave height from Forristall distribution of wave height) to 5th Stokes wave gives smaller wave crest than 100-year wave crest (in this case the 100-year wave crest from Forristall distribution of wave crest). To determine the wave period (T), the 90% band (range of T_p when $F_{\boldsymbol{Tp|Hs}}(T_p|H_{s_{0.01}})$ in the range of 0.05 and 0.95) of T_p for 100-year H_s ($H_{s_{0.01}}$) should be calculated utilizing equation 3.43 then the range of T_p should be multiplied with 0.9. This means $T=0.9\ T_p$. Another way to determine wave period is by using *NORSOK* sugestion [33]. In this case, the range of wave period is determined from 100-year wave height. The relation is presented in equation 3.48.

$$\sqrt{6.5\ H_{0.01}} \leq T_{ULS} \leq \sqrt{11\ H_{0.01}} \tag{3.49}$$

Design wave method is only applicable to analyze the structure statically. By this consideration, it is assumed that the highest load occurs at the highest crest. Therefore, a quasistatic analysis is performed. Moreover, to assign the limited dynamic behaviour of the structure, equivalent dynamic amplification factor (EDAF) must be established. The equivalent dynamic amplification factor is found from the ratio between dynamic response and static response from extreme response distribution. In this case, the dynamic contribution on the structure response is considered as an equivalent acceleration field.

This method is not suitable enough for structure with large dynamic response. Moereover, for mass-dominated structure, the maximum load is not occured at largest crest which indicates this method is questionable to use for mass-dominated structure. In addition, the period of wave also affecting the response of structure and the most critical wave period is not always happen when the most extreme crest (or wave height) occurs. To deal with these issues, the time domain simulation can be utilized. Therefore, it is required to interpret the wave spectrum into a time-set of water surface elevation.

4. Simulation of Irregular Wave

For dynamically sensitive marine structures or marine structures subjected to large displacements, the extreme response is often determined on the basis of short term time-domain simulation. The sea state of short term analysis (H_s and T_p) can be determined by utilizing the contour line method. The time-domain simulation can be done by physical model simulation or numerical simulation. Both methods are performed by summing up a number of harmonic components with various frequency, amplitude and phase angle.

4.1. Wave Spectrum

The sea surface can be assumed as a Gaussian process. The Gaussian model is based on central limit theorem. The considered physical variable is expressed as a sum of variables [26]. This agrees with the formulation for first order water surface elevation in irregular sea condition which is expressed in equation 2.33 where the water surface elevation as function of time is established from sumation of a number of wave component with various amplitude, frequency and phase angle. The mean and standard deviation of one wave component (regular wave) at *x=0* for a period can be determined by:

$$\mu_\zeta = \frac{1}{T}\int_0^T \zeta_{a1}\, cos\,(\omega t)\, dt = 0 \tag{4.1}$$

$$\sigma_\zeta{}^2 = \frac{1}{T}\int_0^T \left(\zeta_{a1}\, cos(\omega t) - \mu_\zeta\right)^2 dt = \frac{\zeta_{a1}{}^2}{T}\int_0^T \left(\frac{1}{2} + \frac{1}{2} cos(2\omega t)\right) dt = \frac{\zeta_{a1}{}^2}{2} \tag{4.2}$$

Therefore, the variance of water surface elevation for irregular condition can be calculated as sumation of one wave component variance:

$$\sigma_\zeta{}^2 = \sum_{i=1}^{N} \sigma_{\zeta,i}{}^2 = \sum_{i=1}^{N} \frac{\zeta_{a1,i}{}^2}{2} \tag{4.3}$$

Instead expressed in time-domain, the water surface elevation can be expressed in frequency-domain by utilizing the Fourier transform. In this case, the sea surface is assumed as periodic process with certain duration (T_f) which also known as fundamental period. This means the

process will repeat after T_f. For numerical purposes, the transformation of sea surface from time domain ($\zeta(t)$) to frequency domain ($\bar{\zeta}(\omega_k)$) can be done by discrete Fourier transform:

$$\bar{\zeta}(m\Delta\omega) = \frac{\Delta t}{T_f}\sum_{n=1}^{N}\zeta(n\Delta t)\, exp(-i\, m\Delta\omega\, n\Delta t)\ ; \Delta\omega = \frac{2\pi}{T_f};\ m = 1,2,\dots,M\ ;\ i = \sqrt{-1} \qquad (4.4)$$

M is the number of frequency component and N is the number of time discrete points in sea surface record. From equation (4.4), it can be conluded that the magnitude of frequency interval is affected by fundamental period. Transfering back from frequency domain to time domain by discrete Fourier transform theoretically should follow equation 4.5 [10].

$$\zeta(n\Delta t) = \sum_{m=\frac{-T_f}{2\Delta t}}^{\frac{T_f}{2\Delta t}}\bar{\zeta}(m\,\Delta\omega)\, exp(i\, m\Delta\omega\, n\Delta t)\ \ ;\ \ i = \sqrt{-1} \qquad (4.5)$$

If equation (4.5) is applied with *m=1,2,3,...* $T_f/\Delta t$, the same result will be produced. This shows that if m is started from component $-T_f/2\Delta t$, $\bar{\zeta}(m\,\Delta\omega)$ only has physiscal definition until $m = T_f/2\Delta t$.

For instance, a Fourier transform is performed for sea surface on Draupner location (the record is taken around 1995 and known as Draupner Wave or New Year's Wave where the freak wave occured). The time series of the sea surface is plotted at figure 4.1.

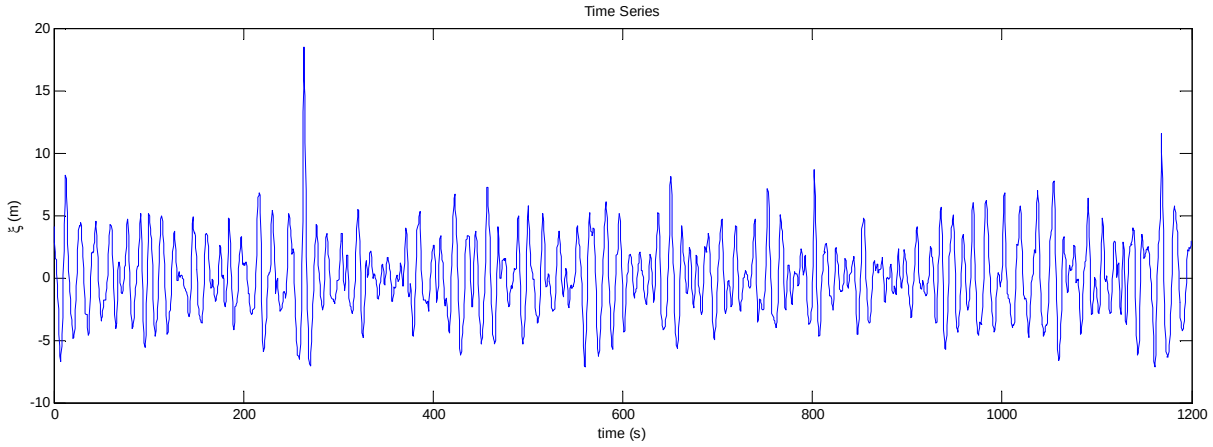

Figure 4.1 Draupner Wave Time Series

By utilizing equation 4.4, the result of discrete Fourier transform (DFT) is presented in figure 4.2. The range of frequency is set between $\Delta\omega$ and $\frac{T_f}{\Delta t}\Delta\omega$.

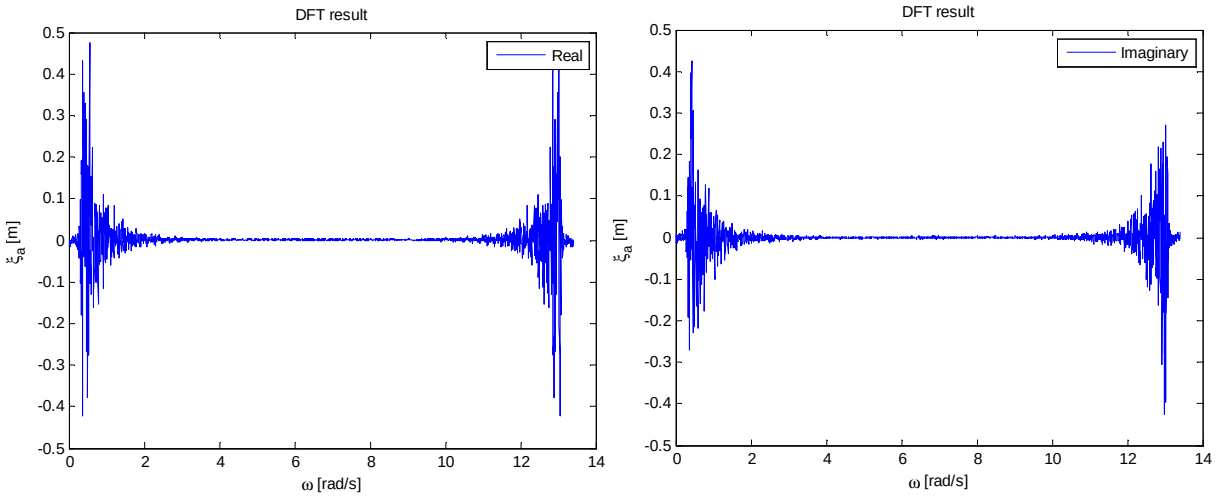

Figure 4.2 Result of Draupner Wave DFT
(Left: Real Part; Right: Imaginary Part)

Theoretically, as presented in equation (4.5), the range of frequency should be set between $\frac{-T_f}{2\Delta t}\Delta\omega$ and $\frac{T_f}{2\Delta t}\Delta\omega$. The result of this configuration is presented in figure 4.3.

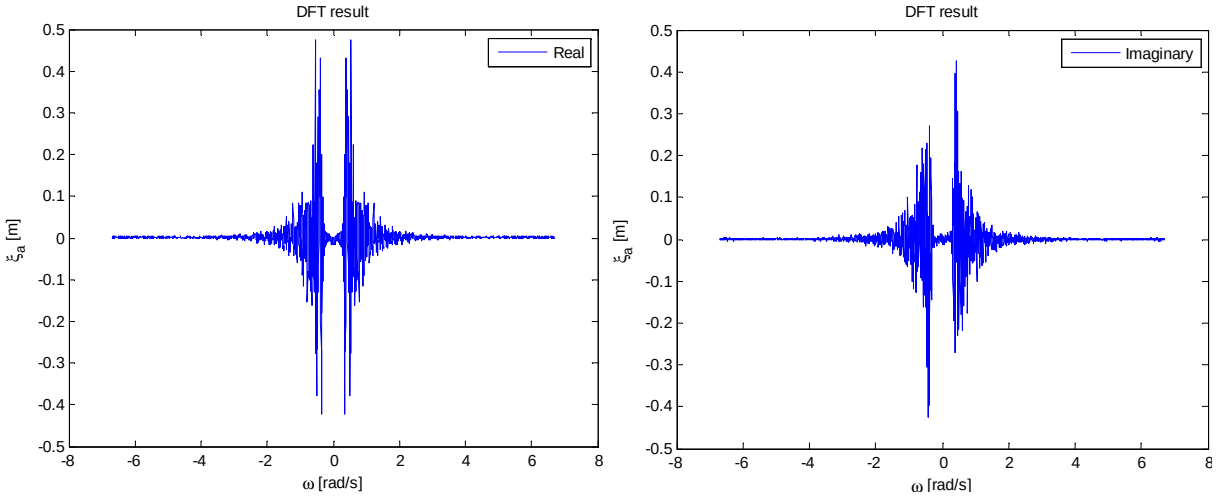

Figure 4.3 Result of Draupner Wave
DFT (Left: Real part; Left: Imaginary part)

The real part of discrete Fourier transformation result is an even function (behaves similar to cosine function) while the imaginary part is an odd function (behaves similar to the sine

function). Therefore, the information from frequency between $\Delta\omega$ and $\frac{T_f}{2\Delta t}\Delta\omega$ is adequate to represent the time series. The largest required frequency is knwon as nyquist frequency (ω_{nyq}).

$$\omega_{nyq} = \frac{T_f}{2\Delta t}\Delta\omega = \frac{T_f}{2\Delta t}\frac{2\pi}{T_f} = \frac{2\pi}{2\Delta t} = \frac{\pi}{\Delta t} \tag{4.6}$$

Since the sea surface is a random process, then it is more convenient to describes the sea surface with a power spectrum. The power spectrum is simply defined by the Fourier transformation of the correlation function of a random process [32]. For sea surface, it is more appropriate to calculate the power spectrum from Fourier transform of the autocorrelation function, as in context the components of the spectrum are the squares of the wave amplitude at each frequency. Since a sea surface can be assumed as a stationary process for certain duration, the autocorelation function of water surface elevation depends on time different ($R(\tau)$).

$$R(\tau) = E[\zeta(t)\ \ \zeta(t+\tau)] \tag{4.7}$$

$R(\tau)$ converges to zero for $t \rightarrow \infty$. The water surface elevation as function of frequency (ω) [10], [32]:

$$s_2(\omega) = \frac{1}{T_f}\int_0^{T_f} e^{-i\omega\tau}\, R(\tau)\, d\tau = |\bar{\zeta}(\omega)|^2 \tag{4.8}$$

$$R(\tau) = R(-\tau) = Re\left[\int_{-\omega_{nyq}}^{\omega_{nyq}} e^{i\omega\tau}\, s_2(\omega)\, d\omega\right]; \quad \tau \geq 0 \tag{4.9}$$

To create a continuous power spectrum, $|\bar{\zeta}(\omega)|^2$ should be divided with $\Delta\omega$ assuming that the energy in interval $\Delta\omega$ is represented by the power spectrum $s_2(\omega)$. The notation *2* for power spectrum in equations 4.8 and 4.9 indicates that the result of the autocorrelation function transformation is a two-sided spectrum. This can be observed by calculating the continuous power spectrum of Draupner time series for $-\omega_{nyq} \leq \omega \leq \omega_{nyq}$ which is presented in figure 4.4.

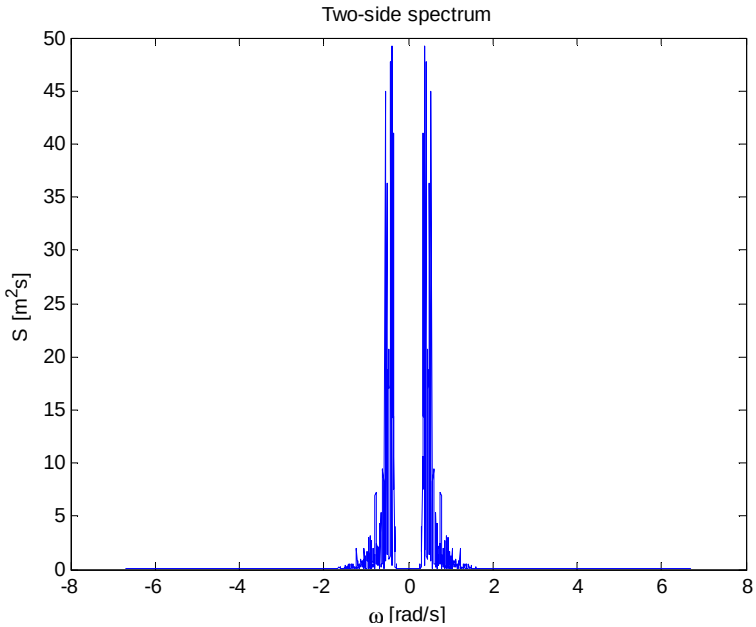

Figure 4.4 Two-sided Continuous Power Spetrum

However, one-sided spectrum is preferable to use since it does not include any negative frequencies which makes it more intuitive. The relation between one-sided and two-sided continous power spectrum is given by equation (4.10).

$$s_1(\omega) = 2s_2(\omega) = \frac{2|\bar{\zeta}(\omega)|^2}{\Delta\omega} = s(\omega) \tag{4.10}$$

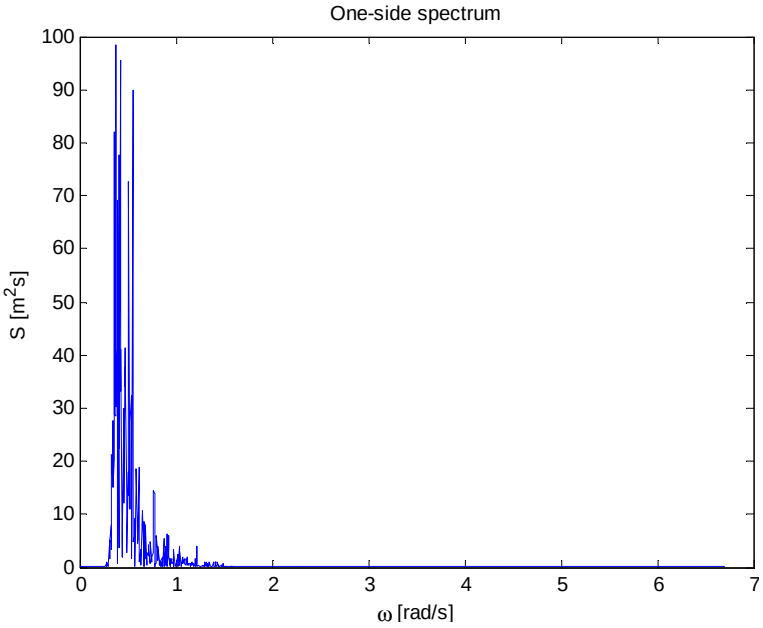

Figure 4.5 One-sided Continuous Power Spectrum

$s(\omega)$ is the wave spectrum. The one-sided continous power spectrum (wave spectrum) from Draupner time series is presented in figure 4.5. Since the calculation is only based on single measurement of sea surface, the shape of the wave spectrum in figure 4.5 is irregular. Methods to make the wave spectrum smoother are not discussed here but in general the methods are based on averaging a number of wave spectrum which refer to several sea surface mesurements.

From equation 4.7, it can be observed that ${\sigma_\zeta}^2 = R(0)$ when $\mu_\zeta = 0$. Therefore, combining equation 4.7 with equation 4.9 and utilizing the information from equation 4.10 gives:

$$ {\sigma_\zeta}^2 = R(0) = \int_0^\infty s(\omega)\, d\omega \tag{4.11} $$

If water surface elevation is expressed as sumation of *N* wave component, the combination of equation 4.3 and 4.11 with discretization for numerical puposes gives:

$$ {\sigma_\zeta}^2 = \sum_{i=1}^{N} \frac{{\zeta_{a1,i}}^2}{2} = \sum_{i=1}^{N} s(\omega_i)\Delta\omega \tag{4.12} $$

If each wave component is observed, it is found that:

$$ \zeta_{a1,i} = \sqrt{2\, s(\omega_i)\Delta\omega} \tag{4.13} $$

Furthermore, the connection between wave spectrum with wave total energy (potential + kinematic) can be determined. The wave energy per unit length for certain wave component ($E_{n,i}$) is defined by [19]:

$$ E_{n,i} = \frac{\rho g {\zeta_{a1,i}}^2}{2} \tag{4.14} $$

The total wave energy is calculated by summing wave energy from each wave component:

$$ \frac{E_n}{\rho g} = \sum_{i=1}^{N} \frac{{\zeta_{a1,i}}^2}{2} = \sum_{i=1}^{N} s(\omega_i)\Delta\omega \tag{4.15} $$

Since it is found that there is a general behaviour in various wave spectrums, then the standardisation is made. By utilizing siginificant wave (H_s) and spectral peak period (T_p), the

wave spectrum for certain location can be estimated. Some standardised wave spectrums are summarized here.

4.1.1. PM (Pierson-Moskowitz)

The *PM* spectrum is valid for fully developed sea and deep-water condition. The wave spectrum is steep for low frequency and has exponentially decay rate for high frequency. The basic form of *PM* spectrum [31]:

$$s(\omega) = \frac{A}{\omega^5} exp\left(\frac{-B}{\omega^4}\right) \tag{4.16}$$

A and *B* are determined by dimensional analysis utilizing H_s and T_p. The modified PM spectrum which is recommended by ISSC (International Ship and Offshore Structure Congress) which is also recomended by 15th ITTC (International Towing Tank Conference) [6], [14]:

$$s(\omega) = \frac{0.05{H_s}^2 T_p}{2\pi}\left(\frac{2\pi}{\omega\, T_p}\right)^5 exp\left[-\frac{5}{4}\left(\frac{2\pi}{\omega\, T_p}\right)^4\right] \tag{4.17}$$

4.1.2. JONSWAP (Joint North Sea Wave Project)

This spectrum based on measurement in North Sea. The result shows that the measured spectrum is more peaked than allowable peak of PM wave spectrum. Therefore, a modification is made for PM wave spectrum. In addition, this spectrum can be used for sea condition with limited fetch. The *B* term from PM spectrum is kept while the *A* term is modified and depend on specific consideration of the location [37]. The formulation of JONWAP spectrum [22]:

$$\begin{aligned} s(\omega) &= \frac{0.05{H_s}^2 T_p}{2\pi}(1 - 0.287\, ln(\gamma))\, \gamma^C \left(\frac{2\pi}{\omega\, T_p}\right)^5 exp\left[-\frac{5}{4}\left(\frac{2\pi}{\omega\, T_p}\right)^4\right] \\ C &= ex\, p\left(-0.5\left(\frac{\omega - \omega_p}{\sigma\omega_p}\right)^2\right) \quad ; \quad \omega_p = \frac{2\pi}{T_p} \end{aligned} \tag{4.18}$$

Where $\sigma = 0.07$ for $\omega \leq \omega_p$ and $\sigma = 0.09$ for $\omega > \omega_p$. γ is peaked parameter. Therefore, JONSWAP spectrum is determined by three parameters: significant wave height (H_s), spectral peak period (T_p) and peaked coefficient (γ). Haver and Torsethaugen (2004) proposed a formula to calculate γ [43]:

$$\gamma = 42.2\left(\frac{2\pi H_s}{g{T_p}^2}\right)^{6/7} \tag{4.19}$$

JONSWAP and PM spectrum are single peak spectrum and are usually used for wave that generated by local wind. In open seas, there will be effect of swell (waves generated from far away, outside the local location) and single peak spectrum is not fully accurate to define the sea condition. To describe the sea condition where affected by swell, Torsethaugen spectrum [43] which is a double peaks spectrum can be used. The JONSWAP and PM spectrum for H_s = 12 m and T_p = 14 second is described by figure 4.6

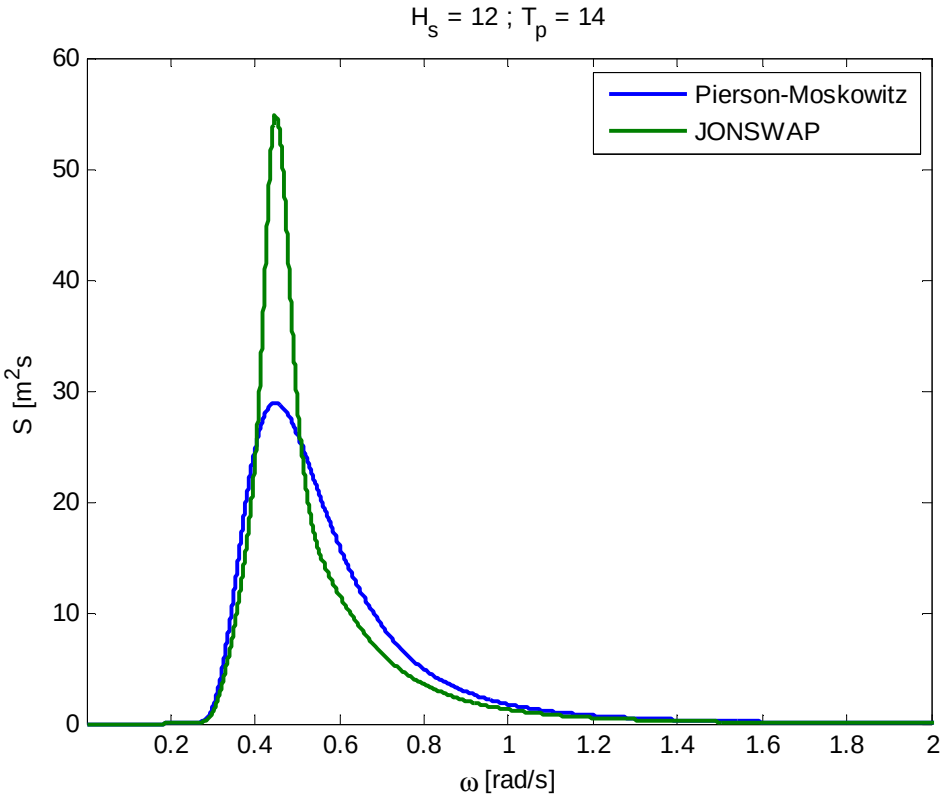

Figure 4.6 PM and JONSWAP Wave Spectrum
(*H_s=14m; T_p=12 s*)

n^{th} moment of wave spectrum can be determined by equation 4.20.

$$m_n = \int_0^\infty \omega^n \, s(\omega) \, d\omega \tag{4.20}$$

If the sea surface is assumed as Gaussian process, some parameter have relation [14].

- $H_s = 4\sqrt{m_0} = 4\sigma_\zeta$
- $T_1 = T_{m01} = 2\pi m_0/m_1$
- $T_2 = T_{m02} = 2\pi\sqrt{m_0/m_2}$; this is the mean zero-crossing period and useful to calculate total number of global maxima for observed time interval
- $T_{m24} = 2\pi\sqrt{m_2/m_4}$; this is the mean period between maxima and can be used to determined wheter the spectrum is narrow banded or broad banded spectrum by comparing T_{m24} wtih T_{m02}. If the different is significant, then the spectrum is considered as broad banded.
- For PM spectrum: $T_1 = 1.086T_2$ and $T_p = 1.408T_2$
- For JONSWAP spectrum: $T_1 = 0.834T_p = 1.073T_2$

4.2. Simulation of First Order Irregular Wave

The wave spectrum contains information about the energy from certain location. Therefore, single wave spectrum may produce different realizations of sea surface. For first order (linear) sea surface, the process is assumed as Gaussian proces and sea surface is expressed sumation of linear components (similar to equation 2.33).

$$\zeta\,(t) = \lim_{N\to\infty} \sum_{i}^{N} \zeta_{a1,i} cos\,(k_i x - \omega_i t + \varepsilon_i) \tag{4.21}$$

$\zeta_{a1,i}$ is first order amplitude which is determined from wave spectrum. The first order amplitude can be calculated from equation 4.13 while the relation between k_i and ω_i is expressed by dispersion relation in equation 2.20. The phase angle (ε_i) is determined by random number which is uniformly distributed between 0 and 2π. Different realizations of sea surface can be produced by changing the ε_i for each simulation.

When modeling the sea surface, a finite number of components (*N*) are used. As a consequence, the model is not perfectly Gaussian process and the repetition occurs. Nevetheless, the sea surface model still can be assumed as Gaussian process for certain duration where the repetition does still not occur. Theoretically, to achieve perfectly Gaussian proccess with no duration limitation, the lowest frequency in wave spectrum $\omega_{min} \to 0$ while the largest frequency

$\omega_{max} \rightarrow \infty$. For finite number of component, ω_{min} is set equal to frequency interval ($\Delta\omega$) and nyqusit frequency (ω_{nyq}) is taken as ω_{max}. In addition, some considerations should be made when determining ω_{max} since it affects the behaviour of velocity potential derivation. Some alternatives to calculate the harmonic component for linear component are presented in this section.

4.2.1. Inverse Fourier Transform (Equidistance Frequency Interval)

The popular way to interpret wave spectrum as harmonic components is by transforming back the spectrum into time series of sea surface using discrete inverse Fourier transform. In this method, the frequency span is set as constant (equidistance frequency interval). The number of wave component (*N*) to model the sea surface is affected by the nyquist frequency (ω_{nyq}) and the frquency interval ($\Delta\omega$).

$$N = \frac{\omega_{nyq}}{\Delta\omega} = \frac{T_f}{2\Delta t} \;\; ; \;\; \omega_{nyq} = \frac{2\pi}{2\Delta t} = \frac{\pi}{\Delta t} \;\; ; \;\; \Delta\omega = \frac{2\pi}{T_f} \tag{4.22}$$

As a consequence, the number of component is determined by the duration of simulation (T_f) and the time interval (Δt). For example, to perfrom complete 3-hour simulation of sea surface with time interval 0.5 seconds, at least 10,800 should be used. In this case, the sea surface profile repeats after 3-hour as explained in section 4.1. If less number of component is used, the sea surface repeats before 3-hour. Therefore, care should be made when determining the number of component and the range of frequency so the repetition does not occur within the considered sea state duration. Furthermore, there are some shcemes to determine the amplitude, frequency and phase of the harmonic component with equidistance frequency.

4.2.1.1. Deterministic amplitude scheme (random phase scheme)

In random phase shceme, the harmonic component is determined by:

$$\zeta_{a1,i} = \sqrt{2 \int_{\omega_{l,i}}^{\omega_{u.i}} s(\omega)\, d\omega} \tag{4.23}$$

$$\omega_i = \frac{\omega_{l,i} + \omega_{u,i}}{2} \tag{4.24}$$

$$\varepsilon_i = rand[0,2\pi] \tag{4.25}$$

Where $\omega_{l,i}$ and $\omega_{u.i}$ is the lower limit and upper limit of frequency component i. The largest harmonic amplitude will be located at components with frequency next to spectrum peak frequency (rich energy part of the spectrum). The illustration of inverse Fourier transform with random phase scheme for JONSWAP wave spectrum with H_s =12 m, T_p = 14 s, $T_f = 100s$ and $\Delta t = 1s$ is presented in figure 4.7.

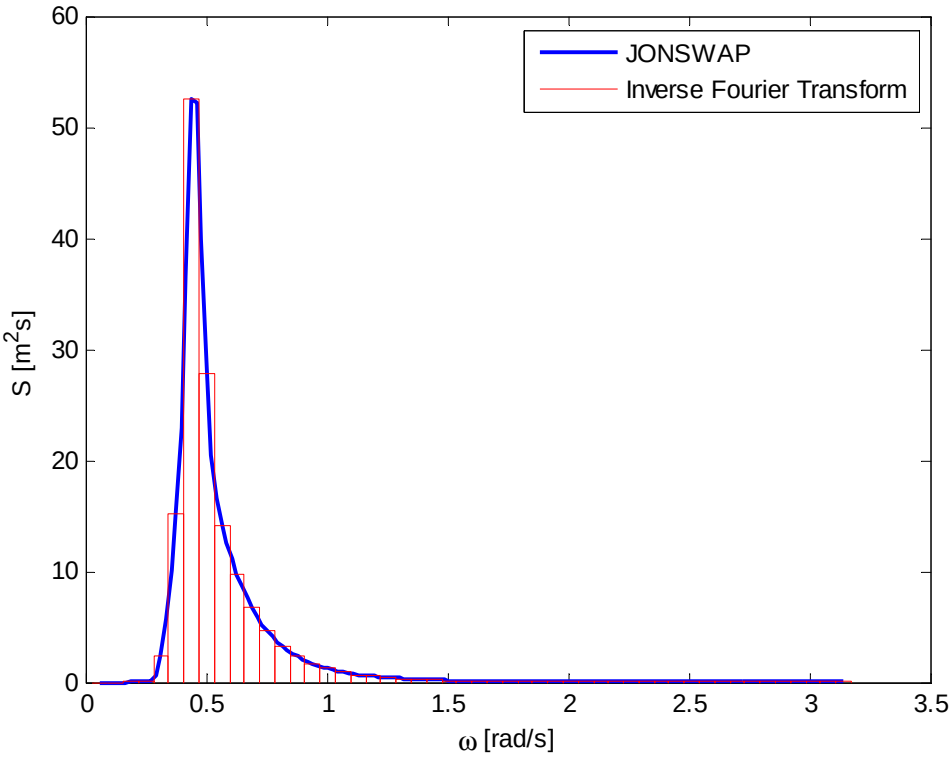

Figure 4.7 Inverse Fourier Transform with Deterministic Amplitude Scheme

4.2.1.2. Random amplitude scheme

The standardized wave spectrum is a result of averaging process (smoothing process) of multiple wave spectrums. As a result, it has a regular shape. However, the real shape of spectrum from measurement has an irregular shape as presented in figure 4.5. Furthermore, when a standardized spectrum is transformed into time series of sea surface by deterministic amplitude scheme and then the sea surface is transformed back again into a spectrum, the same shape of spectrum (the regular shape spectrum) is produced even if the procedures are repeated several times. This means deterministic amplitude scheme eradicates some randomness in the spectrum which causes the realization is not fully Gaussian process. In equation 4.13, the shape of wave spectrum

is determined by the amplitude of harmonic component. Therefore, the set of amplitudes must be modified to restore the lost randomness.

Tucker et al. [45] presented that to create a sea surface based on Gaussian process correctly, the amplitude of particular harmonic component should be determined randomly instead of using equation 4.23. It can be assumed that the wave amplitude follows Rayleigh distribution (equation 3.13) with root mean square value of component i : $\zeta_{rms,i} = \sqrt{2}\,\sigma_{\zeta,i} = \sqrt{2s(\omega_i)\Delta\omega}$. The phase ($\varepsilon_i$) is determined similar to deterministic amplitude scheme (equation 4.25). Figure 4.8 shows the initial JONSWAP spectrum and two possible spectrums from random amplitude scheme for H_s *=12 m*, T_p *= 14 s*, $T_f = 1200s$ and $\Delta t = 1s$.

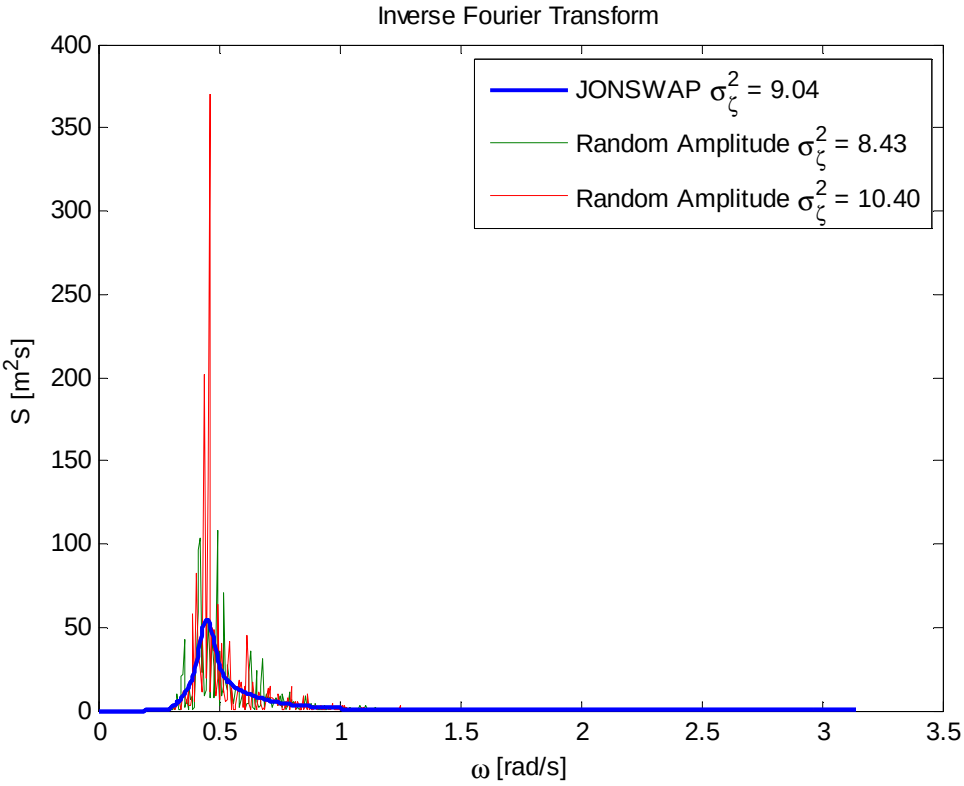

Figure 4.8 Inverse Fourier Transform with Random Amplitide

It can be observed that spectrum of random amplitude scheme amplitude has an irregular shape. However, there is a deviation in the variance of the spectrum. The first realization of random amplitude gives $\sigma_\zeta{}^2 = 10.26$ and the second realization produces $\sigma_\zeta{}^2 = 6.96$ while the actual variance is 9.04. The change in variance is random.

The standardized wave spectrum is an average of several single measured wave spectrum. Therefore, if random amplitude scheme is able to correctly represent this behaviour, the average of several realizations of wave spectrum from random amplitude scheme should converge to its standardized spectrum (the variance and shape). Figure 4.9 shows this behaviour the averaging of 500 wave spectrums with H_s *=12 m*, T_p *= 14 s*, $T_f = 1200s$ and $\Delta t = 1s$.

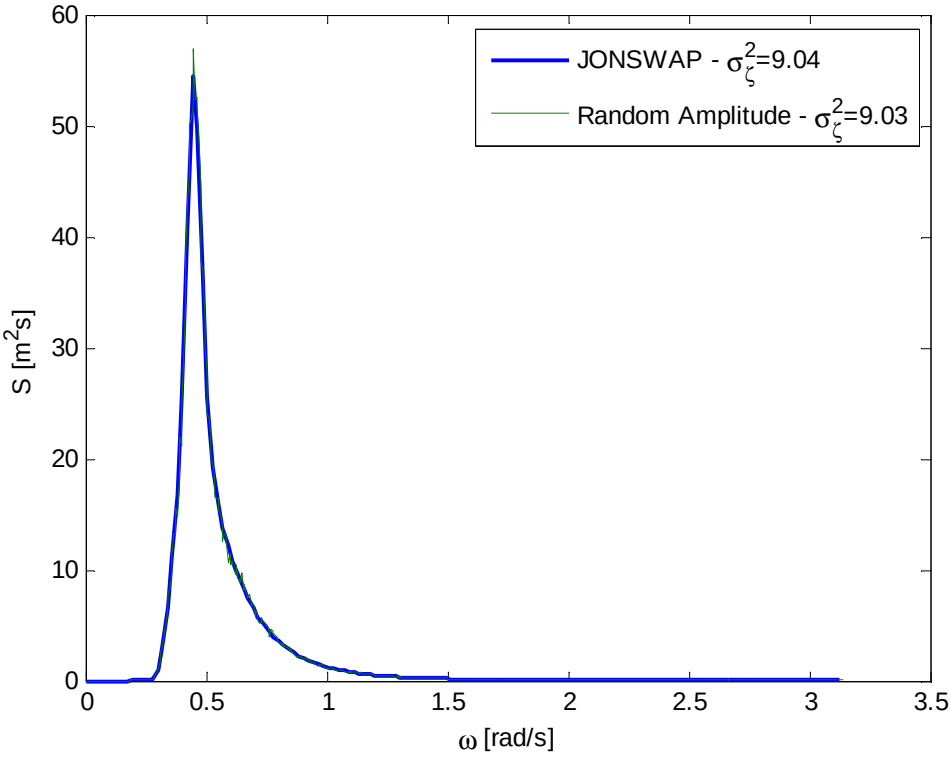

Figure 4.9 Averaging 500 Random Amplitude Wave Spectrum

It is stated before that there is lost of randomness from using deterministic amplitude scheme. Since in each realization the variance of a seastate is the same, the variance of variance is underestimated (this also indicates that the variance of extreme is underestimated since variance of extreme is connected to variance of sea surface). Since the variance $\sigma_\zeta{}^2 = m_0$; then variance of variance [44]:

$$\sigma_{m_0} = \frac{2\pi}{T_f}\int_0^\infty s^2(\omega)d\omega \tag{4.26}$$

Elgar [13] shows that this error can be neglected when the number of component N ≥ 1000. However, for slightly peaked wave spectrum (spectrum where the rich energy part located in

relatively small frequency interval), the random amplitude scheme is suggested. In addition, Bæekaedal [6] suggested using random amplitude scheme for low harmonic component since it is more conservative than deterministic amplitude (random phase scheme).

4.2.2. Alternatives to reduce number of component

For inverse Fourier transform metohd, at least 10,800 should be used to perfrom complete 3-hour simulation of sea surface with time interval 0.5 seconds without any repetition. There is no significant trouble to simulate first order sea surface and the wave particle kinematics regarding computational time and required memory for numerical process. However, to simulate second order wave, the computational time and required memory become prohibitive since the number of component increased to $10{,}800^2$. To tackle this problem, some methods to reduce number of harmonic component are required.

The main reason for a 3-hour simulation requieres a big number of components is to avoid repetition before the 3-hour simulation completes. The repetition is occured because every frequency components synchronizes to the lowest frequency. This means every component of frequency is a multiplication of an integer number (m) to the smallest frequency (which is equal to the frequency interval, $\Delta\omega$). Because of that, the repetition occurs after the wave component with the lowest frequency (the largest period) completes. Figure 4.10 shows this case exactly.

In figure 4.10, five wave component with different amplitudes (*1m, 2m, 3m, 4m* and *5m* respectively) and frequencies (*1 Hz, 0.8Hz, 0.6 Hz, 0.4 Hz, 0.2 Hz*) are combined. The phases are set equal to zero so the repetition is easy to observe (when the phases are included, the same repetition alsco occurs). The combination of five wave components is presented in last plot. Since the lowest frequency is *0.2 Hz* (period 5 second), the repetion occurs after 5 second since all frequencies are synchronized to *0.2 Hz*.

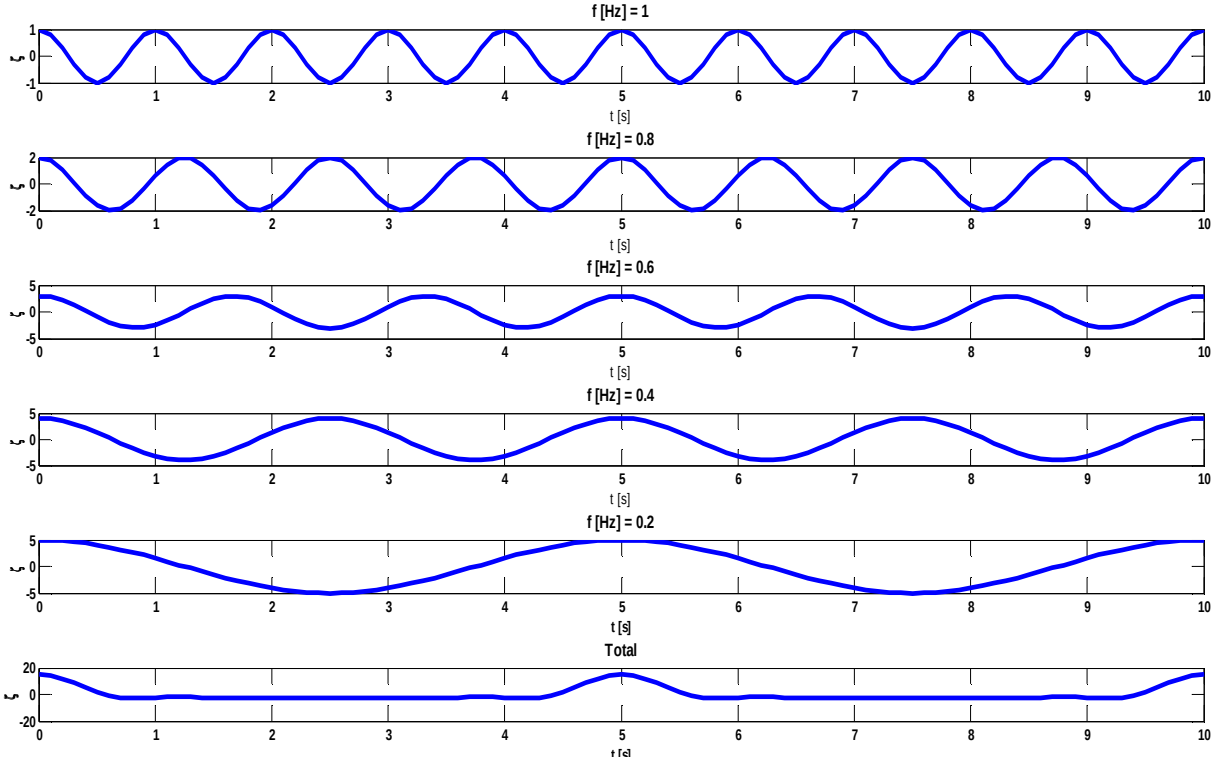

Figure 4.10 Combination of Harmonic Components

Therefore, to manipulate the repetition, the synchronization of wave frequency should be destroyed. Figure 4.11 shows an example where the repetition is manipulated.

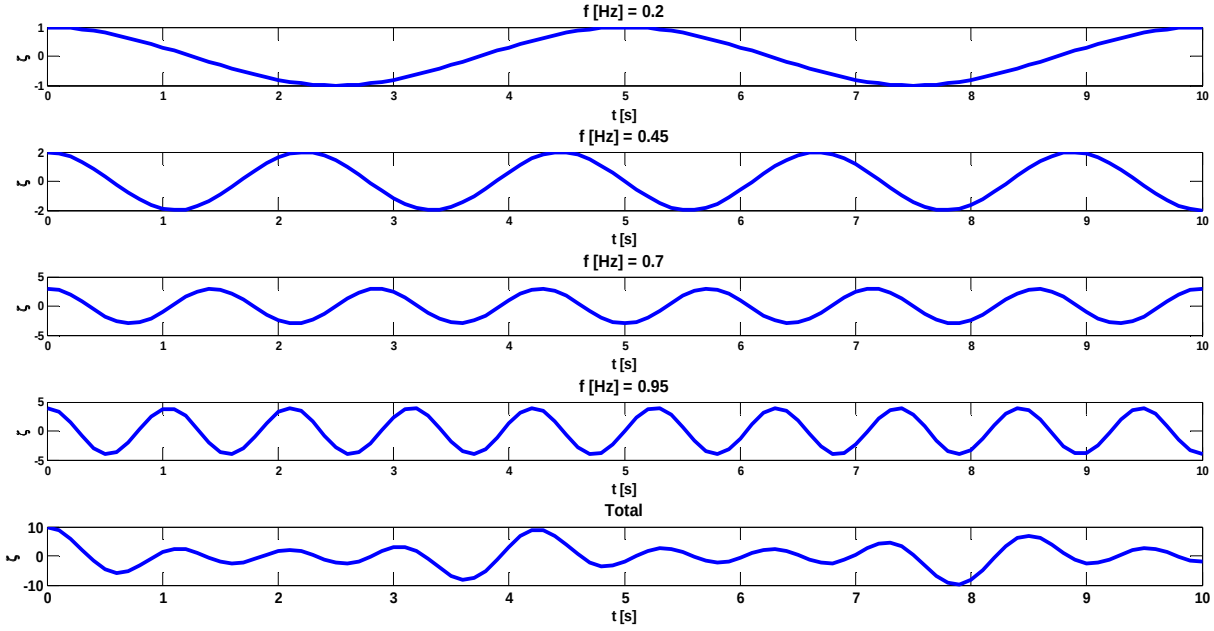

Figure 4.11 Combination of Harmonic Components

In figure 4.11, four wave components are combined with diferent frequencies (0.2 Hz, 0.45 Hz, 0.7 Hz, and 0.95 Hz). All component has the same phase. In this case, the lowest frequency (0.2 Hz) is not equal to frequency interval (0.25 Hz). Because of that, though the lowest wave frequency is 0.2 Hz (period 5 seconds), the repetition is not occurs after 5 second. In general, there are no exact repetition that occurs during 10 seconds. This is because the synchronization of frequency is destroyed. However, if it is observed furthermore, there is a repetition of shape after 4 seconds though the magnitude is not exactly repeated. This indicates that there is still frequency synchronization which caused by the equidistance frequency interval. Therefore, to completely destroy the synchronization, the frequency interval should be totally manipulated. When the frequency synchronization is destroyed, then 3-hour simulation requires less component than 10,800. There are several methods to achieve this.

4.2.2.1. Random frequency scheme

Faltinzen and Zhao [15] presented that if the frequency of wave component is randomly distributed between the component frequency limit, the problem of repeating sea surface realization can be avoided since the frequency is not expressed in preceeding value anymore. In this case, the frequency synchronization is destroyed. Therefore, by using this shceme, fewer components can be used for longer simulation time. Yet there is an issue when small magnitude of N is used.

Tucker et.al. [45] showed that using deterministic amplitude (random phase shceme), the variance of variance of sea surface is underestimated when N is set as 100. However, combining the random phase scheme and random phase amplitude increases the variance of sample since the randomness from amplitude and frequency part directly affect the sample variance. As a consequence, the extreme value of sea surface and its standard deviation can be smaller or higher than theoretical value.

4.2.2.2. Equal area method

The basic idea for equal area method is that the rich energy part of spectrum is the most important part of the spectrum to define an irregular seastate. Therefore, more components should be placed in this part. The wave frequency is set which gives the same energy for each component. As result, the frequency span ($\Delta\omega$) is no longer constant and the frequency

synchronization is broken. The wave frequncy can be taken as the middle value of frequency span in each block similar to equation 4.24. On the other hand, the amplitude is set as a constant value and determined by:

$$\zeta_{a1,i} = \sqrt{\frac{2\int_{\omega_{min}}^{\omega_{max}} s(\omega)\, d\omega}{N}} \tag{4.27}$$

Since the frequency component is no longer constant, repetition of sea surface history can be avoided. This implies that smaller number of harmonic components can be used than equidistance frequency. Figure 4.12 describes the discretization of wave spetrum by equal area method for 20 harmonic components with H_s =12 *m*, T_p = 14 *s*, $T_f = 1200s$ and $\Delta t = 1s$.

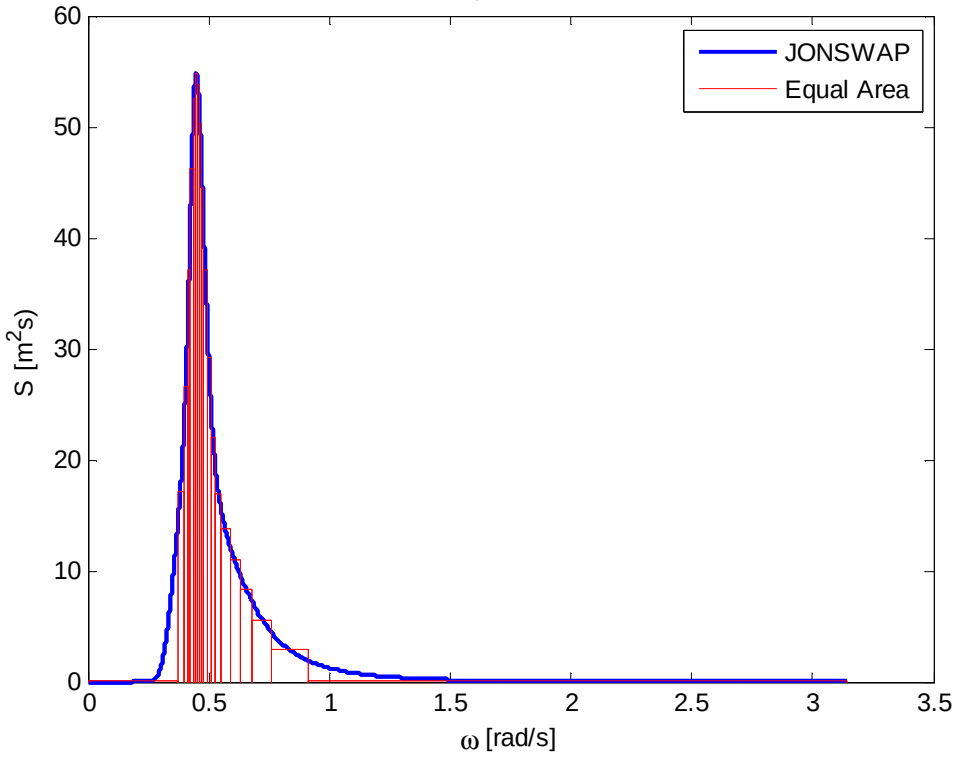

Figure 4.12 Equal Area Method

In general, the structure is designed with eigenfrequency far from the spectrum rich energy part. Therefore, there is a drawback from equal energy method. Biner [5] shows that using equal area method for structure with eigenfrequency far from rich energy part of the spectrum underpredicts the responses since it does not account properly the dynamic behaviour of the structure.

Using equal are method can decrease the number of of required component. Therefore, similar to random phase scheme, care should be made when small number of component is used. By combining equal area method and random amplitude scheme, there is a possibility that the variance of sea surface is changed which lead to changes in variance of extreme. Figure 4.13 shows the possible changes of sea surface variance from combination of equal area method and random amplitude scheme for JONSWAP wave spectrum with H_s =12 *m*, T_p = 14 *s*, $T_f = 1200s$ and $\Delta t = 1s$ utilizing 50 components.

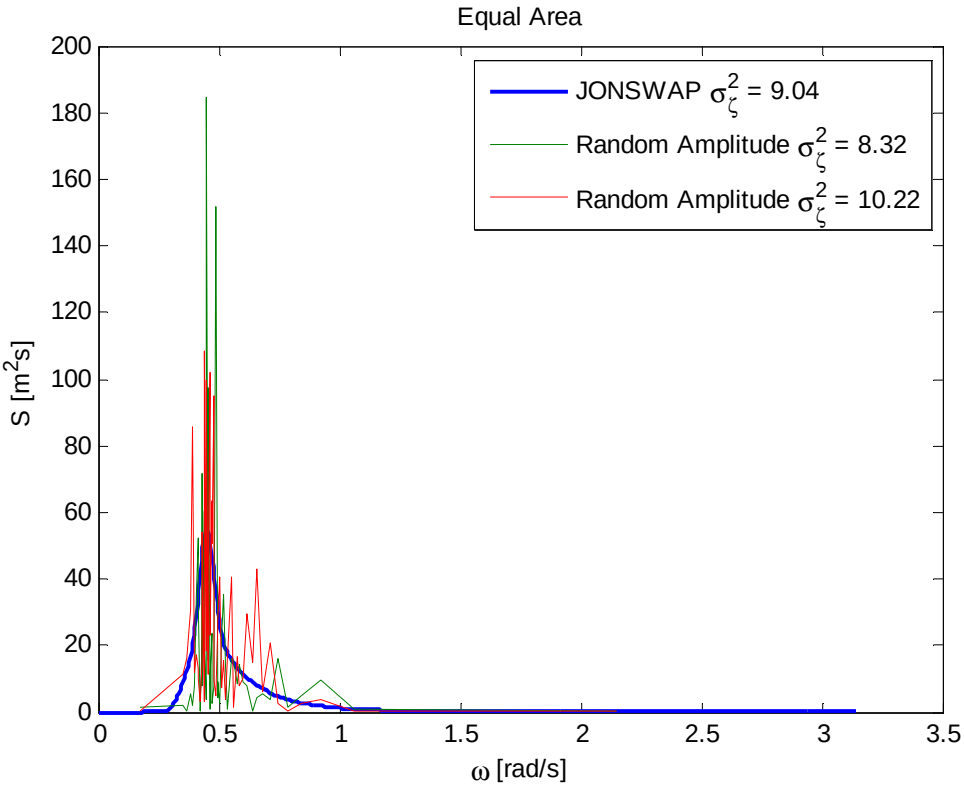

Figure 4.13 Equal Area Method + Random Amplitude Scheme

Therefore, it is also important to determine the optimal number of component to model the sea surface when using combination of equal area method and random amplitude scheme. The average of several spectrum realizations from combination of equal area method and random amplitude scheme converges to its standardized spectrum similar to the explanation in section 4.2.1.2.

In addition, Elgar et al.[13] stated that the adequacy of representing Gaussian condition depends on the effectiveness of placing component in rich energy part, not due to the number of harmonic component. Therefore, equal area method will be better in representing a Gaussian process than inverse Forier transform (equidistance frequency interval). This is also shown by Bæekaedal in his work [6].

4.2.2.3. Peaked equal area method

Since the natural frequency of the sturcture is usually located not in rich energy part of the spectrum, a modification should be made for equal area method. Binner [5] suggests that finer component mesh should be applied close to the natural freqeuncy of the structure. This modification can solve the problem regarding the lack on component around the natural frequency of structure causing more correct load and responses of the structure. This modification is called peaked equal area method.

The first step in this method is dividing components into two groups: N_{EA} (number of equal area method component) and N_{peak} (number of peaked component around natural frequency of the structure). The total harmonic component (N) is [6]:

$$N = N_{EA} + N_{peak} = N(1 - \rho_{EAP}) + N\rho_{EAP} \tag{4.28}$$

Where ρ_{EAP} is a parameter describing the density of component located neared the natural frequency of the structure. The process of peaked equal area method is [6]:

1. N_{EA} is determined by equal area method
2. The block that containing the eigenfrequency and its two-neigbouring block are removed. If the eigenfrequency located at the end of the spectrum, (either low frequency end or high frequency end) only one or none neobouring blocks are removed.
3. The frequency range that does not contain any components (due to the removal in point 2) is split into N_{peak} + *1,2,3,4* or *5* components. It is conditioned such as the frequency span for these components is decreasing towards natural frequency from both sides. One example of function than can be used [6]:

$$\Delta\omega_{\mathrm{i}} = (\omega_n - \omega_{low}) \frac{N_{low} - i + 1}{N_{low}\left(\frac{N_{low}+1}{2}\right)} \tag{4.29}$$

Equation 4.29 is acounted for frequency lower than natural frequency of the structure (ω_n) where ω_{low} is the low limit of freqeuncy range that contains no component and N_{low} is number of component lower than structure eigenfrequency. It can be shown that:

$$\sum_{i=1}^{N_{low}} \frac{N_{low} - i + 1}{N_{low}\left(\frac{N_{low}+1}{2}\right)} = 1 \tag{4.30}$$

For frequncy larger than natural frequency:

$$\Delta\omega_{\mathrm{i}} = \left(\omega_{high} - \omega_n\right) \frac{N_{high} - i + 1}{N_{high}\left(\frac{N_{high}+1}{2}\right)} \tag{4.31}$$

Where N_{high} are number of components larger than structure eigenfrequency and ω_{high} is the upper limit of freqeuncy range that contains no components. Value of N_{low} and N_{high} should be balanced depends on where the eqigenfrequency located. In addition, the sumation of $N_{low} + N_{high} = N_{peak}$.

4. The new frecuency (ω_i) is the middle frequency on each span. The amplitude can be determined either by deterministic amplitude (equation 4.23) or by random amplitude.

Figure 4.13 shows the dicretization using peaked equal area method for JONSWAP wave spectrum with H_s *=12 m,* T_p *= 14 s,* $T_f = 1200s$ and $\Delta t = 1s$. ρ_{EAP} is equal to 30%. For presentation purposes, the applied natural frequency (ω_n) is set as 0.7 rad/s though the magnitude of ω_n is usually larger than 0.7 rad/s for Jack-up platform and located in greatly coarse component mesh.

When peaked equal area method is combining with random amplitude scheme, there is significant change in variance (same problem as equal area method). Moreover, since less component located in rich energy part of spectrum, peaked equal area method is less accurate to model Gaussian sea surface than equal area method for the same value of *N*. However Bækaedal [6] reported that when the eigenfrequency of structure lays on the rich energy part of the wave spectrum, peaked equal area method is better in simulating sea surface for low number of component than the non-peaked equal area method.

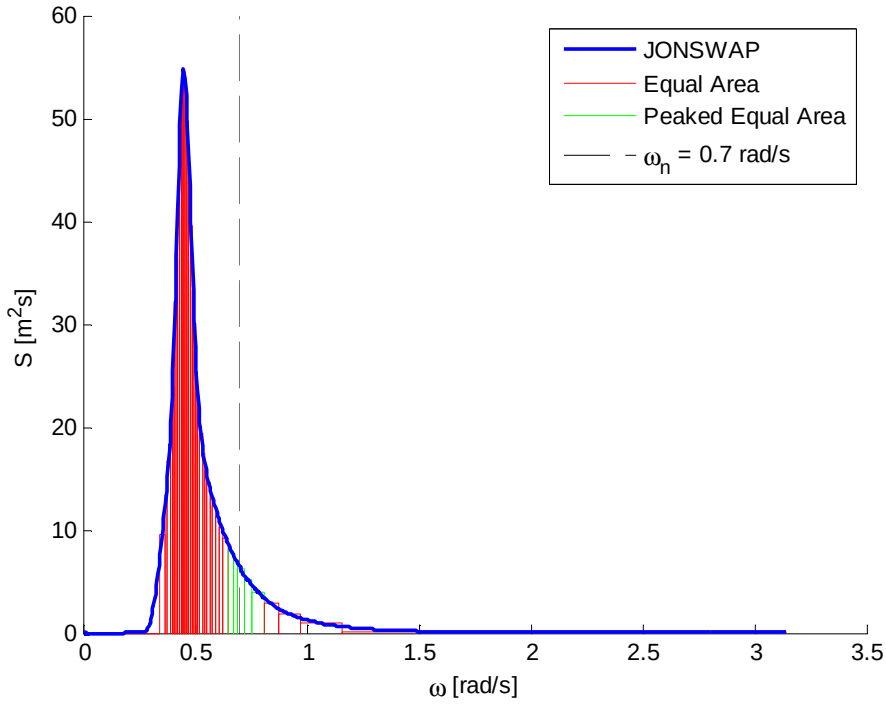

Figure 4.14 Peaked Equal Area Method

4.2.2.4. Partition of time series

Another way to avoid repetition in simulation of irregular wave is by splitting the time series into shorter duration. For example, the 3-hour sea surface simulation is splitted into nine 20-minute simulations. The amplitude for 20-minute simulation can be determined by deterministic or random amplitude scheme while the frequency is established using equidistance frequency interval. However, for each 20-minute simulation, a new set of phase (ε_i) is introduced. As a result, nine different sea surface realizations are generated and combining these different realizations produces 3-hour simulation.

The idea behind this alternative is that larger frequency interval is acquired by decreasing the duration of simulation (T_f). As a consequence, with same nyquist frequency, the number of components decrease significantly. For equidistance frequency interval method either with deterministic or random amplitude scheme, a 3-hour simulation with time interval 0.5 second requires at least 10,800 components while a 20-minute simulation only needs 1,200 components. Therefore, utilizing 20-minutes simulation to represent 3-hour simulation gives a big advantage. However, there are no limitation how small the 3-hour simulation may be split. Due to number of

component which is still considered suifficient, 20-minute simulation is assumed adequate to simulate 3-hour simulations in this study.

This method does not require to destroy the frequency synchronization when using inverse Fourier transform. In addition, this method does not create continous time series of surface elevation. However, the probabilistic model only requires extreme or largest extreme value of time series. Because of that, this method is considered a good option for genrating probabilistic model.

4.3. Simulation of Second Order Irregular Wave

In order to simulate the second order irregular wave, the first order irregular wave must be simulated first. The energy information from wave sepctrum is converted to a set of regular wave components by several methods and scheme that are explained in the previous section. Then the surface elevation can be obtained by superposistion principle. However, to account the second order component, the correction terms which are expressed by equation 2.57 should be calculated and added to the first order sea surface. In this case, the number of harmonic component is significantly increased from N to N^2.

The same case is applied for calculating the kinematics of second order irregular wave. The wave kinematics from first order irregular wave is calculated then the second order correction term, which is gained by deriving the velocity potential expressed in equation 2.56, is added to the first order irregular wave kinematics. The wave particle kinematics are calculated in a grid system which means it is calculated point to point. Hence, the computational time is increased significantly. This condition makes the second order irregular wave simulation becomes unattractive.

A wave spectrum contains energy not only from fist order wave but also second and bigger order wave. However, the first order irregular wave components are determined by utilizing total energy from wave spectrum. Adding second order correction term means adding more variance to sea surface time series which means introducing the second order term correction violates the amount of energy in the wave spectrum. Therefore, when a second order wave is wanted to be introduced, a wave spectrum should be linearized first before calculating first order wave. Some approaches to linearized the spectrum are summarized here.

4.3.1. Iteration to linearize spectrum

In this method, every block in wave spectrum is checked. An iteration process is performed to find the right linear amplitude (ζ_{a1}) that will give right magnitude of the wave spectrum in each block when the second order correction is introduced. Since the number of component could be large, the iteration process could be time consuming. Moreover, the iteration is complicated because one block in wave spectrum is affected by another block through second order correction (through sum and difference term).

4.3.2. Cut-off frequency

Another way to maintain the energy in the wave spectrum when the second order correction is applied is by introducing a cut-off frequency (ω_{cut}). This method was presented by Stansberg [39]. The components with frequency higher than ω_{cut} are assumed as bound waves. Therefore, the energy associate to second-order correction is considered come from the part of the wave spectrum with frequency higher than ω_{cut}. As a consequence, the first order sea surface is determined only from part of the wave spectrum with $\Delta\omega \leq \omega \leq \omega_{cut}$. Figure 4.15 shows a cut-off frequency for JONSWAP spectrum with with H_s =12 m, T_p = 14 s, $T_f = 1200s$ and $\Delta t = 1s$.

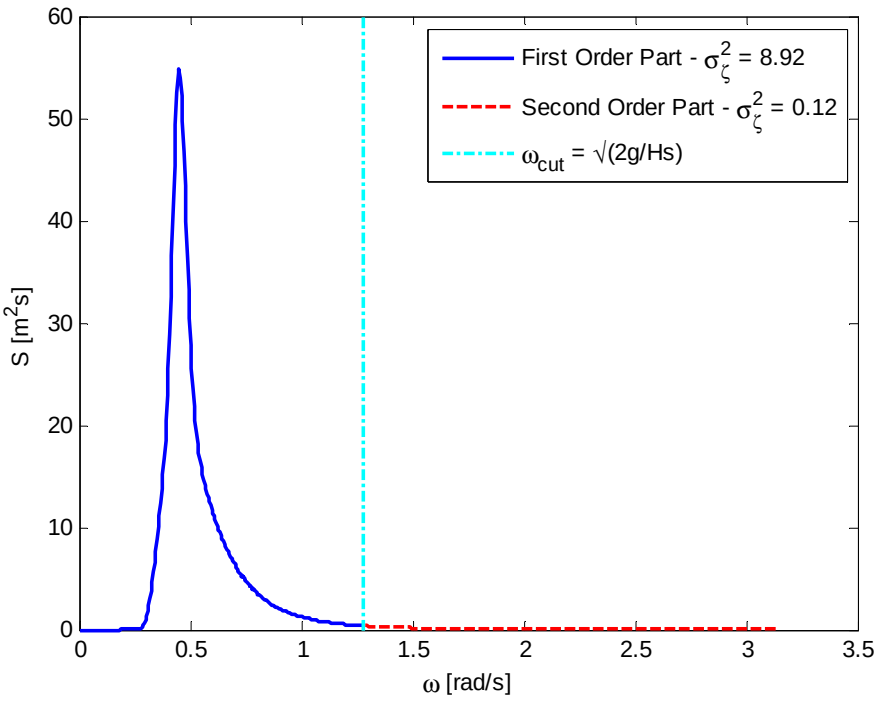

Figure 4.15 Cut-Off Frequency

This method is relatively simple since the iteration process is not required. Futhermore, this method can decrease the required number of component for sea surface simlation. As an example, 3-hour simulation needs 10,800 components for $\Delta t = 0.5s$. By introducing $\omega_{max} = \omega_{cut}$, the required component reduced 2198 for H_s *=12 m*. Therefore, combining the cut-off with the methods to reduce number of component will make the second-order wave simulation becomes feasible.

4.4. Directional Spectrum

To represent a 3-dimensional sea surface (short crest wave), a directional spectrum is introduced. The directional spectrum ($s(\omega, \theta)$) is a multiplication of wave spectrum ($s(\omega)$ as introduced in section 4.1) and a spreading function ($D(\theta)$).

$$s(\omega, \theta) = s(\omega)D(\theta) \tag{4.32}$$

In general, the spreading function is not necessary independent of frequency. In the other word, the form of spreading function could be $D(\theta, \omega)$. However, for simplicity, it is assumed that the spreading function is independent of frequency. To maintain the energy in the spectrum, $D(\theta)$ should satisfy:

$$s(\omega) = \int_0^{2\pi} s(\omega, \theta)\, d\theta = \int_0^{2\pi} s(\omega)D(\theta)\, d\theta \rightarrow \int_0^{2\pi} D(\theta)\, d\theta = 1 \tag{4.33}$$

There are various spreading functions that are proposed [8].The common spreading function which is used [31]:

$$D(\theta) = \begin{cases} K_v \cos^v(\theta), & -\frac{\pi}{2} \leq \theta \leq \frac{\pi}{2} \\ 0, & else \end{cases} \tag{4.34}$$

v is an integer number. $\theta = 0$ is the main propagation direction of the wave. K_v is the normalized coefficient that insurance the satisfaction of equation 4.33. Therefore, K_v can be determined by equation 4.35. Figure 4.16 shows the shape of $D(\theta)$ for various *v*.

$$K_v = \frac{1}{\int_0^{2\pi} \cos^v(\theta)\ d\theta} = \frac{2^{v-1}}{\pi} \frac{\Gamma\left(\frac{v}{2}\right)\Gamma\left(\frac{v}{2}+1\right)}{\Gamma(v)} \tag{4.35}$$

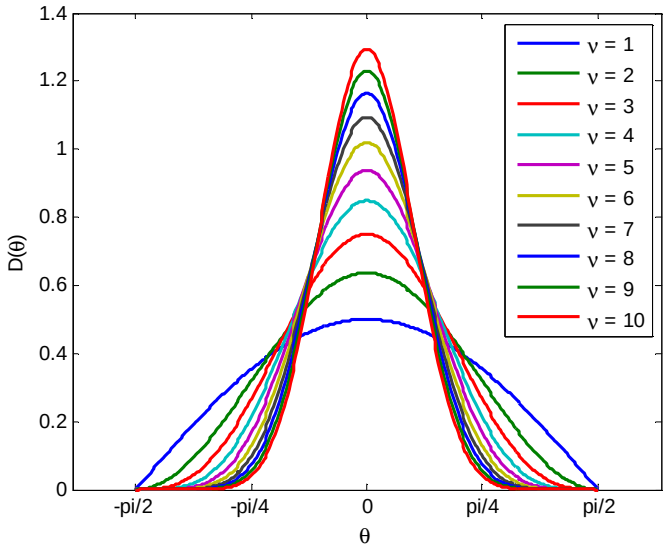

Figure 4.16 Spreading Function

From the directional spectrum, the first order amplitude for component *ij* is determined by:

$$\zeta_{a1,ij} = \sqrt{2\, s(\omega_i, \theta_i)\Delta\omega\Delta\theta} = \sqrt{2\, s(\omega_i) D\left(\theta_j\right)\, \Delta\omega\Delta\theta} \tag{4.36}$$

Then, the first order sea surface can be determined by:

$$\zeta(x, y, t) = \sum_{i}^{N}\sum_{j}^{M} \zeta_{a1,ij}\, cos\left(k_i\left(x\, cos\left(\theta_j\right) + y\, sin\left(\theta_j\right)\right) - \omega_i t + \varepsilon_{ij}\right) \tag{4.37}$$

The particle kinematics can be calculated from equation 2.38 until 2.43 by separating the frequency (*i*) and direction component (*j*) as done in equation 4.37. The number of harmonic component becomes $N\, x\, M$. Hence, applying the spreading function into wave spectrum significantly increases the number of required component for simulation of first order sea surface and wave particle kinematic. Furthermore, the second order wave simulation became greatly prohibitive. Therefore, an alternative method should be used to represent the spreading function.

Another way to express a 3-dimentional wave is by assigning only one direction to each frequency component. In this way, the required component is still equal to *N*. The direction of each frequency component is randomly determined. It is assumed that the direction of each component (θ_i) follows Gauss (normal) distribution. Therefore, θ_i can be determined by:

$$\theta_i = \Phi^{-1}\left(\frac{I}{\sigma_\theta}\right) \tag{4.38}$$

σ_θ is the standard deviation of the direction in radian. $\theta = 0$ is the main direction of wave propagation. Long-crest wave is achieved when σ_θ is set as small number. I is a random number which is uniformly distributed between zero and one. Φ is the standard Gauss cumulative distribution. Because of that, this method is called random direction. Figure 4.17 shows the probability density function of θ as a Gauss distribution with various σ_θ. To simplify, σ_θ is presented in degree though in calculation σ_θ is conversed to radian.

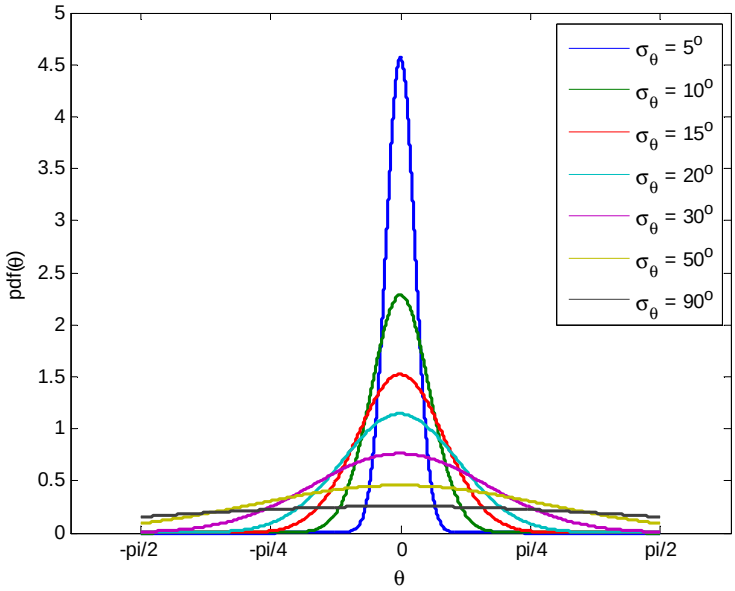

Figure 4.17 Probability Density Function of Wave Direction

The magnitude of probability density function could be larger than one as long the area under the curve is equal to one. When random direction is used with $\sigma_\theta \geq \pi/5$, there is a possibility that θ is larger than $\pi/2$. This contradicts the condition of spreading function which is described in figure 4.16. Therefore, the wave could propagates in the opposite direction since there is a possibility that adequate number of components have direction larger than $\pi/2$. To avoid this issue, it is suggested to use $\sigma_\theta < \pi/5$.

For random direction, the first order sea surface is determined by modifying equation 4.37. In this case, to maintain the energy in the spectrum and to satisfy the condition in equation in 4.33, $D(\theta_j)\Delta\theta$ is not applied to the formula since each frequency component only has one direction.

$$\zeta(x,y,t) = \sum_i^N \underbrace{\sqrt{2\, s(\omega_i)\, \Delta\omega}}_{\zeta_{a1,i}} \cos\left(k_i\left(x\cos(\theta_i) + y\sin(\theta_i)\right) - \omega_i t + \varepsilon_i\right) \qquad (4.39)$$

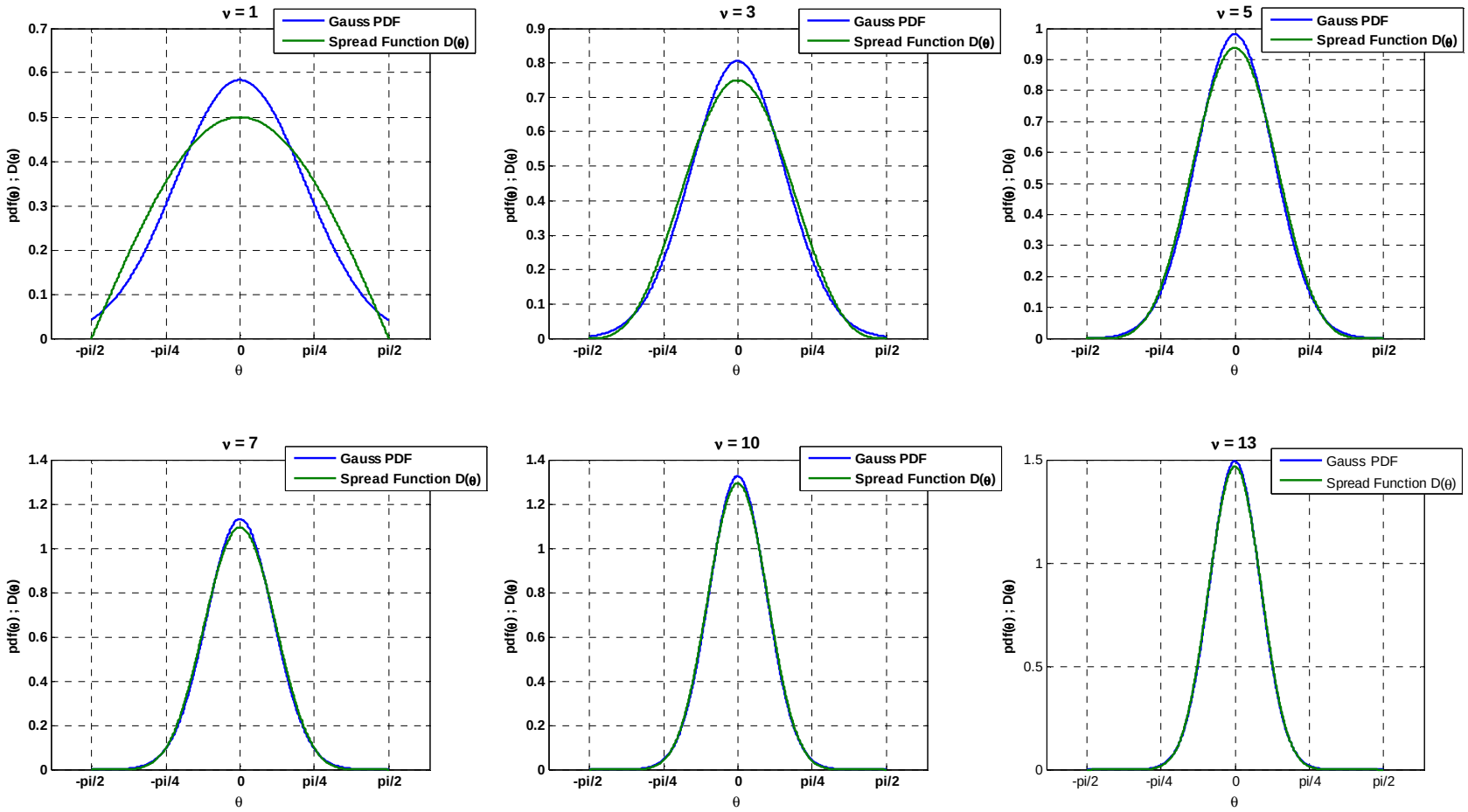

Figure 4.18 Comparisson of Spread Function and Random Direction PDF

The connection between random direction and common spreading function $D(\theta)$ is expressed by the relation of σ_θ and $D(\theta)$:

$$\sigma_\theta = \sqrt{\frac{\sum_j^M \theta_j{}^2 D(\theta_j)}{\sum_j^M D(\theta_j)}} \tag{4.40}$$

Figure 4.18 shows the comparisson of $D(\theta)$ and probability density function of θ for various v. To calculate the second order directional term for sea surface, equation 2.57 can be used with aplying the wave number as a vector. This is briefly explained in section 2.4.2.

4.5. Strategy to Decrease Computational Time in Extetnt

To calculate the load and responses on the structure, the wave particle kinematics could be calculated first on grid system then apply to the structure. This is feasible for small volume structure such as Jack-Up or Jacket platform where the particle kinematics is assumed undistrurbed. Eventhough the number of required components have been reduced, to calculate wave perticle kinematics in grid system still could be very time consuming. Therefore some strategies to reduce the computational time are considered. In this section, some strategies to reduce the computational time of wave particle kinematics are introduced.

4.5.1. Calculating wave kinematics at coarser grid

The wave particle kinematics is first calculated at coarser grid. To find the load at the structure, the wave particle kinematics at structure coordinate are interpolated from adjacent grid coordinates. Therefore, a sensitivity analysis to determine how coarse a grid system that still produces acceptable result is required.

4.5.2. Second order wave at upper layer

Since the wave kineamtics decay exponentially with vertical coordinate both for first order wave and second order wave, then it can be assumed that the difference between second order and first order wave kinematics is negligible at particular location which is close to seabed. Therefore, to decrease the computational time, the second order wave kinematics are only applied close to sea surface (upper layer) while the first order wave kinematics are established at the rest of the depth (lower layer). By this strategy, number of calculation point for second order wave kinematics can be decreased significantly. Therefore, much faster computational time is gained.

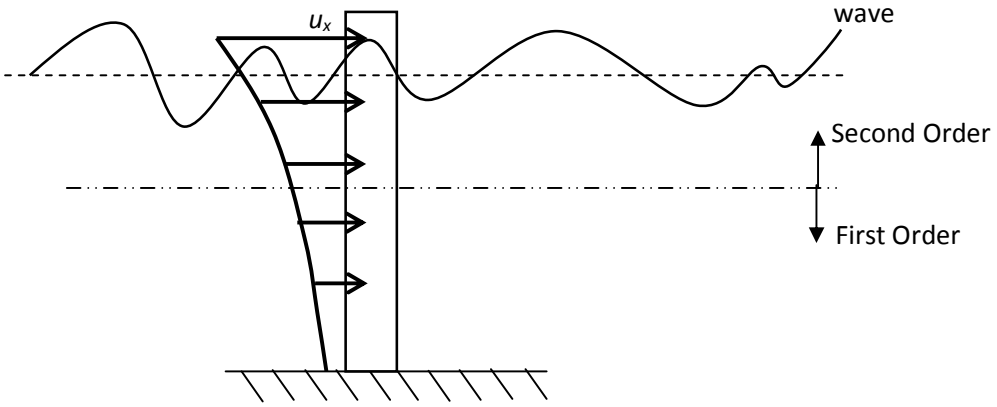

Figure 4.19 Illustration Second Order at Upper Layer Method

This second order at upper layer is illustrated by figure 4.6 for horizontal velocity case. This strategy is useful either for static and dynamic analysis of structure response. From previous project by Lubis [27], it shows that this method could save the computational time significantly for single vertical cylinder case.

4.5.3. Spool-to-extreme wave method

For ultimate limit state analysis, the main interest is the extreme response. In general, the extreme response occurs at extreme load condition. For drag dominated load, which is greatly affected by the wave particle velocity, the extreme load is assumed occurs at the extreme water surface elevation within certain duration. Since the computational time for simulating second order sea surface is relatively faster than for second order wave kinematics, then it is possible to locate when the extreme surface elevation happens. Henceforth, the wave particle kinematics, load and responses are determined only around the extreme surface elevation. For dynamic analysis, the response at certain time instant relies on response at previous time instant (this is presented in section 5.3.2). Thefore, there is no need to calculate wave kinematics from the start of sea surface simulation until the extreme of water surface elevation occurs. The wave particle kinematics then are calculated at a certain time interval before the extreme surface elevation occurs to accomodate the transient effect of the structure. This method is called spool-to-extreme wave and useful for dynamic analysis of structure response. Figure 4.20 illustrates this method.

The first plot in figure 4.20 describes the complete second order sea surface while the second plot shows the sea surface for spool-to-extreme method. There is no specific condition about how long the time interval should be considered before the peak since the transient effect of a

certain structure could be various in irregular sea. In addition, for some cases the maximum response could happen not at the extreme of water surface elevation (for instance for mass dominated structure).

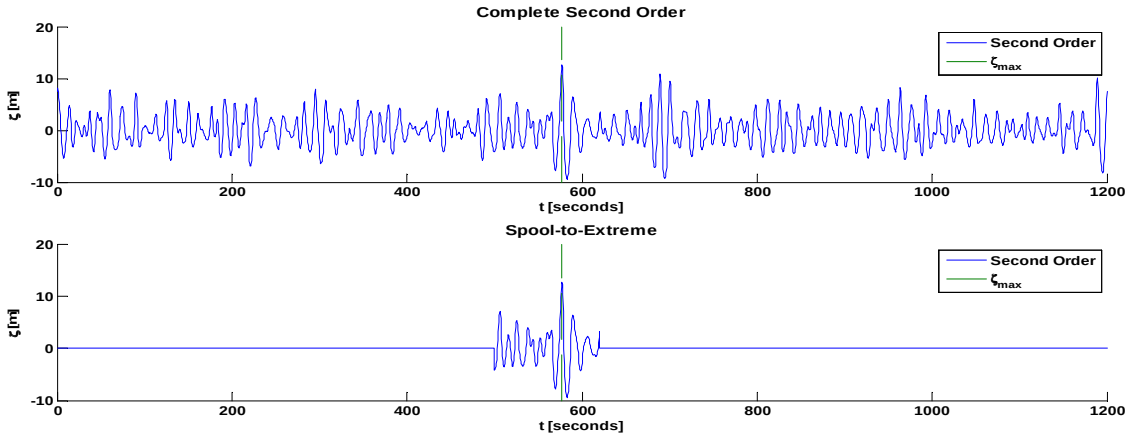

Figure 4.20 Illustration of Spool-to-Extreme Method

4.5.4. Linear theory before maximum (linear-to-extreme)

A further modification is made for spool-to-extreme method. Since the computational time of first order wave kinematics is relatively faster than the second order wave kinematics then on dynamic analysis of structure responses, the load before the extreme surface elevation is calculated from first order wave kinematics to account the structure transient responses. The second order wave is start to apply for a short interval time before the extreme surface elevation. By applying this scheme, it is expected that the duration of calculation can be decreased in extent. This method also does not have specific requirement for how long the load can be applied before the extreme surface elevation. Figure 4.21 illustrates this method.

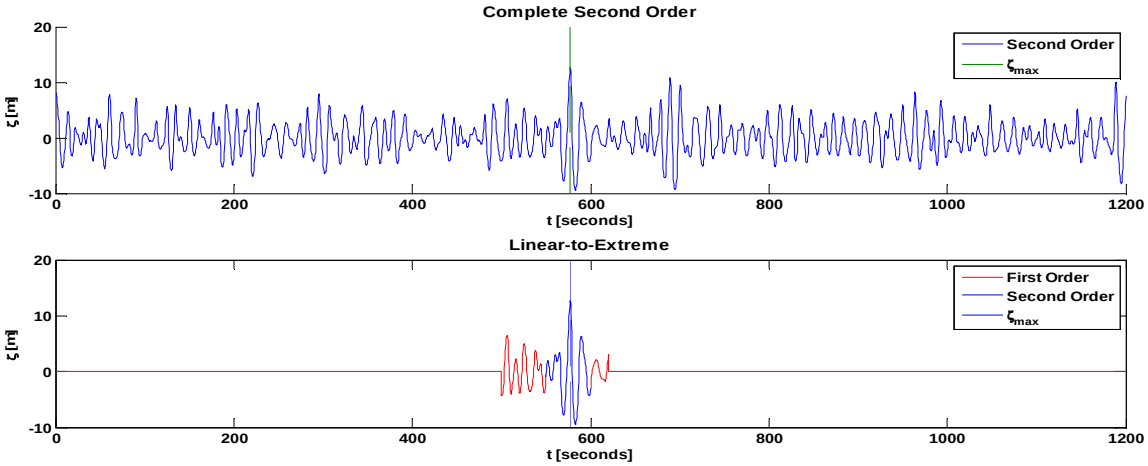

Figure 4.21 Illustration of Linear-to-Extreme Method

5. Structure Model, Loads and Response

In the previous project by Lubis [27], the second order wave is tested on a single vertical cylinder. In this work, the analysis is extended and the second order wave is applied into a jack-up platform. Jack-up is choosen since the jack-up is still categorized as small volume structure and have considerable dynamic behaviour. Then, in this section, the description about the jack-up and the method to calculate the load and responses are presented.

5.1. Structure Model

The jack-up model which is used in this work is CJ62. The model was designed by engineering company GustoMSC and classified by DNV GL. CJ62 is a three legs, cantilever type drilling jack-up patform which is deisgned to operate in moderate to harsh environment. The jack-up is designed to operate with water depth up to 130 meters. The radius of the leg approximately is 35.8 meters with distance between leg center equal to 62 meters. The legs are triangular with x-braces, open truss system. The finite element model is built in USFOS. In the finite element model, the legs are modelled with detail finite element. Figure 5.1 shows the finite element model of CJ62 jack-up.

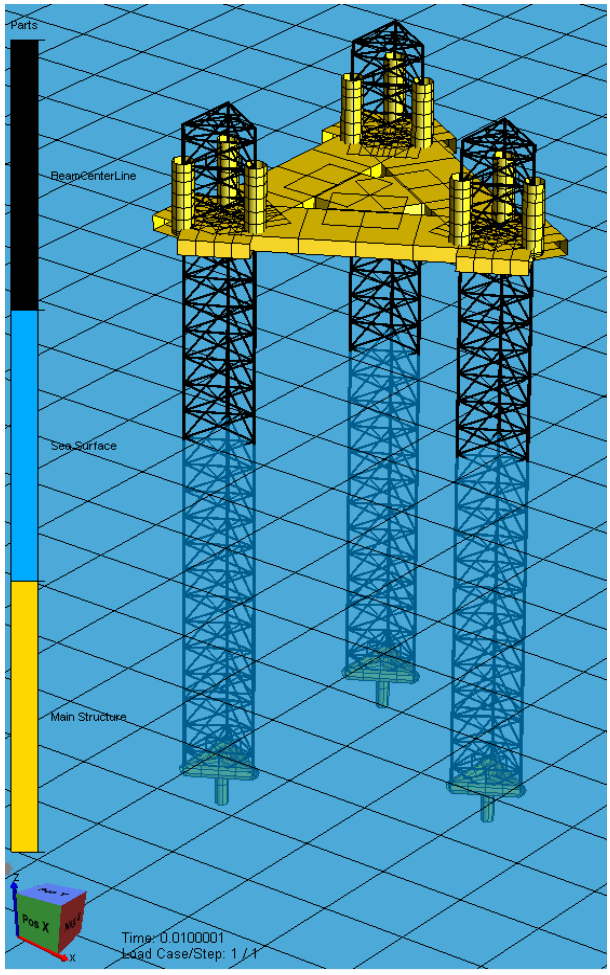

Figure 5.1 CJ62 Finite Element Model

Using the detail finite element model gives more accurate responses, such as deck displacement, baseshear and overturning moment. Eventhough this work is more focus on the difference between effect of first order and second order wave model on the jack-up, the detail finite element model is also useful

in push-over and damage analysis. On the other hand, performing analysis with the detail finite element model leads to longer computational time. In order to save time, an approach to perform several simulations simultaneously is considered. This approach is explained in chapter 6. In addition, the water depth is set to 100 meters for this work.

When determining the response of the structure, the nonlinear behaviour could be too significant to neglect. The nonlinearity on structure behaviour can be caused by [29]:

- Geometrical condition (large displacement)
- Material condition (nonlinearity on stress-strain relationship, e.g. plasticity)
- Bondary condition (contact between structure)

In the previous project, the nonlinearity on structure behaviour is avoided. The cylinder is modelled with very high modulus elasticity of material to avoid the plasticity. Moreover, by introducing very high modulus elasticity, the cylinder stiffness is also increased significantly, which restricts the cylinder from large displacement. As the result, nonlinearity from geomtric condition is avoided.

In this work, the structure is not represented as a linear model anymore. The geometrical and material nonlinearity in the structure are considered in the finite element model. The material of the legs (both the column and the truss) is modelled with elasto-plastic material. In figure 5.2, the purple colour indicates the parts of the structure which have the elasto-plastic material. The rest of the structure are modelled with elastic material. In general, the jack-up model part can be categorized to four groups:

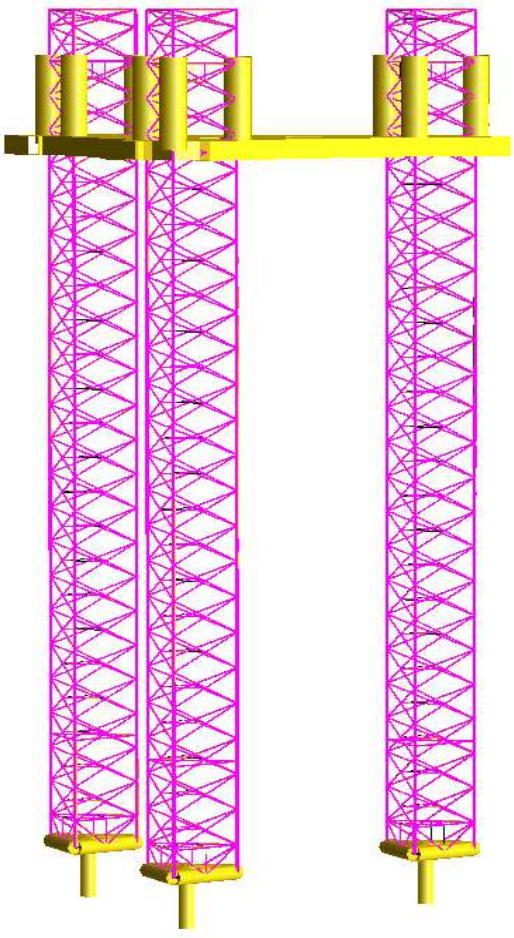

Figure 5.2 Open Truss Model of Leg

- Three sets of leg
- Three sets of support footing
- One Deckbox
- Jack Houses (part of the structure for transfering loads from the deckbox to the legs)

The materials for all part of the structure are summarized in table 5.1. For deckbox, support footings and connecting columns, the yield stress is neglected as the parts are represent with elastic material. In addition, the density of deckbox, support footings and connecting columns are represented by very small number since the mass of these parts is modelled by nodal mass.

Table 5.1 Material Parameter of Jack-up Model

No	Part	Elastic Modulus	Poisson Ration	Yield Stress	Density
1	Legs	210 Gpa	0.3	690 Mpa	7,850 kg/m^3
2	Support Footing	2,100 Gpa	0.3	-	-
3	Deckbox	420 Gpa	0.3	-	-
4	Jack House	210 Gpa	0.3	-	-

Moreover, the stiffness, damping, mass and eigenvalue analysis of the model are explained in this section.

5.1.1. Stiffness

Since geometry nonlinearity is accounted, the stability (Livesley) function [3] is utilized to represent the beam stiffness. In this case, the P-δ effect on element level is included when deriving the stiffness of the beam. The P-δ effect is caused by the axial force on cylinder. The matrix stiffness of the beam is acquired by finding the exact solution of beam moment equilibrium. Figure 5.3 illustrates the beam element with end forces.

For figure 5.3, the internal moment (M_i) and external moment (M_e) at any section $X = x$ are presented respectively in equation (5.1) and (5.2).

$$M_i = -E\, I\, w_{,xx} \tag{5.1}$$

$$M_e = M_A + Q_A X - N_x(w - w_A) \tag{5.2}$$

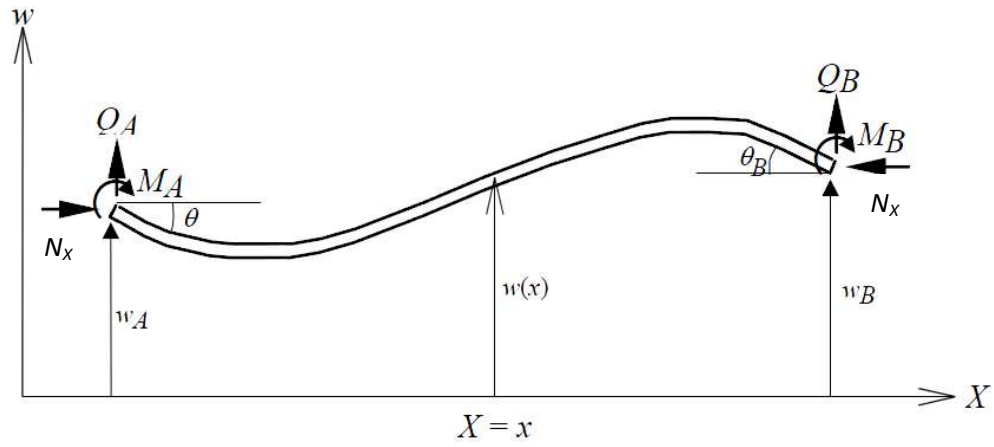

Figure 5.3 Beam Element with End Forces [3]

E and I is the elastic modulus and moment inertia respectively. M_A and Q_A are moment and shear force at point A while N_x is the axial force. $w(x)$ is the lateral displacement of the beam at point x. $w_{,x}$ and $w_{,xx}$ are the first and second x-derivative of w. Therefore, to satisfy the equilibrium:

$$\begin{aligned} M_i = M_e \;\rightarrow\; -E\,I\,w_{,xx} &= M_A + Q_A X - N_x(w - w_A) \\ w_{,xx} + {k_s}^2 w &= \frac{1}{E\,I}(M_A + Q_A X + N_x w_A) \;\;;\;\; {k_s}^2 = \frac{N_x}{E\,I} \end{aligned} \tag{5.3}$$

The differential equation in equation 5.3 is the beam moment equlibrium. The exact solution for equation 5.3 is represented by combination of homogenous (w_H) and particular (w_P) solution:

$$w(x) = w_H + w_P = C_1\,sin(k_s x) + C_2\cos(k_s x) + \frac{1}{N_x}(M_A + Q_A X + N_x w_A) \tag{5.4}$$

In order to find the coefficient C_1 and C_2, the boundary conditions should be satisfied. The boundary conditions are:

$$w(0) = w_A \;;\; w_{,x}(0) = -\theta_A \;\;;\;\; w(L) = w_B \;;\; w_{,x}(L) = -\theta_B \tag{5.5}$$

Combining the bondary condition and equilibrium condition, the relationship between force (or moment) and displacement (or rotation) is presented in equation 5.6 [3].

$$\begin{Bmatrix} Q_A \\ M_A \\ Q_B \\ M_B \end{Bmatrix} = \underbrace{\begin{bmatrix} \frac{12\,E\,I}{L^3}\phi_5 & -\frac{6\,E\,I}{L^2}\phi_2 & -\frac{12\,E\,I}{L^3}\phi_5 & -\frac{6\,E\,I}{L^2}\phi_2 \\ & \frac{4\,E\,I}{L}\phi_3 & \frac{6\,E\,I}{L^2}\phi_2 & \frac{2\,E\,I}{L}\phi_4 \\ & & \frac{12\,E\,I}{L^3}\phi_5 & \frac{6\,E\,I}{L^2}\phi_2 \\ & & & \frac{4\,E\,I}{L}\phi_3 \end{bmatrix}}_{Stiffness\ Matrix\ [k_e]} \begin{Bmatrix} w_A \\ \theta_A \\ w_B \\ \theta_B \end{Bmatrix} \tag{5.6}$$

The ϕ_i can be determined by:

Compression :	Tension :
$\phi_1 = \frac{\beta}{tan(\beta)}$	$\phi_1 = \frac{\beta}{tanh(\beta)}$
$\phi_2 = \frac{1}{3}\frac{\beta^2}{(1-\phi_1)}$	$\phi_2 = \frac{1}{3}\frac{\beta^2}{(\phi_1-1)}$
$\phi_3 = \frac{1}{4}\phi_1 + \frac{3}{4}\phi_2$	$\phi_3 = \frac{1}{4}\phi_1 + \frac{3}{4}\phi_2$
$\phi_4 = -\frac{1}{2}\phi_1 + \frac{3}{2}\phi_2$	$\phi_4 = -\frac{1}{2}\phi_1 + \frac{3}{2}\phi_2$
$\phi_5 = \phi_1\phi_2$	$\phi_5 = \phi_1\phi_2$

$$\beta = \frac{\pi}{2}\sqrt{\frac{N_x}{N_E}} \quad ; \quad N_E = \frac{\pi\,E\,I}{L^2}$$

This stiffness matrix is applied in USFOS. The global stiffness matrix of the structure (***K***) is established by assembling all element stiffness matrices (k_e). N_E is Euler buckling force.

5.1.2. Mass

In order to analyze the dynamic response of the structure, the mass matrix of element has to be defined. In this work, it is choosen to use consistent mass to calculate the mass of the element. Consistent mass means that the mass is based on the same interpolation function as the stiffness matrix. However, in USFOS, the mass is based on the interpolation function of linear 3D beam [37] instead of the nonlinear interpolation function which is described in equation (5.6). Therefore, the mass is not truly consistent with the stiffness matrix but is still considered adequately accurate. For beam element without shear and axial deformation, the mass matrix can be established by [24]:

$$m_e = \int_{-1}^{1} \rho_e {N_s}^T N_s \frac{L}{2} d\xi_F \quad ; \quad s = w, \theta$$

$$N_{w_A} = \frac{1}{4}\left(2 - 3\xi_F + {\xi_F}^3\right) \; ; \; N_{\theta_B} = \frac{1}{4}\left(1 - \xi_F - {\xi_F}^2 + {\xi_F}^3\right)$$

$$N_{w_B} = \frac{1}{4}\left(2 + 3\xi_F - {\xi_F}^3\right) \; ; \; N_{\theta_2} = \frac{1}{4}\left(-1 - \xi_F + {\xi_F}^2 + {\xi_F}^3\right) \tag{5.7}$$

$$m_e = \frac{\rho_e L}{420}\begin{bmatrix} 156 & -22L & 54 & 13L \\ -22L & 4L^2 & -13L & -3L^2 \\ 54 & -13L & 156 & 22L \\ 13L & -3L^2 & 22L & 4L^2 \end{bmatrix} \tag{5.8}$$

Where N_s is the shape function for diplacement (w) or rotation (θ), ρ_e is mass per length (kg/m). The global mass matrix of the structure (***M***) is established by assembling all element mass matrices (m_e). Moreover, the contribution of added mass from hydrodynamic force should be accounted in in mass matrix. Explanation about added mass is presented in section 5.2.

5.1.3. Damping

Damping is the ability of the structure to dissipate kinetic energy energy. Source of damping can be various and modelling them can be complicated. However, damping for structure (***C***) is normally assumed as proportional to stiffness and matrix of the structure [24] which can be expressed by:

$$\boldsymbol{C} = \alpha_1 \boldsymbol{M} + \alpha_2 \boldsymbol{K} \tag{5.9}$$

This damping system is known as Rayleigh damping. It can be shown that the global mass and stiffness matrices have orthogonality behaviour. Therefore, since the Rayleigh damping is proportional to mass and stiffness, it also has the othogonality behaviour. In addition, damping can also be determined as a ratio of structure critical damping for certain eigenmodes (explanation about eigenmodes is presented in section 5.14). The structure critical damping for eigenmode *i* ($\boldsymbol{\phi_i}$) can be expresed as:

$$\overline{c_{cr,\iota}} = \sqrt{2\,\overline{m_\iota}\,\overline{k_\iota}} \quad ; \quad \overline{m_\iota} = \boldsymbol{\phi_i}^T \boldsymbol{M} \boldsymbol{\phi_i} \quad ; \quad \overline{k_\iota} = \boldsymbol{\phi_i}^T \boldsymbol{K} \boldsymbol{\phi_i} \tag{5.10}$$

Then, the damping of the structure can be determined from eqigenmode *i*:

$$\boldsymbol{C} = \boldsymbol{\phi_i}\, \lambda_{c,i}\, \overline{c_{cr,\iota}}\, \boldsymbol{\phi_i}^T \tag{5.11}$$

$\lambda_{c,i}$ is the damping ratio for eigenmodes i. Since the structure has several eigenmodes, the damping ratio also has several values. In addition, each eigenmode refers to certain eigenfrequency. Therefore, the damping ratio (λ_c) can be expressed as a function of eigenfrequency (ω_n):

$$\lambda_c = \frac{1}{2}\left(\frac{\alpha_1}{\omega_n} + \alpha_2 \omega_n\right) \tag{5.12}$$

When $\alpha_1 = 0$, λ_c is proportional to ω_n then α_2 damps high frequency oscillation modes (eqigenmodes). With the same consideration, α_1 damps low eigenfrequency oscillation modes. If two damping ratios ($\lambda_{c,1}$ and $\lambda_{c,2}$) at two structure eigenfrequencies ($\omega_{n,1}$ and $\omega_{n,2}$) are known, α_1 and α_2 can be calculated by:

$$\alpha_1 = \frac{2\omega_{n,1}\omega_{n,2}}{{\omega_{n,2}}^2 - {\omega_{n,1}}^2}\left(\lambda_{c,1}\omega_{n,2} + \lambda_{c2}\omega_{n,1}\right) \tag{5.13}$$

$$\alpha_2 = \frac{2}{{\omega_{n,2}}^2 - {\omega_{n,1}}^2}\left(\lambda_{c,2}\omega_{n,2} - \lambda_{c,1}\omega_{n,1}\right) \tag{5.14}$$

For jack-up case, there are three sources of damping on the structure. They are strutural damping, soil damping and hydrodynamic damping. Structural damping is produced by the material of the jack-up. Soil damping is introduced by the foundation system. The hydrodynamic damping is determined by the velocity of structure relatively to the wave particle velocity. In this case, the hydrodynamic damping is a non-linear damping and known as viscous damping. DNV [11] recommends that the range of structural damping is between 1-3%. For soil damping, the range is recommended between 0-2% while for hydrodynamic damping is between 2-4%. Furthermore, DNV recommends that the total damping for storm condition should be in the range of 6-9%.

Table 5.2 Assumed Damping Ratio

No	Damping Ratio (λ_c)	Eigenfrequency	
		$\omega_n\ [rad/s]$	$f_n\ [Hz]$
1	3%	0.62	0.1
2	2%	62.83	10

In USFOS, the hydrodynamic damping is directly calculated from structure relative velocity. The soil damping is neglected in this case. Moreover, the structural damping determined by specifying two different damping ratios for two different eqigenfrequencies. Table 5.2 shows the

assumed damping ratios for two different eigenfrequencies. In addition, figure 5.4 shows the damping ratio for different eigenfrequencies based on the assumed damping ratio. The eigenfrequencies are presented in Hz instead of rad/s.

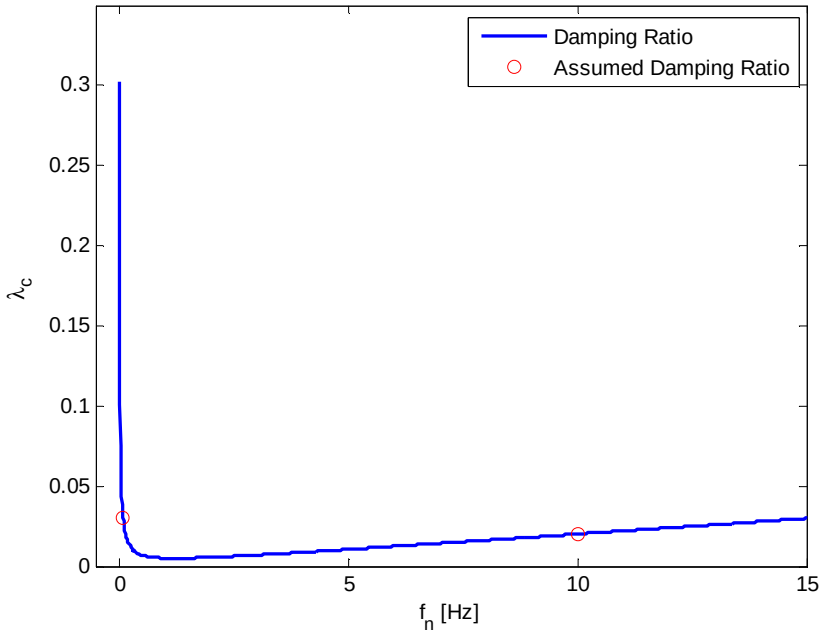

Figure 5.4 Damping Ratio of The Structure

5.1.4. Eigenvalue analysis

For undamped free vibration system, the equation of motion can be written as:

$$\boldsymbol{M\ddot{r} + Kr = 0} \tag{5.15}$$

By assuming $\boldsymbol{r = \phi} sin\ (\omega_n t)$, then equation 5.15 can be rewritten as:

$$(\boldsymbol{K} - \omega_n \boldsymbol{M})\boldsymbol{\phi} = \boldsymbol{0} \tag{5.16}$$

$\boldsymbol{\phi}$ is the vector of eigenmodes and ω_n is the eigenfrequency. This is an eigenvalue problem where $\boldsymbol{\phi}$ is the eigenvector and ω_n is the eigenvalue. The untrivial solution is found by calculating the determinant of $(\boldsymbol{K} - \omega_n \boldsymbol{M})$ that gives zero value. Solving this, the set of eigenfrequency (eigenvalue) and its corresponding eigenmodes are obtained [24].

In order to solve eigenvalue problem for finite element of structure, shifted-inverse itteration method can be used [24]. However, in this work the structure eigenfrequencies are determined by USFOS. The eigenperiods of jack-up model are presented in table 5.3.

Table 5.3 Structure Eigenfrequency

No	Mode	Eigenperiod (T_n) [s]	Eigenfrequency	
			$\omega_n\ [rad/s]$	$f_n\ [Hz]$
1	1st X-Bending	5.91	1.06	0.17
2	1st Y-Bending	5.91	1.06	0.17
3	Rotational	5.41	1.16	0.18
4	2nd X-Bending	0.55	11.4	1.82
5	2nd Y-Bending	0.55	11.4	1.82

5.2. Loads

For jack-up platform, the dimension of members in legs truss system are smaller than the wave length. Because of that, the wave load on jack-up legs can be determined directly from undisturbed wave particle kinematics. In this case, the wave load is calculated by utilizing Morison equation.

5.2.1. Morrison Equation

It is assumed that the strip theory is valid for determining load on jack-up leg. As a consequence, the Morrison equation can be combined with strip theory. The Morrison equation for a strip element of cylinder is expressed by:

$$dF = \underbrace{\rho \frac{\pi D^2}{4} C_M a_x \, dz}_{Inertia\ Term} + \underbrace{\frac{1}{2} \rho \, C_D \, D \, u_x |u_x| \, dz}_{Drag\ Term} \tag{5.17}$$

Where C_M is addedmass coefficient and C_D is drag coefficient. For regular wave, as it can be observed from equation 2.21, and 2.23, u_x has maximum magnitude at wave crest while a_x is equal to zero. At the mean water level, a_x has maximum value while u_x is equal to zero. For irregular wave condition, since it contains a set of regular wave component with different amplitudes, frequencies and phases, the inertia term is not totally zero at wave crest and the drag term is not totally zero at the mean water level. For single vertical cylinder case, when $H > 10\ D$ and $\lambda > 5D$, the drag load (viscous forces) dominates. In this case, H, λ and D are wave height, wave length and cylinder diameter respectively. This is illustrated in figure 5.5.

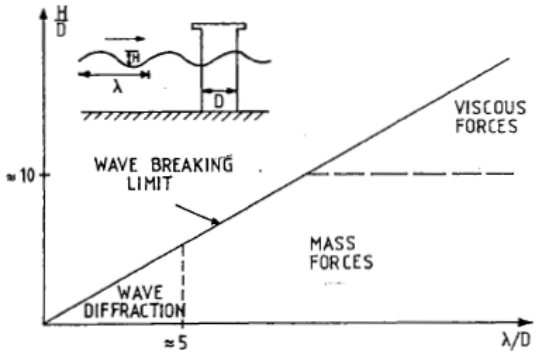

Figure 5.5 Relative Importance of Wave Load [14]

According to NORSOK [33], for slender structure, C_D = 1.05 and C_M = 1.2 for rough member and C_D = 0.65 and C_M = 1.6 for smooth member. The roughness of member can determined by considering the existence of marine growth at the Jack-up leg. NORSOK [33] suggest that the marine growth can be considered exist up to two meters above the mean water level. Therefore, $C_D = 0.65$ and $C_M = 1.6$ for $z > 2m$ while $C_D = 1.05$ and $C_M = 1.2$ for $z \leq 2m$. In this case, sea surface and wave kinematics should be modelled by second order or higher order wave model. On the other hand, when the sea surface is modelled as Gaussian sea (sea surface and wave particle kinematic is determined by first order model), the hydrodynamic coefficient should be modified to give reasonable load level. C_M is kept as previous model while $C_D = 1.15$ for all z coordinate. Figure 5.6 illustrates the applied hydrodynamic coeffien for second order (or higher) wave model and first order model.

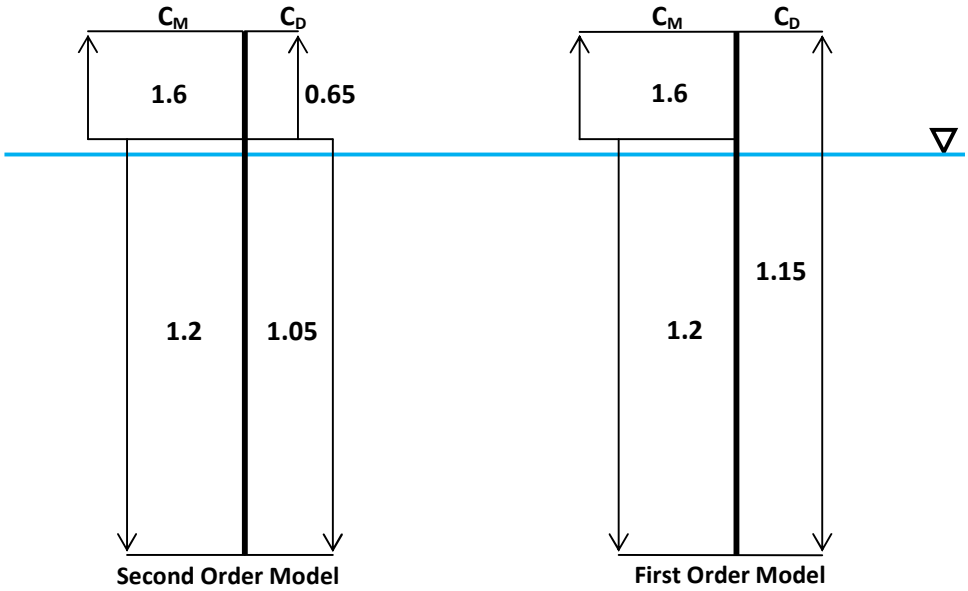

Figure 5.6 Applied Hydrodynamic Coefficient along z-Coordinate

5.2.2. Added Mass

In the potential theory, the inertia force presented in equation 5.17 is a combination of two sources of force. These sources of force are:

- Force comes from diffraction problem. In diffraction problem, the wave comes and hits the structure while the structure is restrained.
- Force comes from radiation problem. In radiation problem, the structure is forced to move and create waves. There is no incident wave in this case, i.e. the generated wave from the motion of structure is the only wave exists.

The diffraction and radiation problems are illustrated by figure 5.4 [14]:

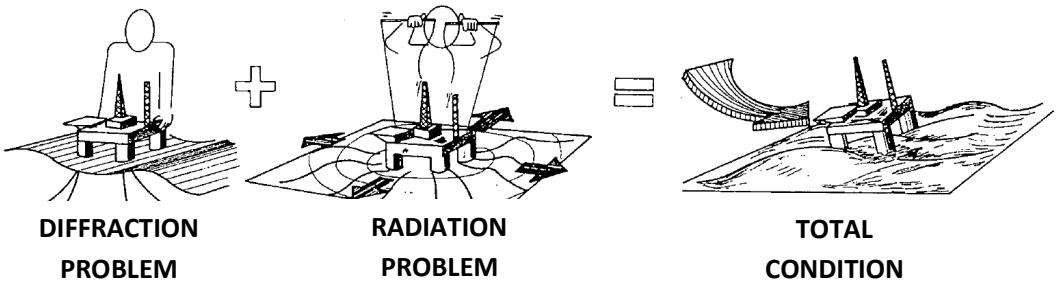

Figure 5.7 Illustration about Diffraction and Radiation Problem [14]

By solving radiation problem, another load terms exist. They are added mass, hydrodynamic damping and restoring. For jack-up system, the hydrodynamic restoring term can be neglected since the magnitude is small compared to stiffness of cylinder. The hydrodynamic damping from potential theory can also be neglected since it is smaller than viscous damping (viscous damping is determined from velocity of the structure relative to the wave particle velocity). However, the added mass force should be considered.

When the structure is oscillating, the added mass term for each strip element of cylinder can be calculated by [25]:

$$dF_a = -\underbrace{\rho \frac{\pi D^2}{4}(C_M - 1)dz}_{added\ mass = A_a}\ \ddot{r} \tag{5.18}$$

The added mass is calculated for each cylinder finite element and added to mass term of the structure (as presented in section 5.1.2).

5.3. Response

The response of structure can be analyzed by two different approaches. The first way is by static analysis. In this method, the contribution from damping and mass is neglected. The second way is dynamic analysis. In this case, the contribution from mass and damping is accounted. In this section, the displacement of the jack-up is taken as response.

5.3.1. Static Analysis

For static analysis, the dynamic behaviour of the structure is assumed can be neglected. Therefore, the displacement ($\boldsymbol{r}$) can be analyzed by:

$$\boldsymbol{K\,r = R} \tag{5.19}$$

Similar to stiffness matrix, the force matrix ($\boldsymbol{R}$) is also needed to assembly before it is included in equation 5.19. The response from static analysis does not depend on previous response. Hence, it is possible to calculate the extreme response by only observing the condtion of sea surface where the extreme load possible to occur. In this way, calculation is relatively simple and fast. To account for the dynamic behaviour of the structure, the static analysis can be extended by utilizing equivalent dynamic amplification factor (EDAF). EDAF is the ratio between dynamic and static response of the structure.

5.3.2. Dynamic Analysis

In dynamic analysis, the displacement is calculated by solving equation of motion. The equation of motion is:

$$\boldsymbol{M\ddot{r} + C\dot{r} + Kr = R}(t) \tag{5.20}$$

$\boldsymbol{\ddot{r}}$, $\boldsymbol{\dot{r}}$ and $\boldsymbol{r}$ respectively are structure acceleration, velocity and displacement. The equation of motion in time domain is solved by utilizing numerical integration. There are several schemes of numerical integration for solving the equation of motion, e.g. constant acceleration method, linear acceleration method and Newmark's β family [24]. In this study, the HHT-α (Hilber, Hughes and Taylor alpha-dissipation) method, the method which is used in USFOS, is utilized. This method averages the damping, stiffness and force term by α-parameter. In general, the lower modes (modes with low eigenfrequency) govern the oscillation of structure. Then, using α method will be advantageous since it introduces artificial damping for higher order modes of vibration.

The equation of motion for HHT-α method is expressed as:

$$\boldsymbol{M}\ddot{\boldsymbol{r}}_{i+1} = [(1+\alpha)\boldsymbol{R}_{i+1} - \alpha\boldsymbol{R}_i] - [(1+\alpha)\boldsymbol{C}\dot{\boldsymbol{r}}_{i+1} - \alpha\boldsymbol{C}\dot{\boldsymbol{r}}_i + (1+\alpha)\boldsymbol{K}\dot{\boldsymbol{r}}_{i+1} - \alpha\boldsymbol{K}\boldsymbol{r}_i]$$
$$\boldsymbol{r}_{i+1} = \boldsymbol{r}_i + \Delta t\,\dot{\boldsymbol{r}}_i + \frac{\Delta t^2}{2}(1-2\beta)\ddot{\boldsymbol{r}}_i + \Delta t^2\beta\ddot{\boldsymbol{r}}_{i+1} \tag{5.21}$$
$$\dot{\boldsymbol{r}}_{i+1} = \dot{\boldsymbol{r}}_i + \Delta t\,(1-\gamma)\ddot{\boldsymbol{r}}_i + \Delta t\,\gamma\,\ddot{\boldsymbol{r}}_{i+1}$$

γ and β are the parameter in Newmark-β method. The stability of the integration is determine by α, β and γ. The unconditional stability is achived when:

$$-\frac{1}{3} < \alpha < 0 \;;\; \gamma = \frac{1}{2}(1-2\alpha) \;;\; \beta = \frac{1}{4}(1-\alpha)^2 \tag{5.22}$$

When α is equal to zero, HHT-α becomes constant average method. In this work, α is set as -0.1. The incremental equations are obtained by substracting the solution at time *i+1* with solution at *i*.

$$\boldsymbol{M}(\ddot{\boldsymbol{r}}_{i+1} - \ddot{\boldsymbol{r}}_i) + (1+\alpha)(\boldsymbol{C}\dot{\boldsymbol{r}}_{i+1} - \boldsymbol{C}\dot{\boldsymbol{r}}_i) + (1+\alpha)(\boldsymbol{K}\boldsymbol{r}_{i+1} - \boldsymbol{K}\boldsymbol{r}_i) = (1+\alpha)(\boldsymbol{R}_{i+1} - \boldsymbol{R}_i) + \boldsymbol{R}_i - \boldsymbol{M}\ddot{\boldsymbol{r}}_i - \boldsymbol{C}\dot{\boldsymbol{r}}_i - \boldsymbol{K}\boldsymbol{r}_i \tag{5.23}$$

$$\Delta\ddot{\boldsymbol{r}}_{i+1} = \ddot{\boldsymbol{r}}_{i+1} - \ddot{\boldsymbol{r}}_i = \frac{1}{\Delta t^2\beta}\Delta\boldsymbol{r}_{i+1} - \frac{1}{\Delta t\beta}\dot{\boldsymbol{r}}_i - \frac{1}{2\beta}\ddot{\boldsymbol{r}}_i \tag{5.24}$$

$$\Delta\dot{\boldsymbol{r}}_{i+1} = \dot{\boldsymbol{r}}_{i+1} - \dot{\boldsymbol{r}}_i = \frac{\gamma}{\Delta t\beta}\Delta\boldsymbol{r}_{i+1} - \frac{\gamma}{\beta}\dot{\boldsymbol{r}}_i - \Delta t\left(\frac{\gamma}{2\beta} - 1\right)\ddot{\boldsymbol{r}}_i \tag{5.25}$$

Then $\Delta\boldsymbol{r}_{i+1}$ will be the only unknown when equation (5.23) is combined with equation (5.24) and (5.25). Therefore, equation (5.23) can be rewritten as:

$$\left[(1+\alpha)\boldsymbol{K} + (1+\alpha)\frac{\gamma}{\Delta t\beta}\boldsymbol{C} + \frac{1}{\Delta t^2\beta}\boldsymbol{M}\right]\Delta\boldsymbol{r}_{i+1} = (1+\alpha)(\boldsymbol{R}_{i+1} - \boldsymbol{R}_i) + \boldsymbol{R}_i - \boldsymbol{M}\ddot{\boldsymbol{r}}_i - \boldsymbol{C}\dot{\boldsymbol{r}}_i - \boldsymbol{K}\boldsymbol{r}_i + \left[\frac{1}{\Delta t\beta}\dot{\boldsymbol{r}}_i - \frac{1}{2\beta}\ddot{\boldsymbol{r}}_i\right]\boldsymbol{M} + \left[(1+\alpha)\left(\frac{\gamma}{\beta}\dot{\boldsymbol{r}}_i + \Delta t\left(\frac{\gamma}{2\beta} - 1\right)\right)\right]\ddot{\boldsymbol{r}}_i \tag{5.26}$$

By knowing $\Delta\boldsymbol{r}_{i+1}$, displacement, velocity and acceleration of the structure can be calculated from:

$$\boldsymbol{r}_{i+1} = \boldsymbol{r}_i + \Delta\boldsymbol{r}_{i+1} \tag{5.27}$$

$$\dot{\boldsymbol{r}}_{i+1} = \frac{\gamma}{\boldsymbol{2}\beta}\Delta\boldsymbol{r}_{i+1} + \left(1 - \frac{\gamma}{\beta}\right)\dot{\boldsymbol{r}}_i - \Delta t\left(\frac{\gamma}{2\beta} - 1\right)\ddot{\boldsymbol{r}}_i \tag{5.28}$$

$$\ddot{\boldsymbol{r}}_{i+1} = \frac{1}{\Delta t^2\beta}\Delta\boldsymbol{r}_{i+1} - \frac{1}{\Delta t\beta}\dot{\boldsymbol{r}}_i + \left(1 - \frac{1}{2\beta}\right)\ddot{\boldsymbol{r}}_i \tag{5.29}$$

6. Numerical Model

In this work, all the calculation and simulation is performed numerically. The works covers the metocean analysis, sea surface simulation, wave particle kinematics calculation and structure response analysis of the jack-up. In addition, since a big number of simulation is needed to perform, a particular scheme should be established to do the numerical simulation efficiently. This section presents the explanation and consideration of the numerical model in this work.

6.1. Flowchart of Simulation

The simulations in this work can be categorized into five main groups, which are:

- Metocean analysis to find the significant wave height and spectral peak period for 100 year return period
- Simulation of sea surface utilizing the significant wave height and spectral peak period from metocean analysis
- Calculation of the wave particle kinematics for each surface evelation
- Calculation of jack-up static and dynamic responses

The first three groups are performed in MATLAB while the last one is performed in USFOS. The works can be presented in a flowchart. Figure 6.1 shows the flowchart of the work.

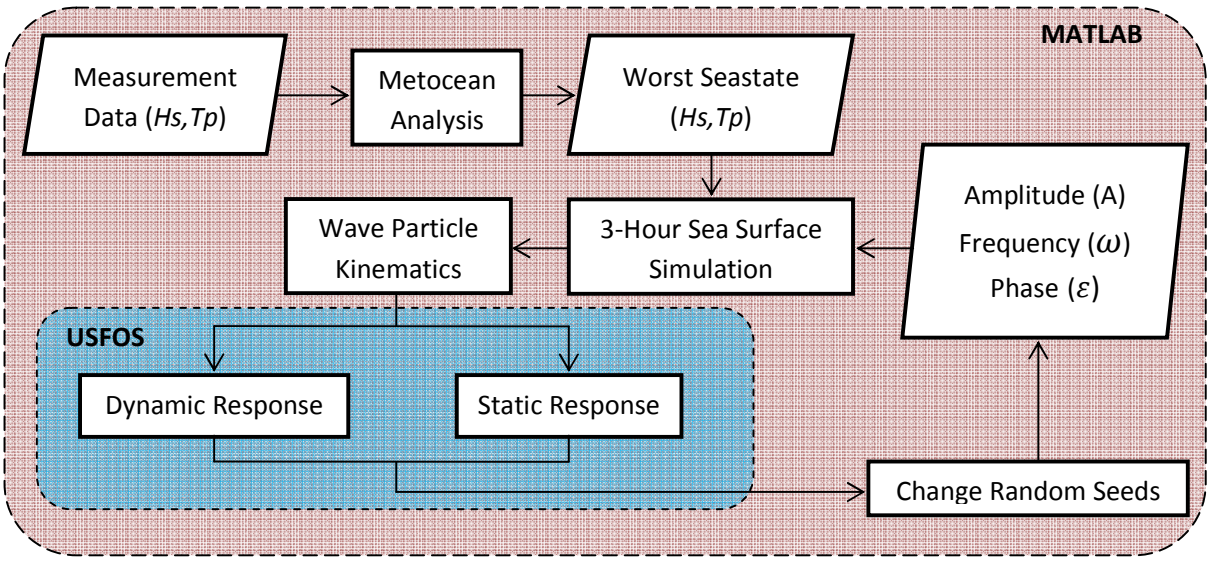

Figure 6.1 Flowchart of Simulation

The parallelogram indicates an input/output while rectangular indicates a process (simulation or calculation). Several three hour simulations of sea surface, wave particle kinematics and responses are acquired by generating new random seeds which means generating new amplitude, frequency and phase of harmonic component (depends on the choosen scheme). The blue colour are indicates the process which are performed utilizing USFOS while the rest of work are performed in MATLAB (red colour).

After certain number of simulations is performed, the distribution of jack-up responses are calculated. In this case, the calculated responses in USFOS are baseshear and overturning moment reaction at the bottom of jack-up. The number of performed simulation is determined differently depends on the focus of analysis. Since the simulation is performed repeatedly, then the best method to do repetition in MATLAB and USFOS is observed.

6.2. Looping in MATLAB

In general, the calculation and simulation in MATLAB requires repetitive process. Choosing the appropriate technique can speed up the calculation. Because of that, several looping techniques are compared. The option which are discussed here is only valid in MATLAB since other computation tools has different environment and library. In this section, four techniques of looping in MATLAB are compared:

1) For-loop : the simplest looping method in MATLAB. Each component of looping is analyzed one-by-one then the result is saved into a result matrix. The result matrix is updated for each looping since the size of result matrix changes in each looping.
2) For-loop with preallocating memory : when the final size of result matrix is known, the final result matrix can be created first. Hence, result from every calculation is assigned into the final result matrix. In this way, the unnecessary computational time for updating result matrix can be avoided.
3) Vectorization : MATLAB uses processor-optimzed for matrix and vector computation. Therefore, a matrix operations could be significantly faster than simple looping process. Therefore, the for-loop process is converted into a set of matrix (or vector) then the matrix operations are performed. In this case, additional vectorization proccess is needed to perform and for some cases the required memory can be larger than simple for-loop process. Moreover, the for-loop process can not be vectorized in several cases.

4) Parallel for-lop : when the for-loop can not be vectorized, pararller for-loop can be used as an aternative technique to speed up the calculation. This technique distributes the looping processes into several *workers* and some processes are executed at the same moment. However, this process depends on the number of available *workers* in MATLAB which is affected by number of computer cores.

To observe the required computational time from four different techniques, a looping is performed to calculate the third power of matrix **A** which is a matrix with size 5000 x 5000. The computational time is measured and summarized in table 6.1. In addition, figure 6.2 shows the result as percentage of simple for-loop computational time. It should be noted that the computational time is also affected by computer processor and memory which gives different computational time in different computer for the same technique. For instance, the pararel for-loop is not very efficient method for computer with small memory and less processor. Therefore, result in table 6.1 and figure 6.2 should be considered as a trend instead of absolute difference. The MATLAB script for comparing different looping technique is presented in appendix 1.

Table 6.1 Computational Time of Different Looping Technique

No	Technique	Computational Time [s]	Percentage [%]
1	For-loop	69.29	100
2	For-loop with preallocating memory	6.13	8.85
3	Vectorization	0.59	0.85
4	Pararel for-loop	44.79	64.64
5	Pararel for-loop with preallocating memory	3.18	4.59

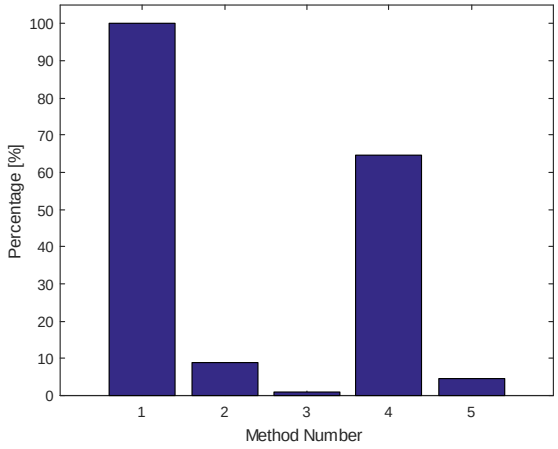

Figure 6.2 Computational Time for Different Looping Technique

From table 6.1, vectorization technique shows the fastest calculation process. Therefore, the MATLAB codes in this work are built based on vectorization technique. A 20-minutes second order-sea surface simulation with time interval 0.5s requires at least 1200^2 looping process. Calculating wave particle kinematics in grid system with size 100m x 100m x 100m (*x*,*y* and *z* coordinate) and interval 1m for 20 minutes means that the looping should be done:

$$Number\ of\ looping = 1200^2 \times 100 \times 100 \times 100 \times \left(\frac{20 \times 60}{0.5}\right) = 3.456 \times 10^{15} \qquad (6.1)$$

Even when the wave can be assumed as long crest wave which makes the grid system in *y*-coordinate can be represented by single *y*-coordinate for each *x* and *z*-coordinate, the process still requires 3.456×10^{13} looping proccess. In this case, the vectorization can not be done due to memory problem. Therefore, a combination of vectorization and pararel for-loop is utilized. All in all, choosing a right looping technique could improve the effiency of calculation in MATLAB.

In this work, several MATLAB scripts and functions has been built. Evethough the arragenment differs which depends on the focus of analysis, each functions and script has its own purposes. The input, output and purpose of the function is explained in the appendix 2.

6.3. USFOS

The responses of jack-up, both static and dynamic responses, are calculated by USFOS. USFOS is a computer program which is built to calculate the nonlinear ultimate strength and anlayze progressive collapse of a frame structure. Bassically USFOS is designed to analyze the collapse of structure like tubular jacket but trough development USFOS is able to analyze other various effects. The installed USFOS package consists of several moduls. Three main modules which is used in this work is *usfos, dynres* and *Xact. Usfos* is the main modul of USFOS which performs all numerical numerical calculation and generates the results. *Dynres* is modul which is used in time domain analysis. *Dynres* converts the time domain result (which is in *.dyn* format) from *usfos* modul into *.plo* format which is usable for further analysis (for example the post analysis in MATLAB). *Xact* or *Graphical User Interface (GUI)* can be used for model setup, execution and post processor. *Xact* can be used to verify the finite element model through graphs. Moreover, *Xact* is really useful modul since it can produce several important graphs to describe the result of analysis.

6.3.1. Input

There are several ways to input model in USFOS. One of them is by using *Xact* modul. The input model can be distributed into three *.fem* files, which are head/control file, load file and model file. The head/control file contains the control parameters. The model file contains the finite element model such as nodes, elements, materials, and mass description. The load on the structure can be included either in head or model file or can be given in separate file as load file.

In this work, all the calculation of sea surface and wave particle kinematics are performed in MATLAB. Therefore, the result of MATLAB calculation shall be transfered into USFOS. The sea surface and wave particle kinematics is transferred into USFOS as *.w132* file format which is the format of gridwave file. The *wavedata* command in USFOS (generally is written in head file) is modified by changing the type into *grid*. This command tells USFOS to utilize the transferred gridwave file as the wave data for calculating load on the structure. In this case, the *usfos* modul is processed first from *Xact* modul then *usfos* asks for the gridwave file. Hence the name of gridwave file is given then the simulation can be continued.

6.3.2. Simulation

The loads in USFOS is determined by utilizing Morison equation. For time domain simulation, the load is introduced as a time series. USFOS applies the wave load only for wet part of the model. Beacause of that, the wet elements are checked before the load applied.

There are two different ways to account the buoyancy force in USFOS. The first way, which is also the default option in USFOS, is by using simple Archimedes calculation. In this case, the displacement of structure is calculated and the buoyancy force is determined using Archimedes formula. The other way to account the buoyancy force is by integrating the pressure (static and dynamic) along the strucre. This method leads to more accurate result with longer computational time as the consequence. In this work, the first option is considered enough to perform in the simulation.

The command *consimas* is used to activate the consistent mass option in USFOS. The comment *CINIDEF* introduces an imperfection in the structure for buckling analysis purposes. The drag coefficients along z-coordinate are determined by *HYDRO_Cd* command while *HYDRO_cm* introduces the addedmass coefficients along z-coordinate of the structure.

In USFOS, the responses are determined by static and dynamic time domain analysis. To perform either static and dynamic time domain analysis, a time history should be set first in USFOS by using command *TIMEHIST*. For wave load, the *switch* should be choosen as timehistory type. However, before the wave load is applied (both in dynamic and static analysis), the weight and buoyancy force should be accounted first. In this case, the weight and buoyancy force is applied as load combination. To avoid the misinterpretation of load as an impact, the combination of weight and buoyancy force is applied gradually for one second with static analysis. The time history with type *S_Curve* is chosen in this case.

Another issue which is needed to consider for time domain simulation in USFOS is the maximum time step. The default maximum timestep in USFOS is 512 step. Using *CMAXSTEP* command, the maximum time step is increased to performs complete 20-minute simulation. In addition, the transient effect of the structure shall be accounted too. Therefore, the responses of structure for certain interval is neglected for further analysis in MATLAB.

USFOS applies the updated Lagrange method to calculate the responses in time domain. For each time instance, the load is applied in steps. The stiffness is updated in each load steps then the displacement of the structure is determined. After each displacement calculation, the structure configuration is updated (nodal coordinate, element force and possible plastic hinge). Therefore, the displacement calculation based on linear analysis which depends on the updated configuration.

DynRes_G command produces the global responses of time domain simulation. In this work, the base shear and overturning moment reaction are chosen as the observed responses. In addition, *DynRes_G* is also used to verify the surface elevation and the wave load.

6.3.3. Multiple simulations in USFOS

The computational time for complete 20-minutes simulation of structure responses in USFOS could be more than 10 minutes (this depends on the specification of the computer). In addition, the result for certain time interval in the begining of simulation is neglected to avoid transient response. Therefore, to do complete 3-hour simulation, at least ten 20-minutes simulation needs to perform. Moreover, this work requires at least 30 simulations of structure response for

statistical purposes. Therefore, performing simulation sequently is very time consuming. To avoid this issues, a parallel computing is performed in the simulation.

USFOS is based on UNIX operating system. Back in 2013, Tange [41] presented a tool to perform parallel computing in UNIX operating system. This tool is called GNU Parallel and still being continuosly developed until now. Since all new computers utilize multicore processors, the concept of GNU Parallel is to optimize the usage of the processors to do parallel computing. The easiest way to perform parallel computing is by spliting the number of *jobs* equally into some *workers* without considering the weight of each *jobs*. On the other hand, GNU Plot optimizes the parallel computing by spawning a new *job* immediately after a *job* finish in particular *worker* [42]. Figure 6.3 illustrates the comparisson of these two different methods where 32 *jobs* are distributed into 4 *workers*.

By utilizing the GNU Parallel, several number of responses simulations by USFOS can be performed simultaneously. In this case, a UNIX script is built to combine the USFOS with GNU Parallel. As a consequence, the computational time is reduced drastically not to mention the convenience which is achived by performing the simulation automatically. In addition, CYGWIN is utilized to run an UNIX script in windows.

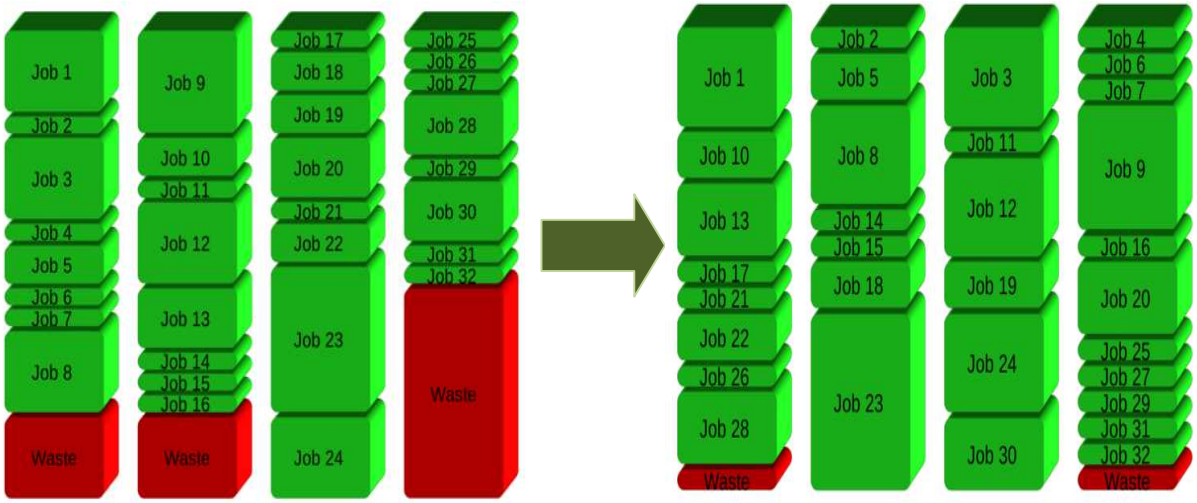

Figure 6.3 Illustration of Parallel Computation
(Left: Simple parallel computing, Right: GNU Parallel scheme) [42]

7. Comparisson and Verification of Model

Before applied to jack-up model, the sea surface model is verified first. The distribution of sea surface model is compared to theoretical distribution. The second order wave particle kinematics are compared to 5th Stokes wave which is the popular wave theory for quasi-static analysis. Some comparissons are also performed between different stretching methods, and schemes to determine the harmonic components. In addition, a verification of transfering sea surface and wave particle kinematics from MATLAB to USFOS is performed. All the simulation in this chapter is performed with $H_s = 14.9\ m$, and $T_p = 15.8$s which are the parameters used in previous work by Evardsen [12]. In addition, the water depth is set as 100 m and $\Delta t = 0.5s$.

7.1. Bootstrapping

When fitting a set of data into a particular distribution, there is a question about the number of data that should be included to produce a fitted distribution with good confidence level. In this case, boostrapping method can be used to show the uncertainty level regarding the number of data (*N*) which are included in the fitting process. The procedure of bootstraping is quite simple and fast to perform.

For example, the largest maximum first order surface elevation (ζ_{lm}) is assumed follows Rayleigh distribution raised to the power of *N*. For bootstraping purpose, ζ_{lm} is determined by:

$$\zeta_{lm} = \sigma_\zeta \sqrt{-2\ ln\left(1 - \left(F_{\zeta_{lM}}(\zeta_{lm})\right)^{T_z/T_f}\right)}\ \ ; T_z = 0.77\ Tp \tag{7.1}$$

$\sigma_\zeta = H_s/4$ for JONSWAP spectrum. $F_{\zeta_{lM}}(\zeta_{lm})$ is determined by random number which is uniformly distributed between zero and one. After calculating a set of ζ_{lm}, the empirical distribution is produced. Repeating the procedures for several times shows the deviation for certain CDF value. Figure 7.1 shows bootstraping result for *N* = 30, 50, 100 and 500. The procedures are repeated 500 times.

In figure 7.1, larger *N* makes the fitted model converges to the theoretical model. This means, using small number of data gives significant uncertainty which is an epistemic uncertainty. Therefore, the deviation in the model shall be accounted when using small number of data.

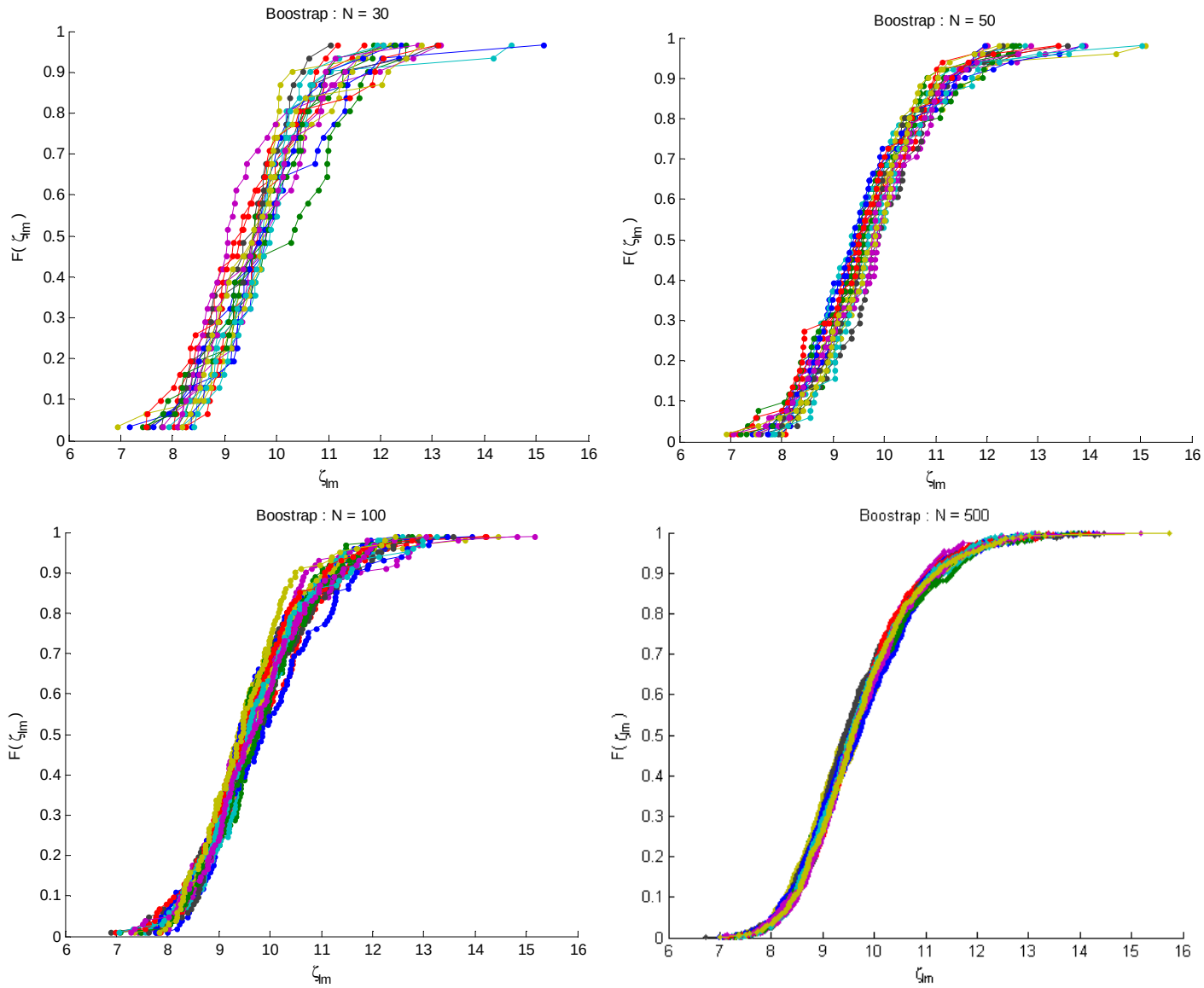

Figure 7.1 Bootstrapping Comparisson

7.2. Verification of Sea Surface Model

To verify the model, the CDF of maximum surface elevation (ζ_m) from the model is compared with theoretical distribution. Furthermore, the CDF of the largest maximum surface elevation (ζ_{lm}) is also observed. In this case, 3-hour simulation of sea surface is performed. Various schemes to determine the amplitude, frequency and phase of harmonic components are tested.

7.2.1. Distribution of maximum first order sea surface

The Rayleigh distribution is compared to distribution of zero-crossing maximum of surface elevation while the Rice distribution is compared to distribution of surface local maxima. Figure 7.2 shows the sea surface at *x=0* for 200s time window with its local and zero-crossing maximums.

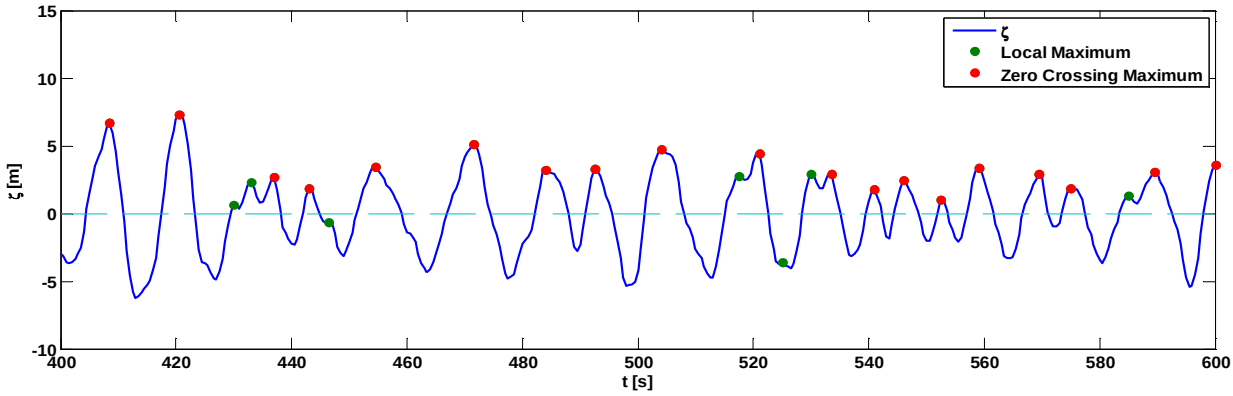

Figure 7.2 Surface Elevation and Maximum Surface Elevation

Figure 7.3 shows the comparisson between empirical and theoretical CDF from two different realizations from equidistance frequency interval with deterministic amplitude (two pictures up) and random amplitude (two pictures down). More realizations are presented in appendix 3 for deterministic amplitude and appendix 4 for random amplitude. From the realizations, Rice distribution tends to underestimate the distribution of local maxima at the lower tail. Based on this fact, the model is not totally broadbanded process as it is assumed in Rice distribution. For some cases, the Rice distribution underestimates the distribution of local maxima at the upper tail though it overestimates the distribution for the other cases. This is due to the epistemic uncertainty in the model. In addition, introducing random amplitude sligthly increases the uncertainty. The uncertainty can be shown by the bootstrapping method as it is shown in section 7.1. Despite all of that, it can be concluded that the local maximum distribution follows Rice distribution.

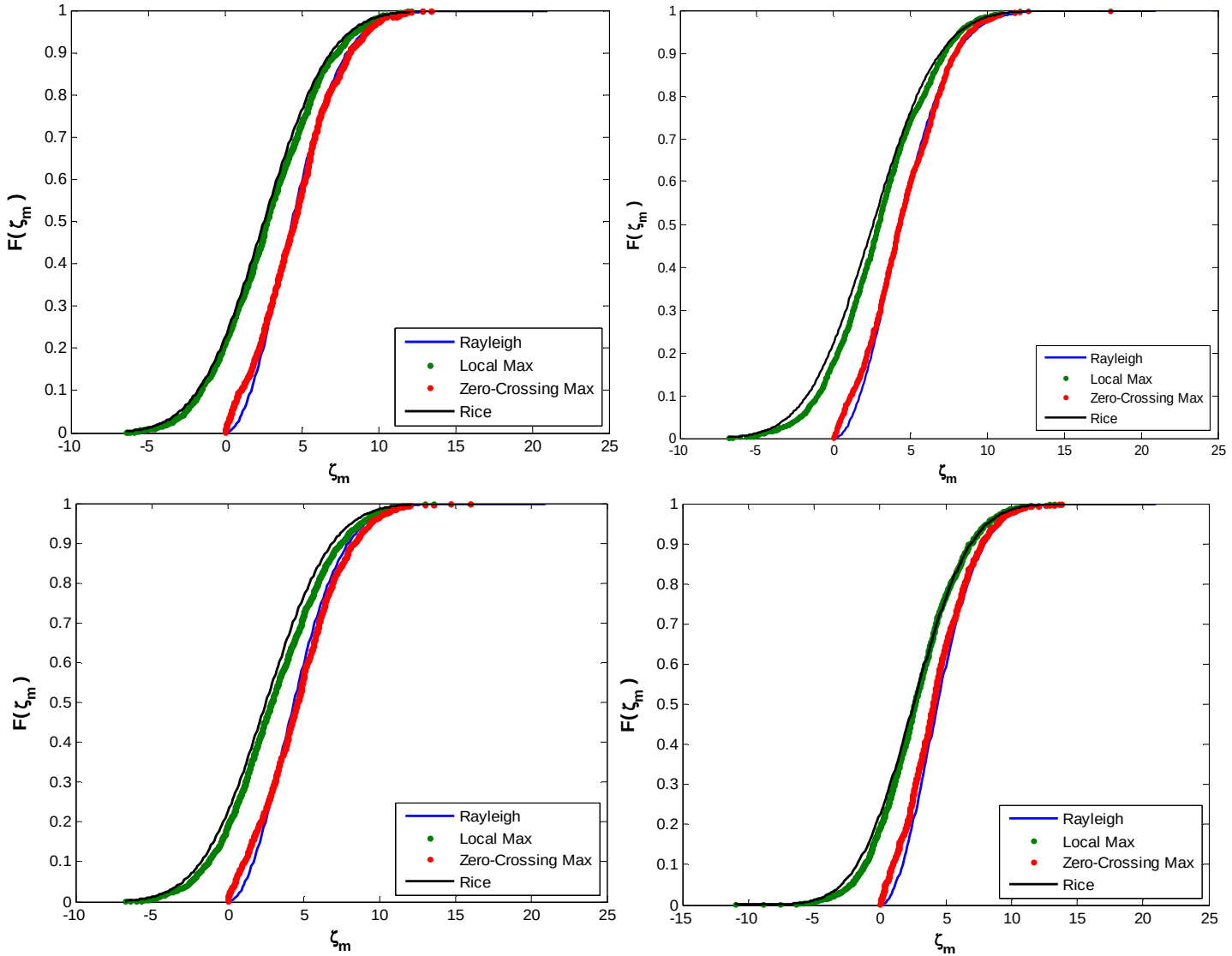

Figure 7.3 Comparisson of Maximum Surface CDF
Up: Deterministic Amplitude; Down: Random Amplitude

The uncertainty of the shape is also observed in the upper tail of maximum zero-crossing distribution. This uncertainty is also can be proven by bootstraping the Rayleigh CDF. However, the empirical model does not follows the Rayleigh distribution at lower tail. At lower tail, the Rayleigh distribution always overestimates the maximum surface elevation. This due to the effect of high frequency harmonic components and indicates that the surface is not totally narowbanded.

When the sea surface is assumed as narrowbanded process, the period between crest is assumed equal to the zero-crossing period. Moreover, the zero-crossing period is assumed not significantly varies. However, real sea surface is greatly irregular and not totally narrowbanded where the period is not concentrated only in a certain range of period. Therefore, when a wave spectrum is converted into time series of surface elevation, high frequency components (which has smaller amplitude) occurs more intense than lower frequency. As a result, when the empirical CDF is constructuted, significant number of maximum surface elevation which refers to the high frequency components will dominate the lower tail of the CDF and shifted the lower tail of empirical CDF to left side of Rayleigh distribution. This means Rayleigh distribution will always overestimates the distribution of maximum surface at the lower tail.

From figure 7.3, Rayleigh distribution gives higher maximum surface elevation than Rice distribution. For ultimate limit state analysis, the main concern of analysis is the upper tail of CDF. Because of that, the Rayleigh distribution is considered as a good distribution for design. All in all, figure 7.3 shows that the surface model is agree well with the theoretical model.

7.2.2. Distribution of largest maximum of first order sea surface

The theoretical CDF of largest maximum is expressed by equation 3.17. To produce the empirical distribution, 100 3-hour simulations of first order sea surface are performed. The largest maximum from each simulation is gathered and sorted to produce the empirical distribution. Figure 7.4 shows one possible realization of largest maximum empirical distribution of first order sea surface with equidistance frequency interval and deterministic amplitude. Another realization is presented in appendix 7.

In addition, the bootstrapping is performed to analyze the deviation as consequence of using 900 data. The procedure of bootstrapping is repeated 500 times. The smallest and largest value for

each CDF level are plotted as dash line in figure 7.4 to show the lower and upper limit of bootstraping. Hence, it is easy to determine wether the empirical distribution is acceptable or not by considering the deviation from boostrapping. Figure 7.4 shows that the empirical distribution agrees well with the theoretical distribution since it is located inside the bootstrapping limit.

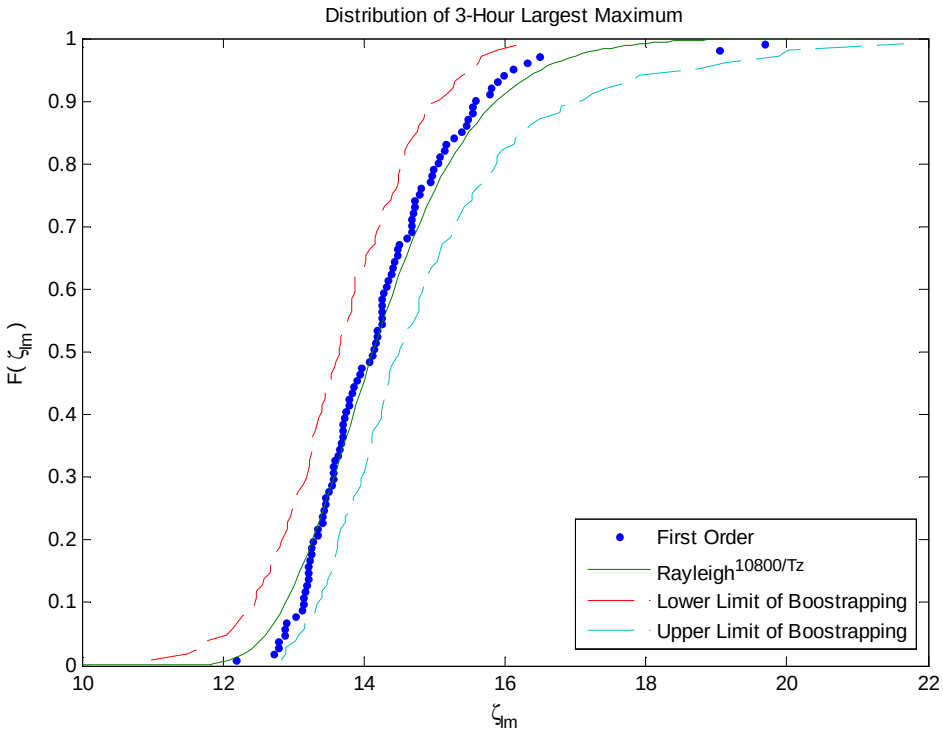

Figure 7.4 CDF of Largest Maximum for for Deterministic Amplitude

Figure 7.5 shows one possible realization of 3-hour largest maximum sea surface distribution with random amplitude scheme. It is explained in section 4.2.1.2 that introducing random amplitude changes the variance of surface elevation from the deterministic amplitude variance. However, figure 7.5 shows that the empirical CDF from random amplitude scheme is located inside the limit of bootstrapping. Therefore, it is conlculed that introducing random amplitude into 3-hour surface elevation still gives good agreement between empirical and theoretical distribution. More distributions of sea surface largest maxima for random amplitude are presented in appendix 8.

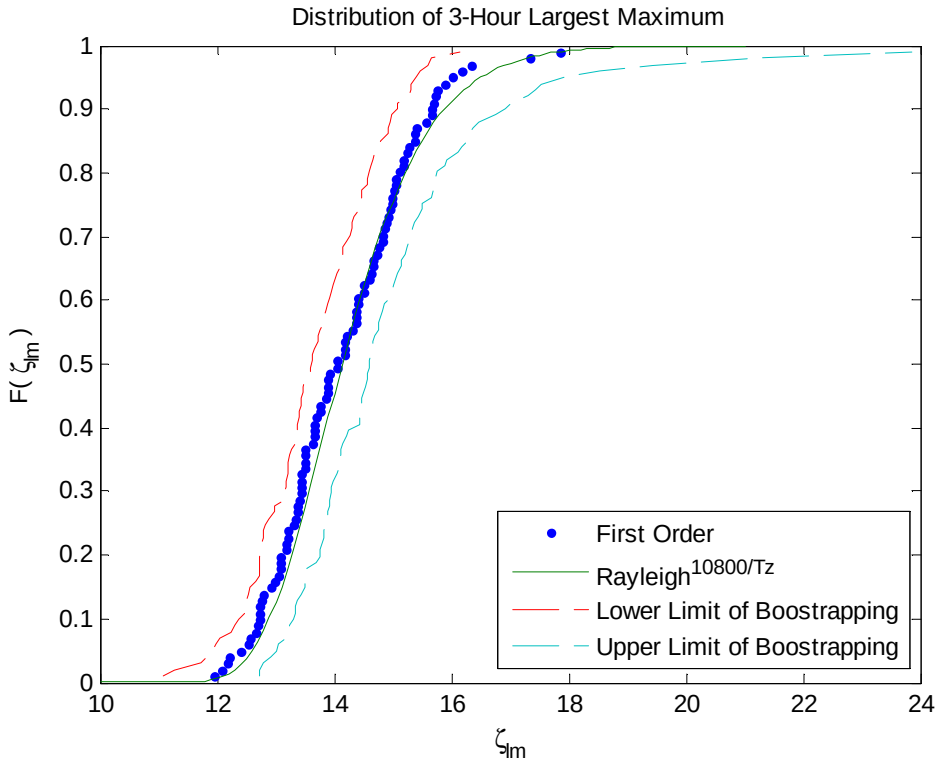

Figure 7.5 CDF of Largest Maximum for for Random Amplitude

7.2.3. Methods of reducing number of component

Generating the distribution of largest maximum of sea surface (or the distribution of largest response of structure) requires more than one simulation. For first order sea, there is no great problem with the computational time. However, the process could be time consuming for second order sea surface. Therefore, methods to reduce number of harmonic component is utilized.

7.2.3.1. Partition of time series

In this case, the partition of time series (explained in section 4.2.2.4) is performed. The three hour simulation is splited into 9 different 20-minutes simulation. To achieve 100 3-hour simulation, 900 20-minute of first order simulations are performed. Each largest maximum surface from each simulation is gathered and sorted to produce empirical distribution of largest maxima. Figure 7.6 shows the distribution of largest maximum of first order sea surface for deterministic amplitude utilizing 900 samples. Another 20-minutes largest maximum distribution is presented in appendix 5.

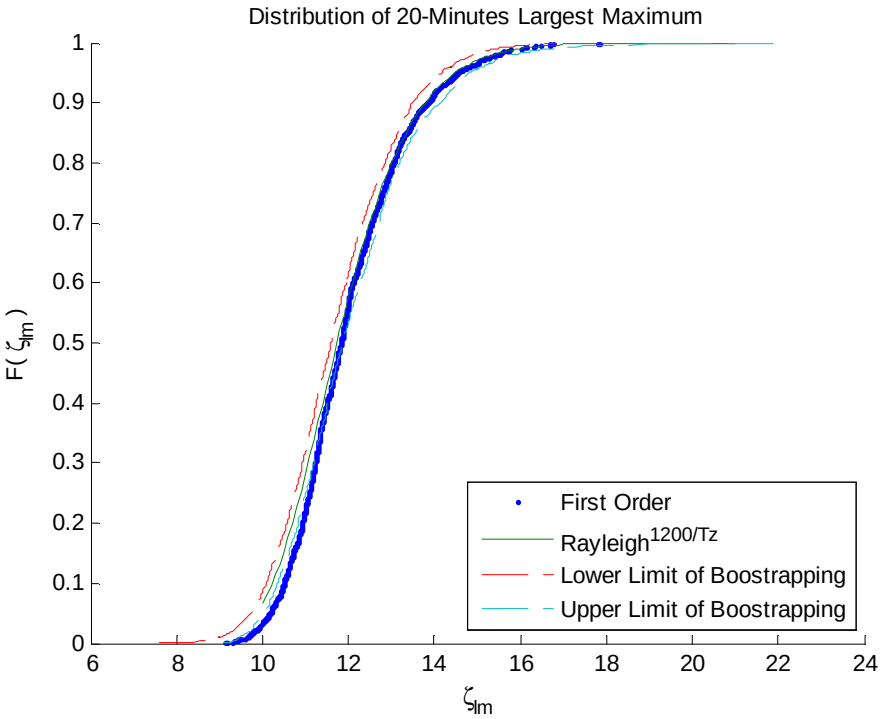

Figure 7.6 CDF of Largest Maximum for Deterministic Amplitude

From the graph, it can be observed that the limit of bootstapping is really close to the Rayleigh CDF. This means the uncertainty in producing empirical CDF is significantly decreased by using 900 samples. The upper tail empirical CDF shows a good agreement with theoretical CDF since it still locates inside the bootstraping limit. Eventhough the lower tail of empirical distribution is slightly out of the bootstraping limit, it is concluded that the empirical CDF agrees with Rayleigh.

To construct the distribution of 3-hour largest maximum, the largest maximums of 20-minute simulation are gathered. Without sorting the value, the 900 20-minutes largest maximum samples are separated into 100 groups where each group consists of 9 samples. Since the sample are not sorted, the randomness of the data is maintained. Hereinafter, the largest maximum of each group is collected and sorted to establish the empirical distribution.

Figure 7.7 shows the distribution of 3-hour largest maximum for the first order sea surface with deterministic amplitude (up) and ramdom amplitude (down). From both figure, it is concluded that partition of time series method produces a good model based on fact the the empirical CDF agrees well with the theoretical CDF and located inside the bootstraping limit. In addition, for

first order sea surface, the partition of time series method requires only 30% of complete 3-hour computational time to create single 3-hour simulation of sea surface. More empirical distributions from utilizing partition of time series presented in the appendix.

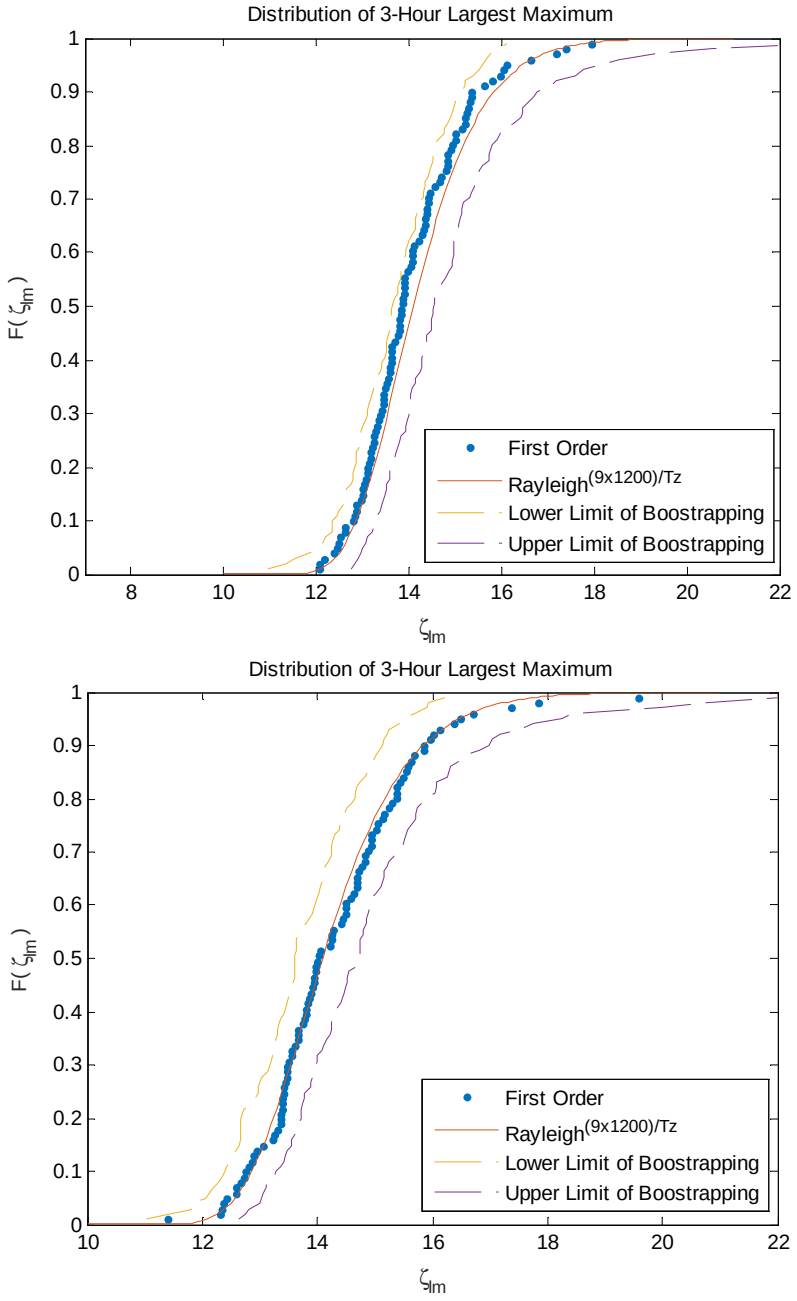

Figure 7.7 CDF of Largest Maximum for for Time Series Partition

7.2.3.2. Random frequency

Figure 7.8 shows the empirical distribution of using random frequency scheme with deterministic amplitude. In this case, the same number of harmonic component as complete 3-hour analysis is used. It shows that the random frequency scheme shows a good agreement between its empirical CDF and theoretical CDF. Therefore, the analysis is continued by reducing number of component.

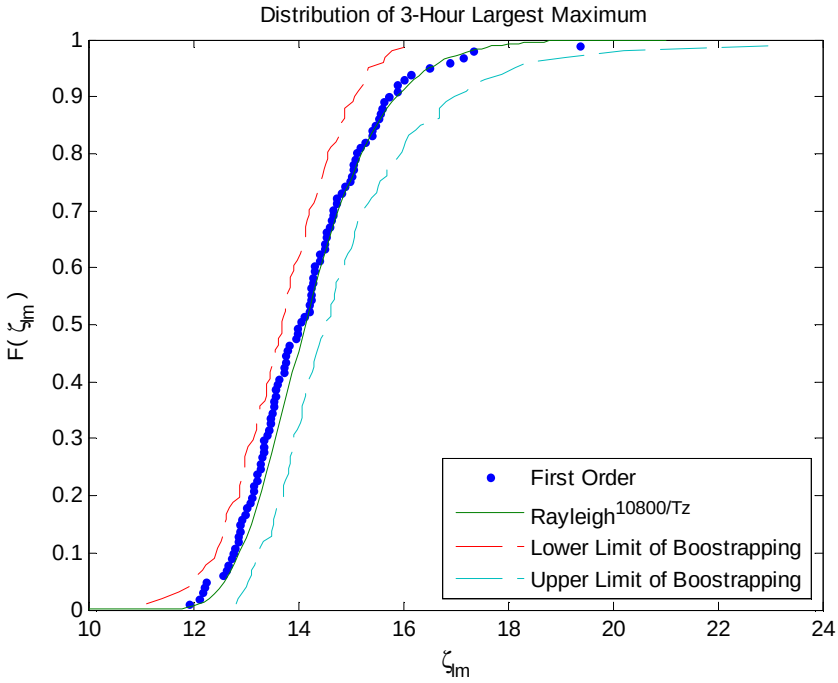

Figure 7.8 CDF of Largest Maximum for Random Frequency

In this case, the minimum frequency is set as $2\pi/T_f = 2\pi/10800$ while the maximum frequency is equal to $2\pi/\Delta t = 2\pi/0.5$. The frequency interval ($\Delta\omega$) is adjusted to give the desired number of harmonic component. To perform complete 3-hour analysis where $\Delta t = 0.5s$, at least 10800 harmonic components shall be used. Therefore, the analysis observes the effect of six different number of harmonic components to the empirical distribution, which are 100, 200, 500, 1000, 2000, and 5000. From the simulation, it is found that even by using 500 harmonic components, the empirical distribution is still in the range of bootstraping limit. When the simulation uses 100 and 200 harmonic component, the empirical distribution falls out of the bootstrapping limit. Hence, it is concludex that in this case, at least 500 harmonic component should be used to simulate 3-hour sea surface when the random frequency and deterministic amplitude method is

performed. However, the effect on structure responses is still questionable. Figure 7.9 shows the distribution of 3-hour sea surface largest maxima.

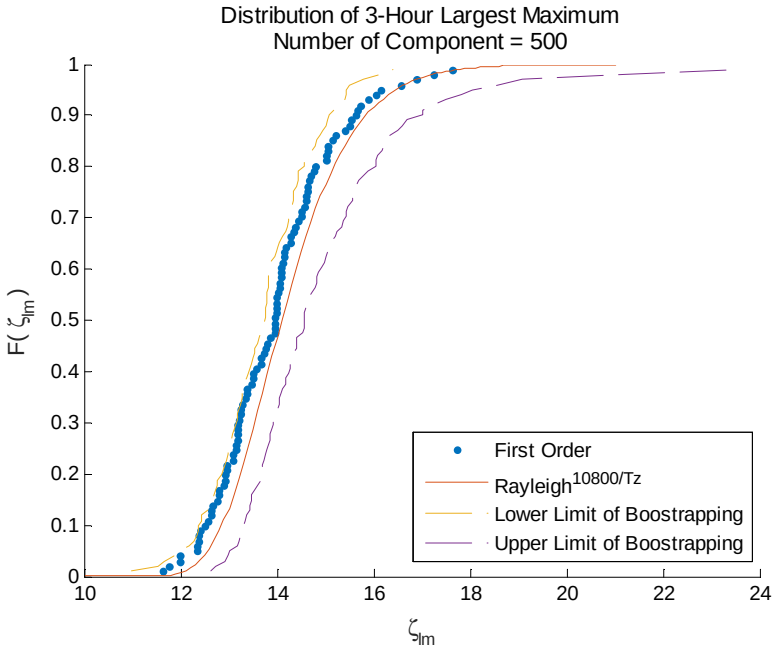

Figure 7.9 CDF of Largest Maximum for Random Frequency with Deterministic Amplitude number of component = 500

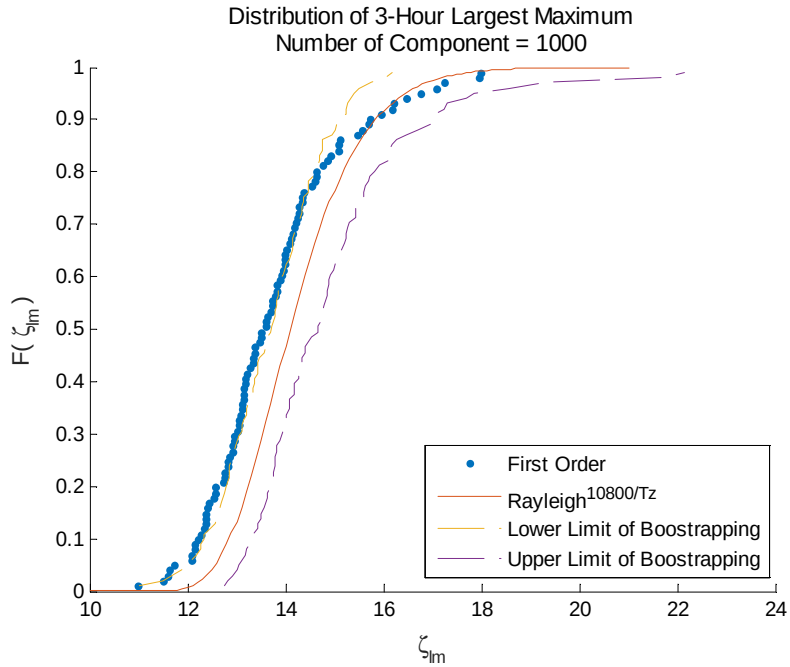

Figure 7.10 CDF of Largest Maximum for Random Frequency with Random Amplitude number of component = 1000

Introducing random amplitude, empirical distribution of largest maximum by using random frequency is already fall out from bootstraping limit when 500 harmonic components are used. Moreover, from different realizations, the lower tail of empirical distribution generally deviate from theoretical distribution. It indicates that combining random amplitude and frequency increasing the uncertainty in the empirical distribution. Figure 7.8 shows the distribution of 3-hour largest maximum sea surface from random frequency and random amplitude with 1000 components. It seems that even by using 1000 components, the empirical distribution shows questionable result. More distributions are presented in appendix 13.

7.2.3.3. Equal Area

Similar to the analysis which is performed in random frequency, the minimum frequency is set as $2\pi/T_f = 2\pi/10800$ while the maximum frequency is equal to $2\pi/\Delta t = 2\pi/0.5$. The frequency interval ($\Delta\omega$) is adjusted to give the desired number of harmonic component. Seven different numbers of component are observed, which are 50, 100, 200, 500, 1000, 2000, 5000. In addition, the deterministic amplitude is used. It is found that even by using 50 harmonic components, the empirical CDF still match correctly with the theoretical CDF. Figure 7.11 shows this result. The other empirical distributions, which corespond to the other number of component, are presented in appendix 14.

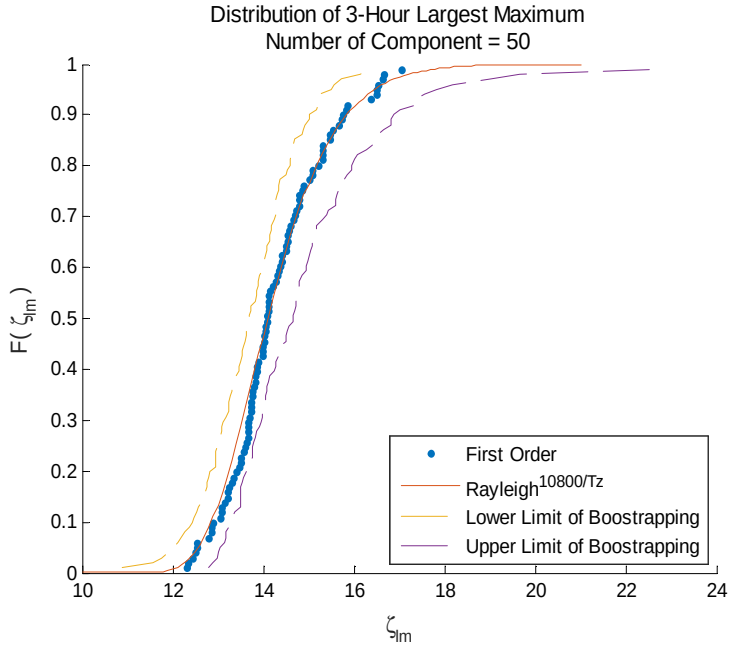

Figure 7.11 CDF of Largest Maximum for Equal Area with Deterministic Amplitude number of component = 50

When utilizing random amplitude, performing equal area with 50 harmonic components still produces an empirical CDF that agrees well with theoretical distribution at the upper tail. However, there is a possibility that the empirical CDF underestimates the value at the lower tail. Figure 7.12 shows distribution of 3-hour largest maximum of sea surface for equal area and random amplitude utilizing 50 harmonic components. Therefore it can be concluded that the equal area method could simulate 3-hour sea surface with smaller number of component than random frequency and partition of time series method. However, similar to the random frequency, the effect on structure response is still questionable.

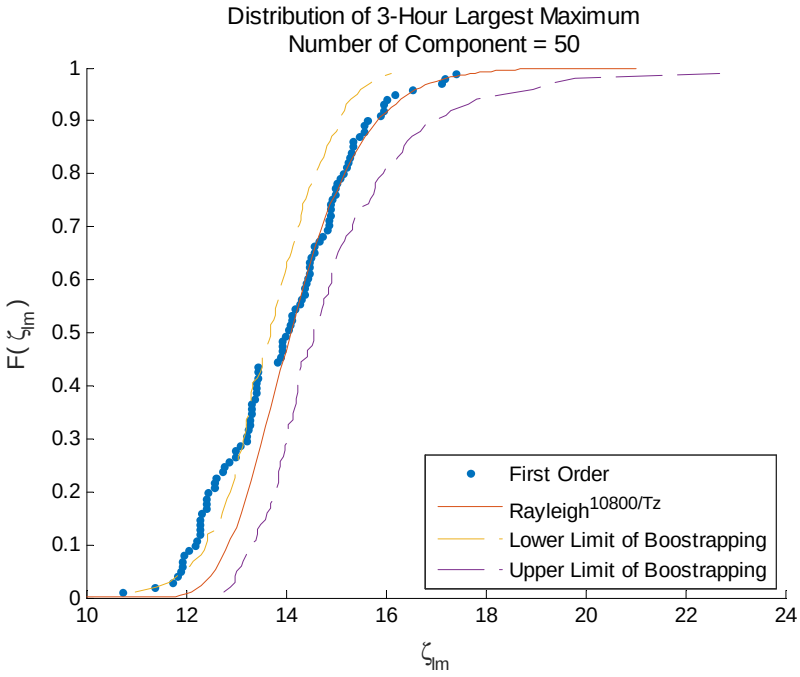

Figure 7.12 CDF of Largest Maximum for Equal Area with Random Amplitude number of component = 50

7.2.4. Effect of cut-off frequency

In section 2.5, for second order wave simulation, some cut-off frequencies are introduced for kinematic calculation purposes. In this section, the effect of introducing cut-off frequency (ω_{cut}) on first order sea surface is observed. The 3-hour time series of first order surface is produced from equidistance frequency interval method with deterministic amplitude. Figure 7.13 shows the effect of introducing different cut-off frequencies to distribution of maximum sea surface (ζ_{lm}) while table 7.1 shows the change in variance of sea surface (σ_ζ) coresponds to the cut-off freuquency. $\sigma_\zeta = 13.95$ when the ω_{cut} is not introduced.

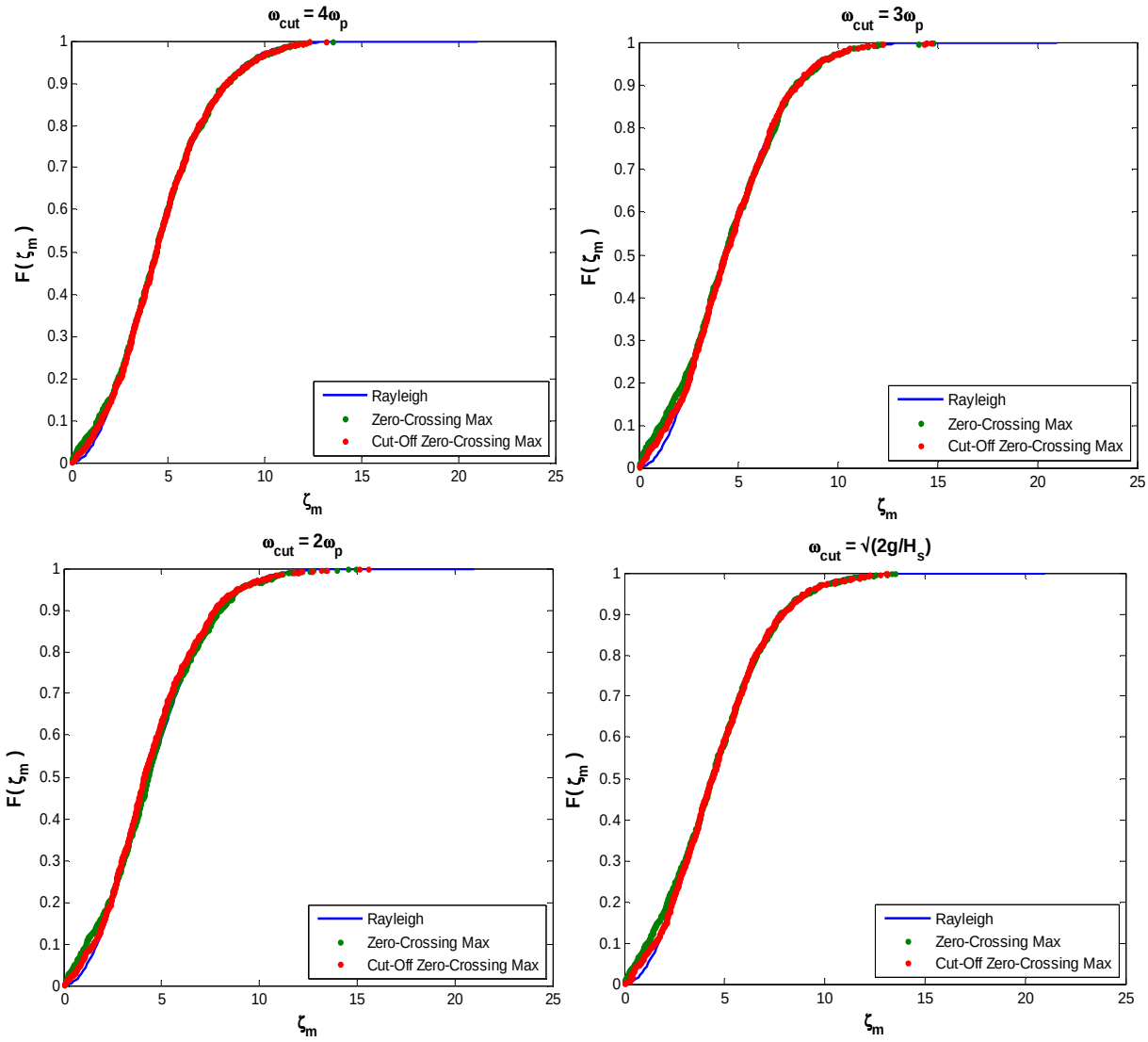

Figure 7.13 Effect of Cut-off Frequency in Maximum Surface CDF

Table 7.1 Variance after Introducing Cut-off Frequency

No	Cut-Off Frequency (ω_{cut})	Spectrum Variance (m_o)	Time-Series Variance (m_o)
1	$4\omega_p$	13.90	13.90
2	$3\omega_p$	13.79	13.79
3	$2\omega_p$	13.19	13.19
4	$\sqrt{2g/H_s}$	13.77	13.77

It can be observed that by introducing ω_{cut}, the lower tail of empirical distribution shift closer to the Rayleigh distribution. This behaviour is more apparent in second order sea surface

distribution. Therefore, it is confirmed that high frequency components is the reason why the lower tail of empirical distribution does not follow Rayleigh distribution as it is explained in section 7.2.1. In addition, introducing stansberg cut-off ($\omega_{cut} = \sqrt{2g/H_s}$) still gives acceptable variance of sea surface. The loss of variance will be covered up by introducing second order corection.

7.2.5. Second Order Sea Surface

The second orer sea surface is generated by utilizing equation 2.57. To save time and the usage of CPU memory, the 3-hour simulation is performed by partition of time series where the 9 different 20-minutes simulations are performed. Figure 7.14 shows the time series of the second order sea surface aroung the largest maximum value. In this case, the random amplitude is used.

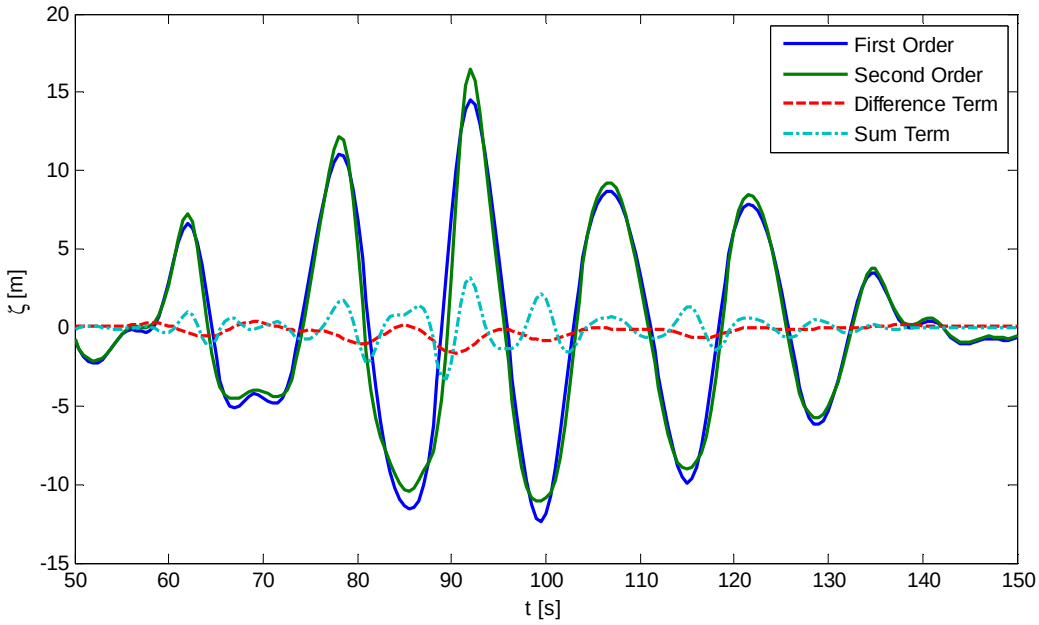

Figure 7.14 Time Series of Second Order Sea Surface

In figure 7.14, the shape of second order surface depends on the first order surface and the correction terms. The correction term consists of two parts, which are sum and difference term. It seems that at the largest maximum second order surface, the sum term has its maximum value (the crest of sum term). However, at the same time instance, the difference term does not has its minimum value (the trough of difference term). Forristal [18] illustrated the same behaviour in his second order model. Therefore, it is concluded that the difference term is not always has the minimum value at the largest maximum second order surface elevation.

7.2.6. Distribution of maximum second order sea surface

For second order sea surface, the distribution of maximum is assumed follows Forristal distribution of wave crest which is expressed in equation 3.26. Therefore, to verify the model of second order sea surface, the empirical CDF is compared to Forristall CDF. Figure 7.15 shows the comparisson between empirical CDF and the Forristall CDF for determinisitic amplitude case without the cut-off frequency. More empirical CDFs are presented in appendix 16.

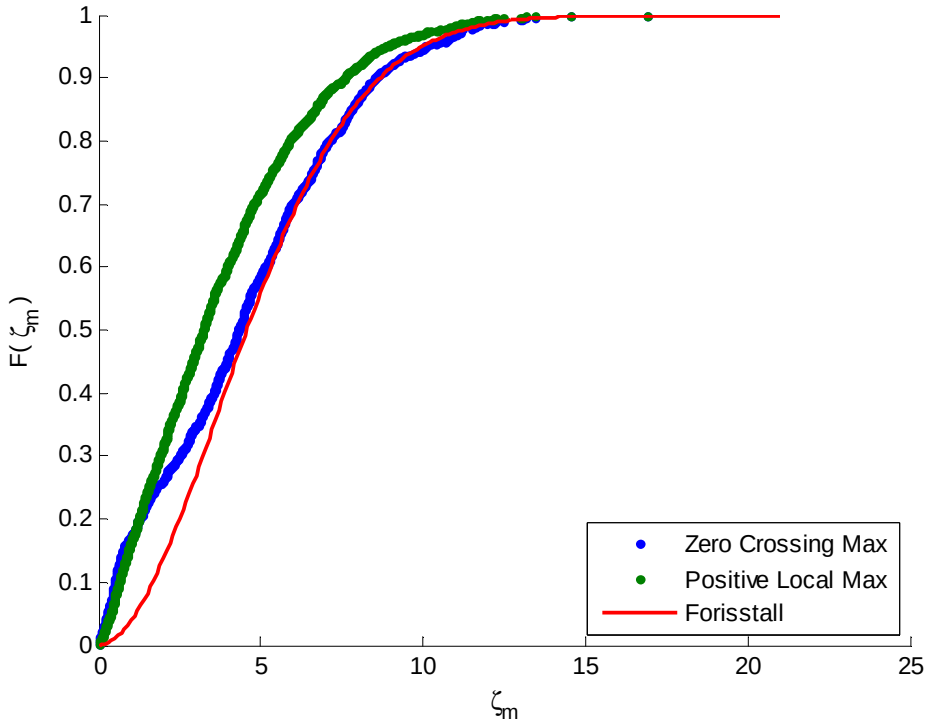

Figure 7.15 CDF of Maximum Sea Surface for Deterministic Amplitude

In figure 7.15, the theoretical distribution is compared to empirical distribution of zero-crossing and positive local maxima. The empirical distribution of zero-crossing maximum shows good agreement with theoretical distribution though the empirical CDF of positive local maxima tends to underestimate the Forristall distribution. This means the Forristal distribution is valid for narrowbanded process. Moreover, the lower tail of zero-crossing maxima CDF does not follow the Forristal distribution. Similar to the first order sea surface, this behaviour is caused by the high frequency components, as it is explained in section 7.2.4. Introducing cut-off frequency will force the lower tail of zero-crossing CDF to follow Forisstall distribution.

Figure 7.15 shows a realization where the spectrum is not linearized. Though the eqmpirical distribution follows theoretical distribution well, the variance of surface elevation which corresponds to second order correction is calculated twice. To maintain the varince, the spectrum should be linearized by iteration process or introducing a cut-off frequency (explained in section 4.3). In this case, a cut-off frequency ($\omega_{cut} = \sqrt{2g/H_s}$) is introduced. Previously, it is explained that introducing the Stansberg cut-off frequency reducing surface elevation variance from 13.95 to 13.77. However, second order correction term produces additional variance with magnitude 0.12 which means the total variance of surface elevation after introducing second order correction term is equal to 13.89. Though this is still smaller than the actual variance from wave spectrum, the difference is negligible.

As explained in section 4.3.2, using ω_{cut} reduces the number of harmonic component. A 20-minutes simulation with $\Delta t = 0.5s$ requires at least 1200 harmonic component for equidistance frequency interval. By introducing ω_{cut}, the number of component is reduced to 244. As a consequence, the simulation save 99% of computational time. Figure 7.16 shows the CDF of maximum sea surface when the cut-off freqeuncy is introduced.

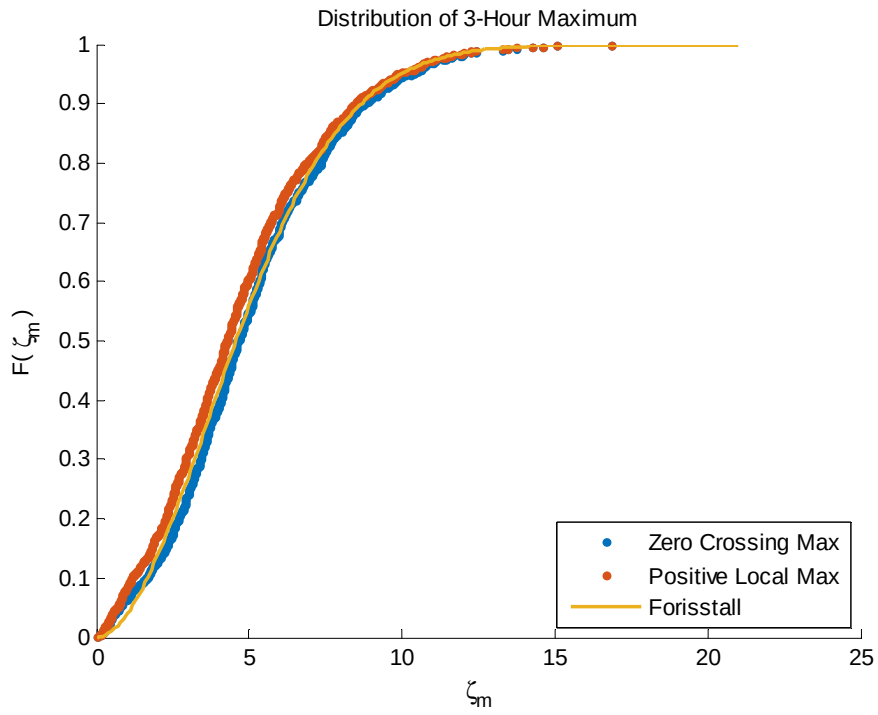

Figure 7.16 CDF of Maximum Sea Surface for Deterministic Amplitude

Introducing cut-off frequency changes the sea surface condition from broadbanded process to narrowbanded. This is proven by the empirical distribution of zero-crossing and positive local maxima which almost coincide. Furthermore, the lower tail of zero-crossing CDF is close to the Forisstall distribution though there is still slight deviation. Therefore, it is verified that the high frequency components are the reason why the lower tail of zero-crossing CDF deviates from theoretical distribution. All in all, the agreement between empirical and theoretical distribution indicates that the model of second order sea surface is verified for partition of time series and determiniestic amplitude.

Figure 7.17 shows the comparisson between theoretical and empirical CDF when random amplitude is introduced. In figure 7.17, empirical CDF of positive local maximum seems also underestimates the Forisstall CDF. Therefore, it is concluded that the Forisstall distribution seems to represent the distribution of zero-crossing maximum which refers to narrowbanded process. In addition, the second order sea surface model is also verified when the random amplitude is introduced.

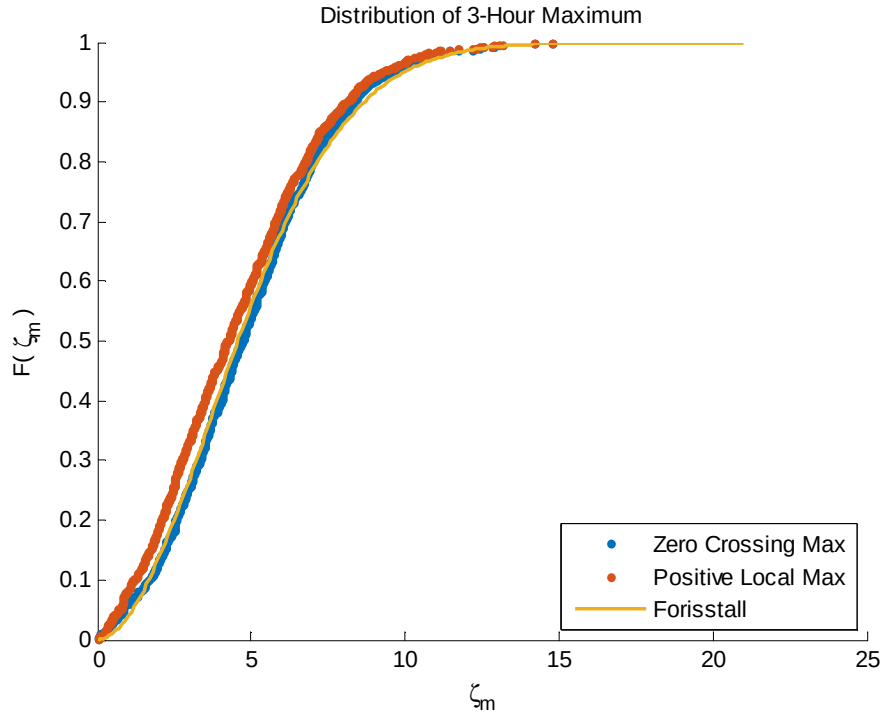

Figure 7.17 CDF of Maximum Sea Surface for Deterministic Amplitude

7.2.7. Distribution of largest maximum second order sea surface

Similar to the first order process, the largest maximum distribution for second order sea surface is expressed as equation 3.17 where $F_{\zeta_M}(\zeta_m)$ is equal to Forisstall CDF. 100 3-hour simulation of second order sea surface is performed. Figure 7.18 shows the comparisson between the empirical CDF and theoretical CDF for second order surface as well as its first order surface component. Equidistance frequency interval with determenistic amplitude method is executed to simulate the surface. The left figure shows the first order part while the right figure coresponds to second order surface. More empirical distributions are presented in appendix 20. Eventhough the shape of empirical CDF does not perfectly follows the theoretical CDF, both first and second order empirical CDF shows good result since they are located inside the bootstraping limit. It is concluded that 100 samples is the main reason for deviation on the shape of empirical CDF. All in all, the second order model with time partition and deterministic amplitude is verified.

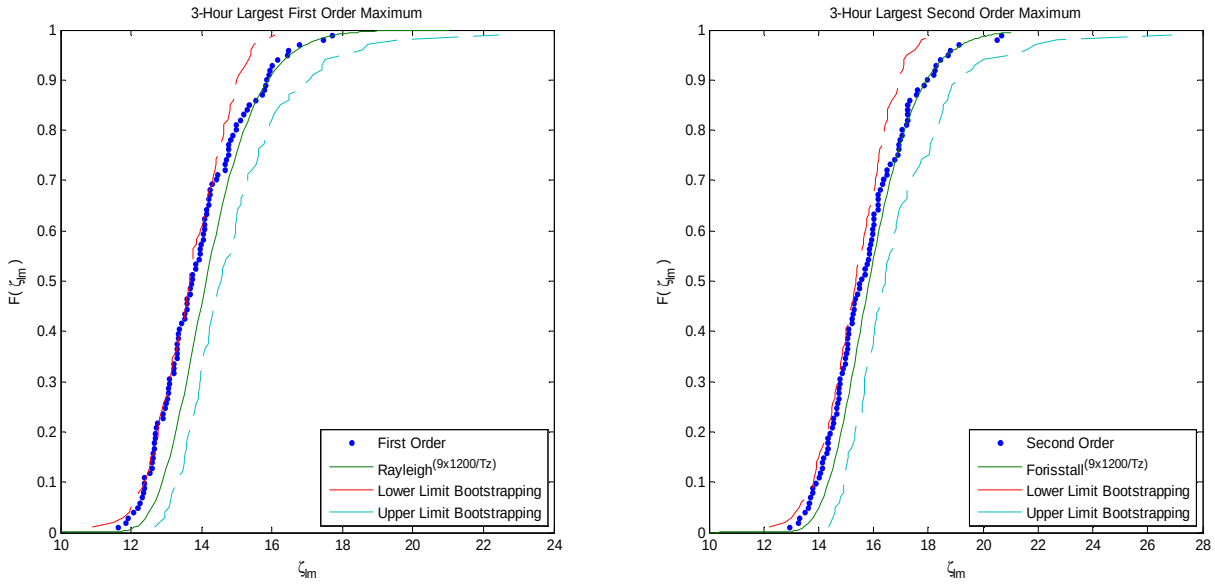

Figure 7.18 Distribution of Largest Maxima for Deterministic Amplitude
Left: First Order; Right: Second Order

CDFs when utilizing the random amplitude are presented in appendix 21. In general, the CDF of second order surface utilizing random amplitude shows a good agreement with theoretical distribution. Therefore, the time partition with random amplitude is considered good enough to simulate 3-hour second order surface.

7.3. Verification of Wave Particle Kinematic

In this case, 20-minute sea surface is performed. The wave particle kinematics along the z-coordinates is observed. In this case, only horizontal velocity and acceleration that is analyzed since the forces on the jack-up are mainly affected by these particle kinematics.

7.3.1. First order wave particle kinematics

Three stretching methods for first order kinematics are compared. They are Wheeler stretching, linear extraploation and constant stretching, which are explained at section 2.5. A 20-minute simulation of first order sea surface is performed. Figure 7.24 shows the horizontal velocity and acceleration along the z-coordinate when the largest maximum sea surface occurs. The points along z-coordinate is set be concentrated next to the sea surface. The left figure shows the horizontal velocity while the horizontal acceleration is presented in right figure.

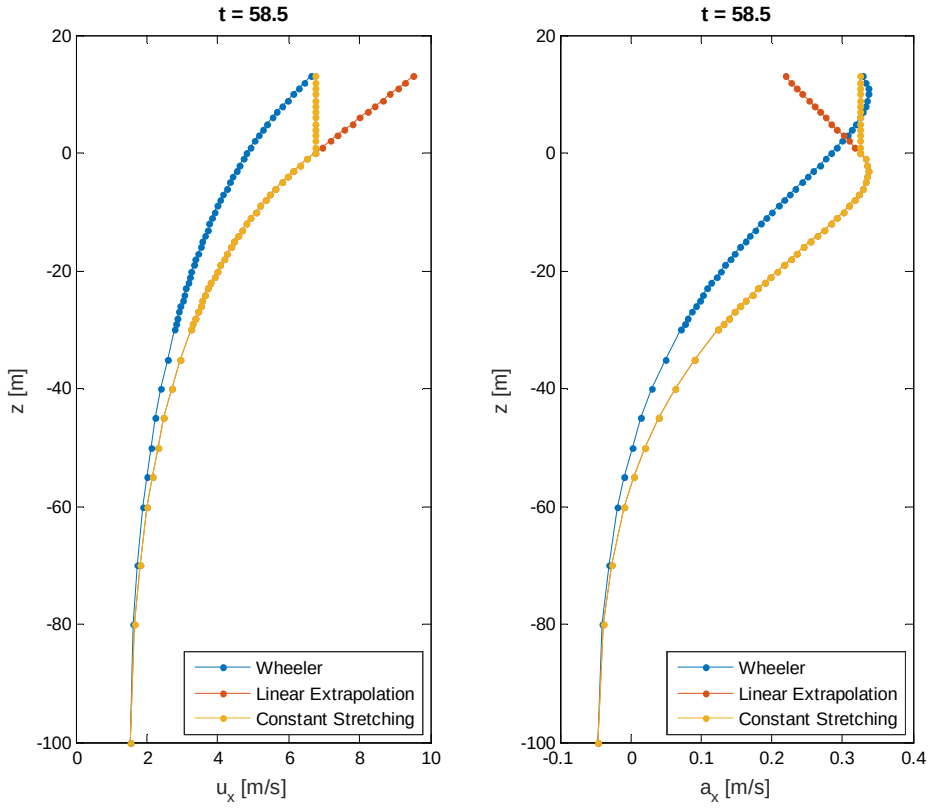

Figure 7.19 Wave Particle Kinematics at Largest Maximum of Sea Surface

In figure 7.19, the linear extrapolation overestimates the surface horizontal velocity while it underestimates the surface horizontal acceleration. The Wheeler stretching is commonly used in

practice while the constant stretching is the stretching method which is proposed when the Airy theory was presented. Therefore, assuming that Wheeler and constant strectching gives the correct value of surface particle kinematics, it is not suggested to use linear extrapolation for first order sea surface. Wheeler stretching mainly produces smaller wave particle kinematics than constant strectching which will cause smaller base shear and overturning moment. Therefore, the usage of Wheeler stretching is questionable for large crest or trough.

From the same simulation, it is found that largest horizontal acceleration exist at the mean sea surface. Figure 7.20 shows the particle kinematics when the horrizontal acceleration occurs. In this case, the particle kinematics from all method are coincided.

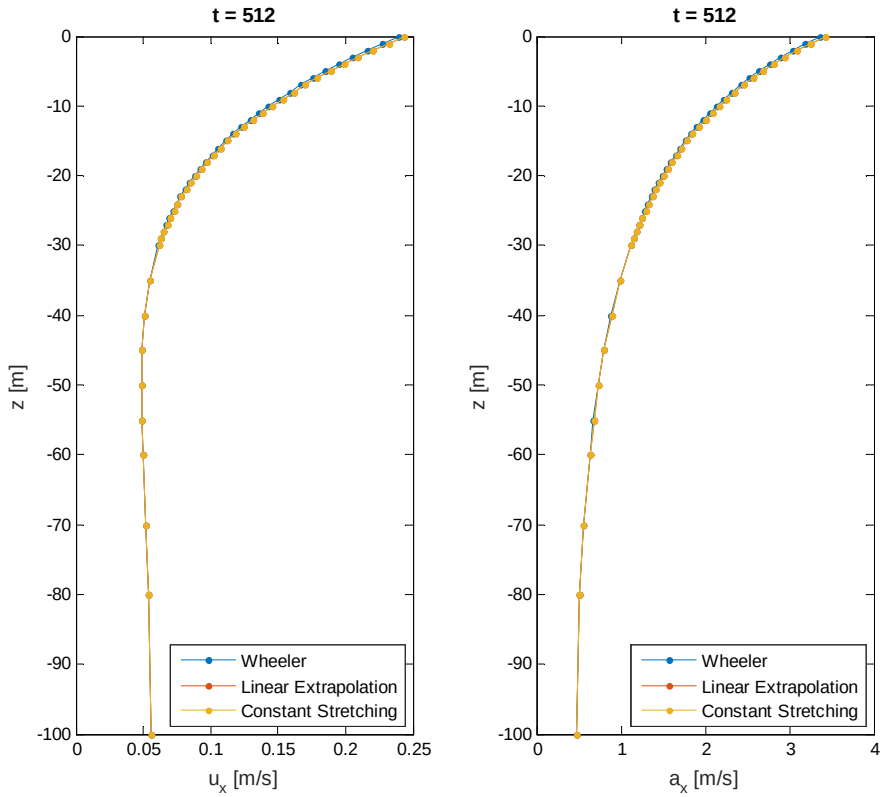

Figure 7.20 Wave Particle Kinematics at Largest Maximum of Sea Surface

For regular wave, larger crest height produces larger horizontal surface velocity while the largest horizontal surface acceleration always occurs at the mean surface. However, for irregular sea, the largest horizontal velocity may occur not at the largest maximum surface elevation. This is illustrated by figure 7.21 where the time instance of maximum value is indicated by dash line.

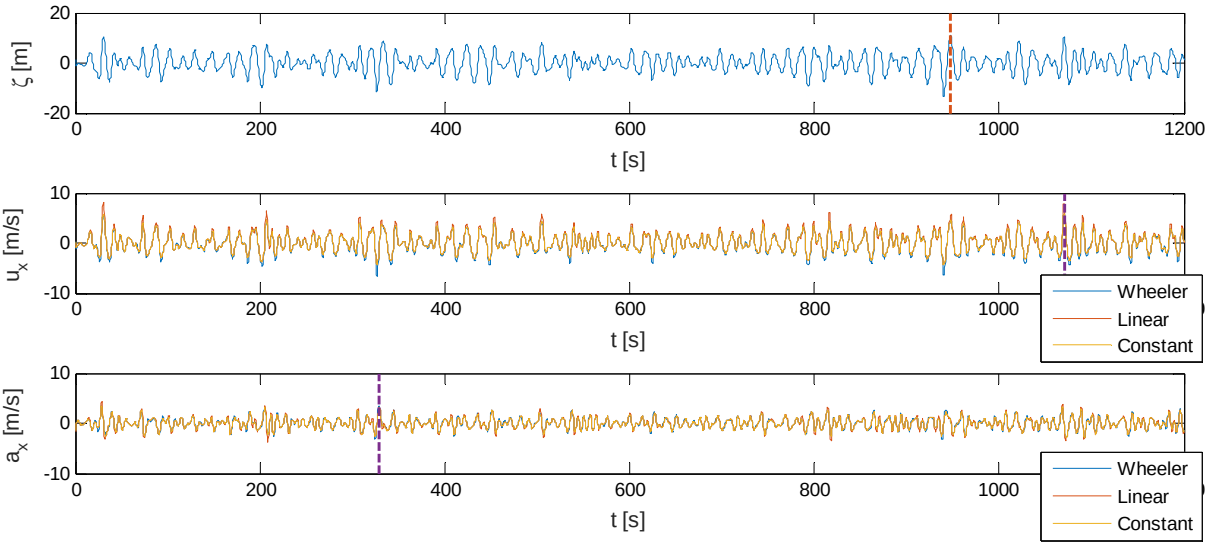

Figure 7.21 First Order Sea Surface, Horizontal Velocity and Horizontal Acceleration

In figure 7.21, the maximum horizontal velocity does not occurs at the same time instant as largest sea surface maximum. In addition, the largest horizontal acceleration does not occur at the mean sea surface. Figure 7.22 shows the particle kinematics when the largest horizontal acceleration occurs. In this case, Wheeler stretching takes the horizontal acceleration at mean surface as the horizontal acceleration at true surface. As a result, Wheeler stretching overestimates the horizontal acceleration at true surface.

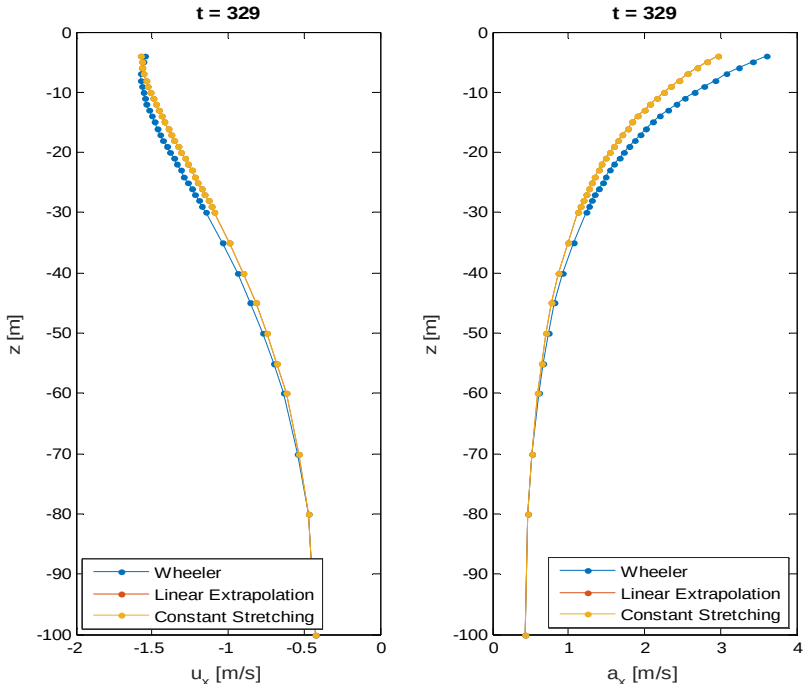

Figure 7.22 Particle Kinematics When Largest Horizontal Surface Acceleration Occurs

7.3.2. Second order wave particle kinematics

For second order wave case, the Wheeler and linear extrapolation method is used to find the wave particle kinematics along the z-coordinate. As explained in section 2.5.2, to perform the Wheeler stretching, the second order sea surface should be linearized first. In this case, the second order surface is determined first by utilizing equation 2.57. By using discrete Fourier transform, which is expressed in equation 4.4), a new set of harmonic component is determined. Combining equation 4.10 and 4.13, the new amplitude of harmonic component i ($\zeta_{a1,i}{}'$) can be determined by:

$$\zeta_{a1,i}{}' = 2|\bar{\zeta}(\omega_i)| \tag{7.2}$$

In this study, the phase is determined by combination of two MATLAB functions which are *angle( )* and *unwrap( )*. *angle*( ) is used to determine the phase angle of complex number while *unwrap( )* corrects the phase angle. The wave particle kinematics are determined from first order kinematics utilizing the new set of harmonic component. In this study, the fast Fourier transform is used where the number of harmonic component is expressed as a power of 2.

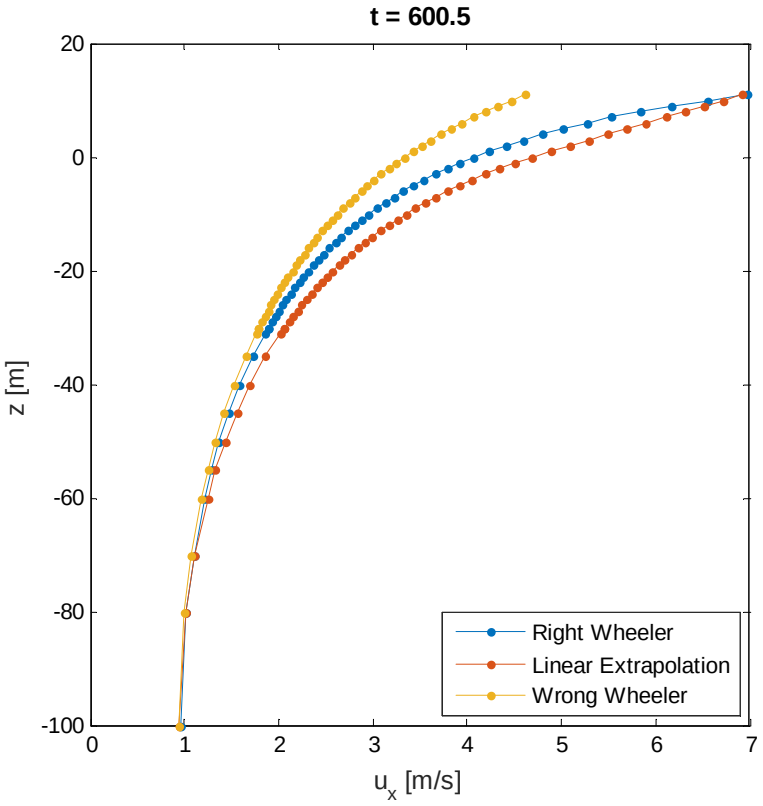

Figure 7.23 Second Order Horizontal Velocity at Largest Sea Surface Maximum

Figure 7.23 shows the comparisson of horizontal velocity along the z-coordinate from linear extrapolation, 'right-way' Wheeler stretching (linearized Wheeler) and 'wrong-way' Wheeler stretching. In figure 7.23, the appropirate way of using Wheeler stretching produces surface horizontal velocity which is similar to linear extrapolation result. Performing Wheeler inappropritely (where the second order kinematics is directly stretched without linearization) greatly underestimates the surface kinematics. In addition, the Wheeler stretching gives lower magnitude of horizontal velocity than linear extrapolation along the z-coordinate.

Figure 7.24 shows the condition of wave particle kinematics when the largest horizontal acceleration from linear extrapolation occurs. From figure 7.25, it can be observed that the linear extrapolation shows lower value than Wheeler stretching for horizontal acceleration. However, there is a disagreement between horizontal velocity profile from Wheeler and linear extrapolation.

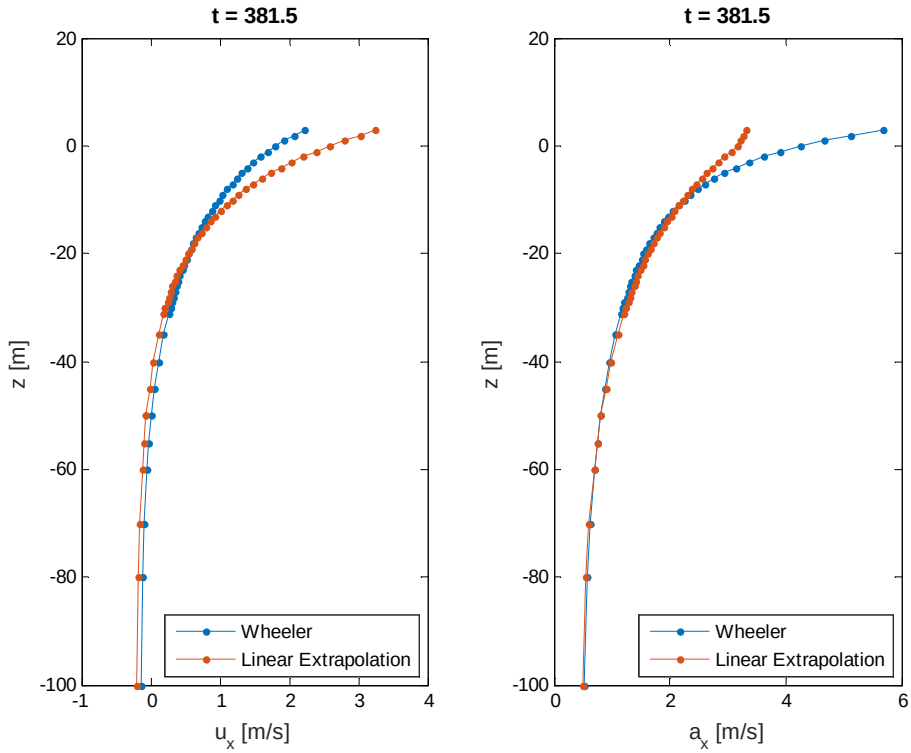

Figure 7.24 Second Order Horizontal Velocity at Largest Horizontal Acceleration

As explained at section 2.5, the cut-off frequency for second order Wheeler and linear extrapolation is different. The suggested cut-off freuqeuncy for Wheeler stretching is $4\omega_p$ which is higher than linear extrapolation cut-off frequency ($\omega_{cut} = \sqrt{2g/H_s}$). As a consequence, range

of the included freqeuncy is broader for Wheeler stretching than linear extrapolation. In addition, the range of difference frequency is also increased. It is suspected that the second order difference term on the rich energy part of the spectrum is the main reason for the difference in figure 7.24. This is because the behaviour of the different between the two methods is more close to the behaviour of high frequency component which has faster decay rate than the lower frequency. However, only difference term that is located on the rich energy part of the spectrum that has adequate amplitude and frequency to give significant different between Wheeler and linear extrapolation kinematics.

Since the linear extrapolation calculates the magnitude of second order kinematics correctly up to the mean sea surface, using Wheeler stretching for second order wave will underestimate the total drag load along the cylinder. Therefore, using linear extrapolation for second order sea is considered better than Wheeler stretching. This consideration is supported with the comparisson of wave load in section 7.4.

7.3.3. Comparisson between second order model and 5th Stokes wave

To verify the particle wave kinematics calculation, the second order model is compared to 5th Stokes. In design, 5th Stokes wave is the common theory to determine the perticle kinematics at the largest crest. The 5th Stokes does not produce the exact particle kinematics around the extreme crest though it shows a good agreement with the exact value. Therefore, if the second order model is good enough, the particle kinematics do not significantly deviate from 5th Stokes wave.

The 5th Stokes wave is generated by using the software which is built by Fenton [16]. First, the effect of wave period and height on the particle kinematics of 5th Stokes wave is observed. Three different combinations of wave height and wave period are presented. In addition, it is checked that the combinations are still inside the wave breaking limit. The water depth is 100 m.

Table 7.2 Combination of Wave Height and Period

No	Wave Height (s)	Wave Period (s)	Upper limit of Wave Height (m)
1	28	13	36.3
2	28	16	49.4
3	31	13	36.3

Table 7.2 shows the combination of wave height and period including its upper limit of wave height for wave breaking. The upper limit of wave height is determined by using equation 2.79. It is confirmed that all the wave height is below their upper limit. Therefore, three different 5th Stokes waves are established and compared. Figure 7.25 shows the sea surface, the maximum horizontal velocity and maximum horizontal acceleration. It seems the maximum horizontal velocity always occurs at wave crest while the maximum horizontal acceleration does not occur at mean surface level as predicted by Airy theory.

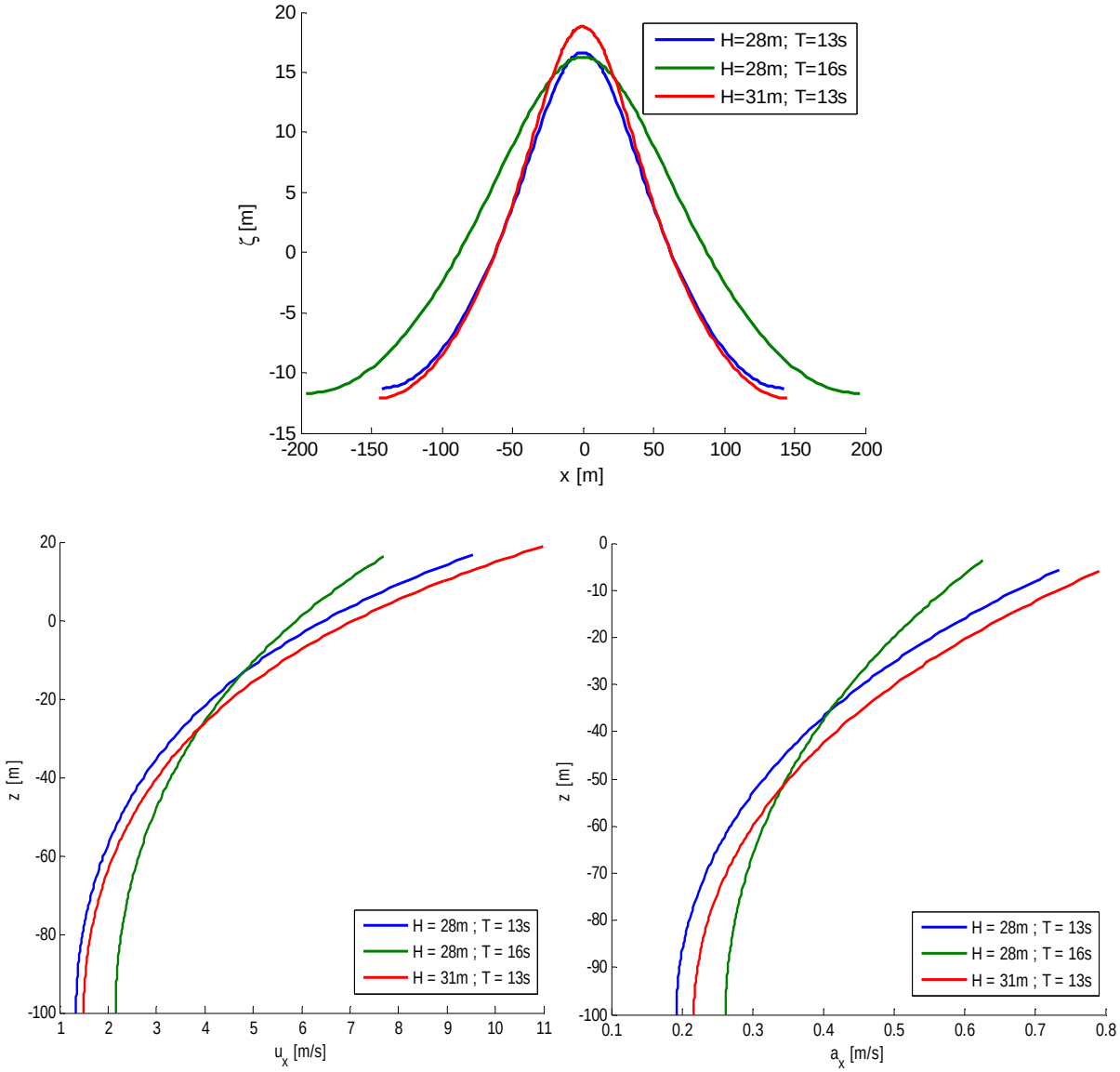

Figure 7.25 5th Stokes from Three Different H and T Combination
Up: Surface; Down Left: Max Horizontal Velocity; Down Right: Max Horizontal Acceleration

Some observations are made and summarized.

1) Increasing wave height increases the wave crest
2) Increasing wave height increases the horizontal velocity and acceleration both at the sea bottom and sea surface
3) Increasing wave period decreases the wave crest
4) Increasing wave period increases both horizontal velocity and acceleration at the sea bottom but decreases them at the sea surface.

As briefly explained in section 2.6.1, the amplitude of surface elevation for 5th Stokes wave component is found from iteration process which is proportional to wave stepness (H/λ). Therefore, point 1) and 3) is acceptable. In additon, horizontal velocity and acceleration is also proportional to wave height which verify the point 2). For Stokes wave, both horizontal velocity and acceleration contain $cosh(k(z+d))$ term. Increasing wave length (decreasing wave number) will decrease the decay rate of $cosh$ ( ) term. Therefore, the behaviour on observation 4) is based on this reason.

In the nextstep, comparisson is made between the second order model and the 5th Stokes. 100 3-hour simulations of second order surface are performed utilizing partition of time series method with deterministic amplitude. The largest surface maximum from each simulation is gathered and sorted then the horizontal velocity is established for each result by utilizing linear extrapolation.

For second order model, the largest surface maximum and its two adjacent troughs are assumed as a single wave. The wave period is determined as the time interval between the two adjacent trough. In addition, the wave height is assumed as the distance between the largest surface maximum and the lowest value between the two neighbouring troughs. For 5th Stokes wave, the wave height is iterated in order to produce the same crest as the largest surface maximum of second order simulation while the period is equal to second order model period.

Figure 7.26 shows an example of fitting a 5th Stokes wave into the second order model. In this case, the period of 5th Stokes is set to be equal to the period of second order model (time interval between two red point). However, to produce the same crest, the 5th Stokes should has a larger wave height than the second order model. The horizontal velocity when the crest occurs is presented in figure 7.27.

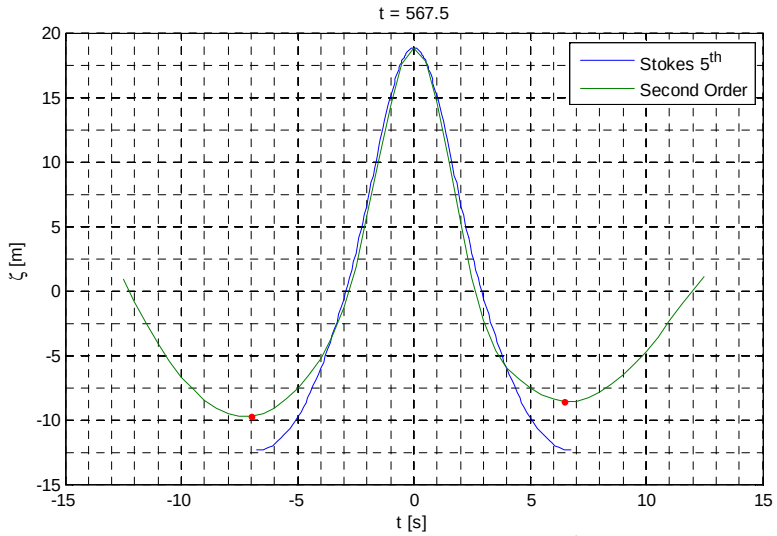

Figure 7.26 Second Order Surface Model vs 5th Stokes Wave

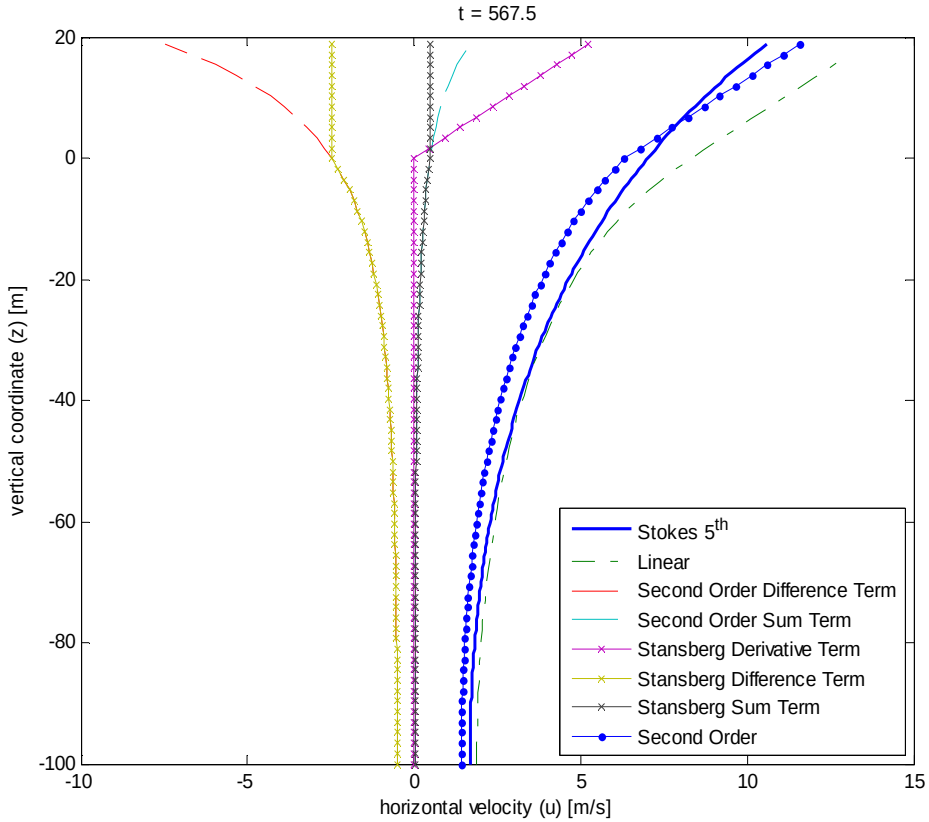

Figure 7.27 Horizontal Velocity: Second Order Model vs 5th Stokes

The Stansberg term refers to linear extrapolation term (since the linear extrapolation method was presented by Stansberg previously) to avoid confusion with linear (first order) term. In figure 7.27, at sea surface, the second order horizontal velocity has smaller magnitude than 5th Stokes. However, 5th order Stokes gives larger result than second order model below the mean surface.

When it is compared to linear (first order) horizontal velocity, the 5th Stokes gives small deviation below certain z coordinate (in this case, below -20m). On the other hand, the second order horizontal velocity produces smaller magnitude than first order horizontal velocity. This is explained by the existance of difference term. It seems that for second order wave, the magnitude of difference term is significant to reduce the first order horizontal velocity along the z coordinate. Moreover, the magnitude of sum term is not adequate to give an important effect to the second order horizontal velocity.

In figure 7.27, it is also obvious why the difference and sum term above the mean sea surface are set equal as the magnitude on mean sea surface (this was indicated by the Stansberg difference and sum term) for linear extrapolation method. If the difference term is not set equal to the magnitude of difference term at mean sea surface, the second order horizontal velocity will greatly be reduced which makes the second order kinematic amiss. As the consequence, the exponential behaviour above the mean surface is lost since the increment of wave particle kinematics only depends on the derivative term.

From the 100 3-hour simulations, to establish the same wave crest, the 5th Stokes wave height does not always has larger magnitude than second order model wave height. Figure 7.28 shows an example of 5th Stokes wave which has smaller wave height than second order model to produce the same wave crest.

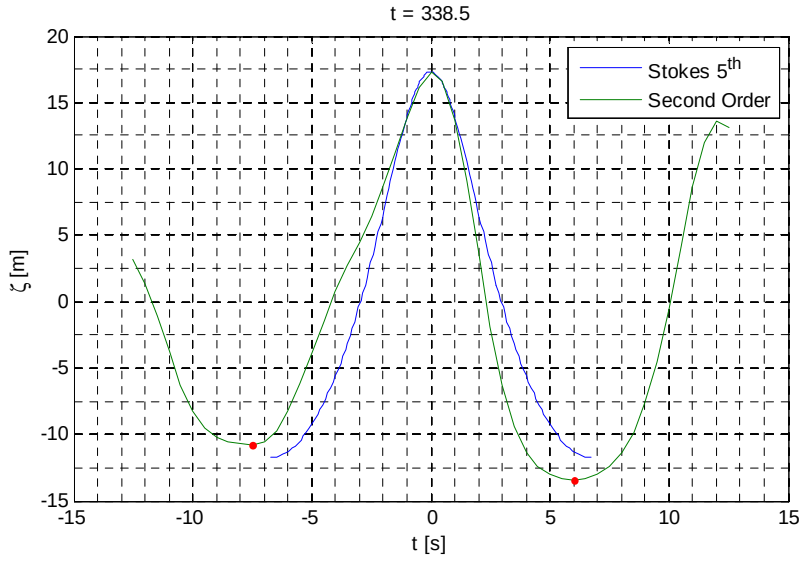

Figure 7.28 Second Order Surface Model vs 5th Stokes Wave

The horizontal velocity at wave crest is presented in figure 7.29. From figure 7.29 and and 7.27, it can be observed that either when the 5th Stokes wave height is smaller or larger than second order model wave height, the 5th Stokes tends to produce larger horizontal velocity below mean sea surface and smaller velocity at the sea surface. However, there is a possibility that this behaviour does not occur.

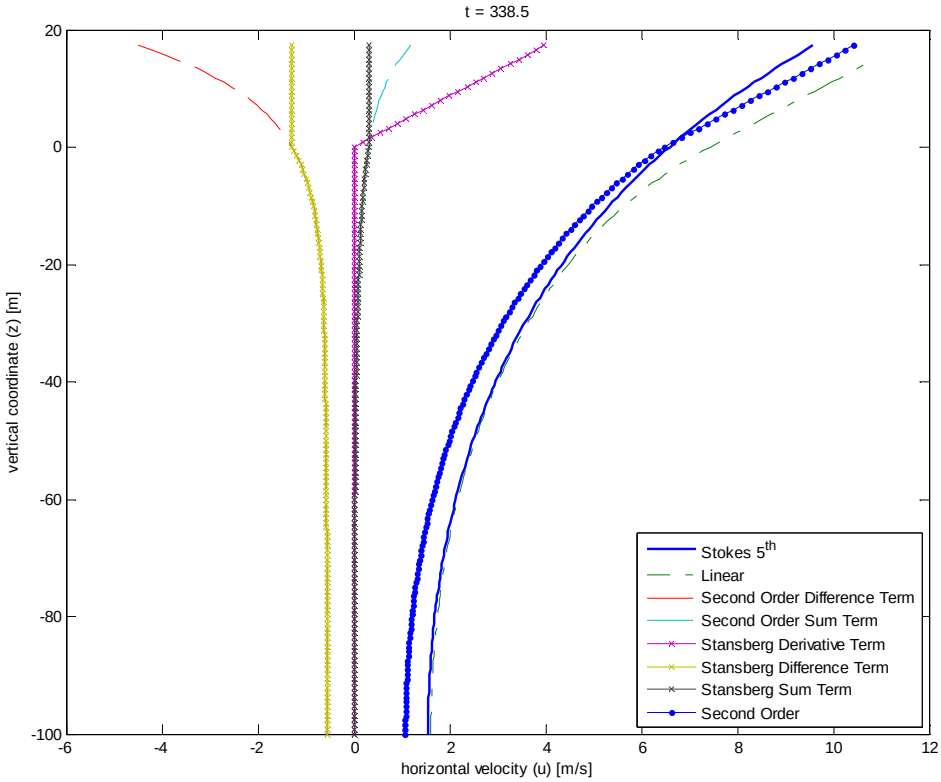

Figure 7.29 Horizontal Velocity: Second Order Model vs 5th Stokes

For linear extrapolation, the magnitude of second order horizontal velocity along the z-coordinate is affected by the first order, sum, difference and derivative term. The sum term contribution to the second order is smaller than the other term. For wave crest, the sum term and linear term exhibits a positive exponential behavior along the z-coordinate while the derivative term follows a positive linear function. However, a special attention should be made on the difference term. For 2-D wave, the difference term of horizontal velocity ($u_{x,min}$) can be simplified as:

$$u_x^- = \sum_{i=1}^{N} A_{u_x^-,i}\, cosh\big(k_i^-(z+d)\big)\, cos\,(k_i^- x - \omega_i^- t + \varepsilon_i^-) \qquad (7.3)$$

$A_{u_x^-,i}$, k_i^-, ω_i^-, and ε_i^- respectively are the amplitude, wave number, wave angular frequency and phase of difference term component *i*. It can be proven that $A_{u_x^-,i}$ and $cosh\left(k_i^-(z+d)\right)$ always have positive value. However, the sign of $cos\,(k_i^- x - \omega_i^- t + \varepsilon_i^-)$ depends on parameter *x* and *t*. To analyze the horizontal velocity along the z-coordinate, the equation 7.3 can be simplified as:

$$u_x^- = \sum_{i=1}^{N} \overline{A_{u_x^-,\iota}}\, cosh\left(k_i^-(z+d)\right) \tag{7.4}$$

At the wave crest, $\overline{A_{u_x^-,\iota}}$ commonly has a negative value. In this case, the difference term profile along the z-coordinate is similar as shown in figure 7.27 and 7.29. However, for particular case, $\overline{A_{u_x^-,\iota}}$ may have positive value for high frequency components. In this case, component with positive $\overline{A_{u_x^-,\iota}}$ has faster decay rate but larger magnitude above mean sea surface. As a consequence, a turning point exists on the horizontal velocity profile along the z-coordinate at the largest surface maximum. Figure 7.30 shows a possible case of this behaviour. More comparisson betwen second order and 5th Stokes horizontal velocity is presented in the appendix.

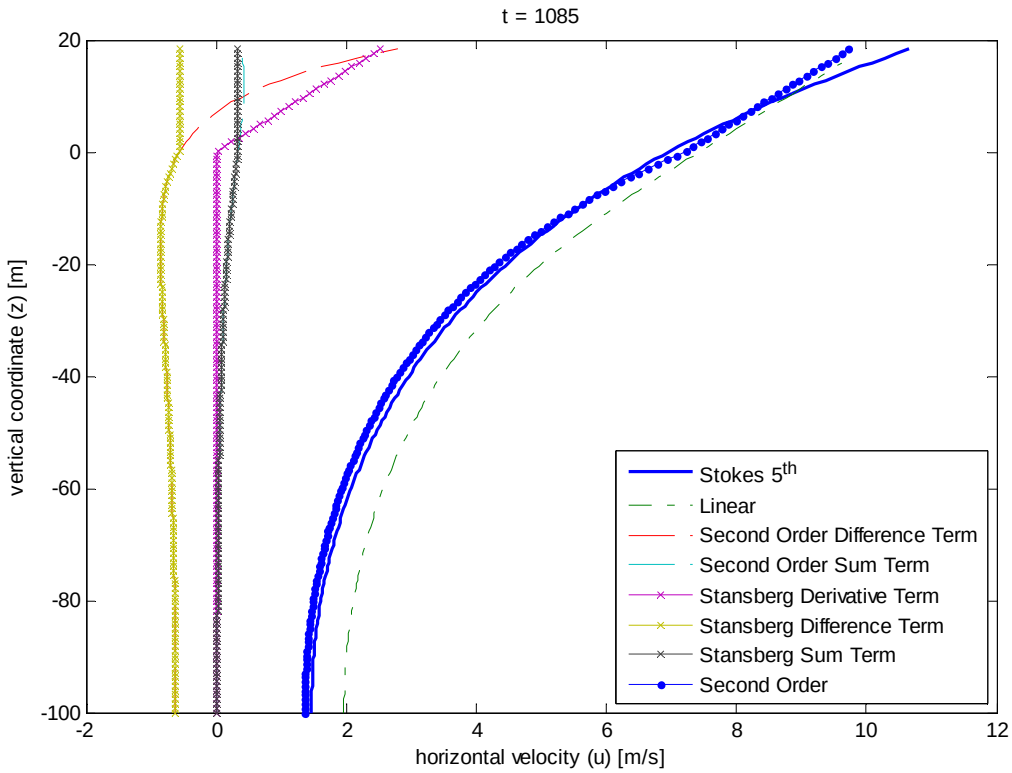

Figure 7.30 Horizontal Velocity: Second Order Model vs 5th Stokes

In this case, there is a possibility that 5th Stokes produces larger surface horizontal velocity at the surface. In addition, for some cases, it is found that the 5th Stokes wave could produces smaller horizontal velocity than second order model at the sea bottom. Therefore, it is concluded that the magnitude of second order model is irregular though it tends to produce larger magnitude at surface and smaller magnitude at sea bottom than 5th Stokes wave. In addition, the 5th Stokes has zero horizontal accelearation along z-coordinated at wave crest while the second order model has certain magnitude. Therefore, using 5th Stokes on non-drag dominated structure is questionable.

Table 7.3 shows the comparisson of wave height between second order model and 5th Stokes wave for 15 different largest surface maximums. In addition, the horizontal velocity is applied to a cylinder with diameter (D) 1m with C_D =0.65 and C_M =1.6 for $z > 2m$ and C_D =1.05 and and C_M =1.2 for $z \leq 2m$. The comparisson of static baseshear and overturning moment (which is calculated in MATLAB) between second order model and 5th Stokes is also presented in table 7.3. In general, the 5th Stokes wave gives larger baseshear and overturning moment. The same behaviour is also presented by Evardsen [12], [22] in his work.

Table 7.3 Second Order Model vs 5th Stokes

No	Stokes Wave Height [m]	Second Order Wave Height [m]	Wave Period [s]	Crest [m]	Stokes Base Shear [kN]	Second Order Base Shear [kN]	Stokes Overturning Moment [kNm]	Second Order Model Overturning Moment (kNm]
1	31.279	28.604	13.500	18.835	1.176	1.016	105.261	95.459
2	30.356	30.720	12.500	18.481	1.123	1.050	104.174	99.237
3	30.378	31.065	13.000	18.334	1.102	1.063	100.006	96.728
4	28.950	30.798	11.500	17.878	1.060	1.043	101.647	95.843
5	29.434	30.152	12.500	17.805	1.038	0.939	95.734	87.287
6	29.565	28.495	13.500	17.635	1.018	0.904	90.070	85.007
7	29.434	28.848	14.000	17.433	0.999	0.872	86.485	81.623
8	28.291	27.878	11.500	17.376	0.992	0.919	94.664	87.784
9	28.357	28.891	12.000	17.228	0.971	0.905	90.846	82.363
10	28.994	28.449	13.500	17.227	0.974	0.883	85.841	83.957
11	28.489	27.018	12.500	17.149	0.957	0.839	87.761	78.349
12	28.247	28.427	12.000	17.146	0.961	0.834	89.803	79.166
13	28.467	29.219	12.500	17.136	0.956	0.862	87.606	81.377
14	28.401	28.777	12.500	17.072	0.949	0.743	86.972	68.824
15	27.522	28.706	11.000	17.055	0.970	0.865	94.023	83.280

Furthermore, from the 100 3-hour second order simulation, the empirical CDF of static baseshear and overturning moment at largest surface elevation on cylinder with diameter 1m is established. The same hydrodynamic coefficient from previous analysis is used. The baseshear and overturning moment are calculated in MATLAB. Figure 7.31 shows, the comparisson of static base shear and overturning moment empirical CDF for second order wave and 5th Stokes model. It can be observed that 5th Stokes gives larger static base shear and overturning momment than second order model. Therefore, it is concluded that for single drag dominaed cylinder case, the 5th Stokes gives a conservative static base shear and over turning moment. More empirical CDFs of static base shear and overturning moment from different method of determining harmonic component are presented in the appendix. For CDF equal to 0.95, the ratio between 5th Stokes baseshear and second order model is 1.08 while for overturning moment is 1.03. This means for CDF equal to 0.95, the 5th Stokes gives 8% larger static base shear and 3% larger static overturning moment than second order model.

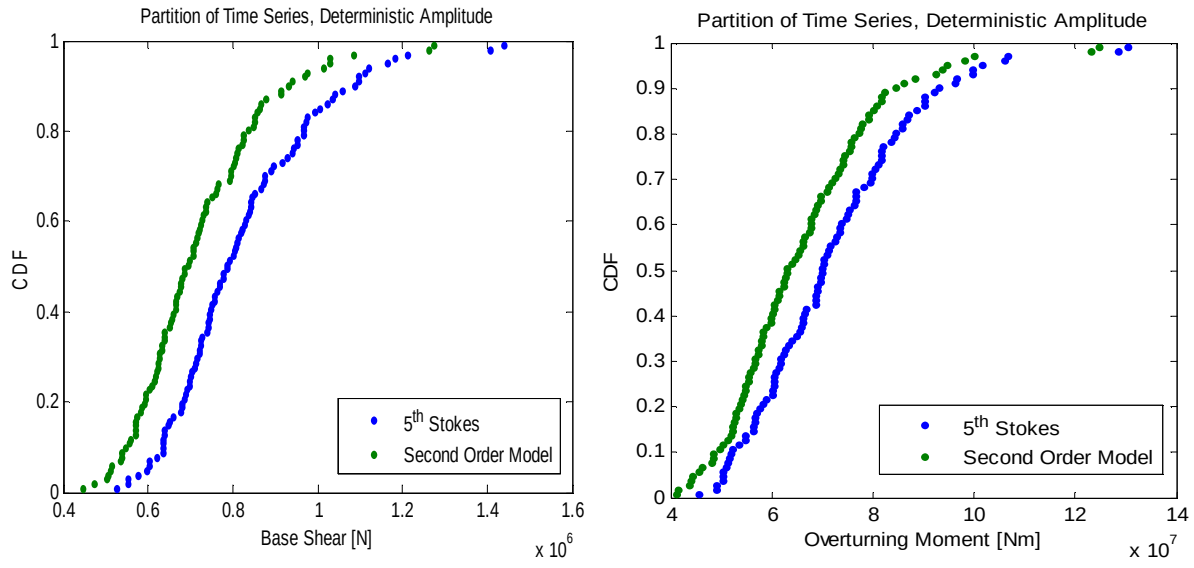

Figure 7.31 Empirical CDF of Base Shear and Over Turning Moment

7.4. Comparisson of Wave Load

For jack-up platform, the wave load is determined by Morrison equation which is expressed in equation 5.17. The hydrodynamic coefficients for first order and second order sea are described in section 5.2.1. In this section, the comparrison of drag load and inertia load along the z-coordinate is presented. Since the jack-up is the drag dominated structure, the comparisson is concentrated in the event where the largest drag load occurs.

Previously, it is shown that the maximum drag load occurs at the wave crest (maximum sea surface). Therefore, the comparisson of drag load is focused on the wave crest. Figure 7.32 shows the horizontal velocity along z-coordinate for 5th Stokes wave, first order and second order model. Moreover, the horizontal velocity above the mean sea surface is determined by various stretching method.

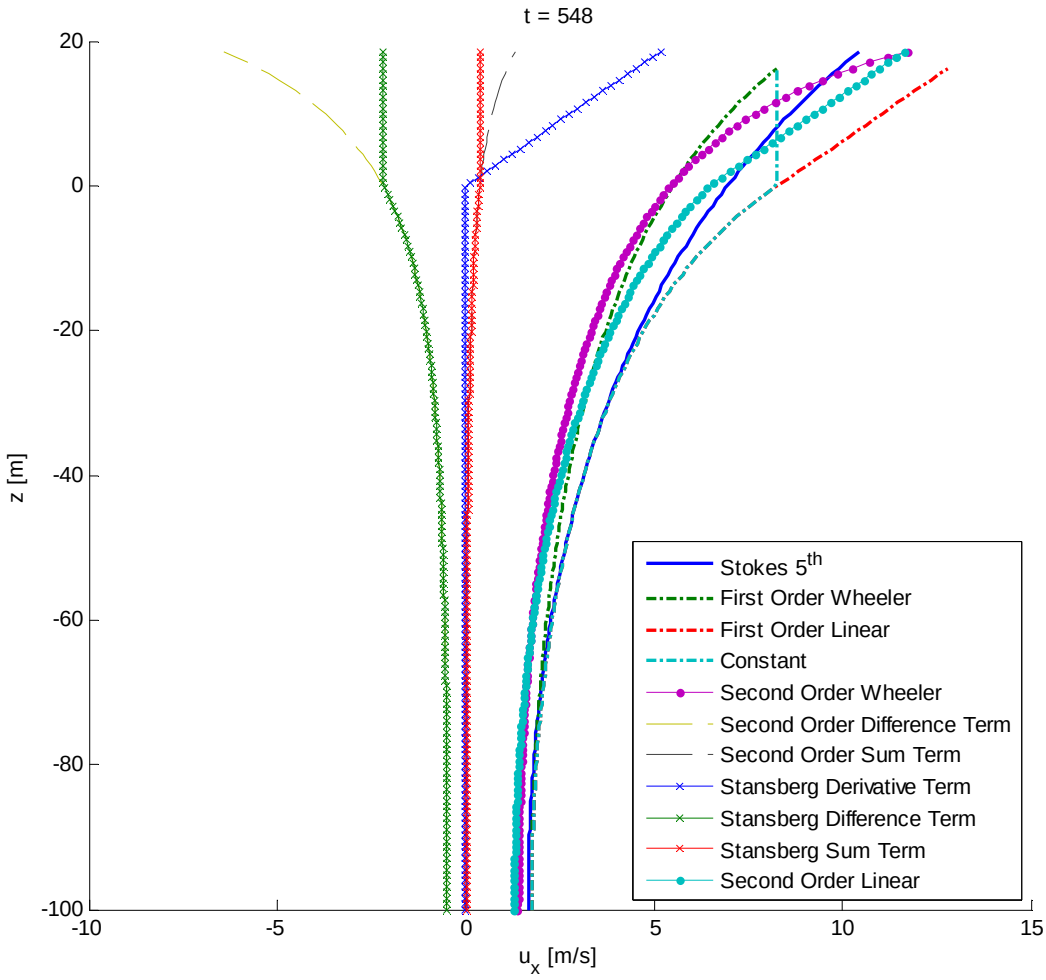

Figure 7.32 Horizontal Velocity along z-Coordinate

First order wheeler and first order linear respectively refer to Wheeler and linear extrapolation of first order horizontal velocity while second order Wheeler and second order linear respectively refer to Wheeler and linear extrapolation of second order horizontal velocity. Constant refers to constant stretching of first order horizontal velocity. In addition, the second order correction terms (derivative, difference and sum term) are also included in the graph.

It can be observed that both first order Wheeler and constant stretching give smaller surface horizontal velocity than second order model (either second order Wheeler or second order linear extrapolation) and 5th Stokes wave. It is also explained before that 5th Stokes tends to produce smaller surface horizontal velocity than second order model. At mean sea surface, the constant stretching produces the largest horizontal velocity. In general, either for first order or second order model, the Wheeler streching underestimates the horizontal velocity around the mean sea surface. In addition, it is explained before that linear extrapolation on first order sea will overestimates the surface horizontal velocity and it is not reccomended to be used.

In section 5.2.1, it is explained that for second order or higher order wave model, $C_D = 0.65$ for $z > 2m$ and C_D =1.05 for $z \leq 2m$. A modification is made to drag coefficient when calculating the load from first order wave where C_D =1.15 for all z-coordinate. Therefore, a comparisson of drag load is made based on these drag coefficients. Figure 7.33 shows the drag load along z-coordinate for single vertical cylinder with diameter 1m.

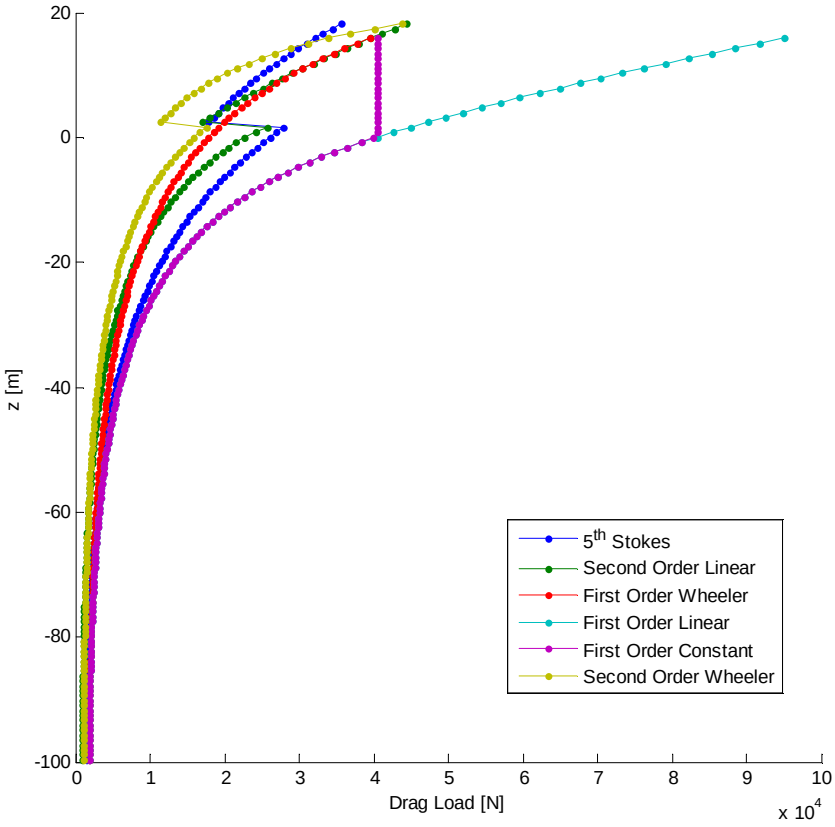

Figure 7.33 Drag Load Along the z-Coordinate

In figure 7.33, there is a jump in second order drag load profile since two different drag coefficients are used along the z-coordinate. For first order drag load, the profile is continous. It can be observed from figure 7.33 that there is a good agreement between the first order Wheeler (red line) and second order linear extrapolation (green line) drag load profile except the jump in the second order linear extrapolation. Though the drag load at the surface is smaller, majority 5th Stokes produces larger drag load than second order linear extrapolation. That is why the empirical CDF of static baseshear and overturning moment of 5th Stokes wave (presented in fugure 7.31) are more conservative than second order linear extrapolation. In addition, first order linear extrapolation greatly overestimates the drag load and is not suggested to be used. The linear extrapolation can be used if only the drag coefficient is modified for *z*-coordinate above the mean surface though this makes the calculation more complicated not to mention the unensured quality of the result. All in all, second order wheeler seems to underestimate the drag load while constant stretching gives the most conservative result.

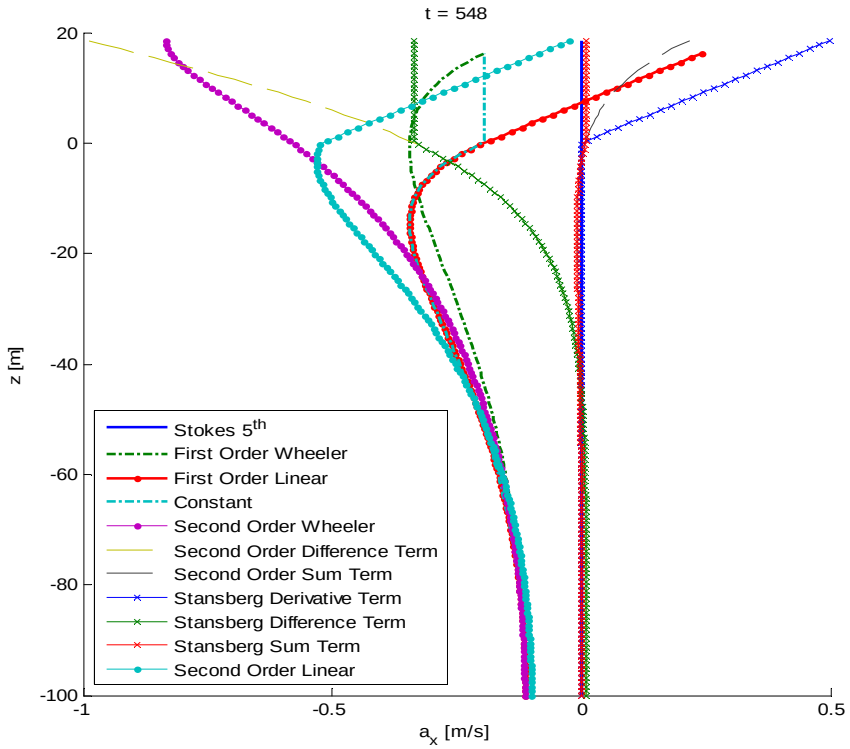

Figure 7.34 Horizontal Velocity along z-Coordinate

The inertia load depends on the horizontal acceleration. Therefore, the horizontal acceleration at the wave crest is observed. Figure 7.34 shows the horizontal acceleration along the *z*-coordinate at the same time instance as the drag load analysis.

In figure 7.34, 5th Stokes shows zero horizontal acceleration along the coordinate. This is because 5th Stokes wave is a regular wave. As explained in section 2.3.1 with first order wave as an example, for regular wave, horizontal acceleration is equal to zero at wave crest while the horizontal velocity has its maximum value. There is a difference regarding the location of maximum horizontal acceleration between 5th Stokes and first order wave as indicated in section 7.3.3. However, the main focus in this analysis is on the wave crest and not at the location of maximum horizontal acceleration.

On the other hand, since both first order and second order model in this work are irregular waves, the horizontal acceleration is not totally zero at the wave crest though the magnitude is small compared to the horizontal velocity. In this case, the horizontal acceleration is irregular along the z-coordinate. It seems that the horizontal acceleration from some components has already have negative value while some high frequency component (which has faster decay rate) still has positive horizontal acceleration. As a consequence, the magnitude of horizontal acceleration at the surface is smaller than at the mean water surface.

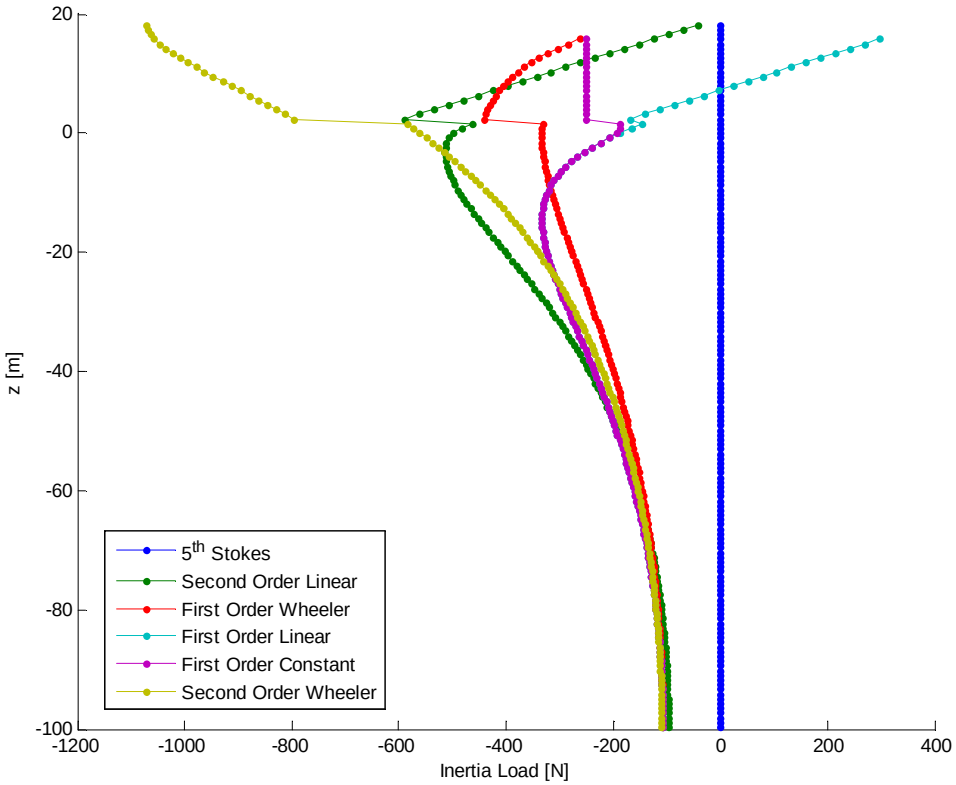

Figure 7.35 Inertia Load Along the z-coordinate

For both first order and second order wave, $C_M = 1.6$ for $z > 2m$ and C_M =1.2 for $z \leq 2m$. The inertia load along the z-coordinate is presented in figure 7.35. There is a different in the behaviour of second order Wheeler stretching (yellow line in figure 7.35) then the other method. This is suspected as the consequence of the different cut-off frequency which is used by second order Wheeler stretching method. As an effect, the second order Wheeler could overestimates the magnitude of inertia load. However, the profile of horizontal acceleration at wave crest is different between various method. Figure 7.36 shows another realization of horrizontal acceleration and inertia load at wave crest. It still can be observed that second order Wheeler stretching overestimates the horizontal acceleration.

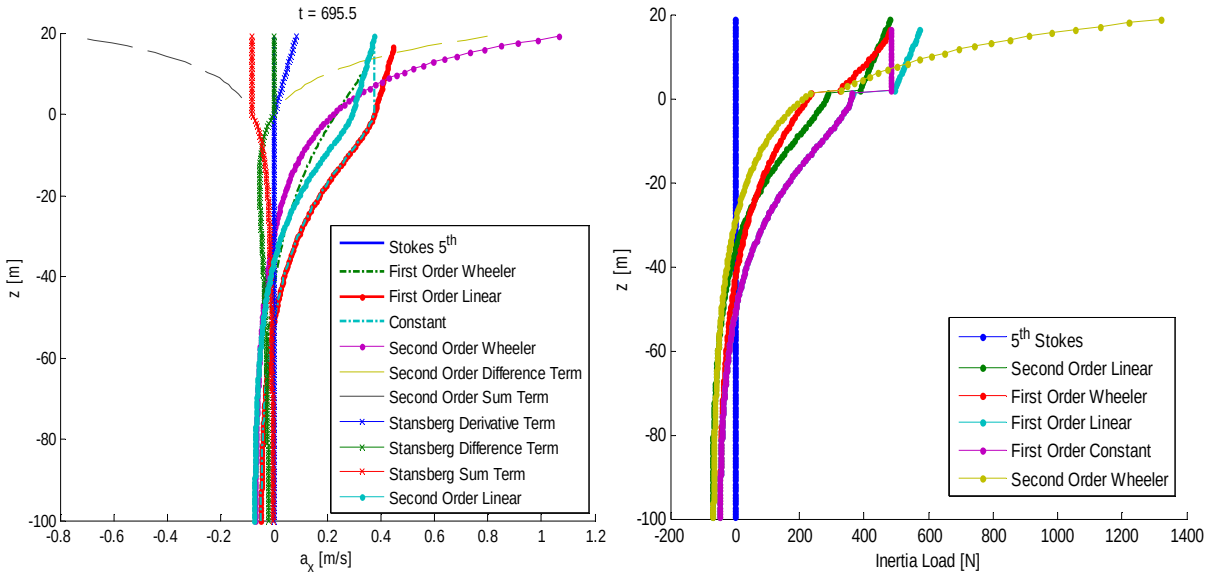

Figure 7.36 Horizontal Acceleration and Inertia Load

For further analysis, the static base shear and overturning moment from 100 3-hour simulation with various stretching method is compared. The analysis is focused on the largest maximum surface elevation from each simulation. Table 7.4 shows 20 different realizations of static base shear and overturning moment from the 20 largest surface maximum. The 5th Stokes wave height is iterated to give the same crest height as the second order model. Figure 7.37 shows the empirical CDF of static baseshear and overturning moment at the largest wave crest from various stretching method. From table 7.4, first order linear extrapolation greatly overestimates the static base shear and overturning moment. In addition, the second order Wheeler gives the lowest static base shear and overturning moment. 5th Stokes and Second Order Linear extrapolation is close to each other.

Table 7.4 Comparisson of Static Base Shear and Overturning Moment

No	Stokes Wave Height [m]	Second Order Model Wave Height [m]	Wave Period [s]	Crest [m]	Static Base Shear [kN]						Static Overturning Moment [kNm]					
					5th Stokes	Second Order Linear Ext.	First Order Wheeler	First Order Linear Ext.	Constant Stretching	Second Order Wheeler	5th Stokes	Second Order Linear Extrapolation	First Order Wheeler	First Order Linear Extrapolation	Constant Stretching	Second Order Wheeler
1	34.55	33.34	11.50	22.15	1.73	1.53	1.29	3.06	2.17	1.06	173.04	154.48	118.16	302.16	202.19	105.63
2	32.25	29.02	13.50	19.54	1.27	1.15	1.04	2.39	1.72	0.85	114.36	112.31	93.87	233.64	158.73	81.36
3	31.49	30.79	13.00	19.13	1.21	1.07	0.95	2.19	1.58	0.77	110.42	105.00	86.65	214.97	146.92	74.58
4	30.95	29.99	13.50	18.60	1.14	0.98	0.93	1.88	1.45	0.74	102.04	93.77	82.13	178.94	131.38	69.72
5	30.63	30.93	15.50	18.09	1.12	1.01	1.01	1.58	1.38	0.86	91.99	89.59	83.23	139.54	116.74	74.53
6	29.86	30.04	13.50	17.83	1.05	0.96	0.88	1.80	1.39	0.74	92.67	90.83	78.18	171.36	125.56	68.67
7	29.96	30.62	15.00	17.66	1.05	0.97	0.99	1.52	1.33	0.85	87.57	85.11	81.15	132.62	112.19	72.52
8	29.38	28.12	13.50	17.50	1.00	0.91	0.85	1.67	1.31	0.71	88.41	85.00	74.76	157.98	118.18	65.89
9	29.10	29.05	13.50	17.30	0.98	0.90	0.83	1.47	1.22	0.71	85.98	82.66	71.74	135.53	108.02	65.12
10	29.10	30.76	13.50	17.29	0.98	0.90	0.80	1.48	1.20	0.68	85.98	85.55	70.41	138.23	107.44	62.75
11	28.66	28.92	13.00	17.12	0.96	0.89	0.82	1.48	1.22	0.72	85.82	82.61	71.83	136.94	108.57	65.67
12	28.80	27.86	14.00	17.00	0.95	0.88	0.86	1.39	1.19	0.74	82.03	77.66	70.73	122.99	100.66	63.97
13	28.36	29.47	13.00	16.91	0.93	0.88	0.88	1.32	1.18	0.75	83.26	77.61	72.80	115.16	99.48	64.64
14	27.59	28.88	11.50	16.87	0.93	0.92	0.83	1.30	1.16	0.74	88.56	84.72	71.55	116.74	101.45	67.33
15	28.84	30.18	15.50	16.86	0.96	0.85	0.90	1.49	1.25	0.75	78.42	73.94	73.54	133.16	105.81	64.25
16	28.38	28.91	13.50	16.81	0.92	0.83	0.78	1.35	1.13	0.67	80.74	75.59	67.01	123.16	99.20	60.12
17	28.38	27.50	13.50	16.80	0.92	0.82	0.77	1.39	1.15	0.65	80.74	76.63	67.38	129.13	102.45	59.75
18	28.26	28.19	13.50	16.72	0.91	0.85	0.79	1.33	1.14	0.69	79.79	78.20	68.10	121.36	100.13	62.55
19	27.89	26.51	12.50	16.72	0.90	0.84	0.72	1.50	1.17	0.63	82.46	81.14	65.78	144.60	107.42	59.96
20	27.05	30.01	11.00	16.71	0.92	0.90	0.71	1.44	1.13	0.64	89.13	86.78	64.04	137.33	103.25	60.69

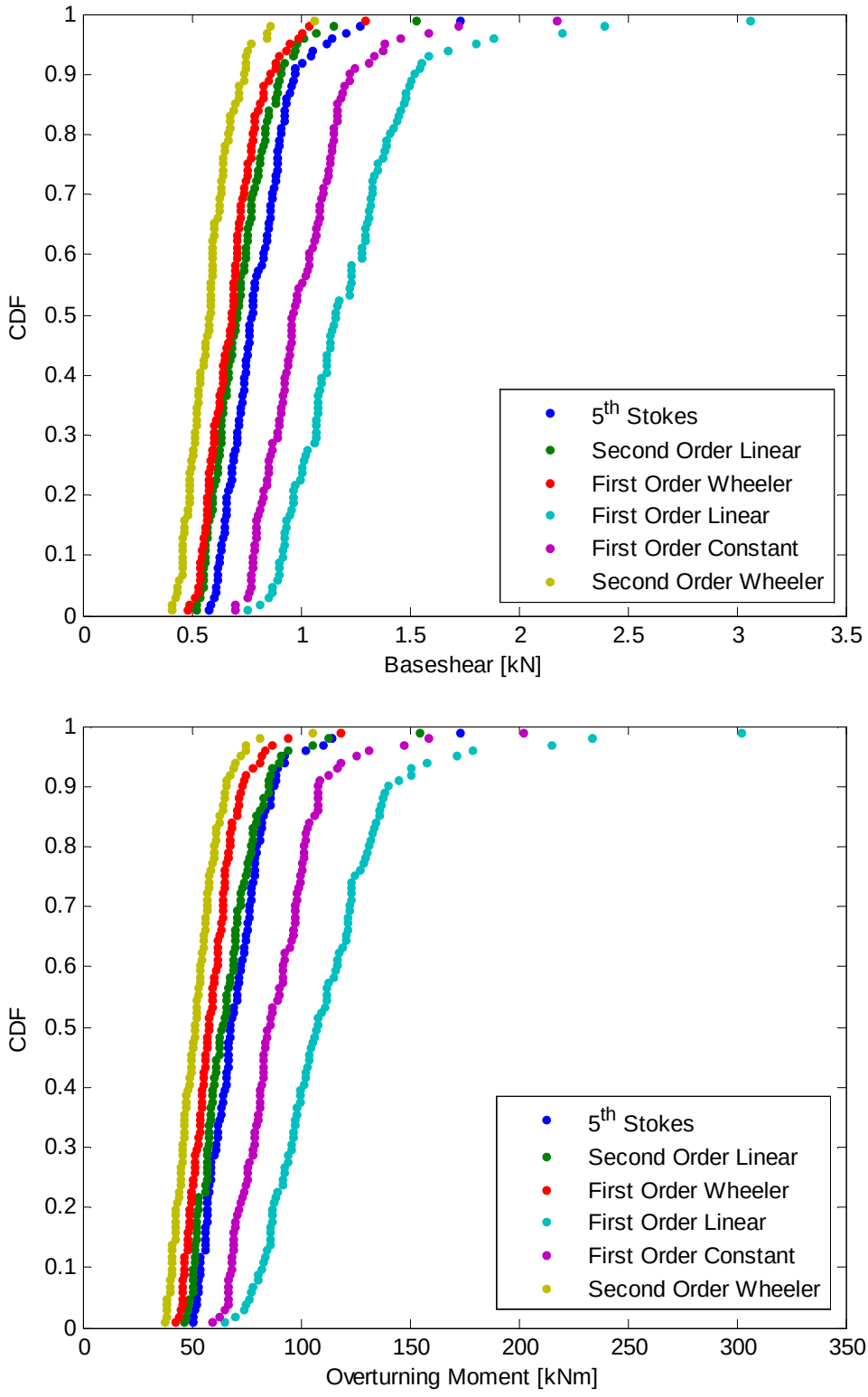

Figure 7.37 Empirical CDF of Static Baseshear and Overturning Moment

7.5. Verification of Transfering Data to USFOS

The sea surface and wave particle kinematics are transferred to USFOS trough wavegrid file since the response of jack-up platform is calculated by using USFOS. Therefore, a brief verification is performed to insure that the data is transfered corretly from MATLAB to USFOS. In this case, a single vertical cylinder with diameter 1m is set as the object of comparisson. A 20-minute first order sea simulation utilizing equal area method and random amplitude with 220 components is performed. The Wheeler stretching is used to determined the particle kinematics along the z-coordinate. In addition, C_D =1.15 and C_M =1.6 along the z coordinate. It should be noted that the focus on this particular verification study is the comparisson of load. Therefore, any methods can be used to simulate the sea surface and wave particle kinematics. Utilizing the result of simulation, the static baseshear and overturning moment on the cylinder from USFOS and MATLAB are compared. Figure 7.39 shows the comparisson of static baseshear and overturning moment between USFOS and MATLAB.

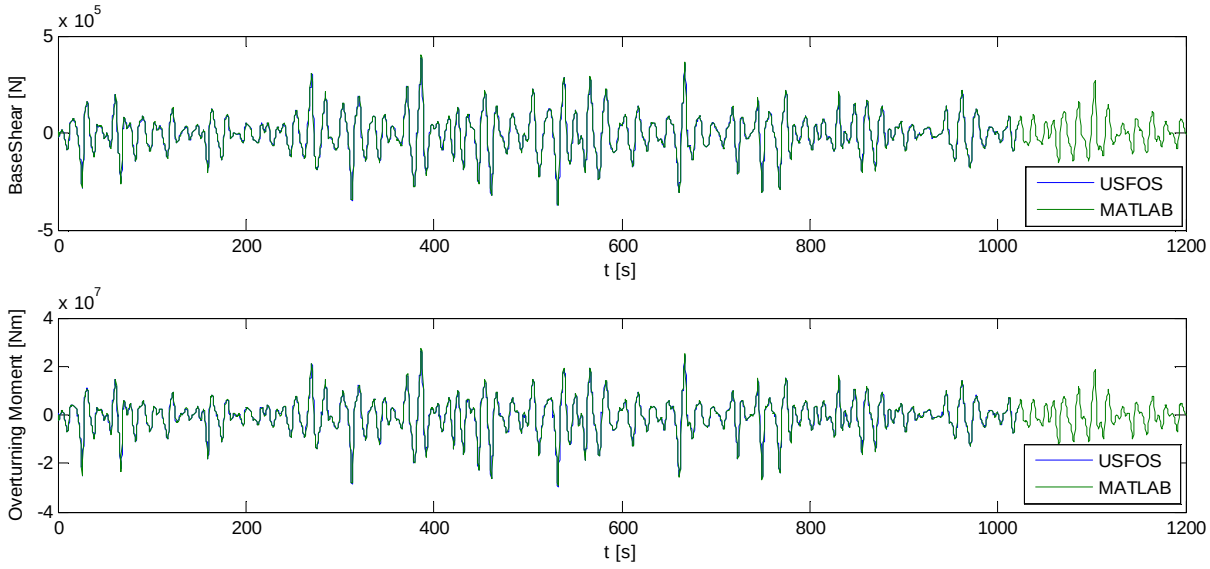

Figure 7.38 Comparisson of Load between USFOS and MATLAB

From figure 7.38, it can be observed that both static baseshear and overturning moment from USFOS and MATLAB model show a good agreement. Therefore it is concluded that the transfer of surface elevation and particle kinematics from MATLAB to USFOS is insured.

8. Reducing Computational Time in Grid System

Eventhough the required harmonic components can be reduced by various method, to calculate 3-hour simulations in a grid system is still prohibitive due to the the large computational time and required memory. To solve this problem, some stategies to reduce the computational time (also the required memory) are introduced. Explanation about the strategies is presented in section 4.5. In this chapter, the effects of applying these strategies to responses calculation of jack-up platform is presented.

In this case, the long crest wave is assumed and the wave is propagates along the x coordinate. The wave particle kinematics on the grid is determined by only oberving a single line on the grid. This is illustrated by figure 8.1.

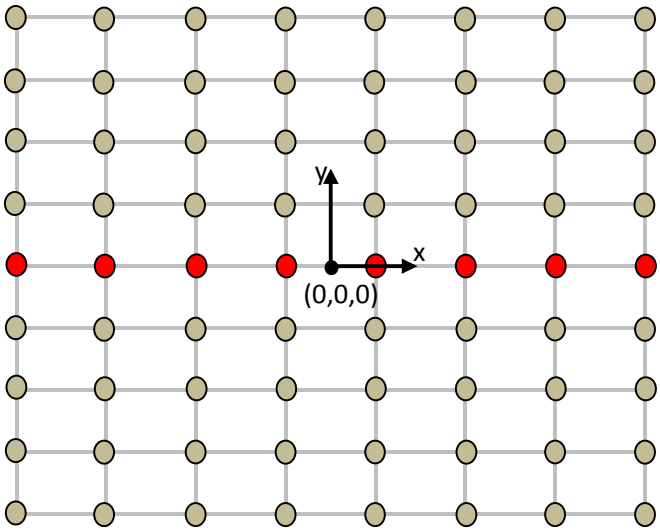

Figure 8.1 Illustration of Grid System

The round shapes shows particular coordinates in the grid system. The red shapes incicates the coordinates where the calculation of sea surface is performed. This coordinates is called the calculation points. Then, all points that has same y-coordinates as the calculation points is set to have the same magnitude of surface elevation and wave particle kinematics as calculation points. As a consequnce, the sea surface which is presented in figure 8.2 is established. All simulation in this chapter is performed utilizing equidistance frequency interval with random amplitude. The time interval is set as 0.5 s. In addition, $H_s = 13m$ and $T_P = 15.9s$. These value is estbalished from metocean analysis which is presented in chapter 9.

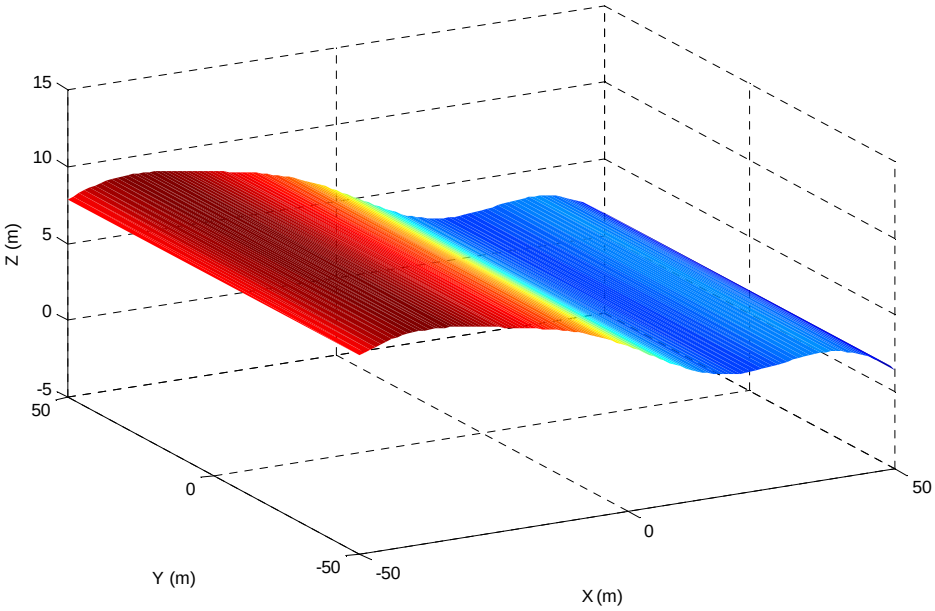

Figure 8.2 Long Crest Surface Elevation

8.1. Calculating Wave Kinematics at Coarser Grid

Calculating wave kinematics at coarser grid decreases the computational time since the number of calculation point is decreased. The sea surface and wave particle kinematics between the calculated points are achieved by USFOS utilizing particular interpolation scheme. Since the wave is assumed as 2-D (long crest) wave, the observation are only performed for x-coordinate and z-coordinate. In this case, the strategy to decrease the number of calculation points along z-coordinate is different than the one which is applied to x-coordinate. In order to verify the accuracy and measure the computational time, 20-minute first order sea with wheeler streetching and 20-minute second order sea with linear extrapolation simulation are perfomed. It shall be noted that the presented baseshear and overturning moment is the reaction baseshear and overturing moment which indicates the negative value occurs when the direction of load on the jack-up is equal to the direction of wave propagation.

8.1.1. Coarser grid for z-coordinate

Since the magnitude of wave particle kinematics are significantly larger around the surface, concentrating the calculation points close to the surface could decrease the number of calculation point along the z-coordinate. To verify this, four different cases of calculation point distribution along the z-coordinate are observed. The interval of z-coordinate is set as equidistance interval with magnitude 0.5, 1, and 2m for first, second and third case respectively. For the fourth case,

the interval of z-coordinate is decreased gradually from sea bottom to the sea surface. In this case, the interval of z-coordinate is set equal to 20m for $z \leq -80m$, 10m for $z \leq -60m$, 5m for $z \leq -30m$ and 1m for $z \leq$ surface elevation. The z-coordinate in grid system is defined up to 30m to accomodate high wave crest. For all case, the interval of x-coordinate is set as 5m to reduce the computational time and memory usage.

Table 8.1 Number of Calculation Point along z-Coordinate and Computational Time

Case	Number of Calculation Points	Computational Time [second]					
		Kinematic (Matlab)		Response (USFOS)			
		First Order	Second Order	First Order		Second Order	
				Static	Dynamic	Static	Dynamic
1	261	1658	33943	1873	1593	1594	1829
2	131	840	16671	1440	1728	1700	1689
3	66	428	8494	1745	1701	1908	1606
4	70	363	9369	1447	1479	1698	1522

Table 8.1 shows the number of calculation points along the z-coordinate and the computational time for each case. The computational of response analysis in USFOS does not have general trend. The possible reason is the pararel computing process. In pararel computing process, several *jobs* are submited into USFOS simultaneously. Therefore, the computational time depends on how many active *jobs* and the available space of CPU memory. Therefore, computational time in USFOS can not be taken as object of comparisson in this case. The comparisson of computational time is focused on kinematic computational time.

From table 8.1, it can be observed that the case 3, where z-interval is set as 2m, shows the smallest number of calculation points along the z-coordinate between the compared cases. As a consequence, the case 3 requires the smallest computational time for second order kinematics. For first order wave, the kinematic computational time for the case 4 is smaller than case 3 though case 4 has more calculation points. This is due to the performed numerical scheme in MATLAB. For first order wave, the kinematics on the calculation points above sea surface is directly set as zero. In this case, the unnecessary multiplication process in MATLAB is avoided. It seems that the fourth case has more calculation points above the sea surface than the third case. As a consequence, the fourth case executes the simulation faster than the third case. This implies that by distributing the calculation points wisely, the computational time could be reduced. However, in order to perform vectorization, the kinematics are calculated on all calculation

points including the calculation points above the sea surface for second order kinematic case. Therefore, in the built MATLAB script, the numerical scheme to calculate second order kinematics is not sensitive to number of calculation points above the sea surface. That is why for second order kinematics, case 4, which has more calculation points, has larger computational time than case 3.In addition, the case 4 cut 78% computational time for first order wave and 72% computational time for second order wave when it is compared to case 1.

In order to verify the accuracy, the mean and standard deviation of baseshear and overturning moment are observed. Table 8.2 presents the mean of baseshear and overturning moment for each case while table 8.3 shows the standard deviation.

Table 8.2 Mean of Baseshear and Overturning Moment

Case	Mean of Baseshear [kN]				Mean of Overturning Moment[kNm]			
	First Order		Second Order		First Order		Second Order	
	Static	Dynamic	Static	Dynamic	Static	Dynamic	Static	Dynamic
1	0.0	0.0	-0.1	-0.1	30.9	54.1	19.8	44.4
2	0.0	0.0	-0.1	-0.1	30.8	53.1	21.0	45.0
3	0.0	0.0	-0.1	-0.1	30.8	54.2	21.5	45.0
4	0.0	0.0	-0.1	-0.1	31.0	53.4	21.0	44.8

Table 8.3 Standard Deviation of Baseshear and Overturing Moment

Case	Std. of Baseshear [kN]				Std. of Overturning Moment[kNm]			
	First Order		Second Order		First Order		Second Order	
	Static	Dynamic	Static	Dynamic	Static	Dynamic	Static	Dynamic
1	0.9	1.1	0.8	1.0	160.9	177.8	157.1	173.2
2	0.9	1.1	0.8	1.0	160.8	176.8	157.7	172.6
3	0.9	1.1	0.8	1.0	160.7	175.5	158.0	172.4
4	0.9	1.1	0.8	1.0	160.8	176.7	157.7	172.7

It is assumed that the case 1 gives the most accurate result since its z-coordinate grid is denser than the other cases. In table 8.2 and 8.3, case 3 mainly produces larger deviation when the mean and standard deviation are compared to the case 1. All in all, the deviations from each case are mainly less than 5% (except for static second order overturning moment of case 3) which indicates case 2, 3 and 4 gives acceptable result. The analysis is continued by observing the maximum baseshear and overturning moment. Table 8.4 to table 8.7 respectively shows the positive maximum baseshear, positive maximum overturning moment, negative maximum baseshear and negative maximum overturning moment.

Table 8.4 Positive Maximum Baseshear

Case	Maximum Baseshear							
	First Order				Second Order			
	Static		Dynamic		Static		Dynamic	
	Mag. [kN]	t [s]	Mag. [kN]	t [s]	Mag. [kN]	t [s]	Mag. [kN]	t [s]
1	3.7	296.5	4.1	297.0	3.0	296.5	3.2	297.0
2	3.7	296.5	4.0	297.0	3.0	296.5	3.3	297.0
3	3.7	296.5	4.0	297.0	3.1	296.5	3.4	297.0
4	3.7	296.5	4.0	297.0	3.0	296.5	3.3	297.0

Table 8.5 Positive Maximum Overturning Moment

Case	Maximum Overturning Moment							
	First Order				Second Order			
	Static		Dynamic		Static		Dynamic	
	Mag. [kNm]	t [s]	Mag. [kNm]	t [s]	Mag. [kNm]	t [s]	Mag. [kNm]	t [s]
1	397.5	296.5	516.8	297.5	337.3	296.5	479.4	601.0
2	397.6	296.5	508.8	297.5	341.6	296.5	470.3	601.0
3	397.8	296.5	508.2	297.5	344.6	296.5	469.2	601.0
4	397.8	296.5	509.2	297.5	341.8	296.5	470.5	601.0

Table 8.6 Negative Maximum Baseshear

Case	Maximum Baseshear							
	First Order				Second Order			
	Static		Dynamic		Static		Dynamic	
	Mag.[kN]	t [s]	Mag. [kN]	t [s]	Mag. [kN]	t [s]	Mag. [kN]	t [s]
1	-4.5	607.5	-5.0	609.0	-4.2	607.0	-4.9	609.0
2	-4.5	607.5	-5.0	609.0	-4.2	607.5	-4.8	609.0
3	-4.5	607.5	-5.0	609.0	-4.1	607.0	-4.8	608.5
4	-4.5	607.5	-5.0	609.0	-4.2	607.5	-4.8	609.0

Table 8.7 Negative Maximum Overturning Moment

Case	Maximum Overturning Moment [kNm]							
	First Order				Second Order			
	Static		Dynamic		Static		Dynamic	
	Mag. [kNm]	t [s]	Mag. [kNm]	t [s]	Mag. [kNm]	t [s]	Mag. [kNm]	t [s]
1	-178.6	584.5	-298.6	609.5	-176.3	584.5	-282.7	609.0
2	-178.7	584.5	-293.9	609.5	-176.4	584.5	-290.6	609.0
3	-179.6	314.0	-296.5	609.5	-176.5	584.5	-287.3	609.0
4	-178.7	584.5	-294.1	609.5	-176.4	584.5	-290.7	609.0

From table 8.4 to table 8.7, compared to case 1, the case 3 generally produces larger deviation then the other cases. It seems the first order negative maximum overtuning moment of case 3 occurs at different time instance than the other cases though it is checked that in the same time

instance as other cases, case 3 does not produce significant deviation on the negative overturning moment. Despite all of that, case 2, 3 and 4 have deviation which is less than 5%. This indicates that all cases give acceptable result. However, the fourth case is the most appealing method to apply since it has the smaller computational time than case 1 and 2 but creates smaller deviation than case 3. Therefore, for further ananlysis, case 4 is used to define the z-coordinate in grid system.

8.1.2. Coarser grid for x-coordinate

Eight different intervals of x-coordinate are observed which are 1m, 2m, 3m, 5m, 7m, 10m, 13m and 15. The interval of z-coordinate gradually decrease from the sea bottom to the sea surface which is similar to case 4 in previous section. The 1m interval is assumed gives the most correct result between the other cases. Therefore, the 1m interval is made as a reference. In addition, the static and dynamic analysis of structure responses are performed. Table 8.8 shows the number of calculation point along the x-coordinate and the computational time for each observed case.

Table 8.8 Number of Calculation Point along z-Coordinate and Computational Time

Case	Interval [m]	Number of Calculation Points	Computational Time [second]					
			Kinematic (Matlab)		Response (USFOS)			
			First Order	Second Order	First Order		Second Order	
					Static	Dynamic	Static	Dynamic
1	1	101	1493	40176	769	1611	1253	1662
2	2	51	756	20365	651	1644	2070	1400
3	3	34	499	13670	606	1833	1956	1331
4	5	21	311	8975	573	1315	1631	1372
5	7	15	221	6075	553	1282	1605	1265
6	10	11	162	4567	934	1257	1500	1328
7	13	8	127	3227	780	1409	1713	1271
8	15	7	105	2784	835	1237	1860	1272

Since multiple calculation in USFOS is performed by utilizing pararellel computing, the calculation speed depends on the available memory and processor when executing the *job*. As a consequence, the comparisson of USFOS computational time is not reliable to perform. Logically, USFOS spends longer duration when executing the grid system with smaller x interval since it requires bigger memory due to the greater number of calculation point. This can be observed by comparing case 1 and case 8 where the case 8 executes the simulation faster than case 1.

The observation is focused on the computational time of wave particle kinematics and sea surface at MATLAB. By setting 1m interval as reference, it is observed that utilizing 5m as interval of x-coordinate cuts the computational time up to 78% for both first order and second order sea. In this case, one simulation of 20-minutes second order sea spends 2.5 hours to be completed. Furthermore, using x-coordinate interval equal to 15 m cuts the 93% computational time of first and second order.

Table, 8.9 shows the mean of baseshear and overturning while figure 8.3 presents the percentage of mean for each x-interval when they are compared to x-interval = 1m. The percentage of mean in figure 8.3 is determined by:

Table 8.9 Mean of Baseshear and Overturning Moment

Case	Interval [m]	Mean of Baseshear [kN]				Mean of Overturning Moment[kNm]			
		First Order		Second Order		First Order		Second Order	
		Static	Dynamic	Static	Dynamic	Static	Dynamic	Static	Dynamic
1	1	0.0	0.0	-0.1	-0.1	26.2	68.6	16.7	53.3
2	2	0.0	0.0	-0.1	-0.1	26.7	68.3	16.9	52.5
3	3	0.0	0.0	-0.1	-0.1	26.8	66.8	17.1	51.8
4	5	0.0	0.0	-0.1	-0.1	26.4	65.6	16.9	50.0
5	7	0.0	0.0	-0.1	-0.1	26.5	63.1	17.1	46.8
6	10	0.0	0.0	-0.1	-0.1	26.9	58.2	17.3	42.9
7	13	0.0	0.0	-0.1	-0.1	26.1	47.7	16.8	34.3
8	15	0.0	0.0	-0.1	-0.1	26.7	48.3	17.5	36.4

From table 8.9, it can be observed that the mean of baseshear is equal to zero for first order sea and -0.1 for second order sea even when the interval of x-coordinate is set as 15m. This is logical since the second order sea has higher crest (produces negative baseshear) and lower trough (produces positive baseshear). For overturning moment, it can be observed that the deviation tends to increase when increasing the x-interval. The deviation of mean of overturning moment could be larger than 5% when x-interval is greater than 5m. Furthermore, for dynamic second order overturning moment, the deviation of mean is equal to 12% when the x-interval is set as 7m. Therefore, assuming the acceptable mean deviation is 5%, the 5m x-interval produces the fastest computational time with acceptable result.

Table 8.10 shows the standard deviation of baseshear and overturning moment. Observing the standard deviation in table 8.10, for static baseshear case from first order sea, it seems all deviation of standard deviation is less than 5%. However, for first order dynamic baseshear case

the deviation of standard deviation could be larger than 5% when the x-interval is set larger than 10m. For overturning moment, all deviation of standard deviation is less than 5%. Therefore, based on standard deviation, interval 10m produces the fastest simulation with acceptable result if 5% is set as the largest acceptable deviation.

Table 8.10 Standard Deviation of Baseshear and Overturning Moment

Case	Interval [m]	Baseshear [kN]				Overturning Moment[kNm]			
		First Order		Second Order		First Order		Second Order	
		Static	Dynamic	Static	Dynamic	Static	Dynamic	Static	Dynamic
1	1	0.8	1.0	0.7	1.0	160.9	177.2	157.9	173.6
2	2	0.8	1.0	0.7	1.0	160.9	177.0	158.0	173.5
3	3	0.8	1.0	0.7	1.0	161.0	176.7	158.0	173.0
4	5	0.8	1.0	0.8	1.0	161.2	176.0	158.2	172.9
5	7	0.8	1.0	0.8	0.9	161.3	174.3	158.2	171.8
6	10	0.8	1.0	0.8	0.9	161.4	172.9	158.5	171.2
7	13	0.8	0.9	0.8	0.9	161.5	170.2	158.6	169.3
8	15	0.8	1.0	0.8	0.9	161.7	171.2	158.8	170.1

The positive maximum (when the jack-up at the wave trough) and negative maximum (when the jack-up at wave crest) of base shear and overturning moment from static and dynamic analysis are presented in table 8.13 and 8.14 respectively. It can be observed that even when the x-interval larger than 1m, the positive maximum of second order dynamic baseshear could occurs at different time instance than x-interval equal to 1m. In addition, the deviation of positive and negative maximum value from all cases could be larger than 5% when the x-interval is larger than 5m. For ultimate limit state, the main focus is the negative maximum baseshear and overturning moment where the wave crest occurs regardless of the time instance. Therefore, it is concluded that based on the maximum baseshear and overturning moment, 5m is the largest interval with acceptable result.

From comparisson of mean, standard deviation and maximum, it is observed that increasing x-interval will not always increase the deviation of result. When x-interval > 5m, it seems the increment in the deviation becomes uncertain while the increment is still predictable for x-interval ≤ 5m. Therefore, it is concluded that too coarse grid could produce uncertainty in the interpolation result. In addition, based on comparisson of mean, standard deviation and maximum value, interval 5m is the largest interval with acceptable result. Therefore, for further analysis, the grid system is established with x-interval equal to 5m.

Table 8.11 Positive Maximum Response

Interval [m]	Baseshear								Overturning Moment [kNm]							
	First Order				Second Order				First Order				Second Order			
	Static		Dynamic		Static		Dynamic		Static		Dynamic		Static		Dynamic	
	Mag. [kN]	t [s]	Mag. [kN]	t [s]	Mag. [kN]	t [s]	Mag. [kN]	t [s]	Mag. [kN]	t [s]	Mag. [kN]	t [s]	Mag. [kN]	t [s]	Mag. [kN]	t [s]
1	3.2	216.5	3.3	674.0	2.8	216.5	3.1	416.5	332.5	962.5	482.5	416.5	304.2	216.5	493.0	416.5
2	3.2	216.5	3.2	674.0	2.9	216.5	3.1	215.0	333.3	962.5	483.4	416.5	307.2	216.5	496.6	416.5
3	3.3	216.5	3.2	674.0	2.9	216.5	3.2	215.0	336.0	216.5	489.5	416.5	308.9	216.5	502.0	416.5
5	3.3	216.5	3.2	674.0	2.9	216.5	3.3	215.0	343.3	216.5	487.8	416.5	312.7	216.5	513.6	416.5
7	3.3	216.5	3.2	215.5	3.0	216.5	3.3	215.0	342.4	216.5	473.8	416.5	315.0	216.5	501.1	416.5
10	3.4	216.5	3.3	215.5	3.0	216.5	3.5	215.0	351.7	216.5	471.5	416.5	318.8	216.5	506.8	416.5
13	3.4	216.0	3.6	216.0	3.0	216.5	3.7	215.0	354.0	216.0	436.6	416.5	319.0	216.5	483.0	215.0
15	3.5	216.5	3.6	215.5	3.0	216.5	3.8	215.5	364.8	216.5	450.0	416.5	324.9	216.5	488.1	215.0

Table 8.12 Negative Maximum Response

Interval [m]	Baseshear								Overturning Moment [kNm]							
	First Order				Second Order				First Order				Second Order			
	Static		Dynamic		Static		Dynamic		Static		Dynamic		Static		Dynamic	
	Mag. [kN]	t [s]	Mag. [kN]	t [s]	Mag. [kN]	t [s]	Mag. [kN]	t [s]	Mag. [kN]	t [s]	Mag. [kN]	t [s]	Mag. [kN]	t [s]	Mag. [kN]	t [s]
1	-3.8	1410.0	-5.2	1410.5	-3.7	1410.0	-5.3	1410.5	-177.5	221.0	-345.2	1410.5	-175.0	38.5	-378.3	1410.5
2	-3.8	1410.0	-5.2	1410.5	-3.7	1410.0	-5.3	1410.5	-183.8	221.0	-343.3	1410.5	-174.7	38.5	-378.0	1410.5
3	-3.8	1410.0	-5.2	1410.5	-3.7	1410.0	-5.3	1410.5	-188.5	1420.5	-344.1	1410.5	-174.5	438.0	-377.2	1410.5
5	-3.9	1410.0	-5.2	1410.5	-3.7	1410.0	-5.3	1410.5	-187.2	220.5	-341.4	1410.5	-174.4	438.0	-374.0	1410.5
7	-3.9	1410.0	-5.2	1410.5	-3.8	1410.0	-5.3	1410.5	-185.1	220.5	-335.8	1410.5	-177.3	392.5	-364.7	1410.5
10	-3.9	1410.0	-5.2	1410.5	-3.8	1410.0	-5.2	1410.5	-181.7	220.5	-328.0	1410.5	-176.1	392.5	-354.8	1411.0
13	-4.0	1410.0	-5.1	1410.5	-3.8	1410.0	-5.0	1410.5	-178.8	392.5	-304.0	1410.5	-174.0	392.5	-334.1	1411.0
15	-4.1	1410.0	-5.1	1410.5	-3.8	1410.0	-5.0	1410.5	-178.0	392.5	-303.8	1410.5	-173.1	392.5	-334.8	1411.0

8.2. Second Order Wave at Upper Layer

As explained in section 4.5.2, applying the second order wave particle kinematics only at the calculation points which are close to sea surface could decrease the computational time. A comparisson study is performed to find how deep the second order wave particle kinematics can be applied with acceptable result. In the previous project about second order wave force on single vertical cylinder by Lubis [27], applying second order surface only at 10% of depth (10m out of 100m) can cut the computational time up to 88% with small deviation on the maximum, mean and standard deviation of responses. In addition, the equidistance interval of z-coordinate is utilized in his work. However, it is explained in section 8.1.1 that concentrating the calculation points close to the sea surface gives significant cut to the computational time. Therefore, instead of applying equidistance z-interval, gradually decreased z-interval is established when observing the effect of applying second order kinematics only at calculation points that are close to the sea surface. The profiles of horizontal velocity at x = 0 when the largest wave crest occurs are presented in figure 8.3.

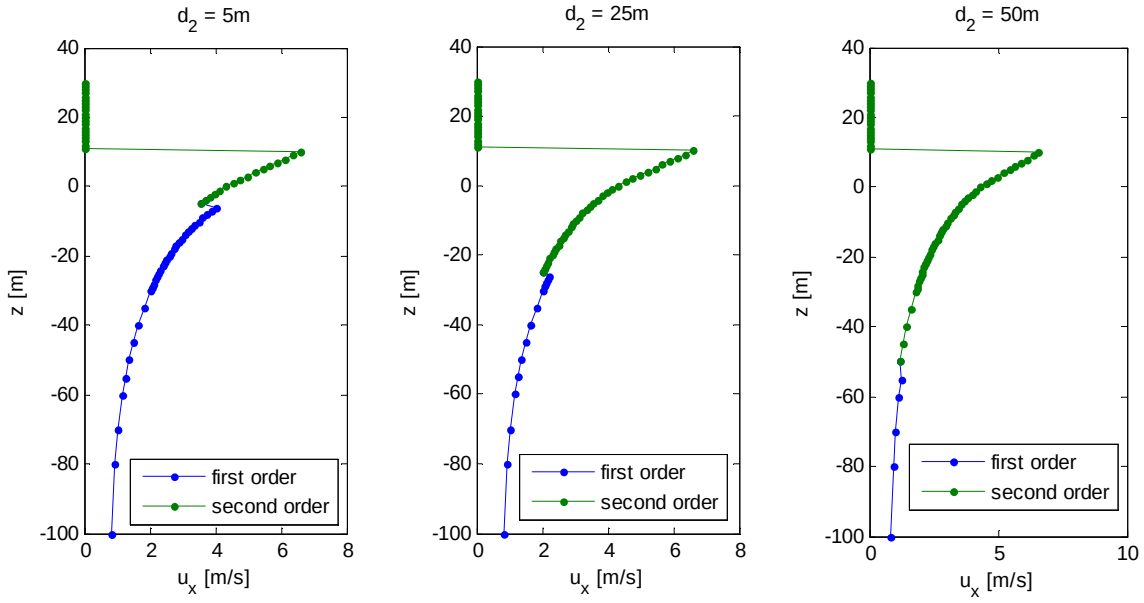

Figure 8.3 Horizontal Particle Velocity Profile

In figure 8.3, the second order kinematics is applied up to three different depths (d_2 which refer to the depth of second order kinematics) which are 5m, 25m and 50m. It can be observed that there is significant jump in the kinematic profile when the d_2 is set as 5m. In this case, the wave load is expected larger than the wave load from complete second order kinematics along z-coordinate. On the other hand, larger d_2 produces smaller deviation in the profile.

In this case, the analysis is focused on the maximum negative (when the crest hit the structure) baseshear and overturning moment. In addition, the comparisson of computational time is concentrated in computational time of kinematics calculation time in MATLAB since the number of calculation points in grid is similar for each observed cases. Table 8.13 presents the observed cases, the kinematics computational time and the maximum responses.

Table 8.13 Combination of First and Second Order Kinematics along Z-Coordinate

Depth of Second Order (d_2)	Computational Time		Maximum Negative Response							
			Baseshear				Overturning Moment [kNm]			
			Static		Dynamic		Static		Dynamic	
	[s]	%	Value[kN]	Dev.[%]	Value[kN]	Dev.[%]	Value[kNm]	Dev.[%]	Value[kNm]	Dev.[%]
Comp.	10298	Ref.	-3.7	Ref.	-0.6	Ref.	-174.4	Ref.	-374.0	Ref.
5 m	4147	40	-4.1	10.8	-0.5	-5.0	-177.4	1.7	-399.0	6.7
10 m	4965	48	-4.1	10.9	-0.5	-6.4	-177.7	1.9	-396.1	5.9
15 m	5616	55	-4.1	10.3	-0.5	-5.8	-177.7	1.9	-394.9	5.6
20 m	6142	60	-4.1	9.3	-0.5	-5.2	-177.8	1.9	-391.9	4.8
25 m	6987	68	-4.1	8.8	-0.5	-4.9	-177.9	2.0	-390.3	4.3
30 m	7415	72	-4.0	7.5	-0.5	-3.9	-178.0	2.0	-386.1	3.2
40 m	7908	77	-4.0	6.0	-0.5	-2.9	-178.1	2.1	-381.7	2.0
50 m	8335	81	-3.9	4.9	-0.5	-2.2	-178.2	2.2	-379.0	1.3

Comp. refers to complete second order kinematic along the z-coordinate and is set as reference result to measure the deviation of the observed case. The percentages of deviation and the percentage of computational time from observed case are presented (indicated by %). From table 8.13, it is observed that by applying second order kinematics up to 40m depth still produces deviation of static baseshear larger than 5%. As presented in figure 8.3, applying second order kinematics only for small depth overestimates the wave load. This is also supported by result in table 8.3, which d_2 = 5m produces larger magnitude of maximum negative baseshear. For overturning moment, the deviation depends on kinematics profile around the mean sea surface on each leg. Therefore, when d_2 is small (which means there is significant jump of kinematics profile close to sea surface), the reduction of overturning moment from wave load close to sea surface equalize the overestimation the overturning moment from wave load close to sea bottom. However, there is an exception for dynamic overturning moment, where the overturning moment is affected by the structure configuration in previous time instance. In addition, d_2=50m only save 20% computational time. This is different than the result from previous work [27] where the cut of computational time is up to 65% for d_2 =30m. Since the calculation points are concentrated close to sea surface, it seems the method produces smaller cut of computational time than equidistance z-interval.

8.3. Spool-to-Extreme and Linear-to-Extreme

To apply spool-to-extreme and linear-to-extreme method, the surface elevation at x=0 is observed. The time instance when the maximum surface elevation occurs is assumed as the time instance for maximum responses. The duration before the maximum surface elevation is varied to observed the effect of spool-to-extreme and linear-to-extreme method on maximum response. Spoll-to-extreme and linear to extreme is used to reduce the computational time of dynamic analysis. However, the static response is observed first since it is easier to explain the deviation in static analysis than in dynamic analysis.

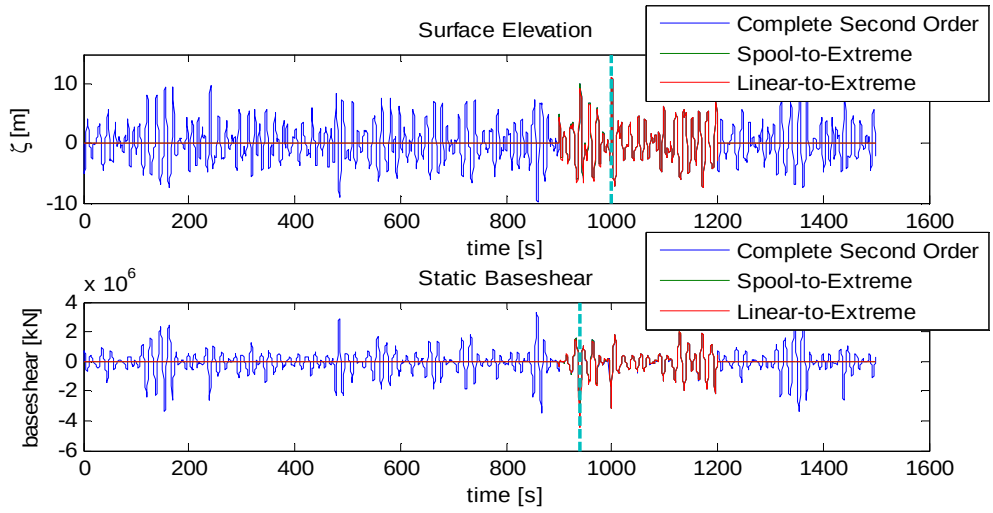

Figure 8.4 Surface elevation and Static Baseshear

Figure 8.4 shows the surface elevation and static baseshear reaction time series. From figure 8.4, it can be observed that the maximum surface occurs at different time instance than maximum negative static baseshear. Therefore, assuming the largest negative static baseshear occurs at the largest surface elevation is not fully correct. This is based on the fact that the largest wave load does not always occur at the largest surface elevation (as presented in section 7.31). In addition, when the largest negative baseshear occurs, the wave crest does not located at x=0. Figure 8.5 shows the surface elevation profile when the largest negative static baseshear occurs. It can be observed that the wave crest is located close to the double leg of jack-up platform (in this case the wave is propagating in x-direction). Therefore, it is more complicated to predict the occurence of maximum baseshear and overturning moment from surface elevation though it can be assumed the wave crest occurs around the double leg location.

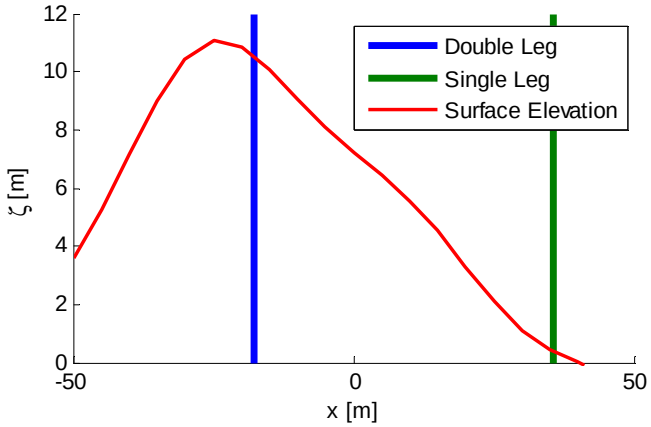

Figure 8.5 Surface Elevation Profile at Largest Negative Static Baseshear

In figure 8.4, though the largest baseshear does not occur at the largest surface elevation, the largest baseshear is still in the range of second order simulation for spool-to-extreme method. In this case the, second order simulation is started 100 seconds before the largest surface time instance which is also the smallest observed duration for spool-to-extreme method. However, for linear-to-extreme method in figure 8.4, the surface elevation is spooled until 100 seconds before the largest maximum and then the first order wave is performed until 10 seconds before the largest surface elevation. As a consequence, the largest base shear is located in the range of first order simulation and the largest baseshear is underestimated. Therefore, due to random occurence of the largest baseshear, spool-to-extreme method is more appealing to be used than linear-to-exteme since it still can cover the maximum static baseshear that occurs around the largest surface elevation. However, when the largest baseshear occurs far away from the largest surface elevation, both spool-to-extreme and linear-to-extreme becomes questionable to be used. To tackle this problem, the observation can be performed not only at single largest surface elevation in 20-minutes but also at second and even third largest surface elevation. As a consequence, the reduction of computational time decreases significantly, especially when the duration of spool is large.

Table 8.14 presents the maximum baseshear and overturning moment. Spool-up-to refers to the duration before largest surface elevation for spool-to-extreme method while linear-up-to refers to duration before the largest surface elevation where the second order wave is applied. The complete refers to complete second order and is taken as reference. Since the occurence of the largest baseshear is located around the largest surface, spool-to-extreme method produces small

deviation for static baseshear and overturning moment for all observed spool duration. However, for linear-to-extreme method, setting the linear-up-to < 70s produces large deviation for static baseshear. The deviation is larger than 25%. However, for static overturning moment, the deviation less than 2% for all observed cases. For dynamic baseshear, except when spool-up-to = 100s, all observed spool-to-extreme cases produces deviation less than 5%. For dynamic baseshear from linear-to-extreme, the deviation is less than 5% only when linear-up-to = 70s and spoo-up-to ≥ 200s. A weird result comes from negative dynamic overturning moment. All the spool-to-extreme result gives large deviation. In addition, only when spool-up-to=100s and linear-up-to < 70s produces small deviation. This is not an expected result. Since duration of second order simulation of linear-to-extreme is small, it is suspected that somehow the transient overturning moment from linear-to-extreme is comparable with the maximum dynamic overturning moment. All in all, based on maximum static baseshear, dynamic baseshear and static overturning moment, spool-to-extreme can be used with spool-up-to ≥ 200s while linear-to-extreme can be used when linear-up-to≥ 70s. In addition, none of the observed cases satisfy the requirement for dynamic overturning moment.

Table 8.14 Maximum Baseshear and Overturning Moment

Negative Static Baseshear [kN]					
Complete	-3,5	**Linear-up-to [s]**			
Spool-up-to [s]		10	30	50	70
100	-3,5	-4,4	-4,4	-4,4	-3,5
200	-3,5	-4,4	-4,4	-4,4	-3,5
300	-3,5	-4,4	-4,4	-4,4	-3,5
400	-3,5	-4,4	-4,4	-4,4	-3,5
500	-3,5	-4,4	-4,4	-4,4	-3,5
600	-3,5	-4,4	-4,4	-4,4	-3,5

Negative Dynamic Baseshear [kN]					
Complete	-4,1	**Linear-up-to [s]**			
Spool-up-to [s]		10	30	50	70
100	-3,7	-5,0	-5,0	-5,0	-3,7
200	-3,9	-5,2	-5,2	-5,2	-4,2
300	-3,9	-5,1	-5,1	-5,1	-4,1
400	-3,9	-5,1	-5,1	-5,1	-4,2
500	-3,9	-5,1	-5,1	-5,1	-4,2
600	-3,9	-5,1	-5,1	-5,1	-4,2

Negative Static Overturning Moment [kNm]					
Complete	-181,8	**Linear-up-to [s]**			
Spool-up-to [s]		10	30	50	70
100	-180,8	-183,8	-183,8	-183,8	-180,8
200	-180,7	-183,9	-183,9	-183,9	-180,7
300	-180,7	-183,9	-183,9	-183,9	-180,7
400	-180,6	-184,0	-184,0	-184,0	-180,6
500	-180,6	-184,0	-184,0	-184,0	-180,6
600	-180,5	-184,1	-184,1	-184,1	-180,5

Negative Dynamic Overturning Moment [kNm]					
Complete	-272,4	**Linear-up-to [s]**			
Spool-up-to [s]		10	30	50	70
100	-204,6	-271,2	-271,2	-271,2	-204,7
200	-234,7	-308,9	-308,9	-308,9	-240,4
300	-230,9	-306,8	-306,8	-306,8	-238,2
400	-233,4	-305,7	-305,7	-305,7	-243,3
500	-233,5	-305,8	-305,8	-305,8	-243,3
600	-233,4	-305,9	-305,9	-305,9	-243,1

However, different than coarser grid method and combination of first order and second order along z-coordinate, the spool-to-extreme and linear-to-extreme can not be based only on one simulation. The analysis requires several simulations for comparisson purposes. However, due to time limitation, the comparisson is not continued. However, the kinematics computational time is summarized in table 8.15 as an estimation for the next work. The left table presents the computational time in seconds while the right table presents the computaitional time in percentage of complete second order computational time. From table 8.15, using spool-to-extreme with spool-up-to=600s can save 42% of computational time. In addition, applying second order wave only on the last 70 seconds of spool-to-extreme while the rest 530s is established by first order wave could save 80% computational time. This indicates the linear-to-exteme could be an appealing method if the correct duration of spool is utilized.

Table 8.15 Kinematic Computational Time from Spool-to-Extreme and Linear-to-Extreme

Computational Time [s]					
Complete	8975	Linear-up-to [s]			
Spool-up-to [s]		10	30	50	70
100	2291	1626	1769	1930	2094
200	3065	1636	1806	1932	2120
300	3870	1620	1777	1910	2107
400	4627	1651	1782	1918	2125
500	5371	1641	1794	1940	2104
600	6103	1623	1776	1937	2080

Computational Time [% of Complete Analysis]					
Complete	100	Linear-up-to [s]			
Spool-up-to [s]		10	30	50	70
100	22	16	17	19	20
200	30	16	18	19	21
300	38	16	17	19	20
400	45	16	17	19	21
500	52	16	17	19	20
600	59	16	17	19	20

8.4. Summary

Observing different x-interval for grid system, it is found that x-interval=5m is the largest interval with the fastest computational time and acceptable result. In addition, applying gradually decreased interval along z-coordinate gives extra cut to computational time. Performing the second order kinematics only up to 50m depth could save 20% computational time for gradually decreased z-interval whiler the spool-to-extreme and linear-to-extreme can save the computational time up to 80%. However, from all observed case, both spool-to-extreme and linear-to-extreme gives large deviation of dynamic overturning moment. In addition, due to the random occurence of largest baseshear and overturning moment, one simulation is not adequate for comparisson study. In the next chapter, the x-interval is set as 5m and gradually decreased z-interval is utilized.

9. Metocean Analysis

The jack-up is designed to withstand the environmental load of the location where the jack-up is planned to be installed. The environmental load is establish from meteorology and oceanography (metocean) analysis. Basically the metocean analysis covers the analysis of wind, current and wave. However, since this work is focused on the wave load, the performed metocean analysis is specified into analysis of wave. In this case, the wave record is observed to find the seastate which produces the extreme jack-up responses.

9.1. Site Location

Figure 9.1 Location of HindcasT Data (www.maps.google.com)

In this work, the typical location of jack-up platform is observed. It is assumed that the jack-up located at the southern part of North sea. The metocean analysis is based on hindcast wave data at latitude 53.61^{o} N and longitude 3.41^{o} E. Figure 9.1 shows the location of the hindcast data from Google map. Comparing the location with map of North Sea from Norwegian Petroleum Directorate (NPD), this coordinate is found around Ekofisk field. This was shown in figure 9.2. The WAM10 wave model [46] is used to hindcast the wave data. The hindcast data is presented in file "*NS south_WAM10_5361N_0341E.txt*" which contains the wind speed, wind direction, and wave parameters (significant wave height and spectral peak period) for each 3 hour from 1st September 1957 to 30th June 2014. In this study, only significant wave height and spectral peak period from total sea is considered.

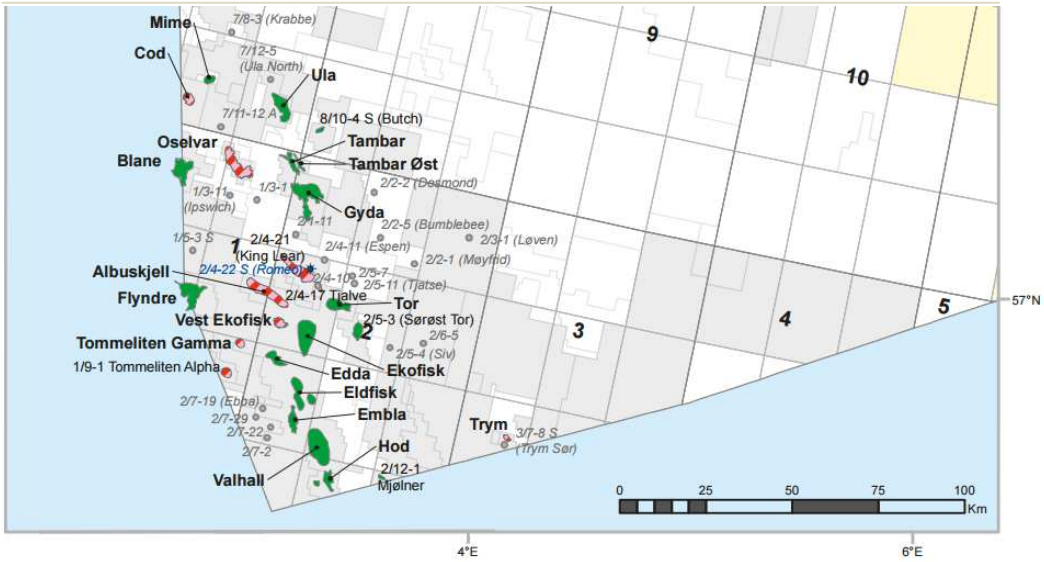

Figure 9.2 Location of Hindcast Data (www.npd.com, [34])

9.2. Scatter Diagram

Table 9.1 illustrates the data inside the hindcast file. From the hindcast file, the significant wave height (H_s) and spectral peak period (T_p) from total sea are processed. They are marked by the red line in table 9.1.

Table 9.1 Illustration of the Hindcast Data

YEAR	MONTH	DAY	HOUR	WIND		TOTAL SEA					WIND SEA			SWELL SEA		
				WSP	DIR	HS	TP	TM	DIRP	DIRM	HS	TP	DIRP	HS	TP	DIRP
1957	9	1	6	4.4	222.	0.9	5.2	4.4	212.	226.	0.2	2.9	227.	0.9	5.2	212.
1957	9	1	9	4.9	214.	0.8	5.2	4.4	212.	218.	0.3	3.2	212.	0.8	5.2	212.
1957	9	1	12	4.3	223.	0.8	5.2	4.4	212.	218.	0.2	2.9	227.	0.8	5.2	212.
1957	9	1	15	2.1	300.	0.8	5.2	4.6	212.	224.	0.1	0.0	220.	0.8	5.2	212.
1957	9	1	18	4.4	350.	0.8	5.2	4.8	212.	229.	0.1	2.7	347.	0.8	5.2	212.
1957	9	1	21	5.6	336.	0.7	5.2	4.8	212.	235.	0.1	3.6	2.	0.7	5.2	212.
1957	9	2	0	7.8	323.	0.8	5.2	3.8	272.	262.	0.5	2.7	287.	0.7	5.2	257.
...	...	...	...	...	...	...	...	...	...	...	...	...	...	...	...	...
2014	6 3	0	12	9.0	320.	1.6	6.9	4.9	347.	340.	1.2	6.3	332.	1.0	7.6	2.
2014	6 3	0	15	8.8	323.	1.6	6.9	4.9	347.	339.	1.3	6.3	332.	1.1	7.6	2.
2014	6 3	0	18	8.4	322.	1.6	6.9	5.0	347.	340.	1.2	6.3	332.	1.1	7.6	2.

Figure 9.3 shows the scatter plot of H_s and T_p. From figure 9.3, it can be observed that rather than random, T_p seems to be grouped. This is due to the limitation of WAM10 model. In order to save memory, WAM10 uses discrete logarithmic spacing when saves the T_p for each 3-hour [1].

In this case, WAM10 model only stores two digit of the $ln(T_p)$. For instance, T_p with magnitude 14.31s ($ln(14.3)=2.66$) and 15.6s ($ln(15.6)=2.74$) are saved into memory as as 2.7. As a consequence, there are only 24 different possible magnitudes of T_p between 2 and 20 s.

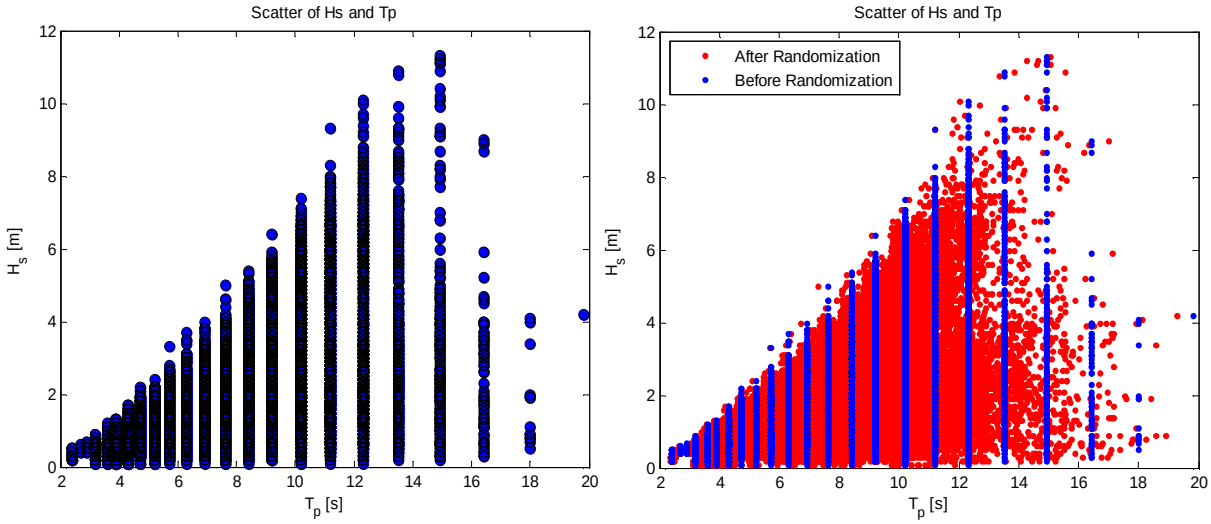

Figure 9.3 The Scatter Plot of H_s and T_p
Left: Without Randomiztaion; Right: With Randomization

The randomness on T_p can be recovered by using equation (9.1) [4].

$$T_p = 3.244\ exp\left[0.09525\left(round\left(1+\frac{ln(T_p'/3.244)}{0.09525}\right)-0.5+rand\right)\right] \qquad (9.1)$$

In this case, T_p' is the spectral peak period from measurement while T_p is the final spectral period for further analysis. In addition, round means round up/down the value inside the bracket into the closest integer while rand indicates a random number which is uniformly distributed between zero and one. Figure 9.4 shows the scatter of H_s and T_p after the randomization. After randomizing the T_p, each combination of H_s and T_p is classed. In this work, the interval of H_s class is 0.5 m while the interval of T_p class is 1s.

9.3. Joint Distribution of H_s and T_p

In section 3.1.1, it is explained that to account the long-term variation, the joint distribution of H_s and T_p should be established. The joint PDF of H_s and T_p is expressed by equation 3.37. Therefore, the marginal distribution of H_s and conditional distribution of T_p should be determined first. This section presents the summary of process to determine the joint distribution of H_s and T_p.

9.3.1. Marginal distribution of H_s

In section 3.3.1, it is explained that 3-parameter Weibull can be used as the marginal distribution of significant wave height ($f_{\boldsymbol{H_s}}(H_s)$). The location ($\lambda_w$), scale ($\alpha_w$) , and shape ($\beta_w$) parameter are determined using method of moment. Figure 9.4 shows the fitted weibull CDF.

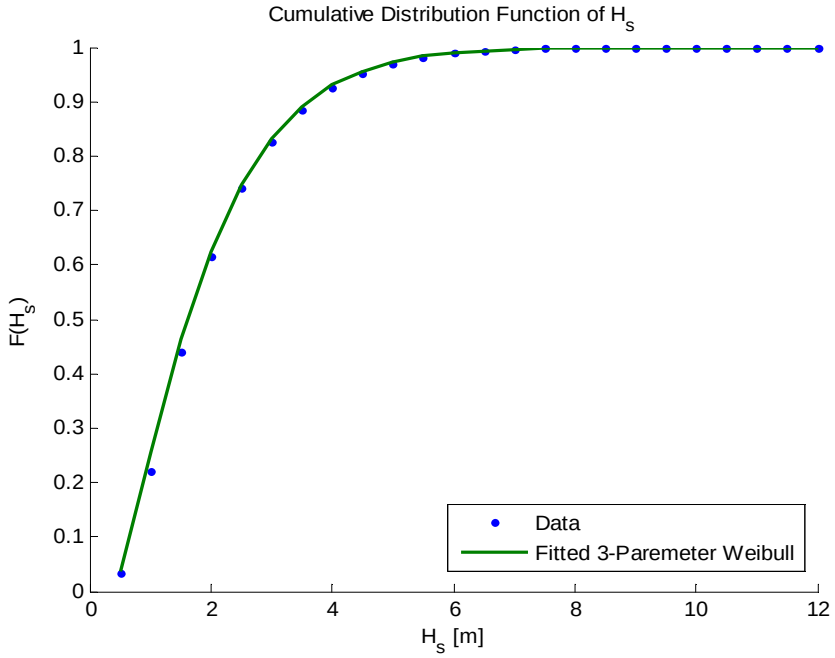

Figure 9.4 Fitted 3-Parameter Weibull

From method of moment, it is found that $\lambda_w = 0.38$, $\alpha_w = 1.64$ and $\beta_w = 1.24$. It should be noted that the mean, variance and skewness coeffcient of H_s should be calculated directly from measurement (before H_s is classed) since determining the mean, variance and skewnwss coefficient from scatter diagram leads to some deviation between the empirical CDF of H_s (blue dot) and the fitted 3-parameter Weibull.

9.3.2. Conditional Distribution of T_p

The distribution of T_p is conditional since it depends on H_s ($f_{\boldsymbol{Tp|H_s}}(T_p|H_s)$). It is assumed that $f_{\boldsymbol{Tp|H_s}}(T_p|H_s)$ follows log-normal distribution which is given in equation 3.42. $f_{\boldsymbol{Tp|H_s}}(T_p|H_s)$ is determined for each class of H_s. To established a log-normal distribution, the mean and variance of $ln(T_p)$ should be found first. Therefore, since the distribution of T_p depends on H_s, mean and variance of $ln(T_p)$ should be analyzed from each class of H_s. Figure 9.5 shows the fitted function of mean of $ln(T_p)$ with H_s as the variable.

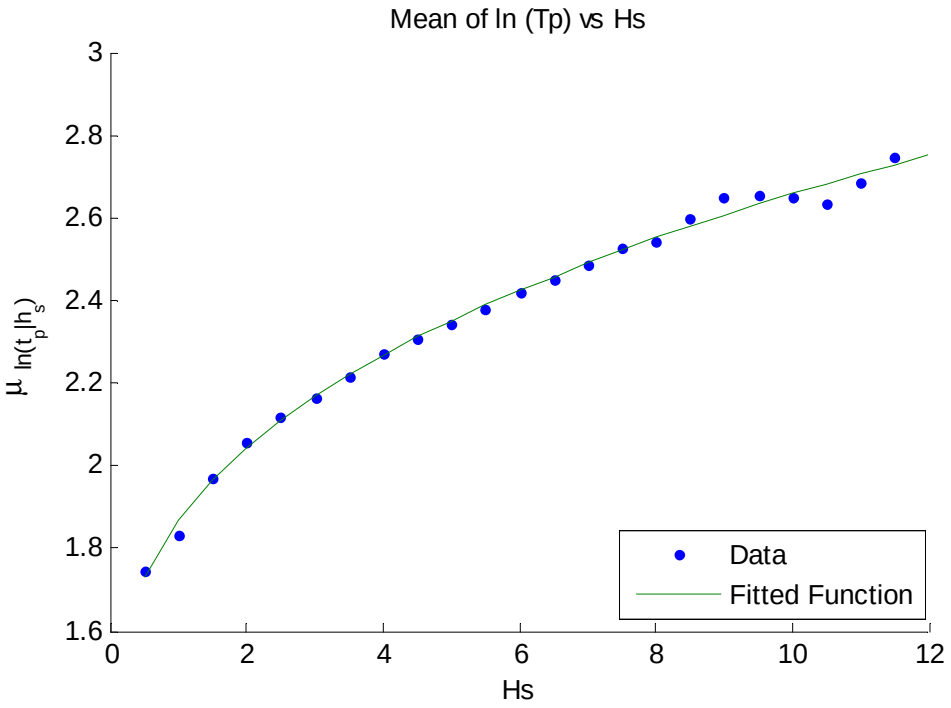

Figure 9.5 Fitted Function of Mean *ln (T_p)*

The mean of *ln(T_p)* can be determined from data by using equation 3.44. The relation between mean of *ln(T_p)* and H_s is assumed follows equation 9.2:

$$\mu_{ln\,(T_p|H_s)} = c_1 + c_2\, {H_s}^{c_3} \tag{9.2}$$

From fitting process, it is found that $c_1 = 1.18$, $c_2 = 0.69$, and $c_1 = 0.33$. For variance of *ln(T_p)*, it is assumed that:

$$\sigma_{ln\,(T_p|H_s)}{}^2 = d_3 + d_1\, exp(-d_2\, H_S) \tag{9.3}$$

The variance of *ln(T_p)* can be established from the data using equation 3.45. By fitting equation 9.3 to the data, it is found that $d_1 = 0.2$, $d_2 = 0.76$ and $d_3 = 0.007$. It is possible for d_3 to have negative value which gives a negative variance of *ln(T_p)* for large H_s. Therefore, d_3 should be restricted from having a negative value. In this work, eventhough d_3 has a positive value from fitting process, it is considered to observe the effect of various values of d_3 on the variance of *ln(T_p)*. Figure 9.6 shows the fitted function of variance *ln(T_p)* when d_3 is not restricted ($d_3 = 0.007$) and when d_3 is set as 0.005 and 0.

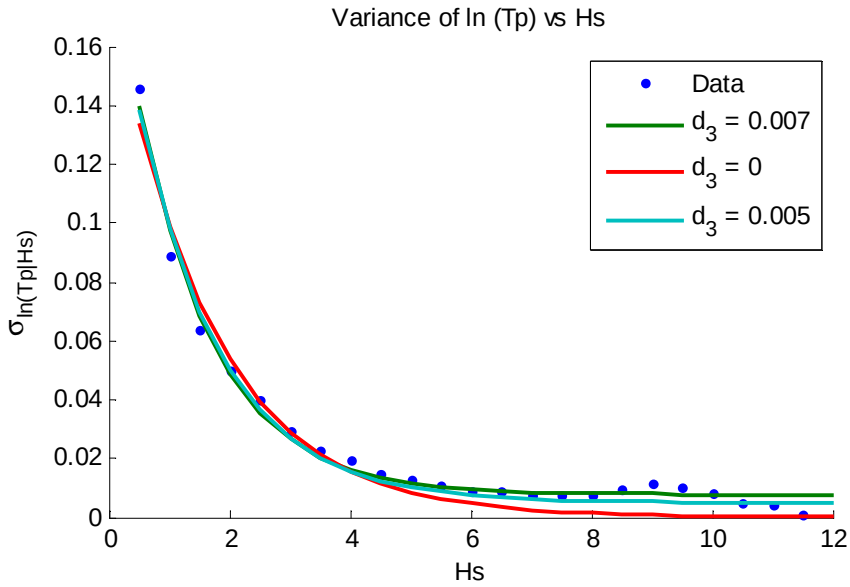

Figure 9.6 Fitted Function of Variance *ln (T_p)*

In figure 9.6, it can be observed that larger d_3 gives increases the variance of $ln(T_p)$ at large H_s. As a consequence, the variability of T_p is also increased at certain H_s when larger d_3 is utilized. This can be proven by checking the 90% band of T_p (range between T_p with CDF 5% and 95%). Figure 9.7 shows the 90% band of T_p on the scatter plot of H_s and T_p.

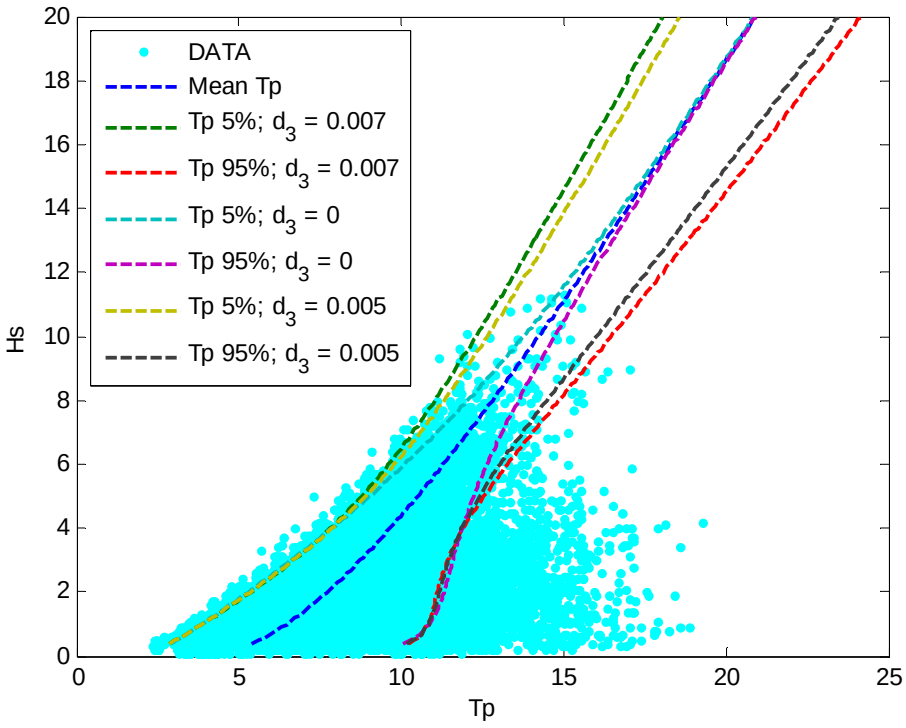

Figure 9.7 90% Band of T_p

In figure 9.7, it can be observed that $d_3 = 0.007$ produces larger 90% band of T_p than the other two values of d_3. The dynamic analysis of jack-up platform not only depends on the wave height but also the wave period. Because of that, larger 90% band of T_p is considered better for dynamic analysis of the jack-up platform since it covers broader range of T_p. Therefore, it is decided that $d_3 = 0.007$ for further analysis.

9.4. Full Long-Term Analysis of Sea Surface

For design wave method, it is assumed that the extreme responses of drag dominated structure, such as jack-up platform, occurs at the largest maximum surface elevation (the largest crest). Therefore, by performing full long-term analysis, the largest crest for certain return period is determined. The full long-term analysis CDF of 3-hour crest is expressed by equation 3.36. In this case, the integration of equation 3.36 is performed numerically where the discretization is introduced in the integration process. Therefore, equation 3.36 can be rewritten as:

$$F_{C_{3h}}(c) = \sum_{T_p}\sum_{H_s} \underbrace{F_{\boldsymbol{C_{3h}|H_s,T_p}}(c|H_s,T_p)}_{\substack{Short-term\\ distribution}} \underbrace{f_{\boldsymbol{H_s}}(H_s) f_{\boldsymbol{Tp|H_s}}(T_p|H_s)}_{\substack{variation\ in\\ H_s and\ T_p}} \Delta H_s \Delta T_p \tag{9.4}$$

In this case, ΔH_s and ΔT_p are assumed constant. However, since the 3-hour wave crest CDF increases significantly, using constant ΔH_s and ΔT_p could lead to numerical error. Therefore a slight modification is made into equation 9.4 for numerical purposes. Instead of using PDF, the marginal distribution of H_s and the conditional distribution of T_p are expressed by CDF. Therefore, equation 9.4 can be rewritten as:

$$F_{C_{3h}}(c) = \sum_{T_p}\sum_{H_s} \underbrace{F_{\boldsymbol{C_{3h}|H_s,T_p}}(c|H_s,T_p)}_{\substack{Short-term\\ distribution}} \underbrace{F_{H_s}(H_s) F_{Tp|H_s}(T_p|H_s)}_{\substack{variation\ in\\ H_s and\ T_p}} \tag{9.5}$$

In this case, the usage of constant ΔH_s and ΔT_p can be neglected then it is assumed that the numerical integration gives result with better accuracy. In addition, theoretically the total sumation of $F_{\boldsymbol{H_s}}(H_s) F_{\boldsymbol{Tp|H_s}}(T_p|H_s)$ is equal to one. However, due to numerical limitation, the total summation of $F_{\boldsymbol{H_s}}(H_s) F_{\boldsymbol{Tp|H_s}}(T_p|H_s)$ is not perfectly one. This could create an upper limit for the 3-hour wave crest CDF. Because of that, the 3-hour wave crest with 100-year return period could not be found since its CDF magnitude could be greater than the introduced upper limit.

To tackle this limitation, the joint distribution is normalized. Therefore, the equation 9.5 is rewritten as:

$$F_{C_{3h}}(c) = \frac{\sum_{T_p}\sum_{H_s} F_{\boldsymbol{C_{3h}|H_s,T_p}}(c|H_s,T_p)\, F_{H_s}(H_s)\, F_{Tp|H_s}(T_p|H_s)}{\sum_{T_p}\sum_{H_s} F_{\boldsymbol{H_s}}(H_s)\, F_{\boldsymbol{Tp|H_s}}(T_p|H_s)} \tag{9.6}$$

The Forisstall wave crest distribution, which are respectively expressed by equation 3.26, is intorduced as $F_{\boldsymbol{C_{3h}|H_s,T_p}}(c|H_s,T_p)$. In addition, the long-term analysis is also performed to find the largest wave height with 100-year return period. In this case, the Forisstall wave height (equation 3.25) is taken as the short term distribution. The result of long term analysis is summarized in table 9.2.

Table 9.2 Result of Long-Term Analysis

Return Period	Wave Height [m]	Wave Crest [m]	Wave Period (*T*) [s]		
			Lower Limit	Mean	Upper Limit
100-year	24.8	15.5	12.7	14.6	16.5

The lower limit and upper limit of wave period is determined by using equation 3.49. The mean wave period is taken as the average between the upper and lower limit of wave period. It is checked that the breaking wave height limit for T=12.7s is 34m and T=16.5 is 51.3 m. Therefore, it is concluded that the wave does not break for combination of wave height/crest and wave period from table 9.2.

Another approach to determine the wave period is by analyzing the 90% band of T_p at H_s with 100-year return period. The wave period is determined as $0.9T_p$. Table 9.5 shows the H_s with 100-year return period, its 90% band of T_p and its range of wave period (T). It can be observed that the presented wave periods in table 9.3 are close the presented wave period in table 9.2 though table 9.3 shows slightly larger wave period than table 9.2. As presented in section 7.3.3, for 5th Stokes, smaller wave period produces slightly larger wave crest which is considered as conservative result. Therefore, the result on table 9.2 is used for further analysis.

Table 9.3 100-year H_s, 90% Band of Tp and Range of T

H_S [m]	13.1 m		
	Lower Limit	Mean	Upper Limit
T_P [s]	14.2	16.3	18.6
T [s]	12.8	14.7	16.7

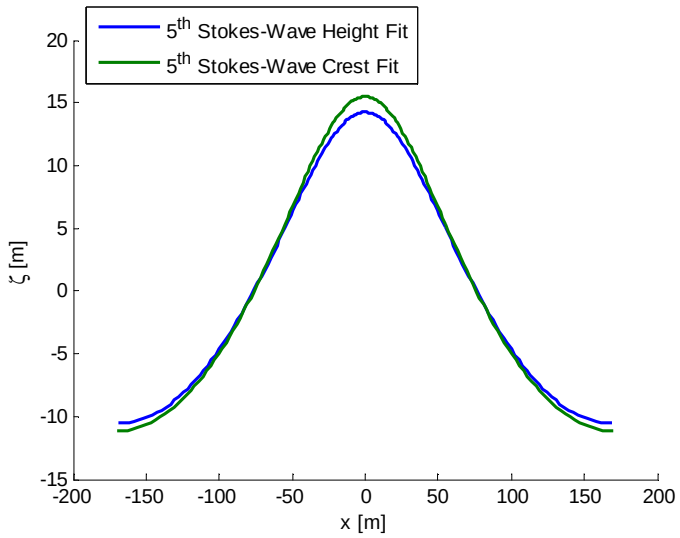

Figure 9.8 5th Stokes Model for 100-year Wave Hight and Wave Crest

Furthermore, the 5th Stokes model is established using combination of wave period and wave height/crest from table 9.2. It is found that the 5th Stokes wave which uses 100-year wave height produces smaller wave crest than 100-year wave crest. This is illustrated by figure 9.8 by taken mean value as the wave period. Therefore, the 5th Stokes wave height is iterated to produce the 100-year wave crest. Table 9.3 shows the 5th Stokes wave height to produce the same 100-year wave crest for each period.

Table 9.4 5th Stokes Wave Height which Produces 100-year Wave Crest

Wave Period [s]	12.7	14.6	16.5
Wave Height [m]	26.2	26.7	26.8

The responses of jack-up are analyzed when hit by the 5th Stokes wave with parameters from table 9.2. As explained in section 5.2.1, hydrodynamic coefficient for second order model is used to determine the responses of jack-up when the 5th Stokes wave is used. Table 9.8 shows the maximum reaction of static baseshear and overturning moment of the jack-up platform. Since table 9.8 shows the reaction, negative maximum occurs when the wave crest hit the jack-up.

Table 9.5 Static Baseshear and Overturning Moment of 100-year Wave Height and Crest

Response	**Wave Height =24.8m**			**Wave Crest = 15.5m**		
	T=12.7s	**T=14.6s**	**T=16.5**	**T=12.7s**	**T=14.6s**	**T=16.5**
Baseshear [kN]	-7.10	-7.84	-8.72	-8.65	-9.85	-11.00
Overturning Moment [kNm]	-397.06	-388.903	-415.45	-541.75	-568.95	-602.87

From table 9.3, it can be observed the fitting 5th Stokes to 100-year wave crest gives greater magnitude than 100-year wave height. In addition, wave period equal to the upper limit (*T=16.5*) produces the most conservative result. However, it decided to use result from mean period to compare with the result of second order analysis in the next chapter.

9.5. Contour Line Method

Beside full long-term analysis of sea surface, contour line method is the other approach to determine the worst responses of jack-up. For ultimate limit state, H_s and T_p with 100-year return period is analyzed. Therefore, the contour line of H_s and T_p with return period 100 year is established. In section 3.3.2, it is explained that the contour line is established by transforming H_s and T_p to standard Gaussian variables (U_1 and U_2). In standard Gaussian space, the contour line is established by creating a circle with radius β_r. For 100-year return period, β_r is determined by equation 9.7. Figure 9.8 shows the contour line for 100-year return period in Gaussian space.

$$\beta_r = \Phi^{-1}\left(1 - \frac{3}{365 \times 24 \times 100}\right) = 4.49 \tag{9.7}$$

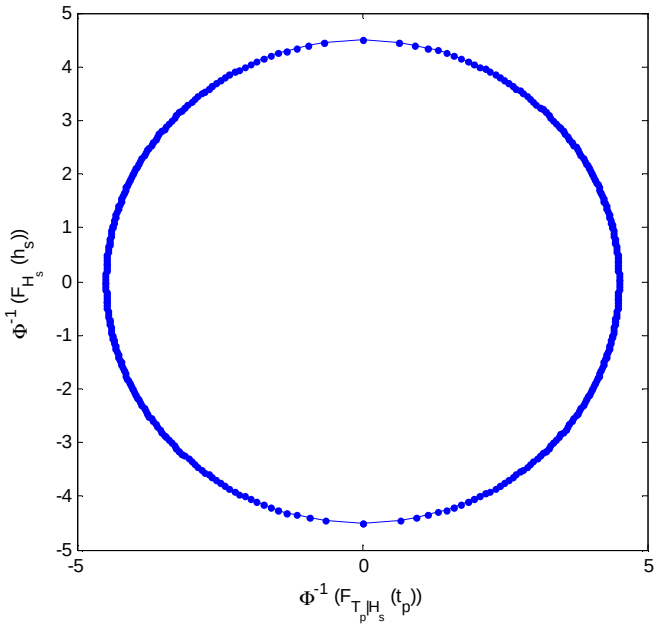

Figure 9.9 100-Year Contour Line in Gaussian Space

The contour line in Gaussian space is transformed back to H_s and T_p by utilizing the CDF of H_s and T_p which are presented in previous section. Figure 9.9 shows the result of contour line when

it is transformed back. In addition, it is also presented the 100-year contour line when $d_3 = 0$ and $d_3 = 0.05$.

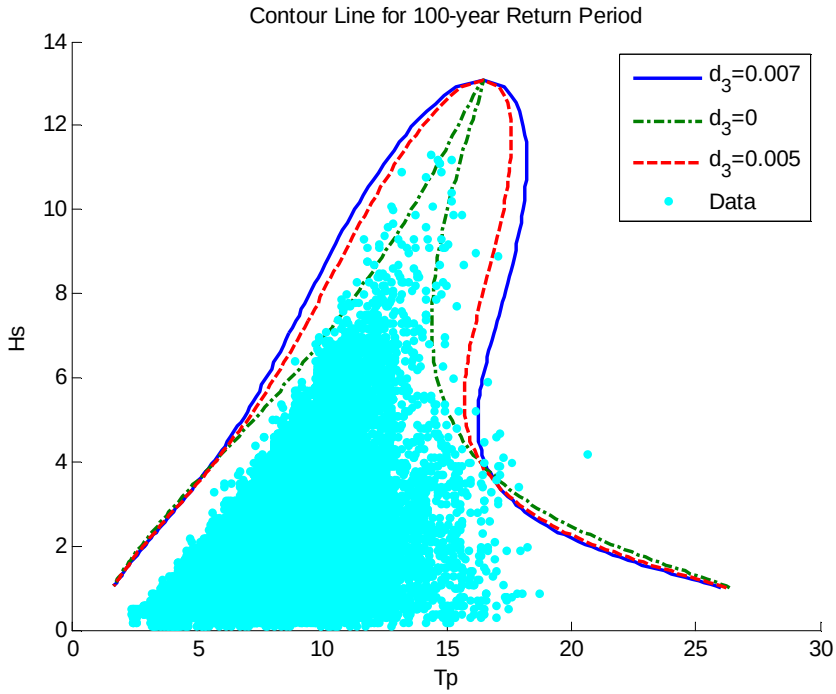

Figure 9.10 100-Year Contour Line with From Various d_3 Coefficient

From figure 9.9, it can be observed that using $d_3 = 0$ produces a contour line with too narrow head. It is considered not conservative when analyzing the worst sea state using the contour line with $d_3 = 0$. Similar to the discussions regarding 90% band of T_p, contour line with $d_3 = 0.007$ is considered the most conservative contour line between the other values.

The quality of the contour line is assessed by counting the number of points that are located outside the contour line. Theoretically, the number of point outside the contour line ($N_{p,outside}$) can be determined as:

$$N_{p,outside} = N_{p,total}\, exp\left(-\frac{1}{2}{\beta_r}^2\right) \tag{9.8}$$

In this case, $N_{p,total}$ refers to total number of data from measurement. By using equation 9.8, $N_{p,outside} = 2$. Observing the data in the Gaussian space and neglecting the data which has $Hs < \lambda_w$, it is found that number of data outside the contour line is 11 which is significatnly greater than the theoretical result. Therefore, the quality of countour line is questionable.

In figure 9.10, it can be observed that points which are outside the contour line are mainly in the H_s range of 3-6m. In addition, these points are located at the right side curve of contour line. The shape of concour line for this specific location depends on the magnitude of parameter d_1 and d_2 in equation 9.3. Therefore, to reduce the number of outside points in these location, the magnitude of d_1 should be increased or d_2 should be decreased. However, this work focus in the extreme condition of H_s and T_p which is commonly located at the head of contour line. Since there are no significant difference for number of outside points at the head part of contour line, it is considered that the current contour line is good enough and modification of contour line is neglected.

9.6. Worst Sea State

A sea state is characterized by combination of H_s and T_p. The worst sea state is the sea state that produces the extreme responses of the jack up. By utilizing the contour line, the worst sea state can be determined. The worst sea state can be used to create a wave spectrum or to establish a probability model of maximum sea surface elevation. There are various considerations to determine the worst sea state in this study which are presented in this section.

9.6.1. Based on the largest maximum surface elevation

For static analysis of drag dominated structure, it is assumed that the largest responses occurs at the largest maximum surface elevation. Therefore, the worst sea state is determined as the sea state which gives the largest of largest maximum surface elevation.

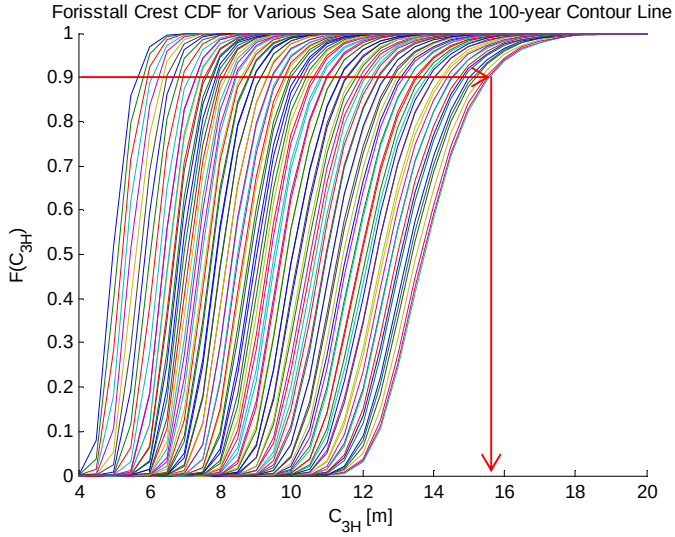

Figure 9.11 Determining Worst Seastate from Largest Surface Elevation

To find this particular sea state, all combination of H_s and T_p are utilized to establish Forisstall crest CDF. For particular level of CDF (in this case when CDF = 0.9), the sea state that gives the largest wave crest is taken as the worst sea state. This was illustrated by figure 9.11. The worst sea state is presented in table 9.6.

Table 9.6 Worst Sea State Based on the Largest Surface Elevation

Worst Seastate	
H_s **[m]**	T_p **[s]**
13	15.9

In this sea state, it is found that the result of 100-year wave crest from full long-term analysis is located at CDF = 0.86. NORSOK [33] suggests that for 100-year return period, the annual exceedence perobability of wave crest is taken as 0.85. This is close to the full long-term result though the result of full long-term gives slight overestimation. Therefore, it is concluded that the presented result in table 9.6 is valid.

9.6.2. Based on the responses from 5th Stokes Wave

The analysis of worst sea state can be extended by fitting the largest wave crest/wave height on 5th Stokes model and simulate the responses of jack-up platform. In this case, the Forisstall distribution of wave height/wave crest is established for several seastates and the wave height/crest with fractile 0.9 is taken to be fitted to 5th Stokes wave.

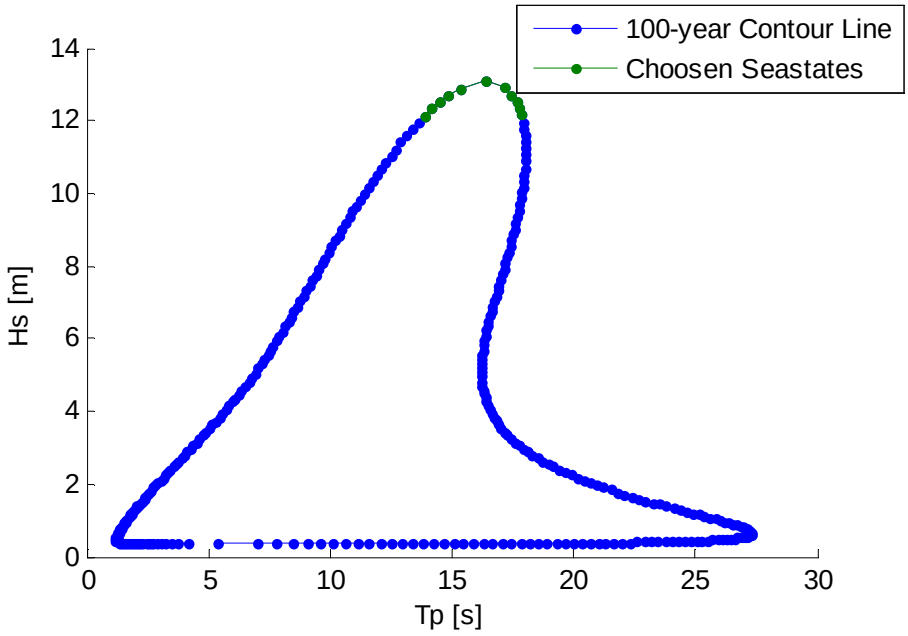

Figure 9.12 Choosen Seastate from Contour Line

Simulating the responses of jack-up platform with 5th Stokes wave can not be performed for all seastates on the contour line since it is time consuming. Therefore, the analysis focus on several seastates. From previous section, it is found that the worst seastate is located around the head of contour line. Therefore, the analysis is concentrated on this area. It is decided that only seastates with H_s larger than 12 m are taken for further analysis. Figure 9.12 shows the location of the choosen seastates. Furthermore, table 9.7 shows the H_s and T_p for the choosen seastates and its largest surface elevation, positive and negative maximum static baseshear reaction and positive and negative maximum overturning moment reaction. Figure 9.13 and 9.14 respectively presents the positive and negative static baseshear reaction and positive and negative overturning moment reaction from each combination of H_s and T_p which are presented in table 9.7.

Table 9.7 Maximum Baseshear and Overturning moment of The Choosen Seastate

No	Hs [m]	Tp [s]	T [s]	H [m]	C [m]	Fitted H [m]	Baseshear [kN]				Overturningmoment [kNm]			
							Positive		Negative		Positive		Negative	
							Crest	Height	Crest	Height	Crest	Height	Crest	Height
1	12.16	18.22	16.40	22.82	13.82	24.20	4.64	4.22	-8.25	-7.31	382.72	368.32	-385.24	-322.50
2	12.34	18.11	16.30	23.18	14.06	24.58	4.74	4.27	-8.47	-7.50	388.24	369.08	-401.85	-337.12
3	12.53	17.96	16.17	23.54	14.32	24.95	4.82	4.32	-8.68	-7.69	392.72	370.56	-417.64	-351.72
4	12.72	17.76	15.98	23.91	14.59	25.36	4.88	4.40	-9.26	-7.84	396.36	372.44	-483.13	-364.88
5	12.91	17.44	15.70	24.29	14.88	25.80	**4.90**	**4.41**	**-9.80**	**-8.00**	**399.01**	**373.92**	-537.85	-379.54
6	13.09	16.55	14.89	24.70	15.29	26.36	4.62	4.17	-9.69	-7.92	387.83	367.27	**-550.12**	**-388.27**
7	12.90	15.42	13.88	24.43	**15.32**	26.25	4.04	3.61	-9.12	-7.15	363.84	340.64	-534.64	-351.44
8	12.71	14.90	13.41	24.11	15.21	25.97	3.71	3.29	-8.74	-6.71	346.40	331.07	-521.33	-329.90
9	12.52	14.50	13.05	23.79	15.08	25.69	3.43	3.03	-8.43	-6.41	333.55	321.52	-508.86	-315.67
10	12.33	14.14	12.73	23.47	14.93	25.39	3.19	2.90	-7.99	-6.11	324.46	315.65	-479.26	-302.07
11	12.14	13.83	12.45	23.14	14.78	25.06	2.95	2.75	-7.64	-5.88	313.83	309.69	-460.58	-290.98

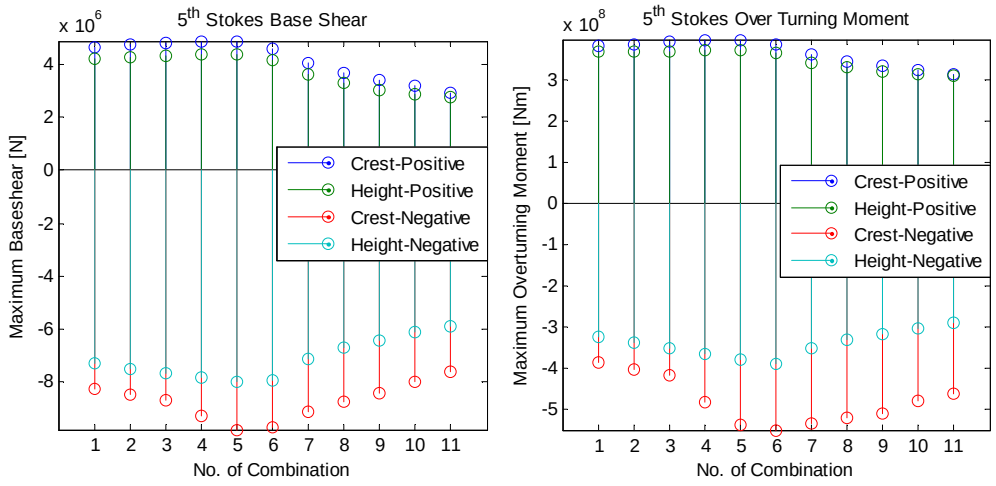

Figure 9.13 Positive and Negative Maximum Baseshear and Overturning Moment

The maximum value of baseshear, overturning moment and wave crest are shaded in table 9.7. The negative maximum baseshear and overturning moment refers to the maximum baseshear and overturning moment when wave crest hit the jack-up (when the wave load has the same direction as the wave propagation). In table 9.7, it is proven again that fitting 5th Stokes to the wave crest produces conservative result than fitting 5th Stokes to the wave height. It can be observed that sea state with H_s = 12.91 m and T_p = 17.44s, which is located slight to the right hand side of the highest point in contour line, gives the largest baseshear (either positive or negative base shear). While the possitive maximum overturning moment also occurs in this seastate, the negative maximum overturning moment occurs at different seastate, which is seastate with H_s = 13.09 m and T_p = 16.55s. This seastate is also the the highest point in the contour line.

In the previous section, the worst sea state refers to H_s = 13.0 m and T_p = 15.9 which is located slightly in the left side of the highest point in contour line. This seastate is not included when calculating the responses of jack-up from 5th Stokes wave. However, it is found that from the presented 11 sea states on table 9.7, seastates with H_s = 12.9 m and T_p = 15.4s produces the largest wave crest which is close to the seastate from previous section.

9.6.3. Based on the responses from irregular sea simulation

The 5th Stokes is only useful when determining the static response of structure. Therefore, to account the dynamic behaviour of the structure when determining the worst seastate along the contour line, the responses of the jack-up are found by simulating an irregular sea. The irregular sea surface is determined from a wave spectrum. To create a wave spectrum, H_s and T_p from each seastates is utilized. In this case, 100 simulations of irregular sea are performed for each seastate. The largest responses from each simlation are gathered and sorted to create an empirical CDF of responses. Furthermore, the comparisson is performed at the empirical CDF=0.9 to determine the worst sea state.

Simulating 100 3-hour second order irregular sea for each seastate is prohibitive due to computational time. Therefore, 100 20-minute first order irregular sea are established for each seastae. The equidistance frequency with random amplitude is used to determine the harmonic component while the Wheeler stretching is utilized to establish the wave particle kinematics. In this case, as explained in section 5.2.1, the hydrodynamic coefficient which refers to first order model hydrodynamic coefficient is used. To avoid the transient effect, the first five minutes of

response time series is neglected. To recover maintain the duration of simulation, additional 5 minutes is included in simulation which makes total duration of simulation equal to 25 minutes. The repetition of sea surface occurs at 20 minute however this does not affect the analysis of responses. In addition, the choosen seastates are the seastates which are presented in table 9.7. Table 9.8 presents the the magnitude of positive and negative maximum of baseshear and overturning moment at fractile 90% while figure 9.14 illustrates the result in table 9.8.

Table 9.8 Maximum Baseshear and Overturning Moment at 90% Fractile

No	Hs [m]	Tp [s]	90%-Baseshear [kN]				90%-Overturningmoment [kNm]			
			Positive		Negative		Positive		Negative	
			Static	Dynamic	Static	Dynamic	Static	Dynamic	Static	Dynamic
1	12.16	18.22	4.84	5.18	-5.60	-6.51	426.66	569.50	-221.90	-391.55
2	12.34	18.11	5.18	5.48	-6.07	-6.74	433.46	598.47	-239.87	-449.36
3	12.53	17.96	5.02	5.37	-6.18	-6.74	437.84	606.71	-253.46	-423.90
4	12.72	17.76	5.31	5.74	-6.18	**-7.31**	437.96	612.36	-263.80	-475.39
5	12.91	17.44	5.23	5.40	-5.71	-7.03	438.49	635.18	-255.02	-480.30
6	13.09	16.55	**5.56**	**6.00**	**-6.44**	-7.29	**467.07**	661.63	**-279.74**	**-490.94**
7	12.90	15.42	4.45	5.67	-5.33	-6.95	417.55	655.69	-210.06	-480.10
8	12.71	14.90	4.81	5.98	-5.41	-6.38	437.65	**722.32**	-228.44	-460.39
9	12.52	14.50	4.60	5.57	-4.85	-6.13	452.45	695.80	-194.54	-450.42
10	12.33	14.14	3.98	5.05	-4.40	-5.80	403.33	706.39	-189.70	-445.24
11	12.14	13.83	3.71	4.80	-4.27	-6.08	386.06	688.85	-190.37	-465.81

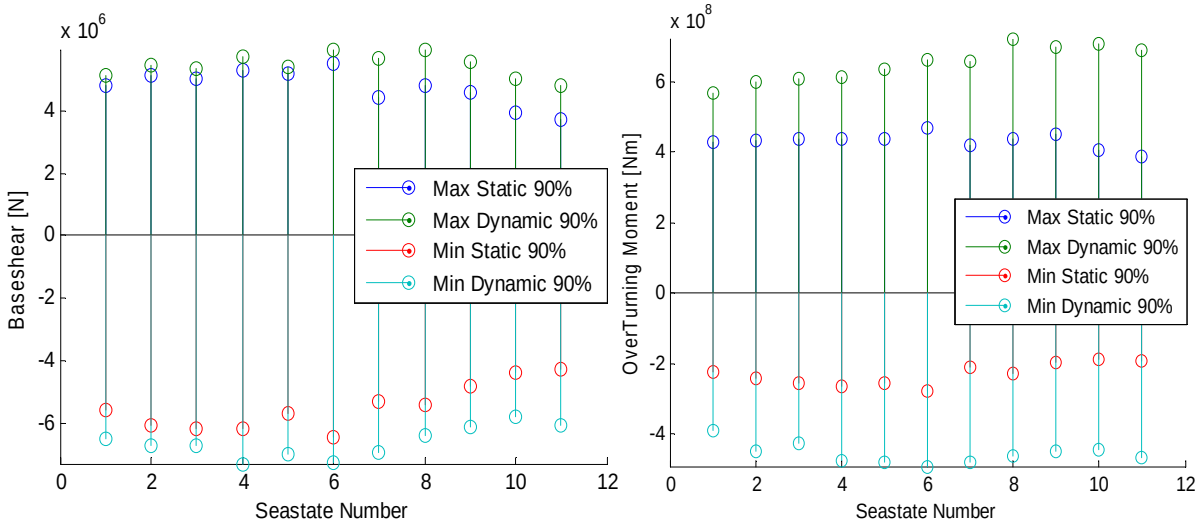

Figure 9.14 Maximum Baseshear and Overturning Moment at 90% Fractile

In table 9.8, it seems that seastate number 6, where H_s = 13.09m and T_p = 16.55s mainly produces the largest maximum response. For maximum negative dynamic baseshear, seastate number 4 gives the largest value though the different between its value and seastate number 6 result is small. In addition, seastate number 8 produces the largest maximum positive dynamic overturning moment.

The positive baseshear and overturning moment mainly occurs when the jack-up hit by the wave trough. In this case, the Wheeler stretching overestimates the load on the jack-up since it set the kinematics on the surface (z = ζ) equal to the kinematics on mean surface (z = 0). Therefore, instead considering the maximum positive result, it is more convincing to determine the worst seastate based on maximum negative baseshear and overturning moment. As a consequence, seastate with H_s = 13.09m and T_p = 16.55s is defined as the worst seastate.

9.6.4. Comparisson of result from three methods

The results of worst seastate from 3 presented method are summarized in table 9.9. From all methods, it seems the H_s is located around 13m while the spectral peak period varies. Due to time limitation, seastate with H_s =13m and T_p =15.9s is not included into the analysis of 5th Stokes and irregular sea. However, the spectral peak periods from 5th Stokes and irregular sea consideration are mainly close to the spectral peak period from surface elevation consideration. It is assumed that when seastate with H_s =13m and T_p =15.9s is included in the analysis of 5th Stokes and irregular sea, it will produce the maximum responses with comparable magnitude as the worst reponses from 5th Stokes and irregular sea consideration. Therefore, it is concluded that the worst sea state along the 100-year contour line is the seastate with H_s =13m and T_p =15.9s. This seastate will be utilized for further analysis.

Table 9.9 Summary of The Worst Seastate

Based on		**Seastate**	
		Hs [m]	**Tp [s]**
Surface Elevation		13	15.9
5th Stokes Wave	**Baseshear**	12.9	17.4
	Overturning Moment	13.1	16.5
Irregular Sea	**Baseshear**	13.1	16.5
	Overturning Moment	13.1	16.5

10. Second Order Wave Effect on Jack-Up Platfrom

To analyze the responses of jack-up platform, several simulations of second order model are performed. Performing complete and continous 3-hour second order analysis is prohibitve since it needs at least $10{,}800^2$ harmonic component for $\Delta t = 0.5s$. Therefore, the partition of time series method is utilized where a 3-hour second order sea is divided into 9 different 20-minute simulations. It was shown in chapter 7 that single 20-minute simulation for first order wave requires at least around 220 harmonic components for equidistance frequency interval method with introducing a cut-off frequency. For second order process, 220^2 harmonic component is utilized. In addition, to avoid the transient effect of the jack-up, the first five minutes in the time series is neglected. To recover the five minutes lost, additional five minutes is introduced. The repetition of wave surface will occur after 20-minute but it is acceptable since the first five minutes in the time series are neglected.

To save memory and computational time, the x-interval is set as 5m and the calculation point is concentrated close to the sea surface (the accuracy and the computational time is presented in section 8.1). The second order model hydrodynamic coefficient, which is described in section 5.2.1 is used. In this case, the worst sea state which is determined in chapter 11 is used. The H_s is set equal to 13m while T_p =15.9s. Various comparissons are performed and presented here.

10.1. 20-Minute Simulation

To establish 30 3-hour of second order simulation with partition of time series method, at least 270 20-minute of second order simulations should be performed. In this work, it is decided to perform 369 20-minute simulations. It is observed that linear extrapolation method takes around 2.5 hours to perform single 20-minute simulation (presented in section 8.1.2). Therefore, due to time and CPU memory limitations, the 369 simulations are distributed equally into 6 computers which are operated simultaneously. Figure 10.1 shows the empirical CDF of maximum negative baseshear for 20-minutes simulation. From figure 10.1, it is observed that there are repetitions in the maximum baseshear. When the data is checked, it is found that there are several 20-minutes simulation that occurs more than once. However, these repetitions occur not on the same computer. Moreover, the repetitions occur not in order. For example, 20-minute case 4 in the first computer is similar to 20-minute case 39 in the second computer. Therefore, it is concluded

that the repetition is random. It is suspected that the method to generate random number in MATLAB is the source of repetition in the simulations where running several simulations on 6 computers simultaneously could creates similar data between the computers.

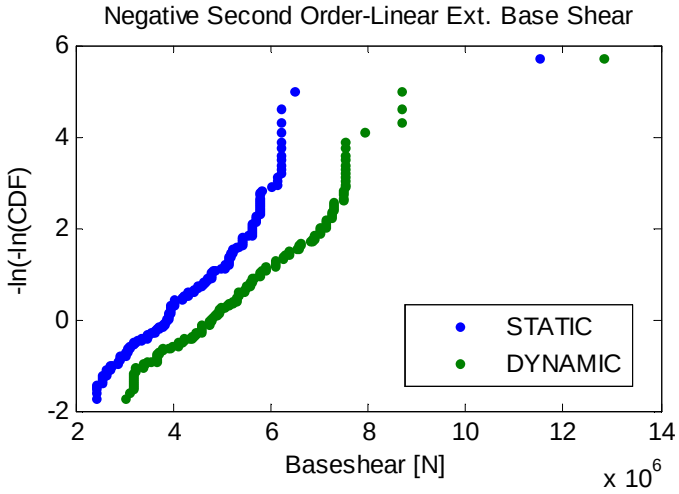

Figure 10.1 Empirical CDF of Maximum Second Order Baseshear

To avoid the repetitions, the data is filtered. The unique maximum negative baseshears (which come from unique surface and kinematics time series) are gathered and sorted. It is found that from the performed 369 20-minutes simulation, there are 124 unique maximum negative baseshears. Therefore, the empirical CDF is established based on these 124 values. Figure 10.2 shows the empirical CDF of maximum negative second order baseshear and overturning moment from linear extrapolation method after neglecting the repetitions.

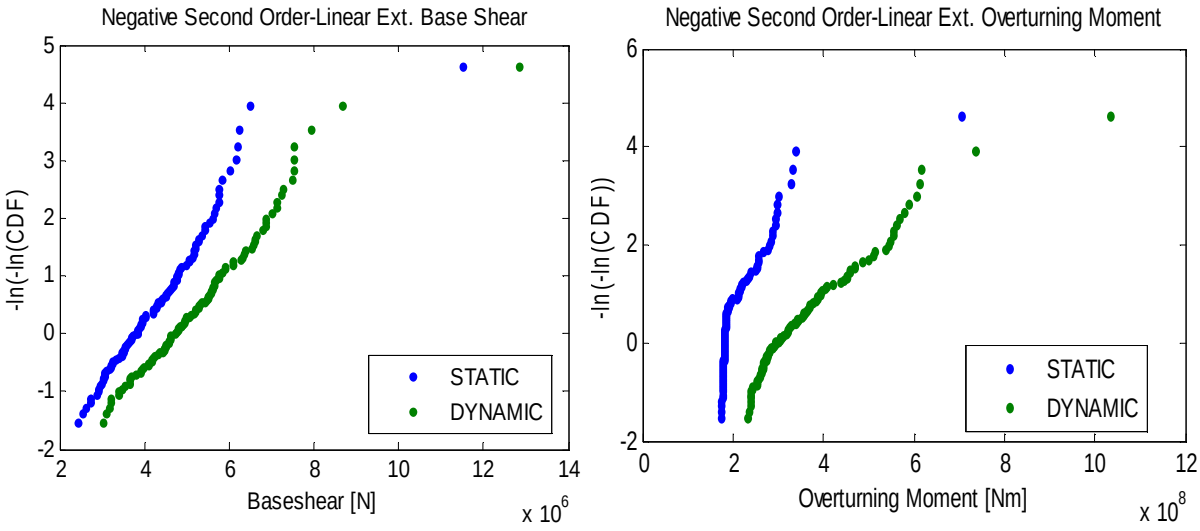

Figure 10.2 Empirical CDF of Maximum Second Order Baseshear and Overturning Moment

In figure 10.3, the empirical CDF of maximum overturning moment seems to have two gradients when it is plotted into Gumbel paper. For static overturning moment, it seems the sample is mainly located around 1.8 kNm and and create a first gradient of the CDF. The gradient of CDF is changed when the overturning moment is larger than 2 kNm for static analysis and 2.9kNm for dynamic analysis. The shift of gradient on the empirical CDF indicating a bad behaving system. One possible reason for this jump is because the kinematics in 3 legs of jack-up occurs at the same phase which creates a larger overturning moment. The change of gradient does not occurs at the empirical CDF of baseshear.

The EDAF is determined by calculating the ratio between dynamic and static result for CDF = 0.9. It is found that for baseshear, the EDAF is equal to 1.25 while EDAF is 1.94 for overturning moment. The analysis is continued by comparing the CDF of baseshear and overturning moment from first order and second order sea and utilizing various stretching method. Utilizing various stretching methods, the computational time of single 20-minutes simulation of first order sea is around 20 seconds which is greatly faster than second order sea simulation. In addition, performing Wheeler stretching into single 20-minutes second order sea only requires 400 seconds approximately. The empirical CDF of largest baseshear and overturning moment for 20-minutes simulation and various model are presented in figure 10.3.

Six methods are compared in figure 10.3. First order refers to first order sea and second order refers to second order sea. Linear extrapolation, constant and Wheeler indicate the performed stretching method to calculate the kinematics along the z-coordinate. In section 5.2.1, it is explained about the hydrodynamic coefficients which are used for first order and second order sea. However, for single cylinder case, which is explained in section 7.4, using the hydrodynamic coefficient of first order model (coef.1) on kinematics from first order linear extrapolation greatly overestimates the wave load and responses. As explained in section 5.2.1, the coef. 1 is a modification of drag and added mass coefficient to produce load from first order sea with comparable magnitude as the load form second order sea. This modification is mainly used for first order Wheeler stretching. That is why using coef. 1 on first order linear extrapolation (or on constant stretching) will produces conservative result. Therefore, it is decided to test the hydrodynamic coefficient of second order model (coef.2) to the first order linear extrapolation.

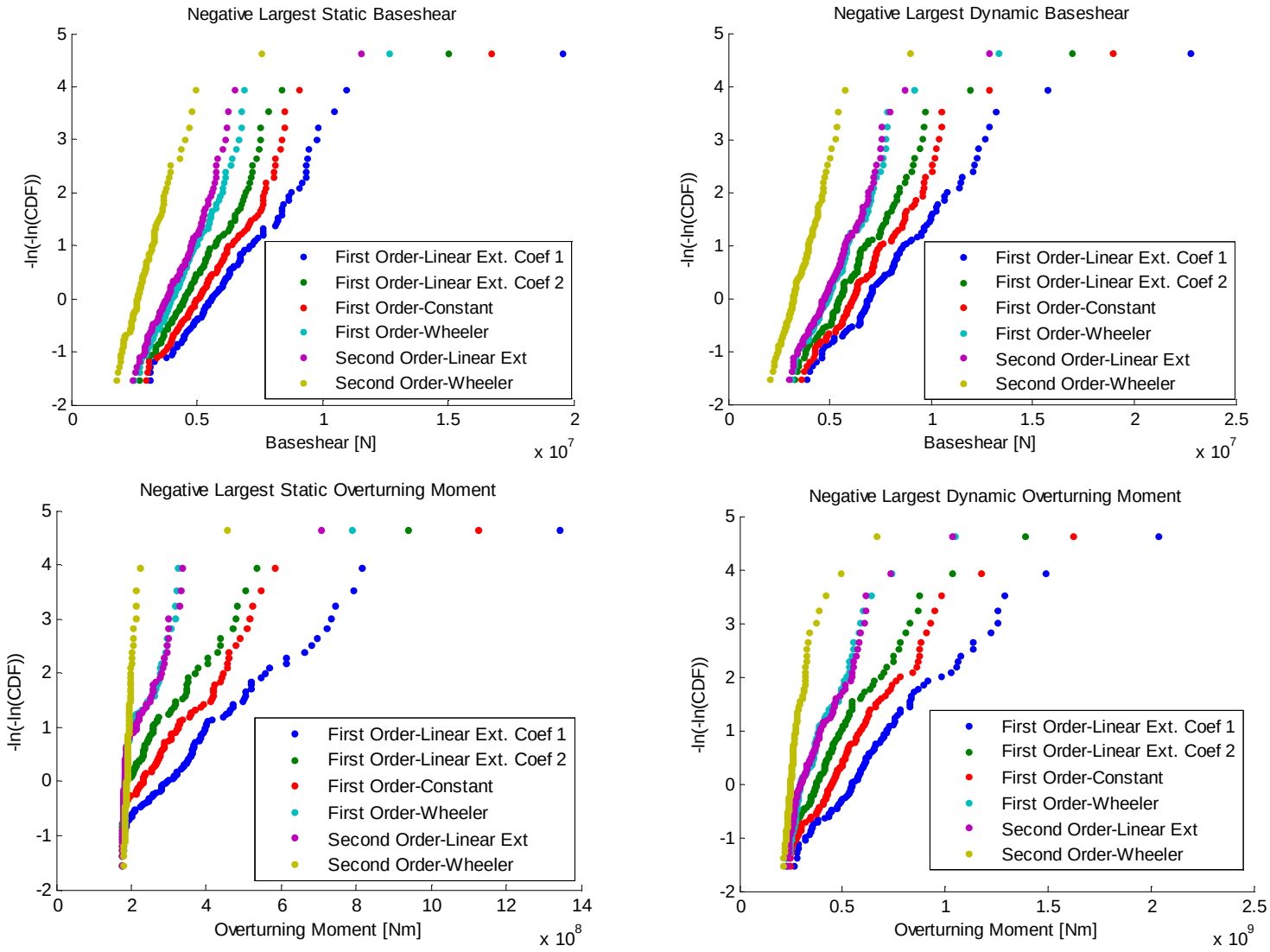

Figure 10.3 Distribution of Maximum Negative Baseshear and Overturing Moment

In figure 10.4, similar to single cylinder case (section 7.4), the Wheeler stretching on second order sea produces the lowest baseshear and overturning moment while the linear extrapolation on first order sea with coef.1 greatly overestimates the response. The constant stretcing on first order sea also overestimates the response. It seems using coef.2 to first order linear extrapolation still produces greater result than linear extrapolation on second order sea. Moreover, there is a good agreement between first order Wheeler and second order linear extrapolation which is also experienced for single cylinder case in section 7.4 though first order Wheeler stretching gives slighly smaller value for cylinder case. This indicates that instead of using linear extrapolation on second order sea which is time onsuming, the irregular sea can be simulated by performing Wheeler stretching on first order sea with modified hydrodynamic coefficient. However, Wheeler streching gives great overestimation of wave load at the wave trough.

10.2. 3-Hour Simulation

The largest responses of each 9 20-minute simulations are gathered and sorted to produces an empirical CDF of 3-hour simulation. In addition, the empirical CDF is fitted into Gumbel distribution. The magnitude at 90% fractile is presented in table 10.1. In addition, the EDAF, which is taken as ratio between dynamic and static responses at 0.9 freactile, is also presented.

Table 10.1 Maximum Baseshear and Overturning Moment at 0.9 Fractile

Method	Negative					
	Baseshear [kN]			Overturning Moment [kNm]		
	Static	Dynamic	EDAF	Static	Dynamic	EDAF
First Order Linear Extrapolation (Coeff.1)	14.2	17.5	1.2	793.2	1592.5	2.0
First Order Linear Extrapolation (Coeff.2)	10.9	12.9	1.2	672.0	945.8	1.4
First Order Constant	12.1	14.3	1.2	763.0	1260.4	1.7
First Order Wheeler	9.2	10.4	1.1	522.0	790.7	1.5
Second Order Linear Extrapolation	8.3	10.0	1.2	471.3	817.8	1.7
Second Order Wheeler	4.5	6.7	1.5	310.6	418.6	1.3

In addition, table 10.2 shows the 5th Stokes static responses for 100-year crest with middle wave period (T=14.6s) which is presented in section 9.4.

Table 10.2 5th Stokes Static Responses for 100-year Return Period

5th Stokes Static Responses	Wave Crest = 15.5m
	T=14.6s
Baseshear [kN]	9.85
Overturning Moment [kNm]	568.95

From single cylinder case, the linear extrapolation on second order wave produces comparable 3-hour static baseshear to the result from 5th Stokes. Therefore, for jack-up cases, the static baseshear of 5th Stokes wave utilizing longterm analysis of wave crest is compared to the 3-hour static baseshear from linear extrapolation on second order wave. It should be noted that the comparisson between 5th Stokes and irregular wave for cylinder case is based on the same wave occurence (the 5th Stokes is fitted to produce the same wave crest as irreular wave simulation). However, for jack-up case, the wave profile for 5th Stokes is different than the second order wave profile since the 5th Stokes wave is based on wave crest from longterm analysis.

By comparing result from table 10.1 and 10.2, the ratio of static baseshear between 5th Stokes and second order linear extrapolation is around 1.18. This implies that the Stokes wave produces conservative result. However, the empirical CDF of 3-hour jack-up responses is merely based on 13 data. As a consequence, the epistemic uncertainty on the CDF shape is great. The epistemic uncertainty can be illustrated by performing bootstrapping to the fitted CDF. Left figure in figure 10.4 shows the fitted CDF (Gumbell distribution) of baseshear and its bootstrapping limit for second order linear extrapolation case.

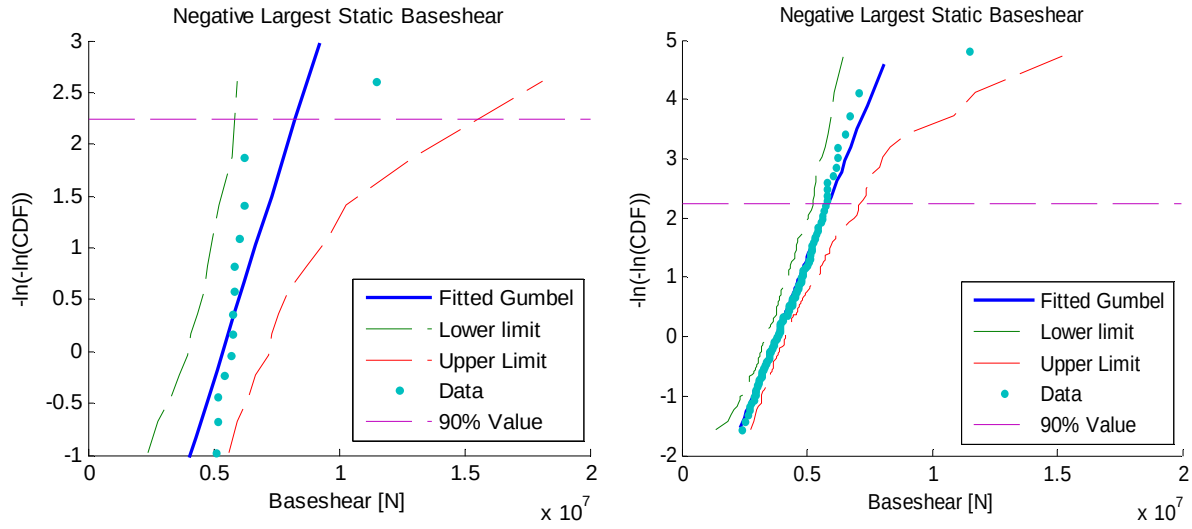

Figure 10.4 Maximum Static Baseshear Empirical CDF for Second Order Linear Ext. (Left: 3-hour Static Baseshear; Right: 20-Minute Static Baseshear)

From figure 10 left side, it can be observed that the range of deviation at 90% percentile is around 10kN. This indicates that the quality of 3-hour static baseshear CDF is bad. Therefore, another approach to extablish the empirical CDF of 3-hour static baseshear is performed. For 20-

minute simulation, 124 data exists. Therefore, the Gumbel distribution is fitted into 20-minutes static baseshear data and presented as right side figure in figure 10.4. By assuming that the maximum of static baseshear is statistical independent and identical distributed, the Gumbel distribution of 3-hour static baseshear can be established by:

$$F_{X3H}(X) = \left(F_{X20M}(X)\right)^9 \tag{10.1}$$

Therefore, the new Gumbel distribution and its bootstapping limit is presented in figure 10.5. Table 10.3 shows the 90% fractile value of 3-hour static responses from second order linear extrapolation including its lower and upper bootstraping limit. From table 10.3, the 90% fractile of 3-hour static baseshear is 7.9 kN which is smaller than previous result. However, the range of deviation at 90% level is 1.7kN indicating the new baseshear CDF has better quality than the previous baseshear CDF. Ratio between 5th Stokes and 90% fractile of 3-hour static baseshear is 1.2. Utilizing the upper limit of bootstaping, the ratio between 5th Stokes and 3-hour static baseshear is 1.1 which is close to the ratio from sinle cylinder case (1.08).

Table 10.3 3-Hour StaticResponse from Second Order Linear Extrapolation

Static Responses	90% Value	Bootstrapping Limit	
		Lower	Upper
Baseshear [kN]	7.9	7.2	8.9
Overturning Moment [kNm]	404.2	367.9	462.48

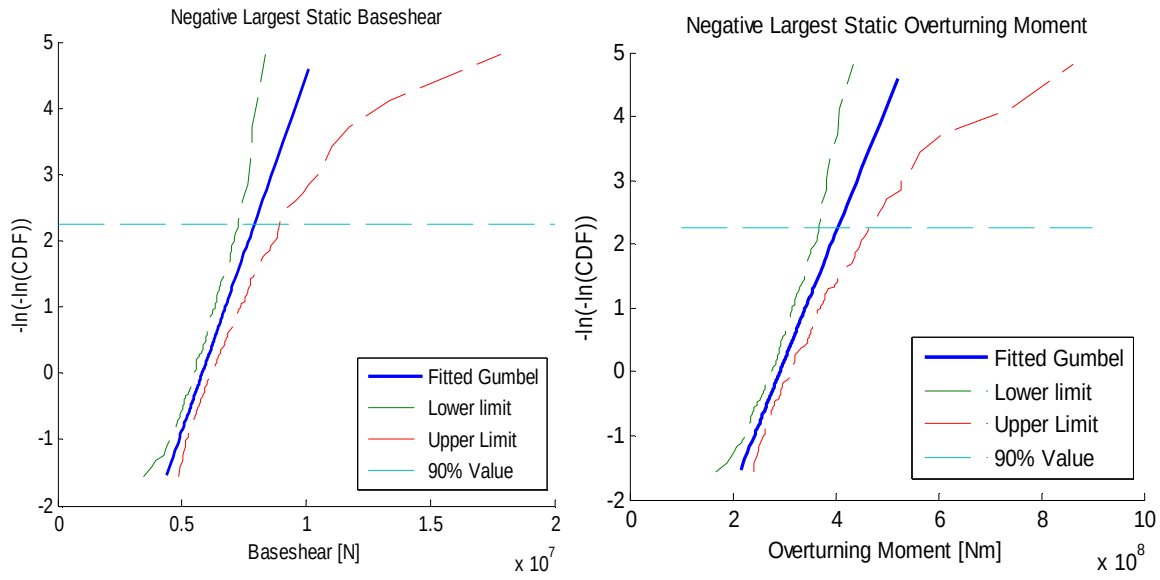

Figure 10.5 3-Hour Maximum Static Baseshear Empirical CDF (Using linear extrapolation on second order wave)

For static overturning moment, the ratio between 5th Stokes and 90% value of second order linear extrapolation result is 1.4. In addition, the ratio between 5th Stokes and upper bootstrapping limit of 90% value is 1.2. The analysis is continued by observing the CDF of wave crest (maximum surface elevation). In this case, the largest wave crest at x=0 is observed from 124 20-minute simulations. Left side figure in figure 10.6 shows the CDF of largest wave crest for 20-minute simulation. Furthermore, the CDF of largest wave crest for 3-hour simulation is established from CDF of largest wave crest for 20-minute simulation by utilizing equation 10.1. Right side figure in figure 10.6 shows the CDF of largest wave crest for 3-hour simulation.

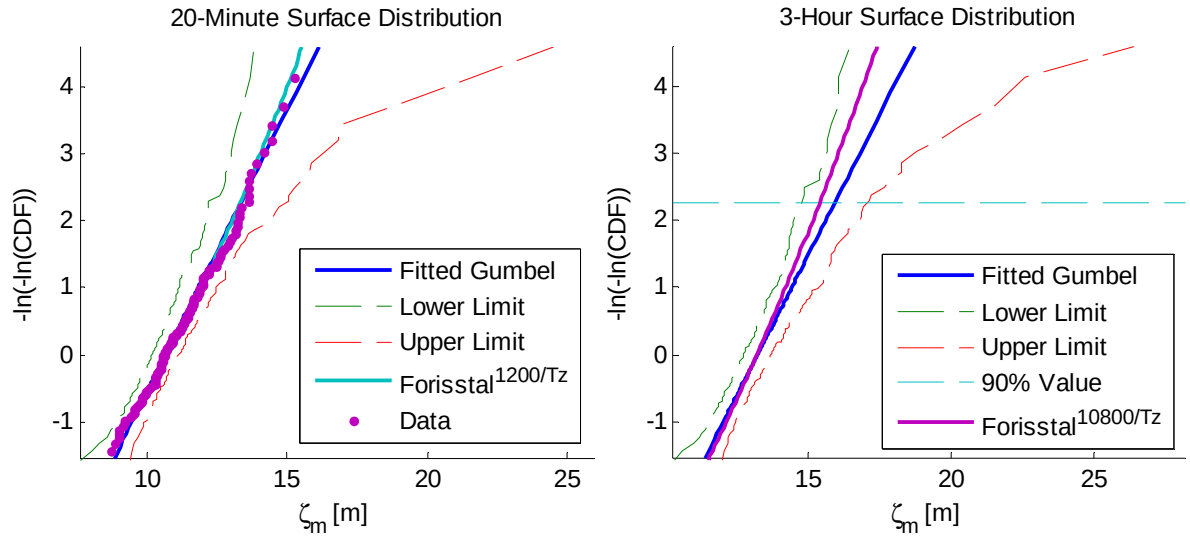

Figure 10.6 Distribution of Largest Wave Crest
(Left: 20-Minutes Largest Crest; Right: 3-Hour Largest Crest)

As explained in section 3.2.3, Gumbell distribution is an asymptotic extreme distribution which is a good distribution when $N \rightarrow \infty$. Therefore, it can be observed in figure 10.6 that the fitted Gumbell distribution gives larger wave crest than Forisstall crest distribution. In addition, for high fractile, the data is closer to Forisstall distribution than the fitted Gumbell. However, the difference between Gumbell and Forisstall crest at 90% percentile can be tolerated. The 90% value of wave crest from Gumbell and Forisstall including the bootstraping limit of Gumbell distribution is presented in table 10.3.

Table 10.4 90% Wave Crest

Forisstall 90% crest[m]	Gumbell 90% Crest	Lower Limit	Upper Limit
15.5m	15.9m	15.1m	17.1m

However, for jack-up, the largest baseshear and overturning moment does not only depend on the crest magnitude. In addtion, the crest tends to be located close to the leg location than at x=0 when largest baseshear and overturning moment occurs. Therefore, the surface and kinematic profile when the largest baseshear and overturning moment occur are observed.

10.3. Surface and Wave Kinematic Profile at Jack-Up leg

The observation is focused on horizontal particle velocity since it greatly affects the wave load for jack-up leg. In addition, the observation is concentrated to second order linear extrapolation method. There is no data that perfectly coincides with 90% responses value which are presented in table 10.3. Therefore, the the observation is performed with data which has the closest responses to the result in table 10.3. The observed baseshear and overturning moment is smaller than result in table 10.3. In addition, the kinematics and surface profile when the largest observed responses occurs from second order model is also observed. Figure 10.7 shows the illustration of surface elevation profile from event close to 90% static baseshear (left figure) and overturning moment (middle left figure). The middle right figure shows the largest observed responses from second order model while the right figure shows the 5th Stokes wave profile which gives the largest static baseshear and overturning moment. In figure 10.7, the surface elevation it coarser than the real data. The exact surface profile can be found in appendix 29.

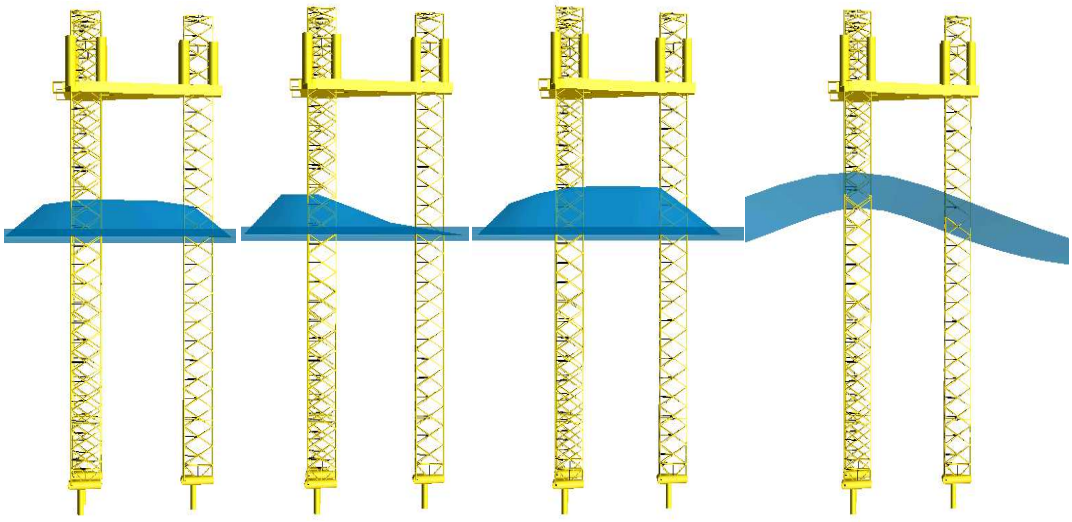

Figure 10.7 Surface Elevation Profile at Largest Responses
(Left: 90% Baseshear; Middle-Left: 90% Overturning Moment; Midle-Right: Largest Observed Response;Right: 5th Stokes)

From figure 10.7, it can be observed that when the maximum static baseshear and overturning moment occurs, the 5th Stokes wave crest is located at the location of the double leg of the jack-

up. The same surface elevation profile is observed for the 90% overturning moment from second order sea. However, for 90% baseshear, it seems that all jack-up legs are located at two adjacent wave crests. In addition, the magnitude of wave crest for the 90% baseshear is smaller than the 100-year wave crest and the magnitude of wave crest for the largest overturning moment. Table 10.5 shows the magnitude of wave crest from the four observed cases.

Table 10.5 Wave Crests from The Four Observed Cases

5th Stokes	90% Baseshear	90% Overturning Moment	Largest Response
15.5m	13.4m	15.0m	17.3m

In table 10.4, the wave crest of 90% baseshear is smaller than 5th Stokes wave crest. This is because the observed case that represents 90% baseshear does not really produces the 90% value of static baseshear. However, this indicates that due to the spacial effect, the largest response in irregular seas could be smaller than 100-year wave crest. Therefore, it is concluded that for irregular wave, the largest value could come from two adjacent waves with magnitude of crest smaller than 100-year wave crest.

Figure 10.8 shows the kinematic profile along z-coordinate at the double and single leg of jack-up when the largest baseshear and the largest overturning moment occurs, both from second order wave and 5th Stokes wave. In addition, the largest observed response from second order model is also presented.

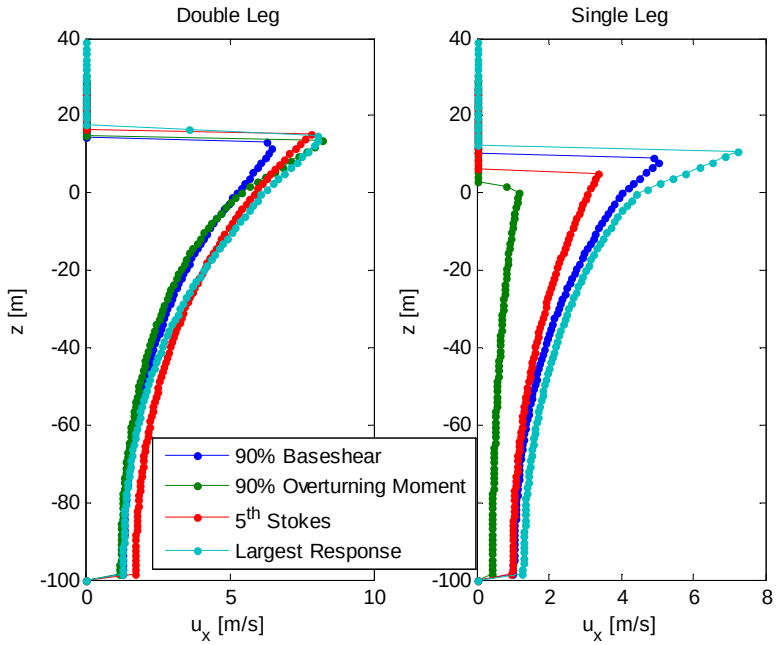

Figure 10.8 Kinematic Profile along z-coordinate at Jack-Up Leg

Based on the kinematic profile at figure 10.7, when the largest baseshear occurs, 5th Stokes tends to have larger wave crest and larger magnitude of horizontal velocity than second order wave model at the double leg location. However, at the single leg location, second order wave model has larger wave crest and larger magnitude of horizontal velocity than 5th Stokes. Since the drag load depends on square of horizontal velocity, it seems the difference on double leg location is the source of overestimation on 5th Stokes baseshear. The difference between 5th Stokes and second order model in each leg is measured by the ratio of drag load normalized by leg diameter.

$$Ratio\ of\ Normalized\ Drag\ Load = \frac{\left[\sum_L \frac{1}{2}\rho\ C_D\ u_x|u_x|\ dz\right]_{5^{th}\ Stokes}}{\left[\sum_L \frac{1}{2}\rho\ C_D\ u_x|u_x|\ dz\right]_{Second\ Order}} \qquad (10.2)$$

At the double leg location, the ratio of normalized drag load is around 1.5 while the ratio in the single leg location is around 0.6. This means, Stokes 5th produces 50% larger drag load then second order model at double leg location while it produces 40% smaller drag load at single leg location. In total, the ratio of normalized drag load between 5th Stokes and second order model is 1.3 which explain the ratio of static baseshear in previous section.

For overturning moment, it seems that the largest values is more affected by the horizontal velocity around the surface. In figure 10.8, large horizontal velocity are located around sea surface at double leg location for 90% overturning moment configuration which produces larger overturning moment that 90% baseshear configuration. The ratio of normalized overturning moment in double leg is 1.3 while the ratio is 7.9 in single leg. This means, 5th Stokes gives 30% larger overturning moment from drag load than second order model in double leg location. In addition, the overturning moment in double leg location seems dominating the total overturning moment since the ratio of total normalized overturning moment is 1.4 though 5th Stokes wave produces almost 8 times larger overturning moment than second order model.

10.4. EDAF for Jack-Up

Table 10.1 presents the EDAF for every observed case. However, it is explained before that the EDAF is merely based on 13 data. Thefore, as the new EDAF is established by fitting a Gumbel distribution to 20-minutes responses and raised it to the power 9. Table 10.4 shows the new 90% fractile value and its EDAF.

Table 10.6 Maximum Baseshear and Overturning Moment at 0.9 Fractile

Method	Negative					
	Baseshear [kN]			Overturning Moment [kNm]		
	Static	Dynamic	EDAF	Static	Dynamic	EDAF
First Order Linear Extrapolation (Coeff.1)	13.0	16.3	1.3	918.6	1516.2	1.7
First Order Linear Extrapolation (Coeff.2)	10.1	12.3	1.2	592.1	1030.4	1.7
First Order Constant	11.2	13.7	1.2	699.6	1197.5	1.7
First Order Wheeler	8.5	10.0	1.2	421.3	747.5	1.8
Second Order Linear Extrapolation	7.9	9.7	1.2	404.3	768.8	1.9
Second Order Wheeler	5.4	6.6	1.2	266.4	440.4	1.7

In table 10.1, it seems by including the dynamic behaviour of the structure, the baseshear increases around 20-30% while overturning moment increases around 70-90%. This indicates that the dynamic behaviour is crucial when analyzing overturning moment reaction. In addition, performing Wheeler stretching on first order sea by utilizing first order hydrodynamic coefficient produces comparable result to second order linear extrapolation. Since it spends only 0.1% second order linear extrapolation computational time, it is recommended to use first order Wheeler for analyzing the ultimate limit state of jack-up on irregular seas.

10.5. Summary

Similar to cylinder case, performing Wheeler stretching on second order sea significantly underestimates the wave load on jack-up. However, performing Wheeler stretching on first order sea and using the modified hydrodynamic coefficients (first order hydrodynamic coefficients) produces comparable result to linear extrapolation on second order sea.

By utilizing linear extrapolation on second order sea, the responses (reaction baseshear and overturning moment) from second order iregular sea is smaller than responses from 5^{th} Stokes wave. This indicates that utilizing 5^{th} Stokes is a conservative approach to measure the responses of jack-up. Moreover, responses from iregular seas is a random process which requires big number of data to establish result with high confidence level. In this work, the 3-hour extreme distribution is predicted from 20-minute extreme distribution. However, it is more reliable to established 3-hour distribution directly from 3-hour simulation.

The extreme baseshear is possible coming from wave with smaller crest that 100-year wave crest. In this case, the extreme baseshear is greatly affected by the wave length. However, the extreme overturning moment is greatly affected by the kinematic profile around the surface.

11. Conclusion and Recomendation for Future Work

11.1. Conclusion

This thesis work deal with the time domain simulation of structure responses on irregular seas. The main focuses are the effects of second order irregular sea on jack-up paltform and the alternative methods to reduce the computational time. In the begining, the verification of second order wave model is performed by comparing the distribution of second order crest with Forisstal crest distribution. The analysis in continued by observing the effect of second order on single vertical cylinder with diameter 1m before tested on jack-up platform.

The first approach to reduce computational time is by reducing the number of harmonic component. Dividing 3-hour analysis into 9 20-minute simulations could significantly decreases the number of component from 10,800 components to 1,200 components (when time interval is 0.5 seconds) since smaller duration of simulation has greater frequency interval. In addition, a cut-off frequency is utilized to maintain the energy on the wave spectrum when the second order correction is introduced. When introducing the cut-off frequency, the required harmonic component is reduced from 1,200 to around 220 components (depend on the significant wave height) which gives additional cut to the computational time. In addition, cut-off frequency changes the surface elevation process from broadbanded process to narrowbanded process. All in all, the crest distribution from second order surface model shows a good agreement with Forisstall distribution which verifies the quality of second order surface model.

Various extrapolation methods to define the kinematics along vertical coordinated are observed. Utilizing Wheeler stretching on second order wave gives comparable surface horizontal velocity to surface horizontal velocity of linear extrapolation on second order wave. However, Wheeler stretching on second order wave underestimates the horizontal velocity below the surface. To verify the wave particle kineatics, the horizontal particle velocity from linear extrapolation on second order wave model is compared to horizontal particle velocity from 5^{th} Stokes wave. In this case, the second order wave model tends to produces larger surface horizontal velocity than 5^{th} Stokes wave though the second order model produces smaller horizontal velocity than 5^{th} Stokes below mean surface.

In single vertical cylinder tests, the Wheeler stretching on second order wave greatly underestimates the static response of the cylinder. On the other hand, linear extrapolation method on second order wave produces comparable responses of the structure to the responses from 5th Stokes wave. In addition, performing Wheeler stretching on first order wave (Gaussian sea) with utilizing the modified hydrodynamic coefficients produces comparable static baseshear to the static baseshear from 5th Stokes wave though it underestimates the static overturning moment.

For jack-up case, various altervatives to reduce computational time in grid system are observed. It is found that utilizing grid system with x-interval = 5m and gradually decrease z-interval produces the smallest computational time with accepatable deviation of static and dynamic response. By applying the second order kinematics only up to 50m (where the depth is 100m) can decrease the computational time up to 20% with acceptable deviation of responses. In this case, the cut on computational depends on the distribution of calculation points along the z-coordinate. In addition, only applying the second order kinematics at location close to water surface increases the magnitude of static and dynamic responses.

It is found that the maximum baseshear and response do not always occur at the largest surface elevation. Therefore, the assumption which is made in spool-to-extreme and linear-to-extreme method is not fully correct. As a consequnce, the deviation of extreme responses may be great and the actual extreme response on the time series may be not observed. However, the analysis for spool-to-extreme and linear-to-extreme method is only based on one simulation. Since the occurence of largest response is a random process, analysis based on statistical comparisson should be performed.

For jack-up case, the responses from irregular seas is compared with the responses from longterm analysis of the wave. In this case, the 5th Stokes wave is fitted to wave with 100-year return period. Similar to the result from single cylinder case, in jack-up case, Wheeler stretching on second order wave greatly underestimates the static responses while linear extrapolation on second order wave gives comparable static responses to the static responses from 5th Stokes wave. In addition, in irregular seas, the largest static baseshear could occurs when the jack-up hit by the wave with smaller crest than 100-year wave crest but comparable length to the distance between jack-up leg. On the other hand, the largest static overturning moment tends to occurs from wave with crest close to 100-year wave crest since the static overturning moment is greatly

affected by length of moment arm and the kinematic profile along the surface. Furthermore, from the observed jack-up, dynamic analysis produces 20% larger baseshear and 90% larger overturning moment than static analysis. This indicates that performing quasistatic analysis without including the EDAF could greatly underestimates the baseshear and overturning moment of jack-up in irregular seas.

11.2. Recommendations for Future Work

In this work, to analyze the jack-up responses, the 3-hour simulation is divided into 9 differents 20-minute simulation to decrease the harmonic component. The analysis can be continued to observed the effect of utilizing equal area and peaked equal area method to the jack-up responses. In addition, the effect second order irregular wave on various jack-up natural periods should be observed. The jack-up natural period can be changed by adjusting the mass on the jack-up.

It is found from this study that using small z-interval at location close to sea surface and large z-interval around the sea bottom can decrease the computational time. Therefore, another analysis can be performed by only using small x-interval around the jack-up leg. In addition, several 3-hour simulation should be performed to verify the quality of spool-to-extreme and linear-to-extreme method since the verificantion is based only on one simulation in this study.

Due to time limitation and repetition in data, only 13 3-hour simulation exists. Therefore, the distribution of 3-hour extreme response is predicted by raising the distribution of 20-minute extreme response to the power of 9. The distribution of 20-minute extreme response is determined by fit a Gumbell distribution to the data. Since the Gumbell distribution is a asymptotic distribution of extreme, it overestimates the extreme response at high percentile. Therefore, raising the distribution of 20-minute extreme response to the power of 9 could increase the overestimation in the Gumbell. Therefore, for future work, it is important to check distribution of 3-hour extreme response by directly fitting the Gumbell distribution to adequate number of 3-hour simulation. In addition, it is also interesting to check the effect of second order irregular wave on jack-up for short crest sea. A validation of the approach to simulate second order irregular wave with small number of harmonic component which is presented in section 4.4 should be performed.

References

[1] Aarsnes, L.H. (2015) *Estimation of Extreme Response –in a Jack-Up Platform by Application of Stochastic Model*, Master Thesis, Department of Marine Technology (NTNU), Trondheim

[2] Adcock T.A.A. and Draper, S. (2015) "The Second Order Contribution to Wave Crest Amplitude," *Proc. 25th ISOPE Conf., Vol III, Hawaii, USA*

[3] Amdahl, J. (2005) *TMR4205: Buckling and Ultimate Strength of Marine Structures*. Trondheim: Department of Marine Technology (NTNU)

[4] Andersen, O.J. (2009) *Statoil Memo Describing Why and How Tp should be Corrected*

[5] Binner, I. (2011) *Time-domain Simulation of Floating Wind Power Plants in Irregular Seas*, Master Thesis, Department of Marine Technology (NTNU), Trondheim

[6] Bækkedal, E. (2014) *Time-domain Simulation of Marine Structures in Irregular Seas*, Master Thesis, Department of Marine Technology (NTNU), Trondheim

[7] Cartwright, D. E. M and Longuet-Higgins, M.S. (1952) "The Statistical Distribution of The Maxima of A Random Function," *Proc. R. Soc. Lond., Series A 1956, XI (3)*

[8] Chakrabarti, S.K. (2005) *Handbook of Offshore Engineering*, Oxford: Elsevier

[9] Dean, R.G. (1965) "Stream Function Representation of Non-Linear Ocean Waves," *J. Geophys, Res., 70, pp 4561-4572*

[10] Dean R.G. and Dalrymple R.A. (1991) *Water Wave Mechanics for Engineers and Scientists Advanced Series on Ocean Engineering, Vol II*, Singapore: World Scientific

[11] DNV (2012) *DNV-RP-C104: Self-Elevating Units*, Oslo: DNV

[12] Edvardsen, K. (2015) *Forces on Simplified Offshore Structures According to Different Wave Models*, Master Thesis, University of Stavanger, Stavanger

[13] Elgar, S; Guza, R.T. and Seymour, R.J. (1985) "Wave Group Statistics from Numerical Simulations of A Random Sea," *Applied Ocean Reasearch, 1985, Vol.7, No. 2, pp.93-96*

[14] Faltinsen, O.M., (1990) *Sea Loads on Ships and Offshore Structures*, Cambridge: Cambridge University Press

[15] Faltinsen, O.M. and Zhao, R. (1985) "A Comparative Study of Theoretical Models for Slowdrift Stray Motion of A Marine Structure," *Journal of Ship Research, 1988, pp 153-158*

[16] Fenton, J.D. (2014) *Use of The Programs FOURIER, CNOIDAL and STOKES for Steady Waves*, [online], Available at: http://johndfenton.com (Accessed 15 March 2015)

[17] Forristal, G.Z. (1978) "On The Statistical Distribution of Wave Height in a Storm", *Journal of Geophysical Research, Vol. 83, No. C5 pp2353-2358*

[18] Forristall, G.Z. (2000) "Wave Crest Distributions: Observations and Second-Order Theory", *Journal of Physical Oceanography, 30, pp, 1931-1943 (2000)*

[19] Greco, M. (2012) *TMR 4215: Sea Loads [Lecture Notes]*, Trondheim: Department of Marine Technology (NTNU)

[20] Haver, S. (2014) *Statistic for Offshore Structure [Lecture Notes]*, Department of Marine Technology (NTNU), Trondheim

[21] Haver, S. (2014) *Description of Metocean Characteristics for Planning of Marine Operations [Lecture Notes]*, Stavanger: University of Stavanger

[22] Haver, S.K.; Evardsen, K. And Lian,G. (2015) *Uncertainties in Wave Loads on Slender Pile Structures Due to uncertainties in Modelling Waves and Assiciated Kinematics*, Submitted for Possible Presentation at ISOPE 2016, Rhodes, Greece, 2016

[23] Johannessen, T.B. (2008) "On the Use of Linear and Weakly Nonlinear Wave Theory in Continuous Ocean Wave Spectra: Converge with Respect to Frequency," *Proc.27th OMAE Conf.*, Estoril, Portugal

[24] Langen, I. and Sigbjörnsson, R. (1975) *Utdag fra Dynamisk Analyse av Konstruksjoner*. SINTEF, Avdeling for konstruksjonsteknikk

[25] Larsen, C.M. (2015) *Added Mass on Cylinder [Lecture Notes]*, Trondheim: Department of Marine Technology (NTNU)

[26] Leira, B.J. (2010) *TMR 4235: Stochastic Theory of Sealoads: Probabilistic Modelling and Estimation*, Trondheim: Department of Marine Technology (NTNU)

[27] Lubis, M.B. (2015) *Alternative Methods of Realizing The Sea Spectrum for Time-Domain Simulations of Marine Structures in Irregular Seas*, Project Thesis, Departement of Marine Technology, Trondheim

[28] Moan, T. (2003) *TMR 4190: Finite Element Modelling and Analysis of Marine Structures*, Trondheim: Department of Marine Technology (NTNU)

[29] Moan, T. (2012) *Nonlinear Anlysis of Structure [Lecture Notes]*, Trondheim: Department of Marine Technology (NTNU)

[30] Myrhaug, D. (2005) *TMR 4235: Stochastic Theory of Sealoads: Statistics of Narrow Band Processes and Equivalent Linearization*, Trondheim: Department of Marine Technology (NTNU)

[31] Myrhaug, D. (2009) *TMR 4182: Marine Dynamics*, Trondheim: Department of Marine Technology (NTNU)

[32] Newland, D.E. (1993) *An Introduction to Random Vibrations, Spectral and Wavelet Analysis, 3rd Edition*, Essex: Longman Scientific and Technical

[33] NORSOK (2003) *N-003: Actions and Action Effects*, Oslo: Norwegian Technology Standards Institution

[34] NPD (2015) *Map of Norwegian Continental Shelf – The North Sea*, Available at: http://www.npd.no/Global/Norsk/4-Kart/Sokkelkart2015/Kontsok15-NS.pdf (Accessed 12 May 2016)

[35] Reinecker, M. M. and Fenton, J. D. (1981) "A Fourier Approximation method for Steady Water Waves," *J. Fluid Mech. 104, 119-137*

[36] Sharma, J.N. and Dean, R.G. (1981) "Second-Order Directional Seas and Associated Wave Forces," *Society of Petroleum Engineers Journal 4, pp. 129-140*

[37] SINTEF Marintek (2010) *USFOS Hydrodynamics: Theory Description of Use Verification*, Trondheim: SINTEF Marintek

[38] Stansberg, C.T. (1993) "Second-order Numerical reconstruction of laboratory generated random waves," *Proc. 12th OMAE Conf., Florence, Italy, pp 103-110*

[39] Stansberg, C.T. (1998) "Non-Gaussian Extremes in Numerically Generated Second-Order Random Waves in Deep Water," *Proc. 8.th ISOPE Conf., Vol III, Montreal, Canada, pp 103-110*

[40] Stansberg, C.T.; Gudmestad O.T. and Haver S. (2008) "Kinematics Under Extreme Wave," *Journal of Offshore Mechanics and Arctic Engineering-Transactions of The ASME, vol. 130 (2)*

[41] Tange, O. (2011) *GNU Parallel - The Command-Line Power Tool, ;login: The USENIX Magazine, February 2011:42-47*

[42] Tange, O. (2013) *Tool: GNU Parallel-Pararellize Serial Command Line Programs without Changing Them*, Available at: https://www.biostars.org/p/63816/ (Accesed 1 May 2016)

[43] Torsethaugen, K. and Haver S. (2004) "Simplified Double Peak Spectral Model for Ocean Waves," *Proc. 14th ISOPE Conf., Vol III, Toulon, France, pp76-84*

[44] Tucker, M.J. (1957) "The Analysis of Finite-Length Record of Fluctuating Signals," *British Journal of Applied Physiscs, 1984, Volume 8, April 1957, pp 137-142*

[45] Tucker M.J.; Challenor, P.G. and Carter, D.J.T. (1984) "Numerical Simulation of A Random sea: A common Error and Its Effect upon Wave Group Statistic," *Applied Ocean Research, 1984, Volume 6, No.2, pp118-122*

[46] Wamdi, T.G. (1988) "The WAM Model-A Third Generation Ocean Wave Prediction Model," *Journal of Physical Oceanography 18, 1775-1810*

APPENDIX

APPENDIX 1-MATLAB Script for Computational Time Comparisson

```
close all
clearvars
clc

A=rand(5000);
%matlabpool('open',4)

%% SIMPLE FOR-LOOP
tic
for i=1:5000
    for j=1:5000
        B1(i,j)=A(i,j)^3;
    end
end
dur1=toc;

%% FOR-LOOP WITH PREALLOCATING MEMORY
tic
B2=zeros(5000);
for i=1:5000
    for j=1:5000
        B2(i,j)=A(i,j)^3;
    end
end
dur2=toc;

%% VECTORIZATION
tic
B3=A.^3;
dur3=toc;

%% PARALLEL FOR LOOP
tic
parfor i=1:5000
    for j=1:5000
        B4(i,j)=A(i,j)^3;
    end
end
dur4=toc;

%% PARALLEL FOR-LOOP WITH PREALLOCATING MEMORY
tic
B5=zeros(5000);
parfor i=1:5000
    for j=1:5000
        B5(i,j)=A(i,j)^3;
    end
end
dur5=toc;
%matlabpool('close')
```

APPENDIX 2-Built Matlab Function

Function()/Script.m	Input – Output – Usage
apf**()**	amplitude, frequency, frequency limit, method (1,2,3 or 4)
	amplitude, frequency, phase
	Determine the amplitude, frequency and phase of harmonic component from choosen method: 1. Random phase; 2. Random amplitude; 3. Random frequency; 4. All random
BOOTSTRAPING**.m**	Performing bootstrapping for Rayleigh and Forristall crest distribution then taking the lower and upper limit. numelBOT refer to the number of repetition
bsovtm**()**	horizontal particle velocity, horizontal particle acceleration, z-coordinate, depth, diameter, condition (1 or 2)
	Baseshear, Overturning moment
	Calculating baseshear and overturning moment for a single vertical cylinder. The drag and added mass coefficient is determined by the condition: 1. Linear wave consideration; 2. Second or higher order consideration
cdfHs**()**	scatter data, significant wave height from data, spectral peak period from data
	c-coefficients,d-coefficients,location parameter (λ), scale parameter (α), shape parameter (β),alternative 1 d-coefficient, alternative 2 d-coefficient
	Fitting Significant wave height data to 3-parameter weibull distribution (represented by λ, α and β). In addition, fitting a function to find relationship between mean of ln (Tp) and Hs (represented by c-coefficients); and between variance of ln (Tp) and Hs (represented by d-coefficients). Another d-coefficients is presented when $d_3 = 0$ and $d_3 = 0.005$. In the end, th 90% band of Tp is ploted
constantstretch**()**	wavenumber, wavefreqeuncy, phase, x-coordinate, time instance, velocity potential amplitude, horizontal particle velocity amplitude, vertical particle velocity amplitude, horizontal particle acceleration amplitude, vertical particle acceleration amplitude
	potential velocity, horizontal particle velocity, vertical particle velocity, horizontal particle acceleration, vertical particle acceleration
	Performing constant stretching to establish kinematics along z-coordinate
contourg**()**	set of significnat wave height, set of spectral peak period, annual probability,c-coefficients, d-coefficients, location parameter (λ), scale parameter (α), shape parameter (β),
	Theoreticel probability of point outside the contour line, number of actual data outside the contour line, set of seastate along the contour line
	Creating the environmental contour line based on the desired annual probability then counting the point outside the contour line
EAP**()**	type of spectrum ('PM' or 'JONSWAP'), significant wave height, spectral peak period, option for plot ('yes' or 'no'), number of harmonic component, minimum frequency, maximum frequency, gamma (only used for JONSWAP spectrum)
	amplitude, frequency, frequency limit
	Performing equal area method to determine the amplitude and frequency from the chosen spectrum (PM or JONSWAP)
EAPP**()**	type of spectrum ('PM' or 'JONSWAP'), significant wave height, spectral peak period, option for plot ('yes' or 'no'), natural frequency of structure, number of harmonic component, density of peaked component, minimum frequency, maximum frequency, gamma (only used for JONSWAP spectrum)
	amplitude, frequency, frequency limit
	Performing peaked equal area method for given structure natural frequency to determine the amplitude and frequency from the chosen spectrum (PM or JONSWAP)
FFT**()**	type of spectrum ('PM' or 'JONSWAP'), significant wave height, spectral peak period, option for plot ('yes' or 'no'), frequency interval, minimum frequency, maximum frequency, gamma (only used for JONSWAP spectrum)

	Amplitude, frequency, frequency limit
	Performing peaked equidistance frequency method (inverse discrete Fourier transform) to determine the amplitude and frequency from the chosen spectrum (PM or JONSWAP)
fiitingstokes**()**	wave height, wave crest, wave period, water depth
	wave height
	Adjusting the 5th Stokes wave weight to produce the desired wave crest for certain wave period and water depth using Fenton's software
gridwave**()**	name of girdwave file, x-coordinate, y-coordinate, z-coordinate, time instance, surface elevation, x-horizontal particle velocity, y-horizontal particle velocity, vertical particle velocity, x-horizontal particle acceleration, y-horizontal particle acceleration, vertical particle acceleration
	gridwave file
	Creating a gridwave file for further analysis is USFOS
HC3H**()**	annual probability, water depth, c-coefficients, d-coefficients,location parameter (λ), scale parameter (α), shape parameter (β)
	number of iteration for wave height, number of iteration for wave crest, wave height, CDF for wave height result, CDF for wave crest result, summation of joint probability PDF
	Determining the 3-hour extreme wave crest and wave height from full long-term analysis
Hcin**()**	annual probability, water depth, c-coefficients, d-coefficients,location parameter (λ), scale parameter (α), shape parameter (β)
	number of iteration for wave height, number of iteration for wave crest, wave height, CDF for wave height result, CDF for wave crest result, mean of zero-crossing frequency, summation of joint probability PDF, summation of joint probability PDF x zero-crossing frequency
	Determining the individual wave crest and wave height from full long-term analysis
HsTp**()**	name of measurement data
	significant wave height, spectral peak period without randomization, spectral peak period with randomization
	Extracting the significant wave and spectral peak period (with and without randomization) from WAM10 data
JONSWAP**()**	significant wave height, spectral peak period, minimum frequency, maximum frequency, frequency interval, gamma parameter
	spectrum for given wave frequency, wave frequency, 0th spectral moment, 1st spectral moment,2nd spectral moment, 3rd spectral moment, 4th spectral moment
	Establishing JONSWAP spectrum and its n-th spectral moment
kinematictest**.m**	Extracting the horizontal velocity from Fenton's software result and compare it with irregular sea model. In addition, the baseshear and overturning moment are determined
linkinematic**()**	amplitude, frequency, phase, surface elevation, x-coordinate, time instance, number of z-coordinate (considered to be revised), depth, method (1,2 or 3)
	horizontal particle velocity, vertical particle velocity, horiznontal particle acceleration, vertical particle acceleration, z-coordinate, potential velocity
	Determining the kinematics of first order sea based on the choosen method: 1.Wheeler stretching; 2. Linear extrapolation; 3. Constant stretching
linsurface**()**	amplitude, frequency, phase, x-coordinate, time instance, water depth
	surface elevation
	Establishing the first order surface elevation
metocean**.m**	Main script for performing metocean analysis
perex**()**	water depth, seastate along the contour line, wave crest from long-term analysis, wave height from long-term ananlysis
	percentile of long-term analysis on the worst seastate CDF, worst seastate based on wave

	height, worst seastate based on wave crest, 90% wave crest on the worst sea state, 90% wave height on the worst sea state
	Determining the worst seastate along the contour line including the 90% value on the worst sea state
plotfenton**.m**	Plot the surface elevation and horizontal particle velocity of Fenton's software
PM**()**	significant wave height, spectral peak period, minimum frequency, maximum frequency, frequency interval
	spectrum for given wave frequency, wave frequency, 0^{th} spectral moment, 1^{st} spectral moment,2^{nd} spectral moment, 3^{rd} spectral moment, 4^{th} spectral moment
	Establishing PM spectrum and its n-th spectral moment
qprob**()**	annual probability, c-coefficients, d-coefficients,
	significant wave height for desired annual probability, mean spectral peak period of significant wave height for desired annual probability, 5% spectral peak period of significant wave height for desired annual probability, 95% spectral peak period of significant wave height for desired annual probability
	Determining the significant wave height for the desired annual probability and its mean, 5% and 95% spectral peak period
scatdiag**()**	set of significant wave height, set of spectral peak period
	scatter diagram
	Creating a scatter diagram
seckinematic**()**	amplitude of first order wave, amplitude of second order wave, wave frequency, wave number, phase, second order surface, Dmin, Dplus, wave number of difference term, wave number of sum term, wave frequency of difference term, wave frequency of sum term, x-coordinate, number of z-coordinate (considered to be revised), time instance, water depth, lower point of z-coordinate, method (1 or 2), spectral peak frequency, multiplication of wave frequency, PSImin, PSIplus, plot option (1 or 0)
	horizontal particle velocity, vertical particle velocity, horiznontal particle acceleration, vertical particle acceleration, z-coordinate, potential velocity
	Determining the kinematics of second order sea based on the choosen method: 1.Wheeler stretching; 2. Linear extrapolation
secspect**()**	amplitude, frequency, frequency limit, water depth
	spectrum for given wave frequency for difference term, spectrum for given wave frequency for sum term, 0^{th} spectral moment
	Determining the second order spectrum from second order correction term
secstansberg**()**	wave number, wave frequency, phase, x-coordinate, time instance, PSImin, PSIplus, amplitude of surface difference term, amplitude of surface sum term, amplitude of horizontal velocity difference term, amplitude of horizontal velocity sum term, amplitude of vertical velocity difference term, amplitude of vertical velocity sum term, amplitude of horizontal acceleration difference term, amplitude of horizontal acceleration sum term, amplitude of vertical acceleration difference term, amplitude of vertical acceleration sum term, amplitude of first order velocity potential, amplitude of first order horizontal velocity, amplitude of first order vertical velocity, amplitude of first order horizontal acceleration, amplitude of first order vertical acceleration, amplitude of horizontal velocity derivative term, amplitude of horizontal acceleration derivative term, amplitude of potential velocity difference term, amplitude of vertical velocity derivative term, amplitude of vertical acceleration derivative term
	second order velocity potential, second order horizontal velocity, second order vertical velocity, second order horizontal acceleration, second order vertical acceleration, horizontal velocity difference term, horizontal velocity sum term, horizontal velocity derivative term, horizontal acceleration difference term, horizontal acceleration sum term, horizontal acceleration derivative term

	Performing linear extrapolation (presented by Stansberg) for second order wave kinematics
secsurface**()**	wave amplitude, frequency, frequency limit, phase, water depth, lower point for kinematics calculation, x-coordinate, number of z-coordinate (considered to be revised), time instance, method (1 or 2), spectral peak frequency, velocity condition (1 or 0), plot option (1 or 0), first order surface
	second order surface, second order surface correction, second order horizontal velocity, second order vertical velocity, second order horizontal acceleration, second order vertical acceleration, z-coordinate, second order potential velocity, surface correction difference term, surface corretion sum term
	Calculating second order surface and its wave kinematics based on the choosen method: 1.Wheeler stretching; 2. Linear extrapolation. When velocity condition is set as 0, the second order kinematics is not calculated. Lower point of kinematic is used when performing combination of first and second order kinematic along z-coordinate
stansberg**()**	wave number, wave frequency, phase, x-coordinate, time instance, amplitude of first order velocity potential, amplitude of first order horizontal velocity, amplitude of first order vertical velocity, amplitude of first order horizontal acceleration, amplitude of first order vertical acceleration, amplitude of horizontal velocity derivative term, amplitude of horizontal acceleration derivative term, amplitude of potential velocity difference term, amplitude of vertical velocity derivative term, amplitude of vertical acceleration derivative term
	First order velocity potential, first order horizontal velocity, first order vertical velocity, first order horizontal acceleration, first order vertical accelaration
	Performing linear extrapolation (presented by Stansberg) for first order wave
statwave**()**	time instance, surface elevation
	time of maximum surface elevation, positive maximum surface elevation, sorted maximum surface elevation, CDF of positive maximum surface elevation
	Determining the positive maximum surface elevation from time series
stokesresult**.m**	Extracting largest surface elevation from time series of surface elevation, fitting the 5^{th} Stokes wave to produce the same wave crest, comparing the kinematics and then calculating the baseshear and overturning moment
surfacekin**()**	kinematic
	surface kinematic
	Extracting the kinematic on surface elevation from kinematics along z-coordinate
theorydist**.m**	Establishing Rayleigh and Forristall crest distribution
wavefreq**()**	wave number, water depth
	wave frequency, number of iteration
	Establishing wave frequency from given wave number
wavenum**()**	wave frequency, water depth
	wave number
	Establishing wave number from given wave frequency
wheeler**()**	amplitude, wave number, wave frequency, phase, surface elevation, x-coordinate, z-coordinate, time instance, water depth
	velocity potential, horizontal velocity, vertical velocity, horizontal acceleration, vertical acceleration, pressure
	Performing wheeler stretching to determine the kinematics along z-coordinate
zerocross**()**	time instance, surface elevation
	time of maximum zero-crossing surface elevation, maximum zero-crossing surface elevation, sorted maximum zero-crossing surface elevation, CDF of positive maximum zero-crossing surface elevation
	Determining the maximum zero-crossing surface elevation from time series

APPENDIX 3-CDF of First Order Surface Maxima

Equidistance Frequency, Determinisitic Amplitude

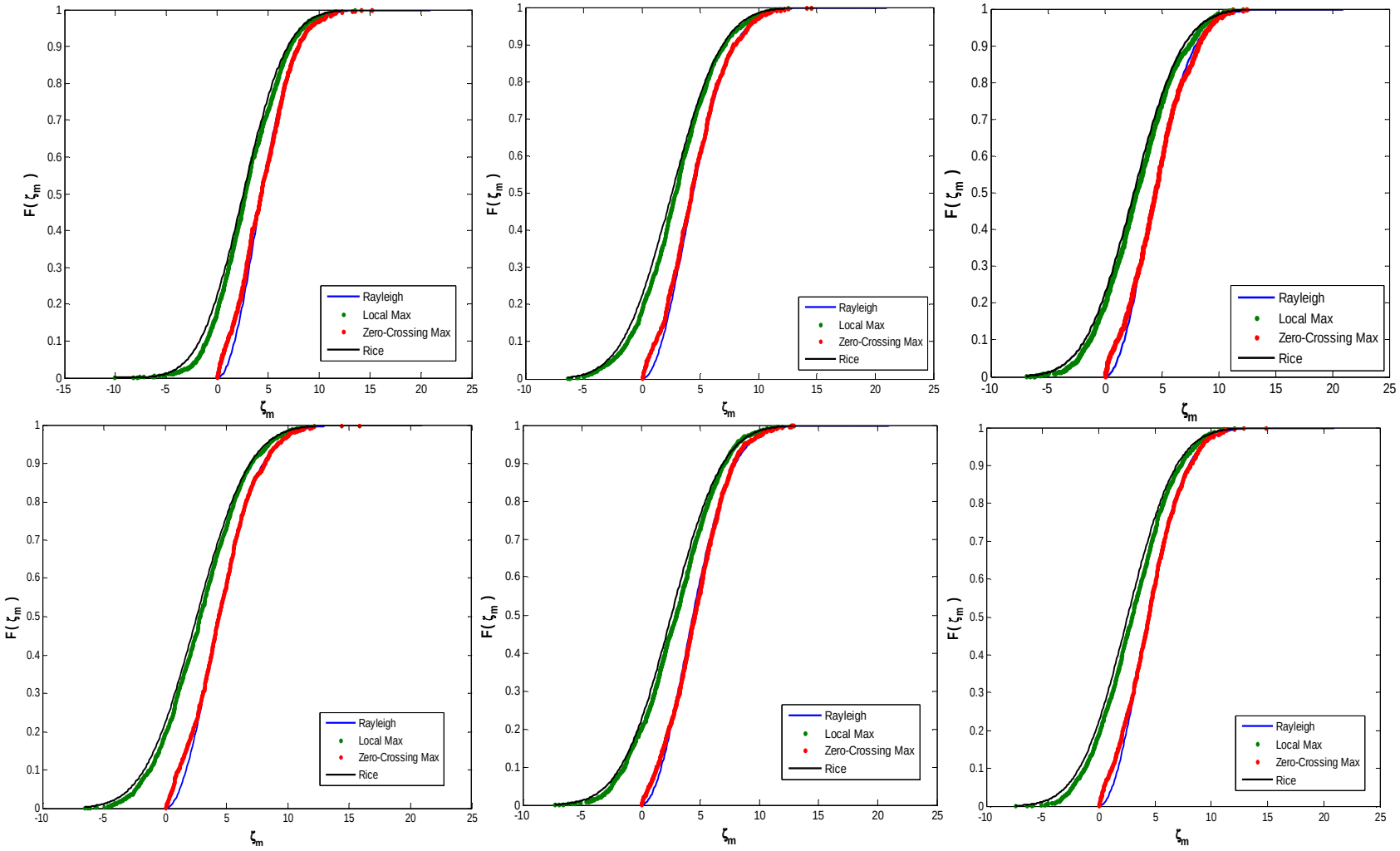

APPENDIX 4-CDF of First Order Surface Maxima

Equidistance Frequency, Random Amplitude

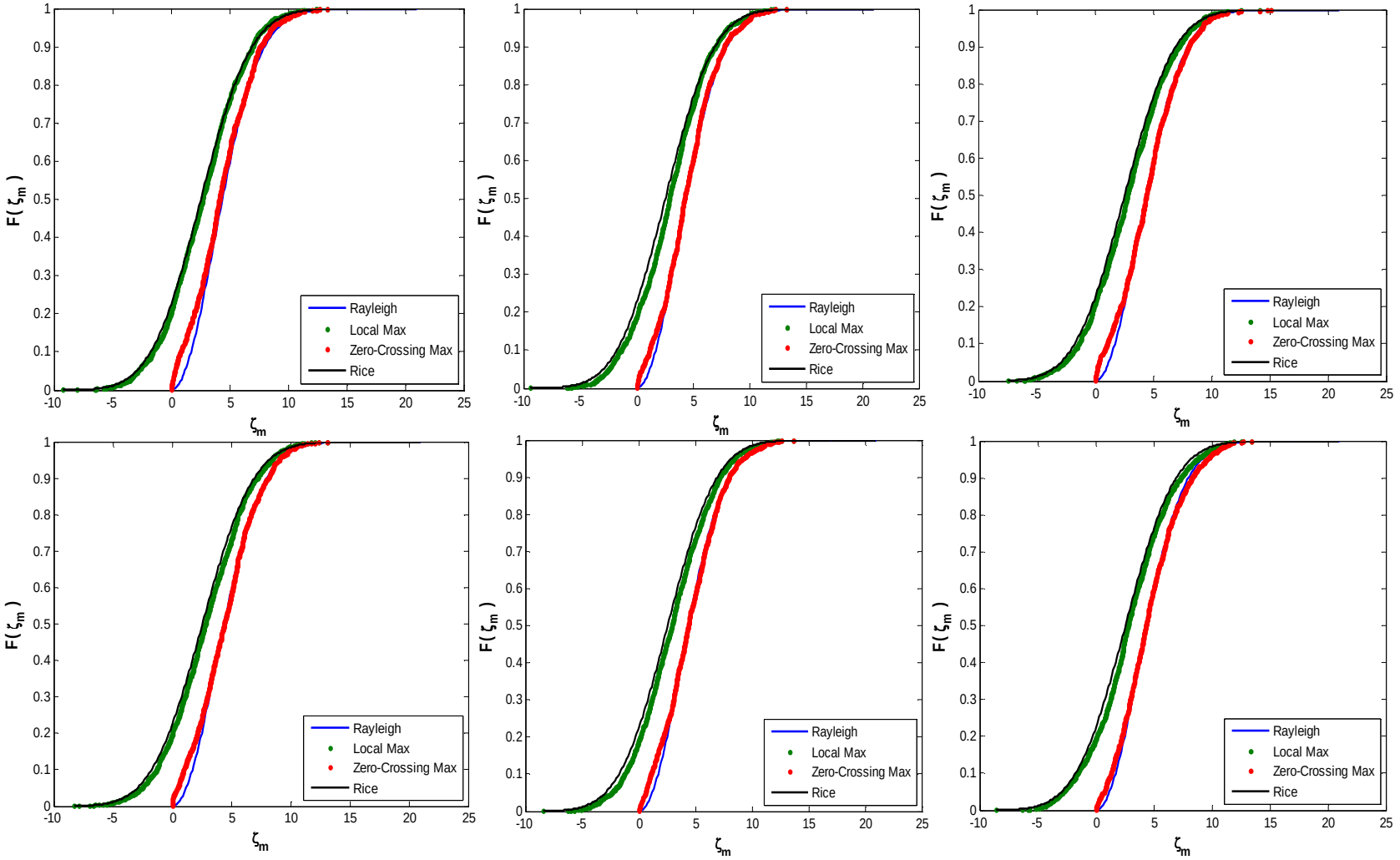

APPENDIX 5-CDF of 20-Minute Largest First Order Surface Maxima :
Equidistance Frequency, Deterministic Amplitude

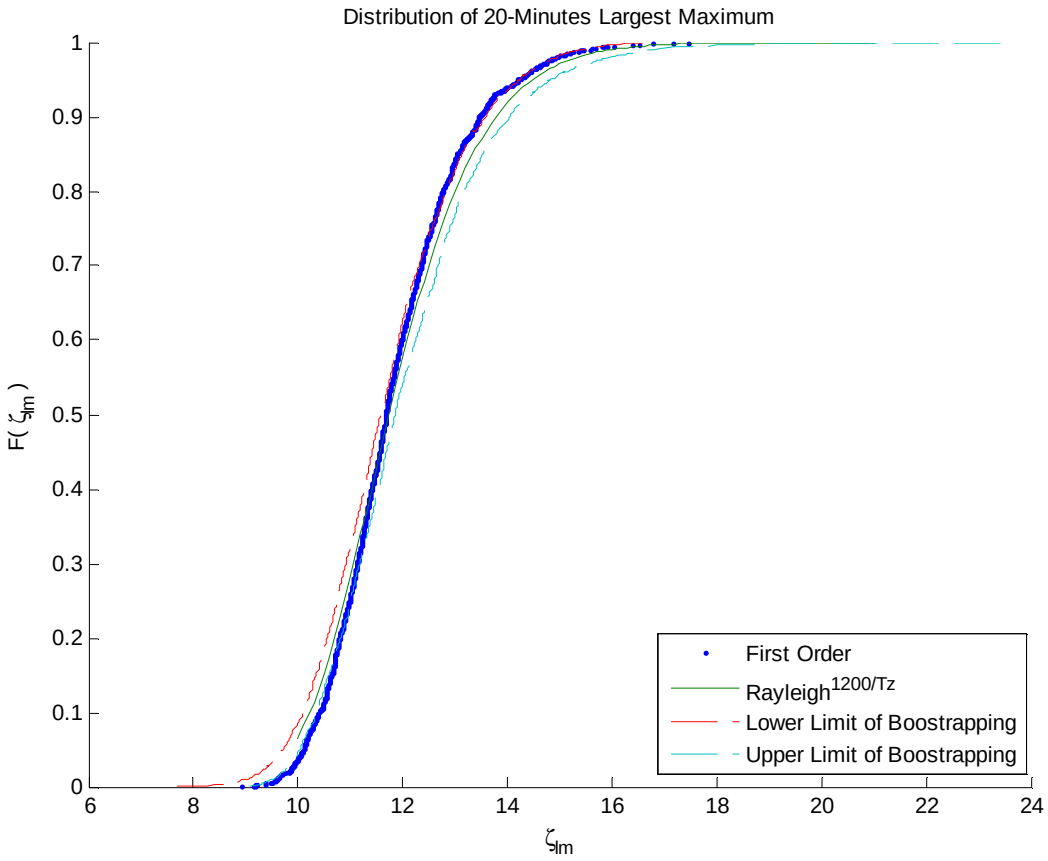

APPENDIX 6-CDF of 20-Minute Largest First Order Surface Maxima :

Equidistance Frequency, Random Amplitude

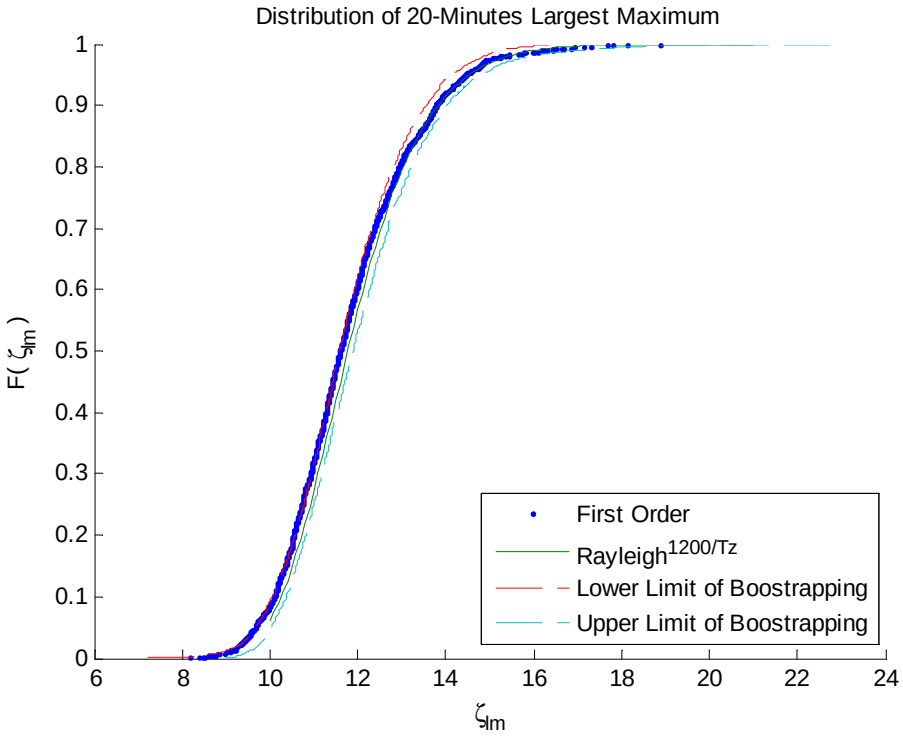

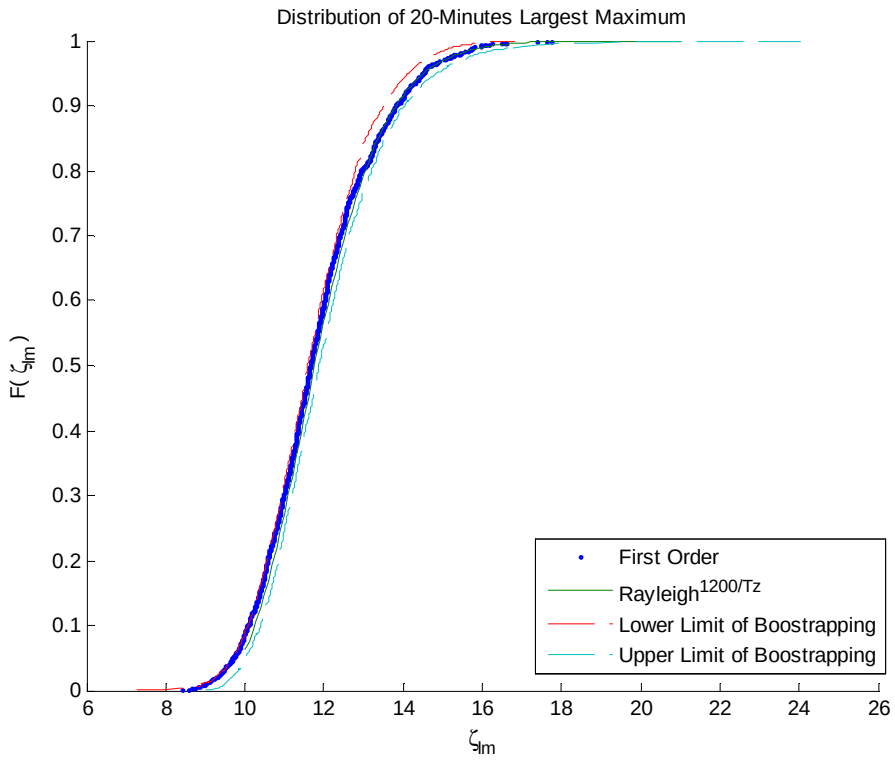

APPENDIX 7- CDF of 3-Hour Largest First Order Surface Maxima :

Equidistance Frequency, Deterministic Amplitude

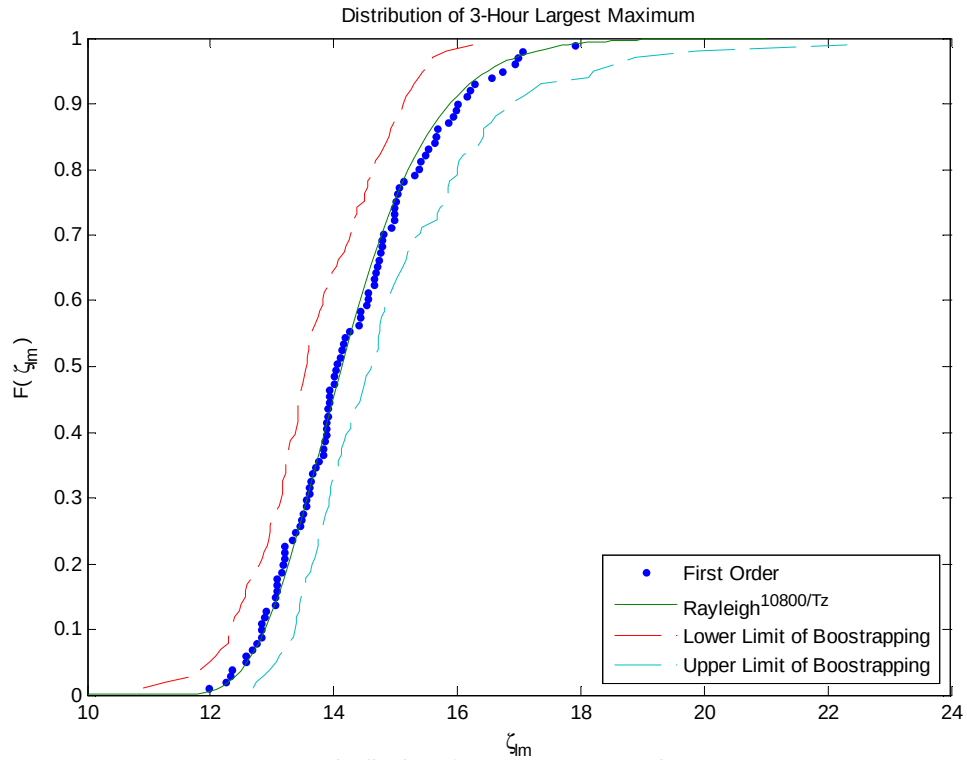

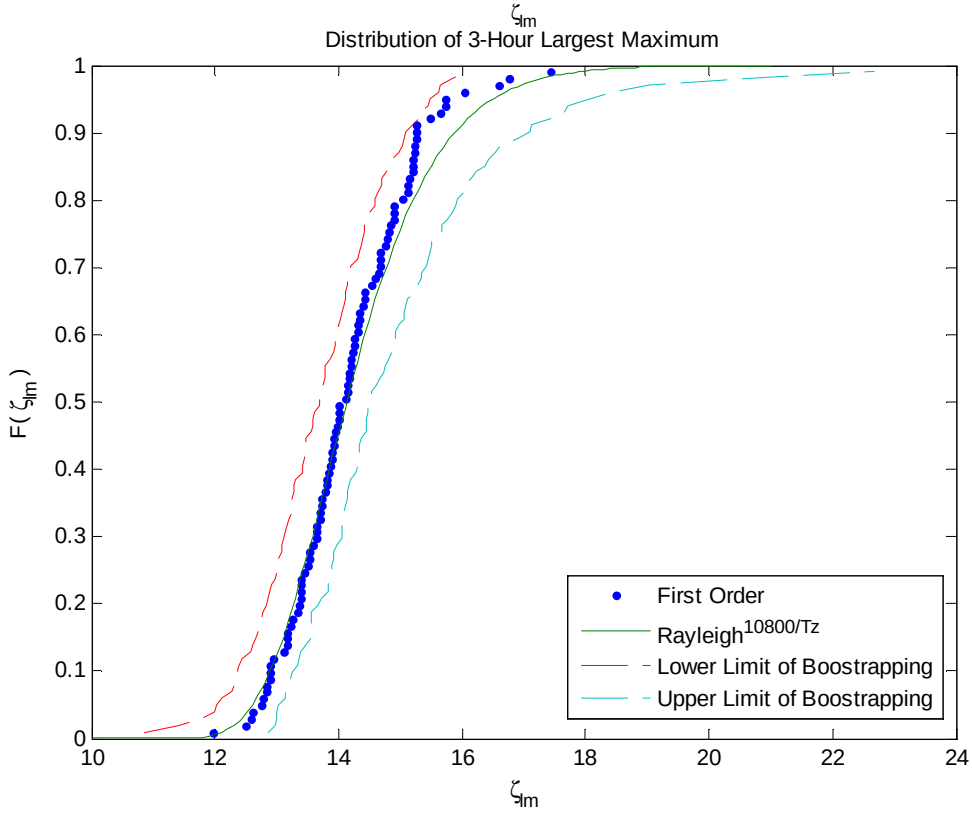

APPENDIX 8-CDF of 3-Hour Largest First Order Surface Maxima

Equidistance Frequency, Random Amplitude

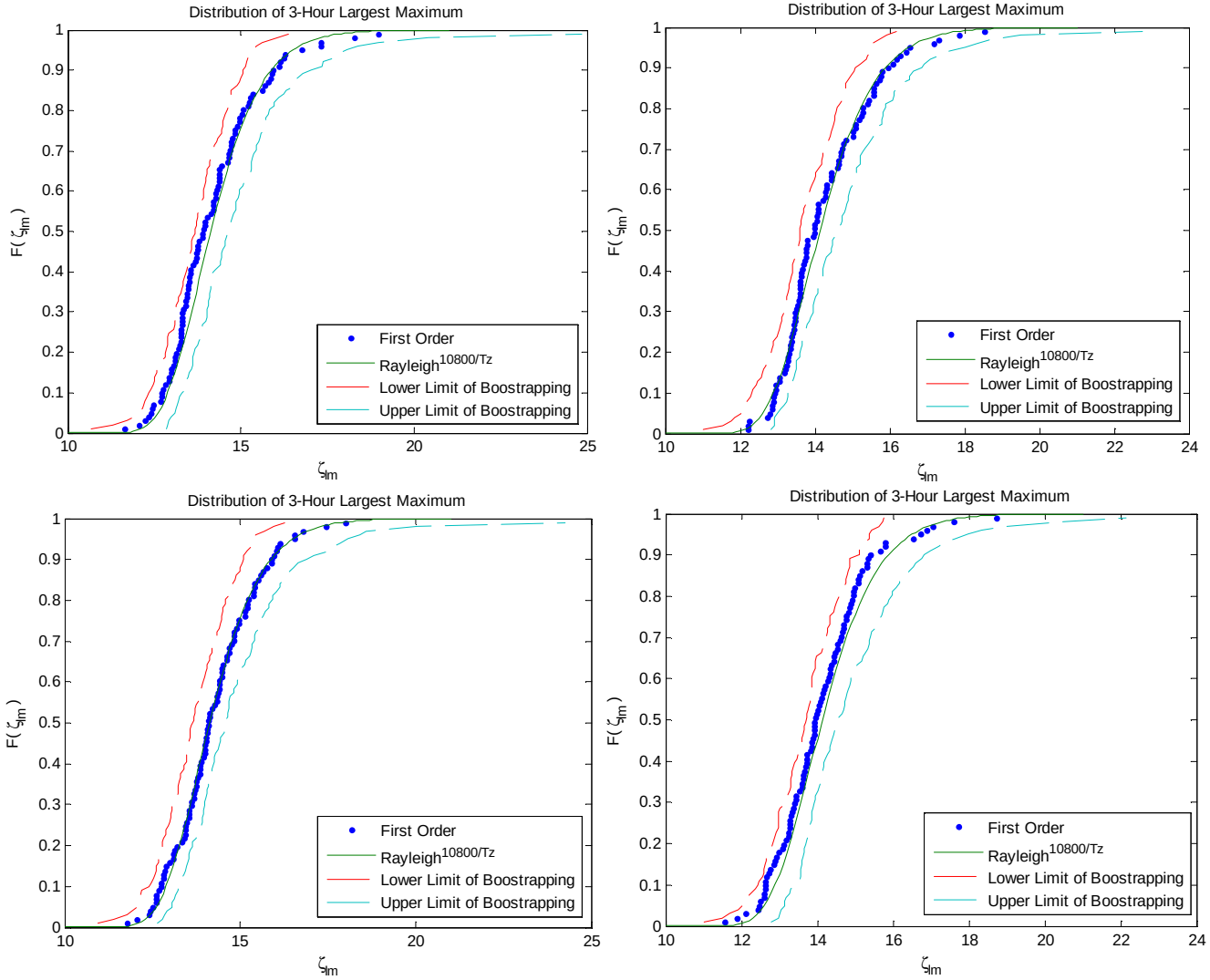

APPENDIX 9-CDF of 3-Hour Largest First Order Surface Maxima

Random Frequency, Deterministic Amplitude (Number of component = 10800)

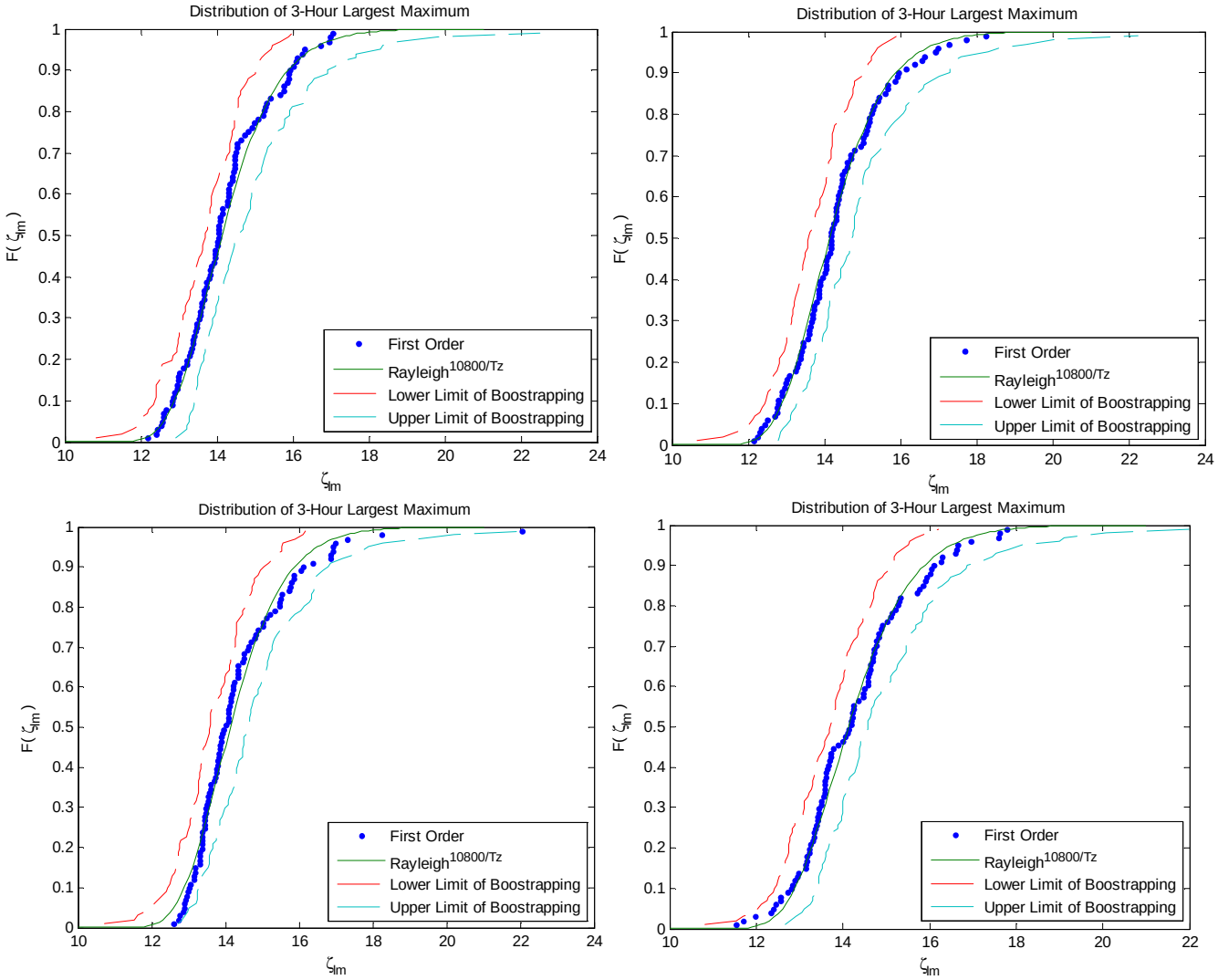

APPENDIX 10-CDF of 3-Hour Largest First Order Surface Maxima

Time Series Partition, deterministic Amplitude

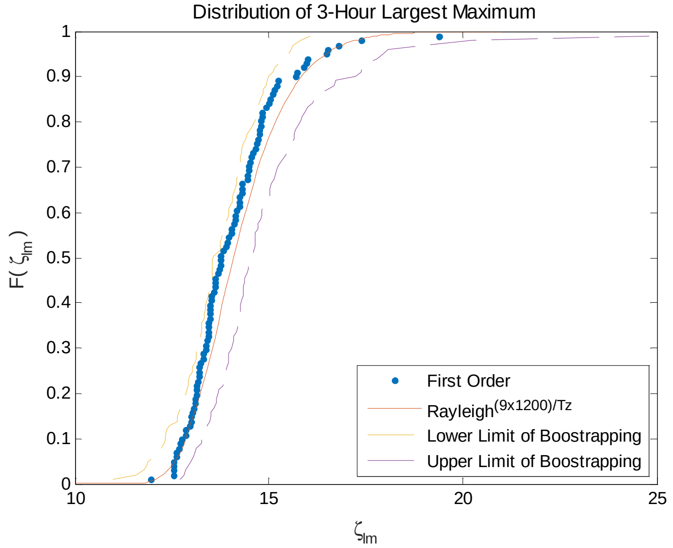

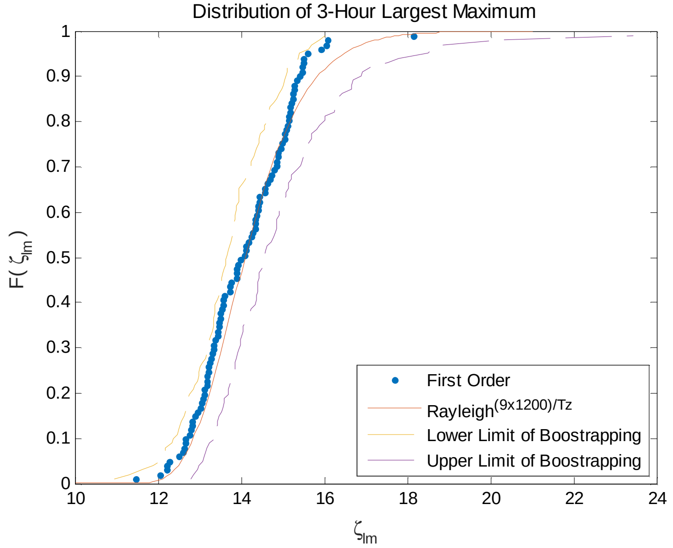

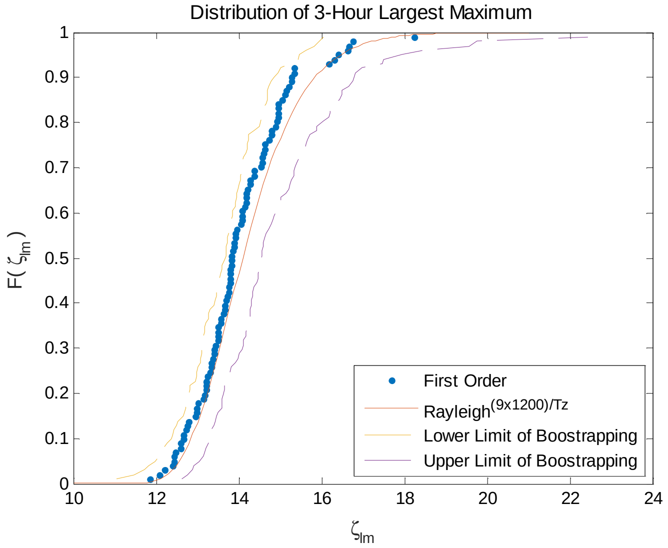

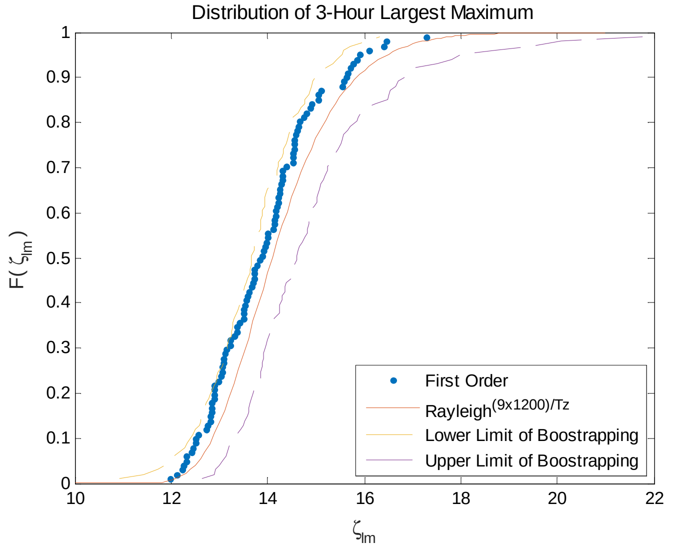

APPENDIX 11-CDF of 3-Hour Largest First Order Surface Maxima

Partition of Time Series, Random Amplitude

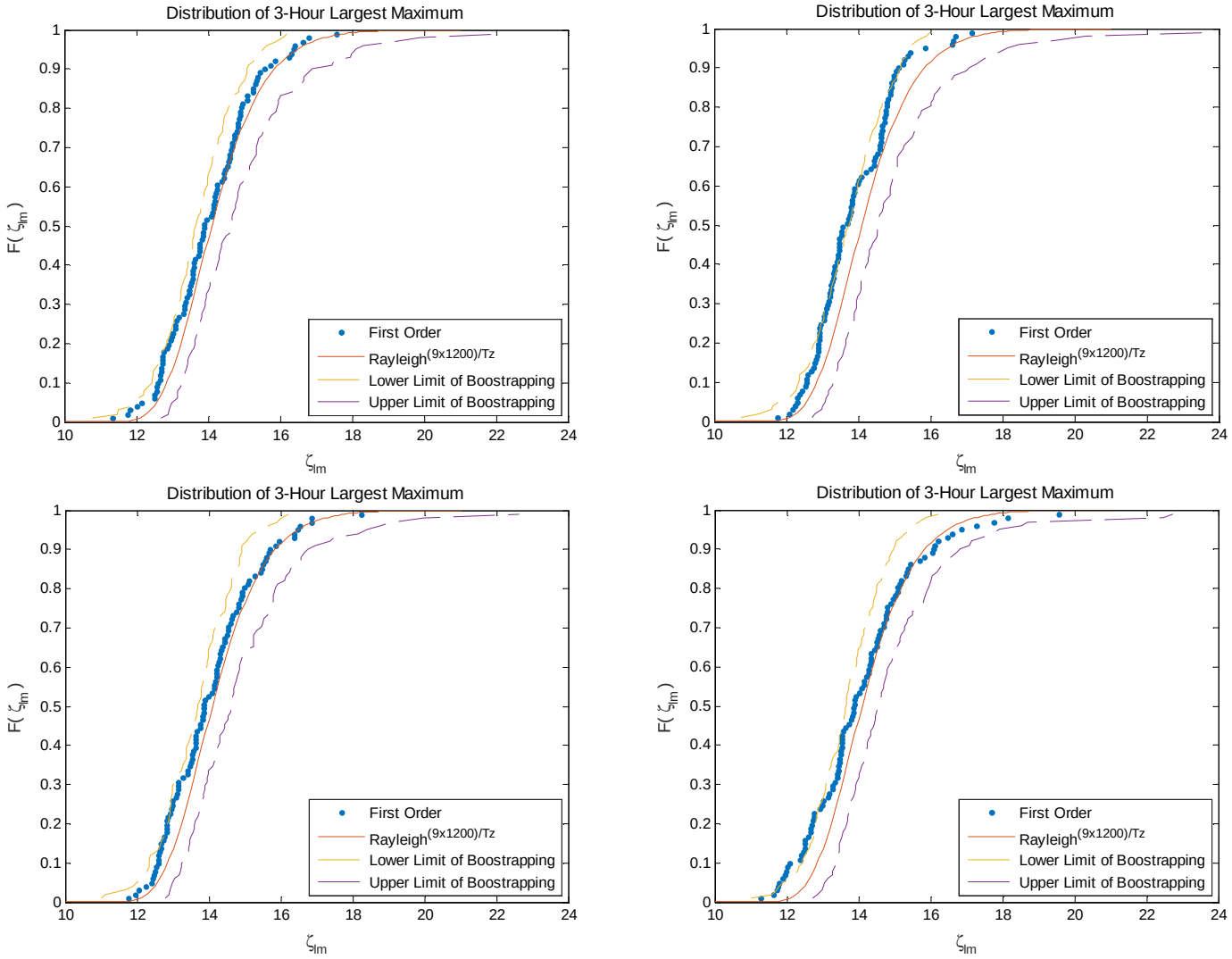

APPENDIX 12-CDF of 3-Hour Largest First Order Surface Maxima

Random Frequency, Deterministic Amplitude (Reducing Number of Component)

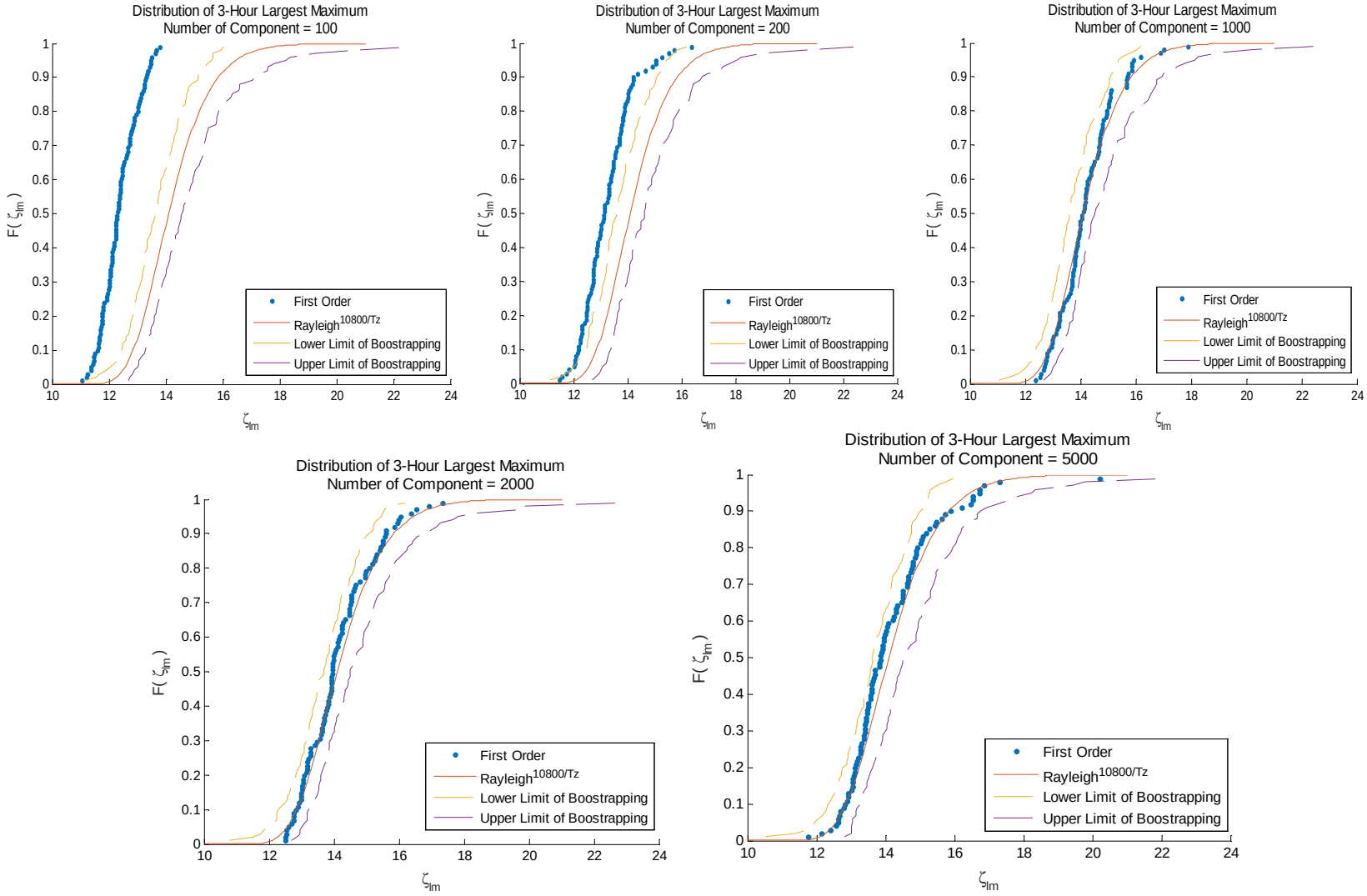

APPENDIX 13-CDF of 3-Hour Largest First Order Surface Maxima

Random Frequency, Random Amplitude

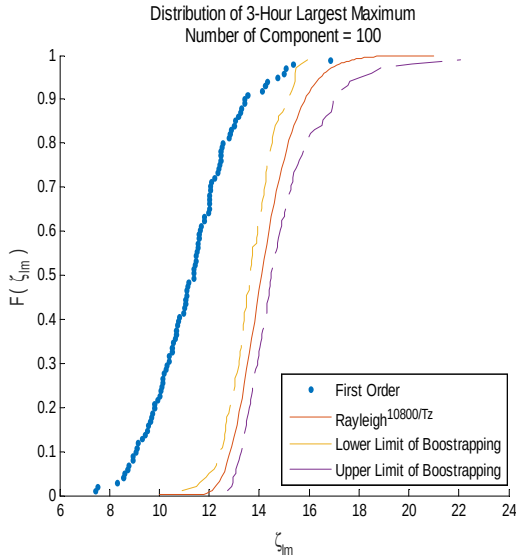

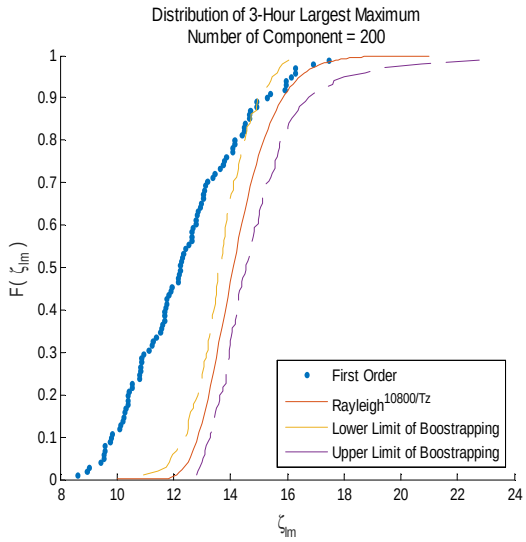

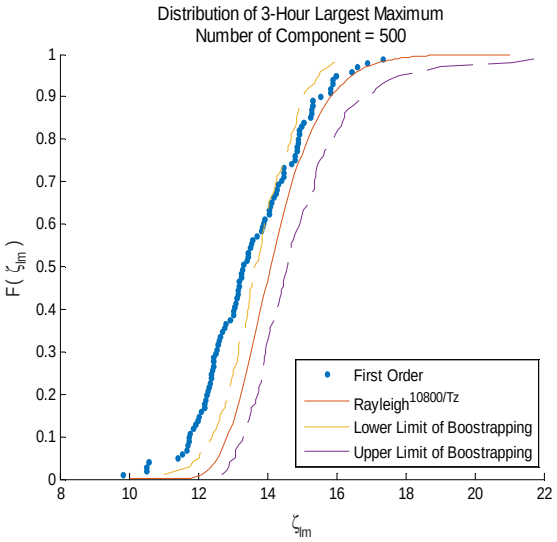

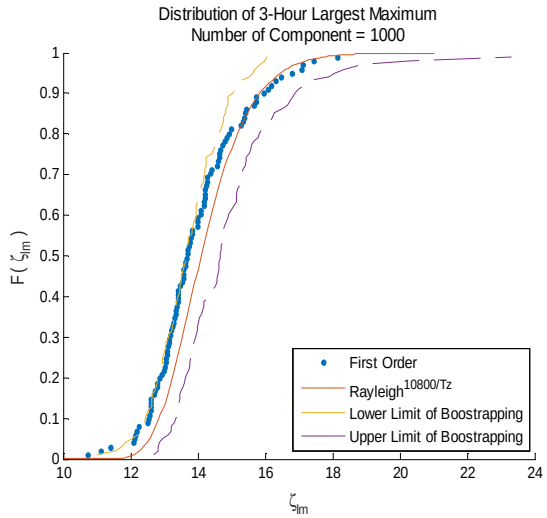

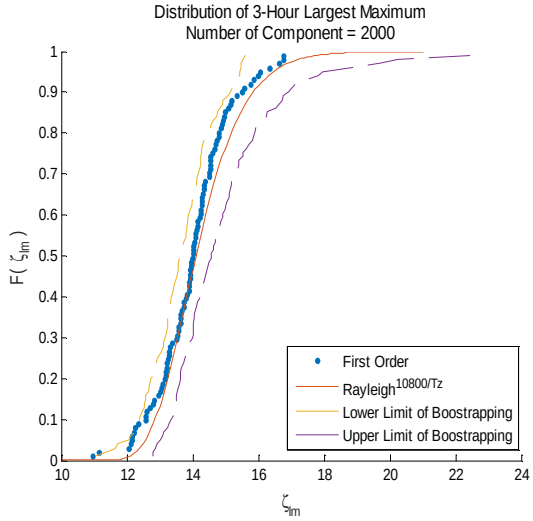

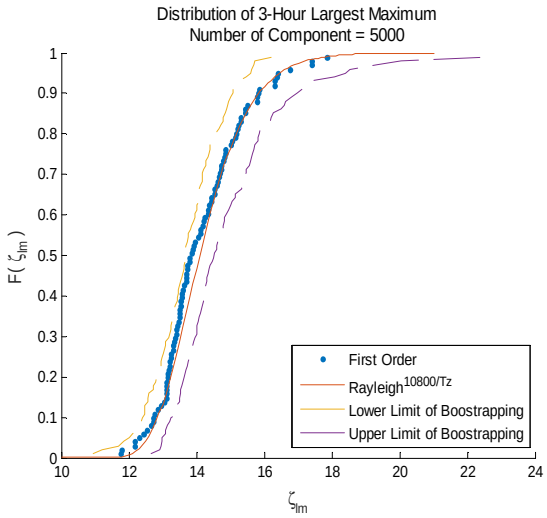

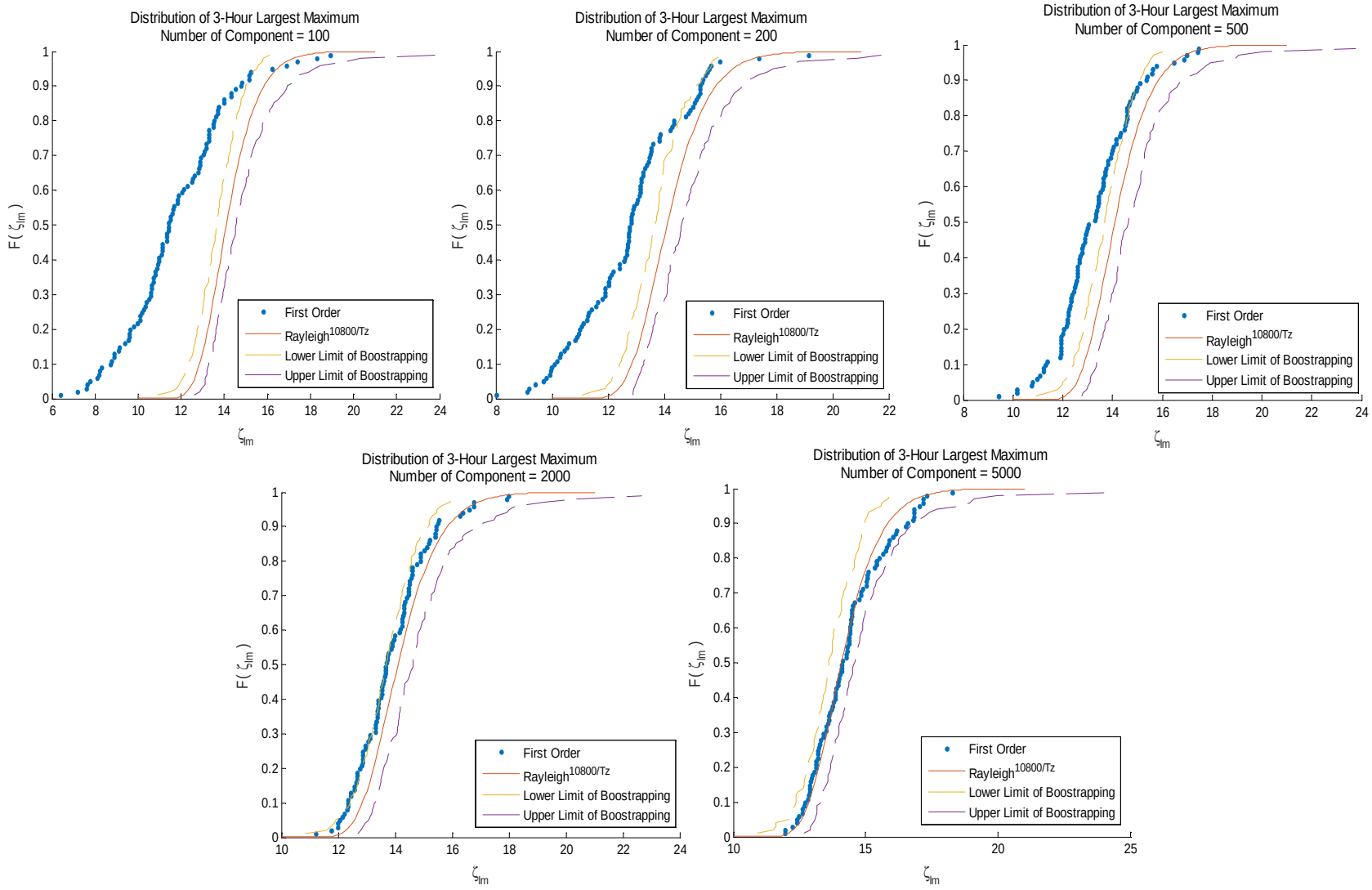
Distribution of 3-Hour Largest Maximum
Number of Component = 100
Distribution of 3-Hour Largest Maximum
Number of Component = 200
Distribution of 3-Hour Largest Maximum
Number of Component = 500
Distribution of 3-Hour Largest Maximum
Number of Component = 2000
Distribution of 3-Hour Largest Maximum
Number of Component = 5000
First Order
Rayleigh10800/Tz
Lower Limit of Boostrapping
Upper Limit of Boostrapping
F(ζlm)
ζlm

APPENDIX 14-CDF of 3-Hour Largest First Order Surface Maxima

Equal Area, Deterministic Amplitude

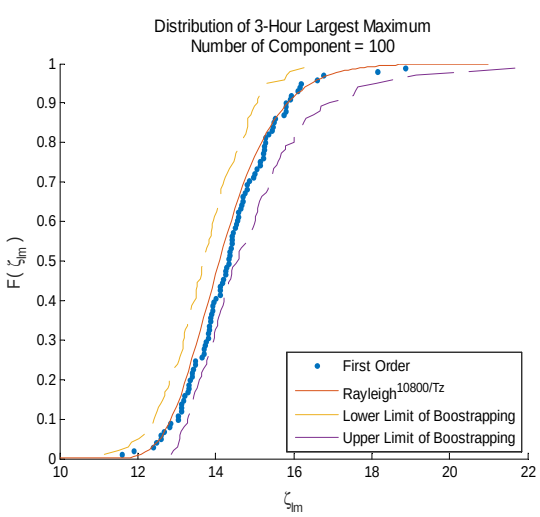

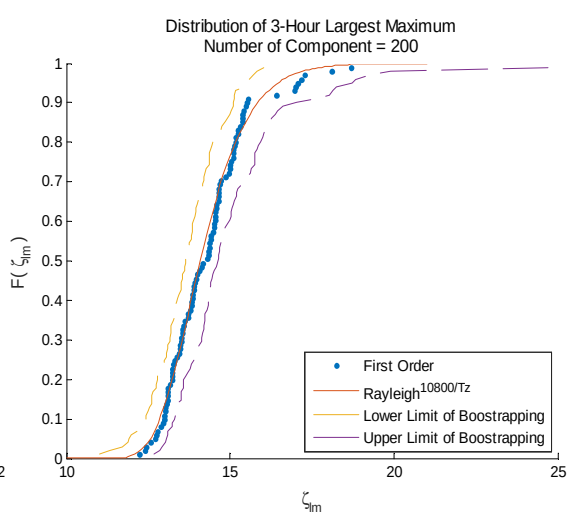

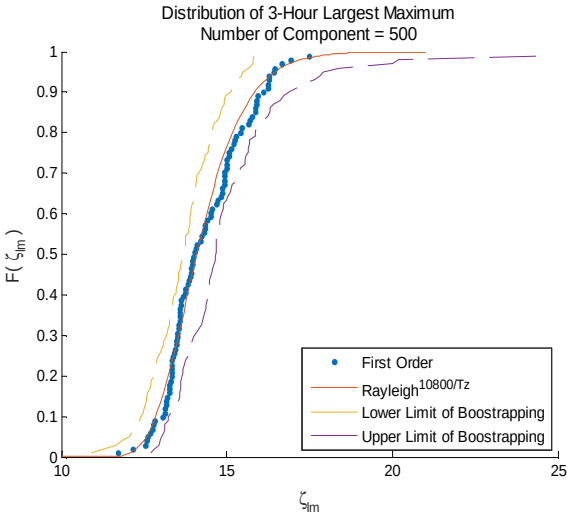

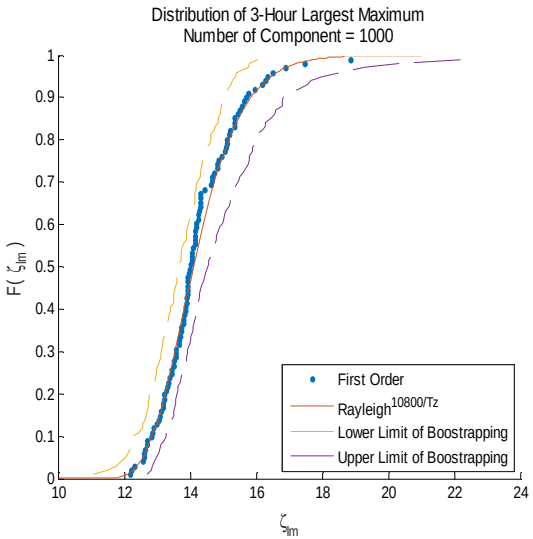

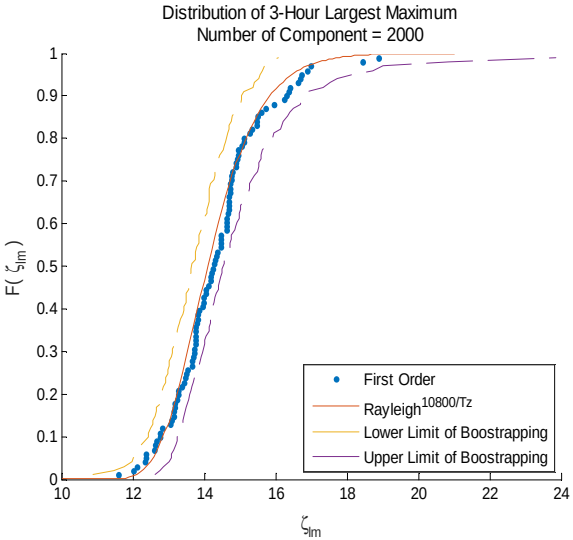

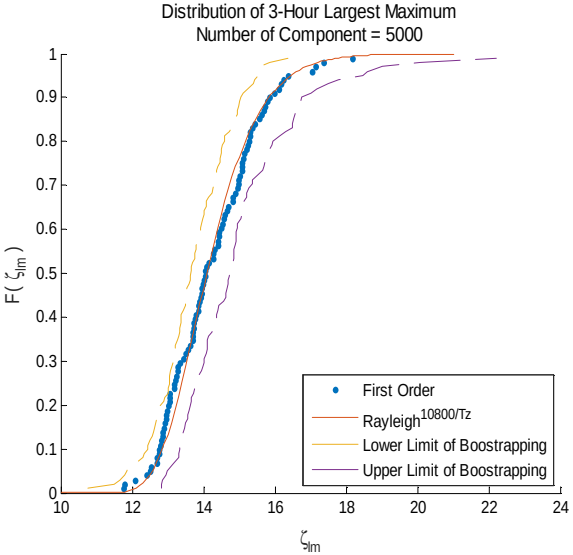

APPENDIX 15-CDF of 3-Hour Largest First Order Surface Maxima

Equal Area, Random Amplitude

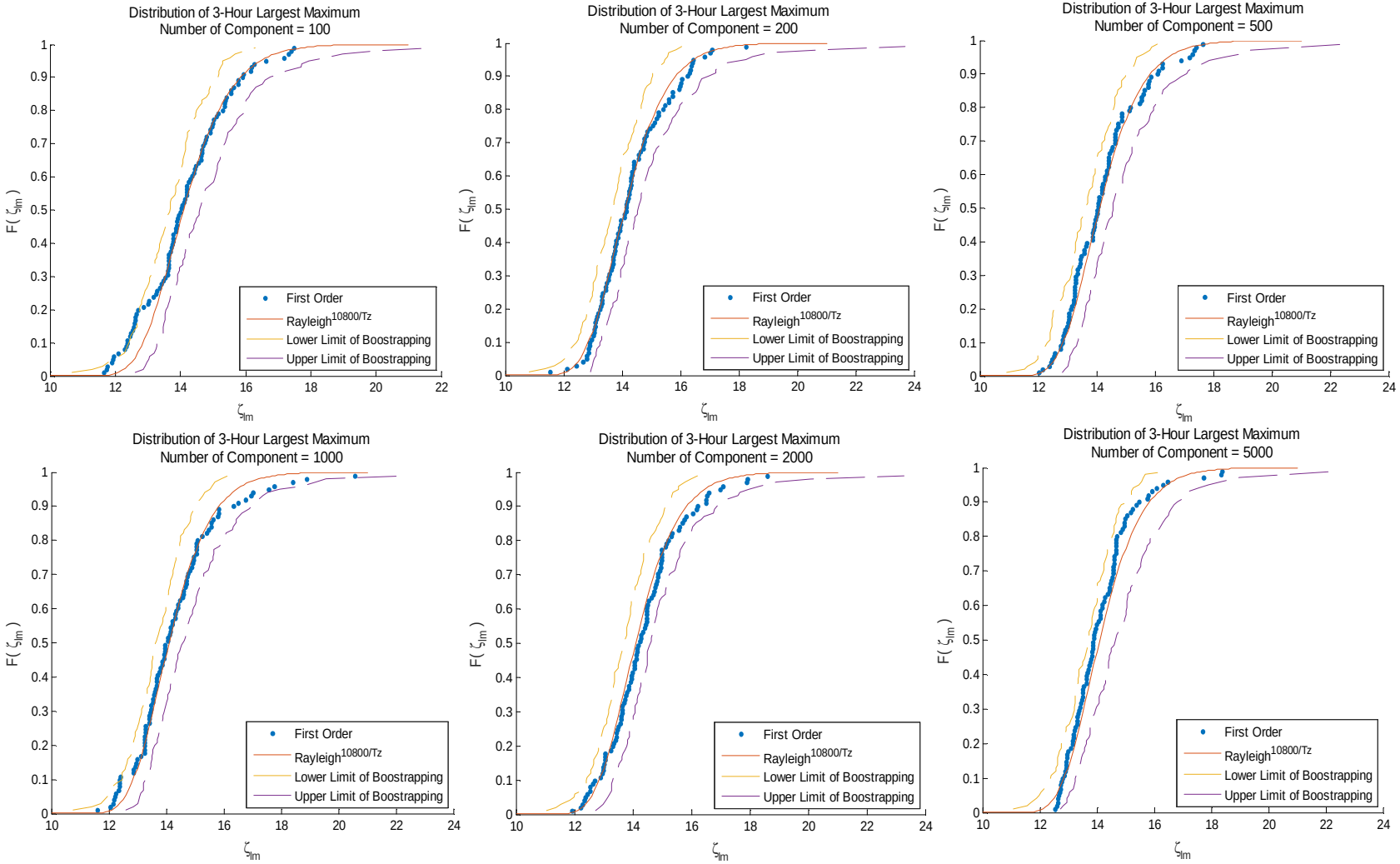

APPENDIX 16-CDF of 3-Hour Second Order Surface Largest Maxima

Partition of Time Series , Deterministic Amplitude without Cut-Off frequency

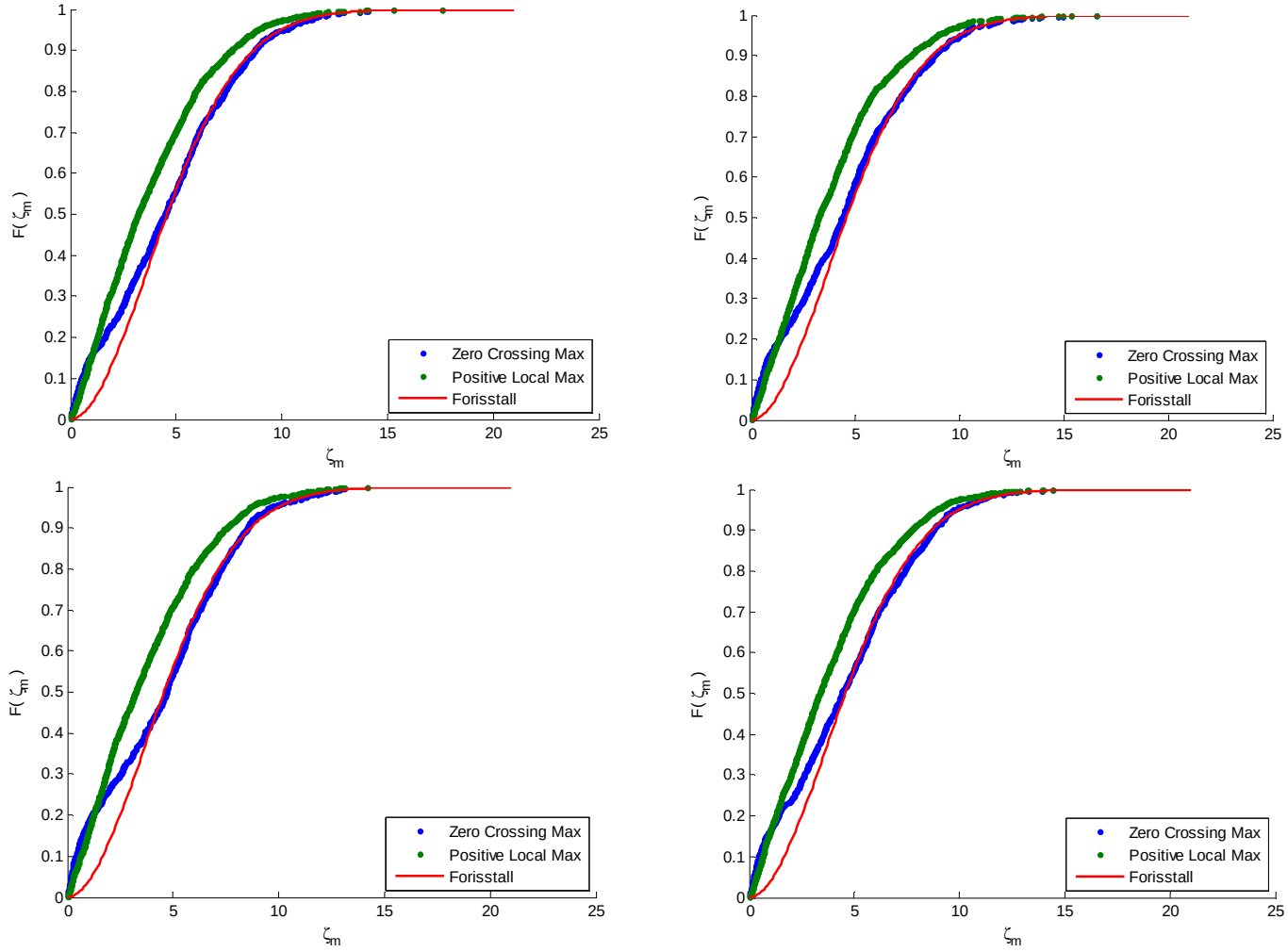

APPENDIX 17-CDF of 3-Hour Second Order Surface Largest Maxima

Partition of Time Series, Random Amplitude without Cut-Off frequency

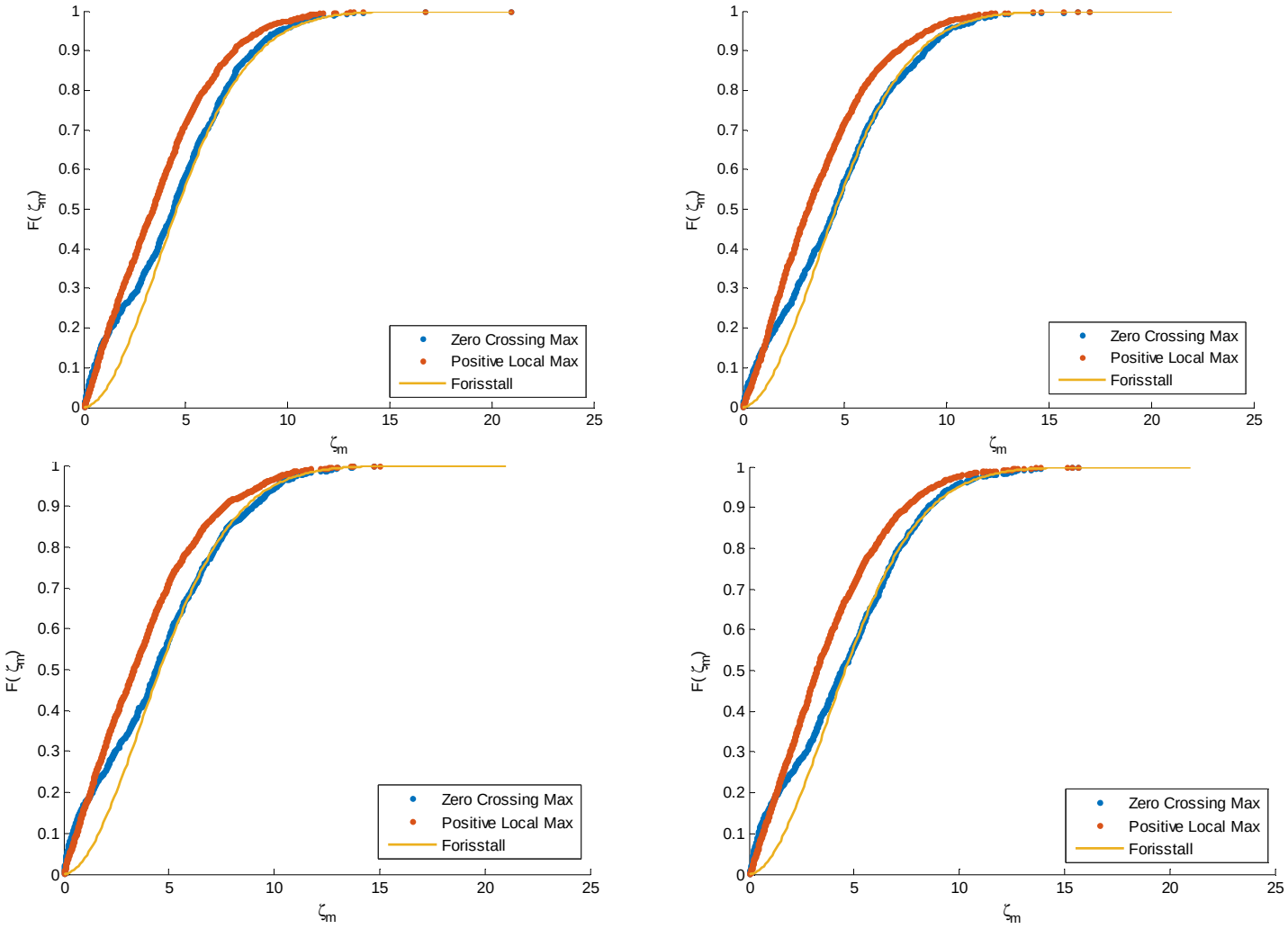

APPENDIX 18-CDF of 3-Hour Second Order Surface Largest Maxima

Partition of Time Series, Deterministic Amplitude with Cut-Off frequency

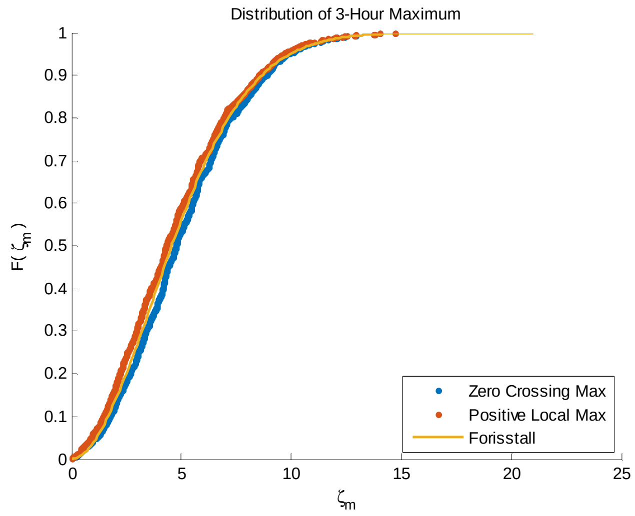

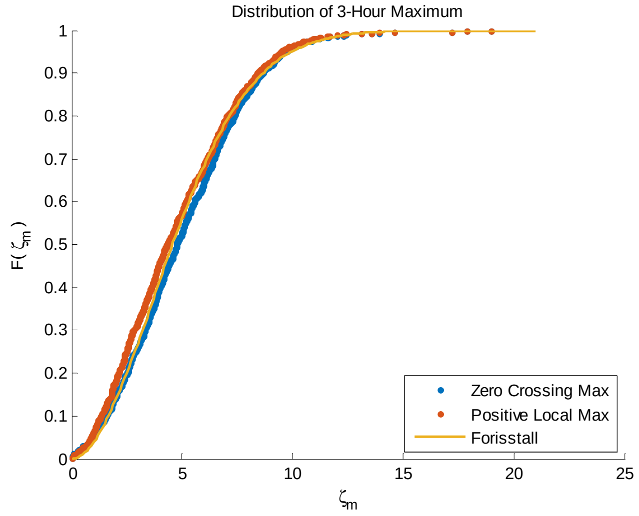

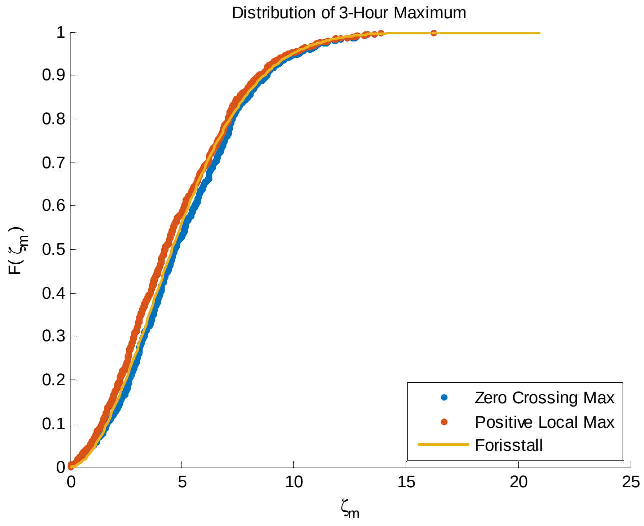

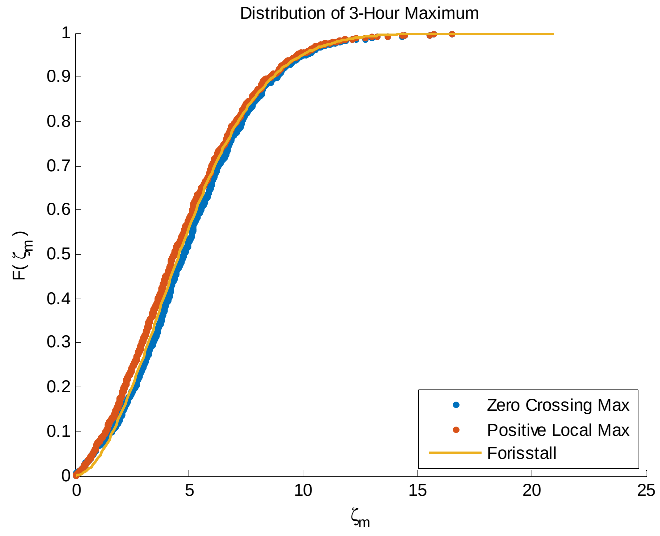

APPENDIX 19-CDF of Second Order Surface Maxima

Partition Time Series, Random Amplitude with Cut-off Frequency

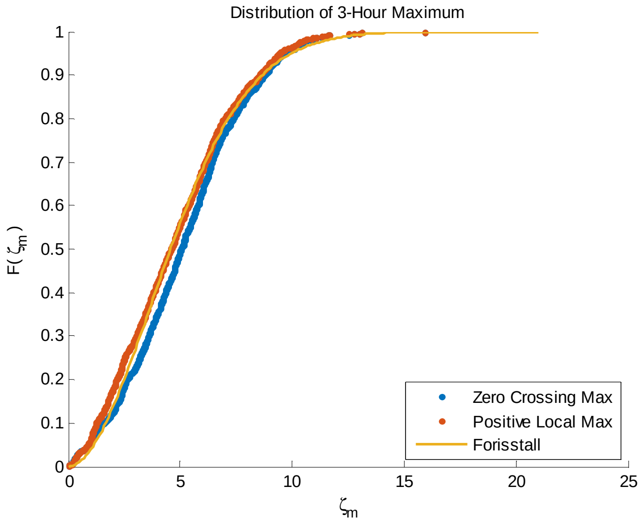

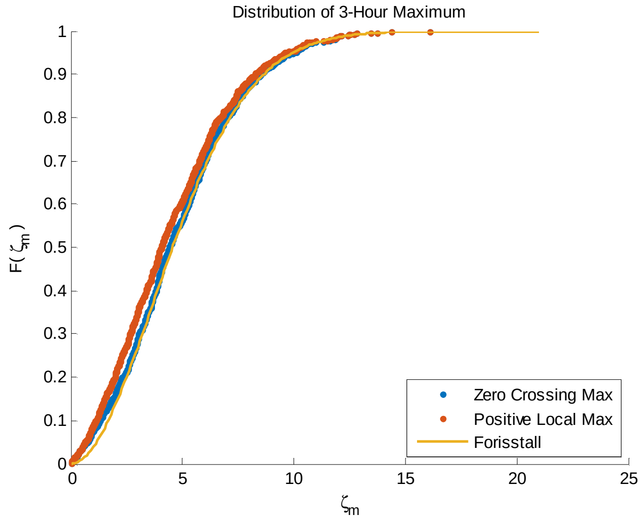

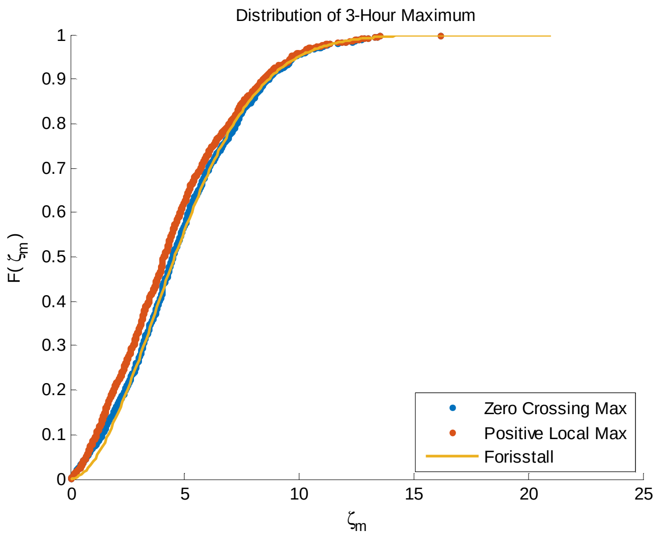

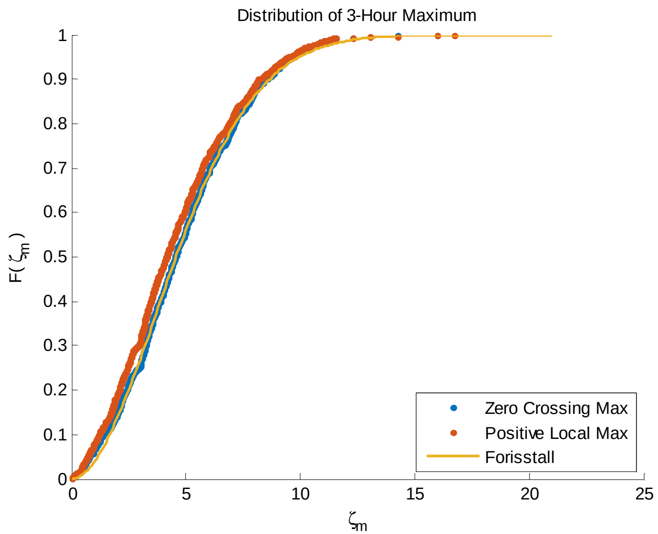

APPENDIX 20-Distribution of Second Order Largest Maxima

Equidistance Frequency, Deterministic Amplitude

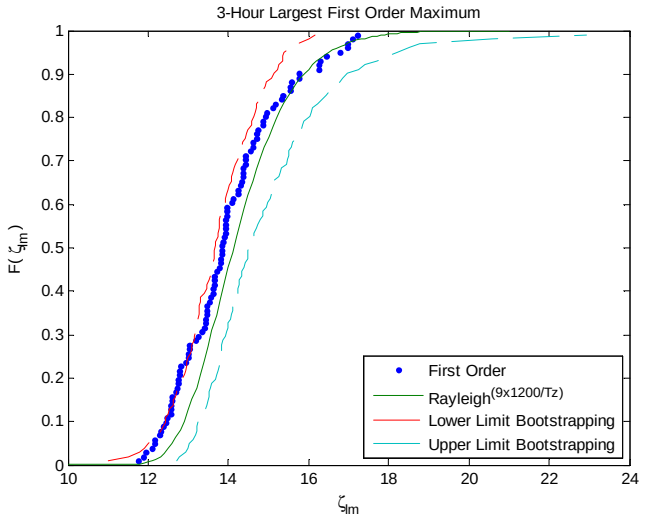

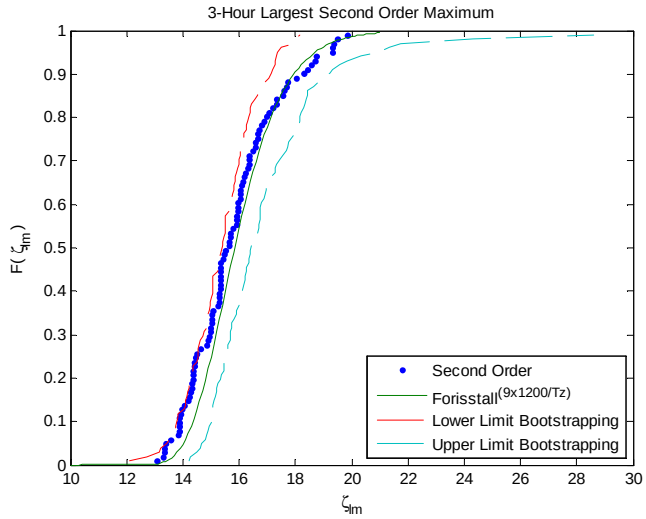

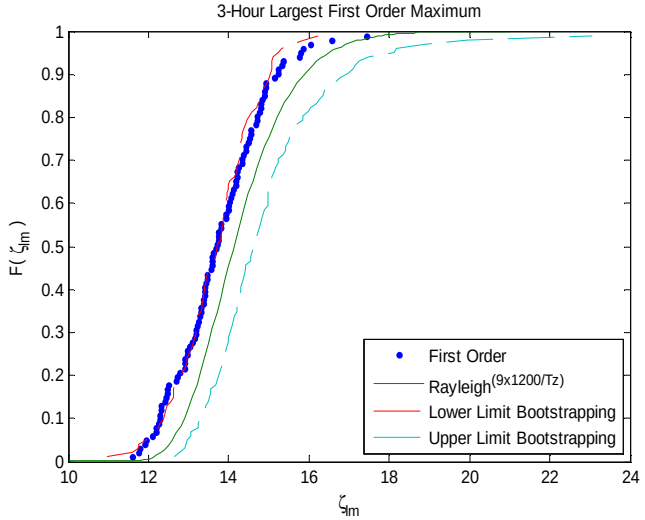

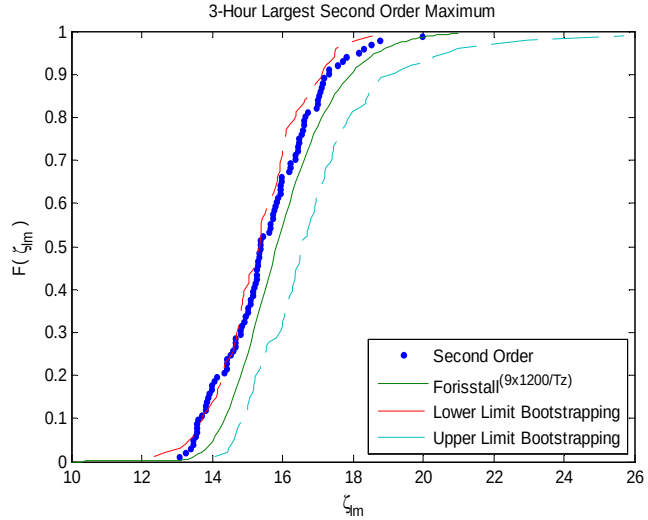

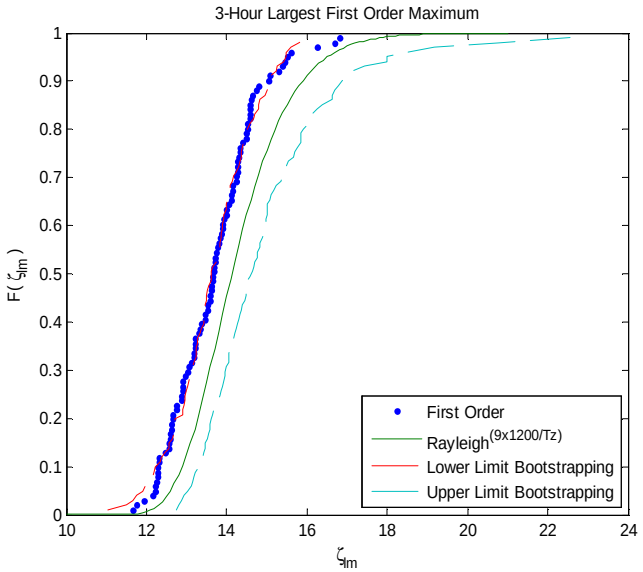
3-Hour Largest First Order Maximum
F(ζlm)
ζlm
First Order
Rayleigh(9x1200/Tz)
Lower Limit Bootstrapping
Upper Limit Bootstrapping

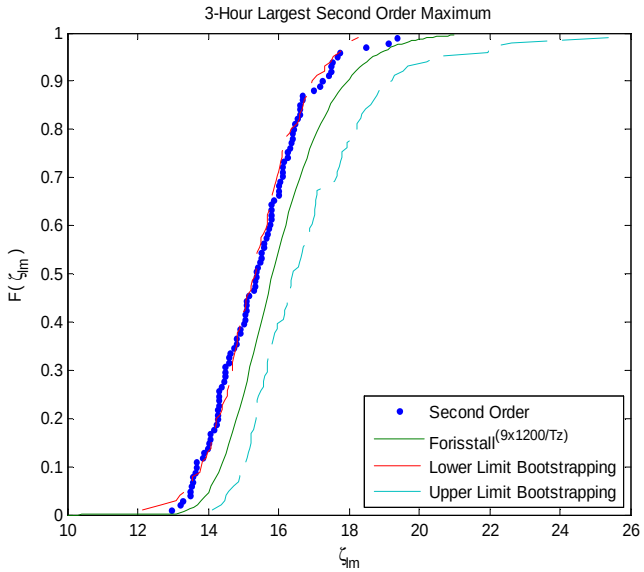
3-Hour Largest Second Order Maximum
F(ζlm)
ζlm
Second Order
Forisstall(9x1200/Tz)
Lower Limit Bootstrapping
Upper Limit Bootstrapping

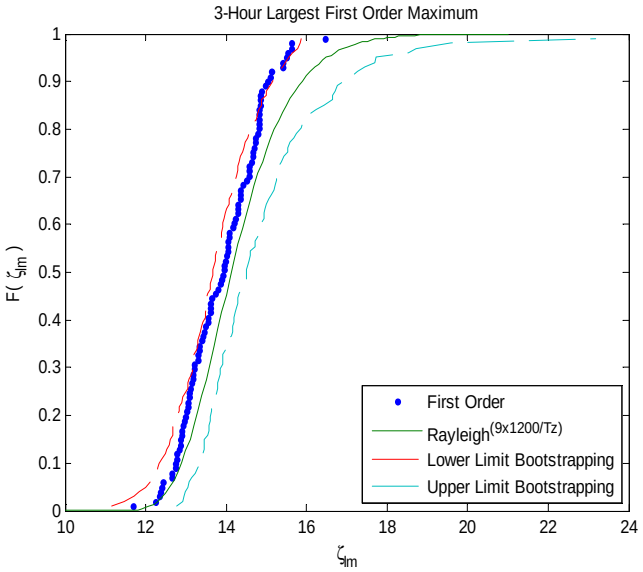
3-Hour Largest First Order Maximum
F(ζlm)
ζlm
First Order
Rayleigh(9x1200/Tz)
Lower Limit Bootstrapping
Upper Limit Bootstrapping

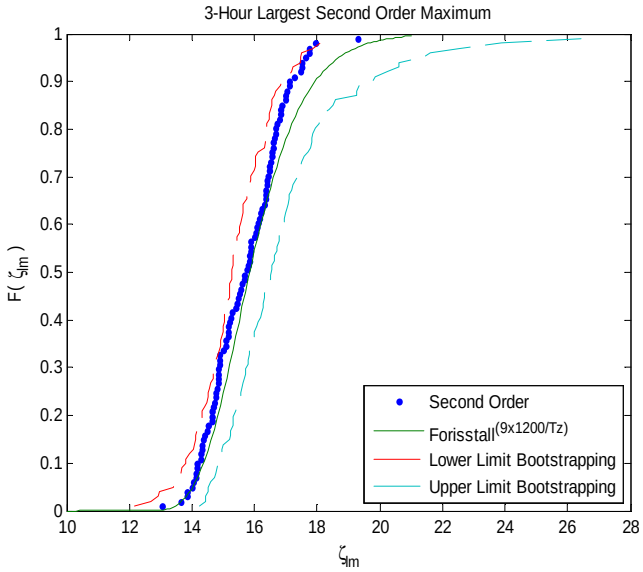
3-Hour Largest Second Order Maximum
F(ζlm)
ζlm
Second Order
Forisstall(9x1200/Tz)
Lower Limit Bootstrapping
Upper Limit Bootstrapping

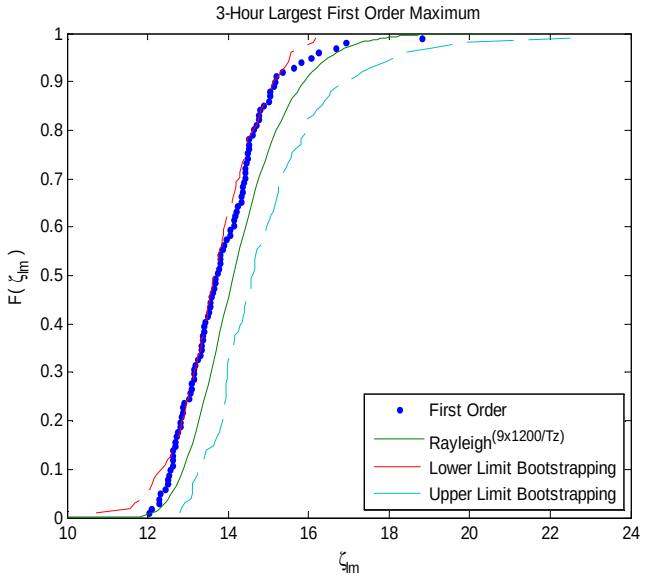
3-Hour Largest First Order Maximum
F(ζlm)
ζlm
First Order
Rayleigh(9x1200/Tz)
Lower Limit Bootstrapping
Upper Limit Bootstrapping

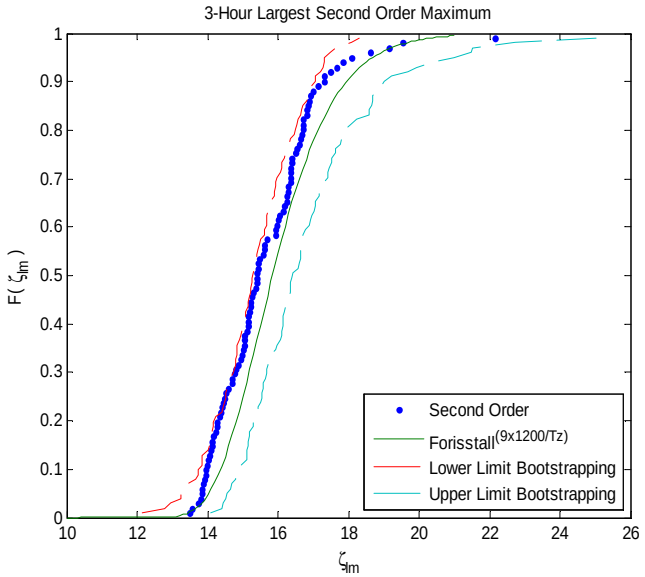
3-Hour Largest Second Order Maximum
F(ζlm)
ζlm
Second Order
Forisstall(9x1200/Tz)
Lower Limit Bootstrapping
Upper Limit Bootstrapping

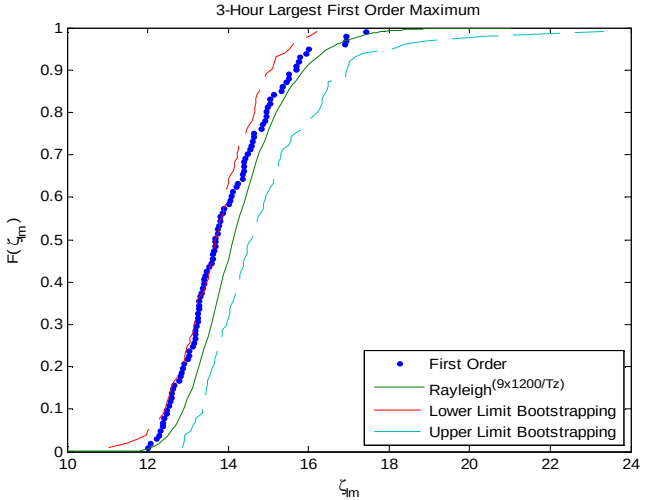
3-Hour Largest First Order Maximum
F(ζlm)
ζlm
First Order
Rayleigh(9x1200/Tz)
Lower Limit Bootstrapping
Upper Limit Bootstrapping

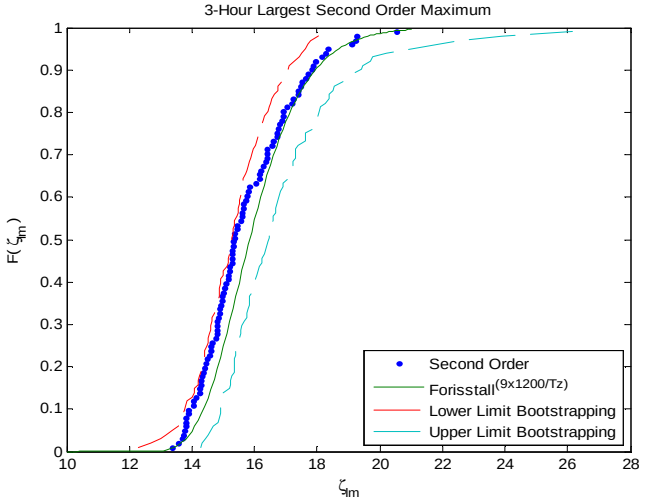
3-Hour Largest Second Order Maximum
F(ζlm)
ζlm
Second Order
Forisstall(9x1200/Tz)
Lower Limit Bootstrapping
Upper Limit Bootstrapping

APPENDIX 21-Distribution of Second Order Largest Maxima

Partition of Time Series, Random Amplitude

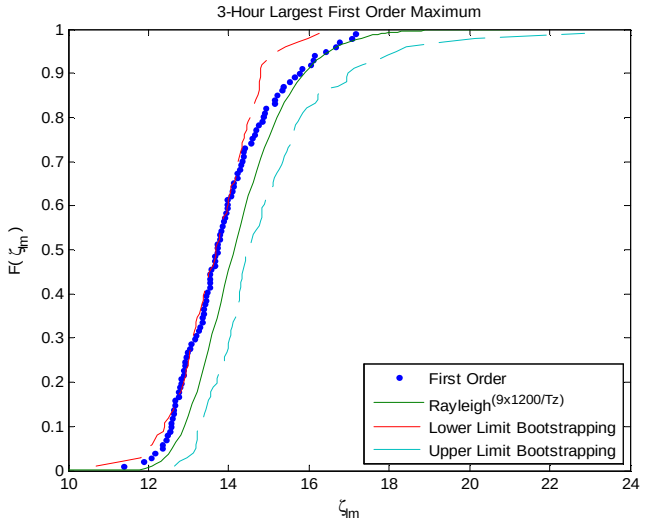

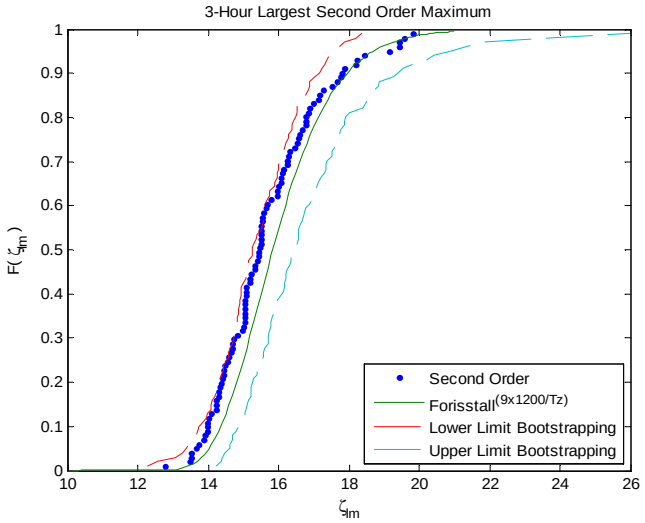

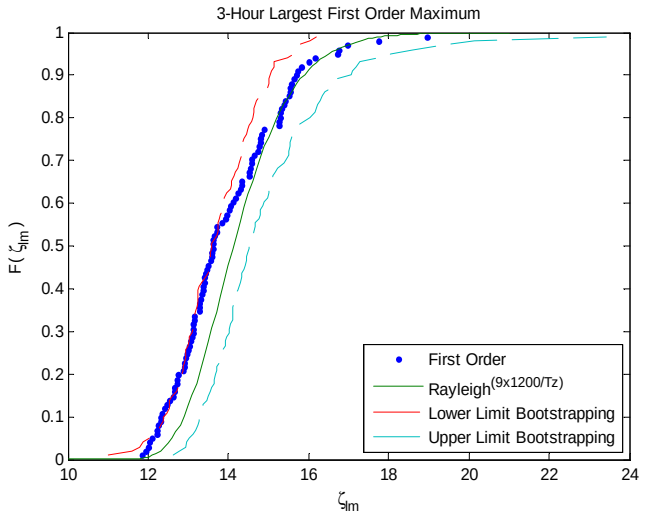

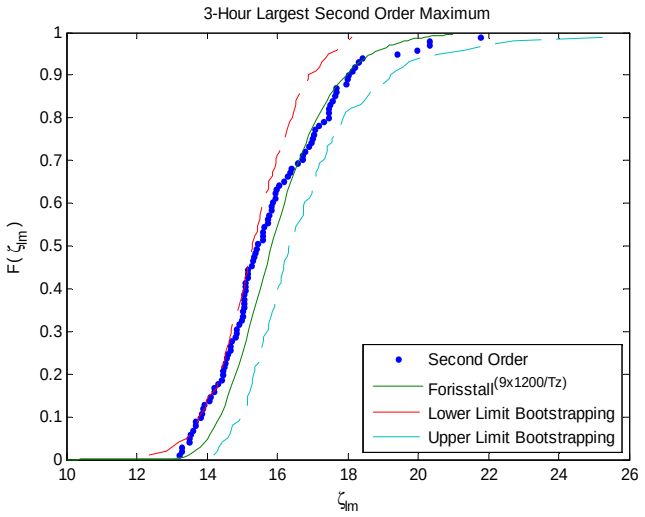

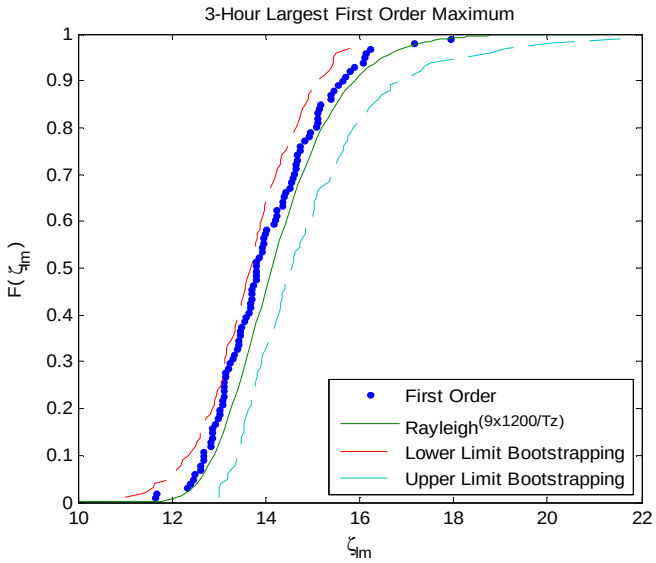
3-Hour Largest First Order Maximum
F(ζlm)
ζlm
First Order
Rayleigh(9x1200/Tz)
Lower Limit Bootstrapping
Upper Limit Bootstrapping

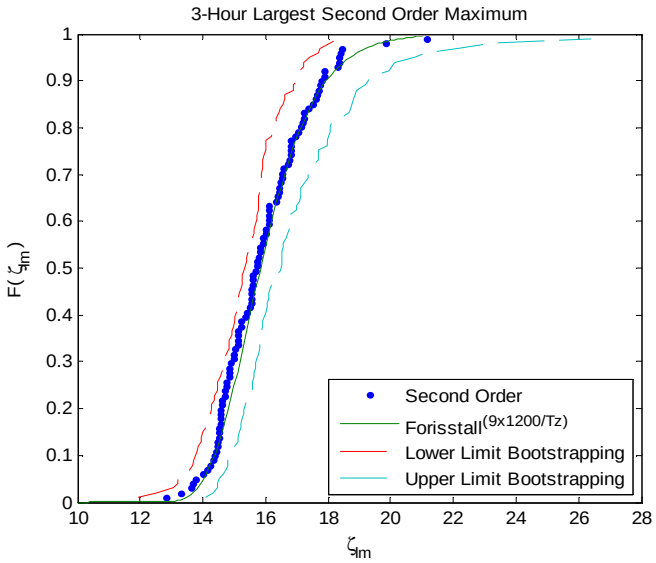
3-Hour Largest Second Order Maximum
F(ζlm)
ζlm
Second Order
Forisstall(9x1200/Tz)
Lower Limit Bootstrapping
Upper Limit Bootstrapping

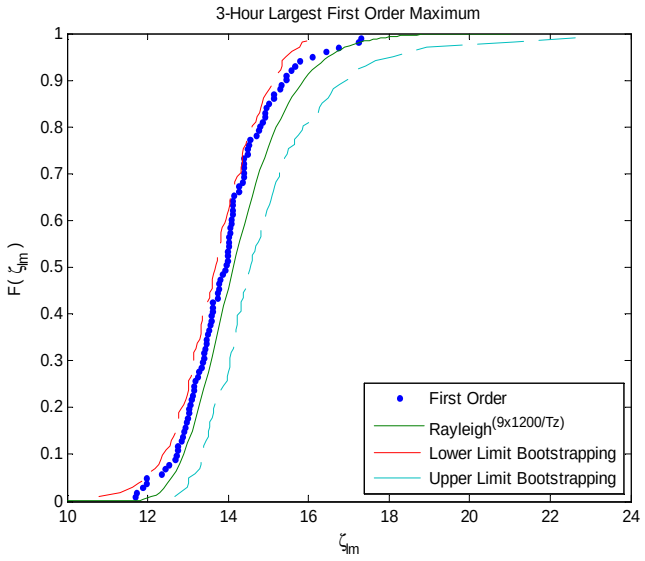
3-Hour Largest First Order Maximum
F(ζlm)
ζlm
First Order
Rayleigh(9x1200/Tz)
Lower Limit Bootstrapping
Upper Limit Bootstrapping

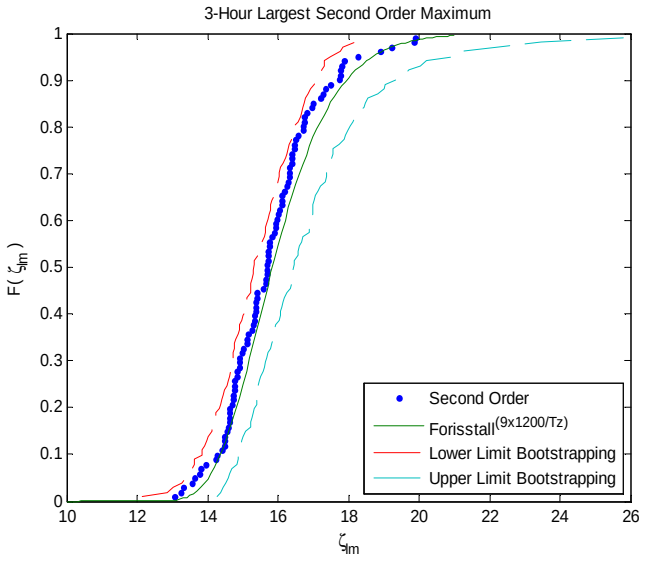
3-Hour Largest Second Order Maximum
F(ζlm)
ζlm
Second Order
Forisstall(9x1200/Tz)
Lower Limit Bootstrapping
Upper Limit Bootstrapping

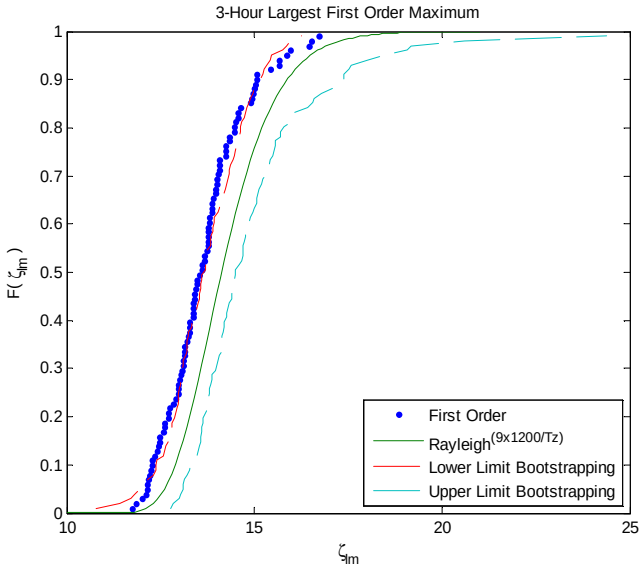
3-Hour Largest First Order Maximum
F(ζlm)
ζlm
First Order
Rayleigh(9x1200/Tz)
Lower Limit Bootstrapping
Upper Limit Bootstrapping

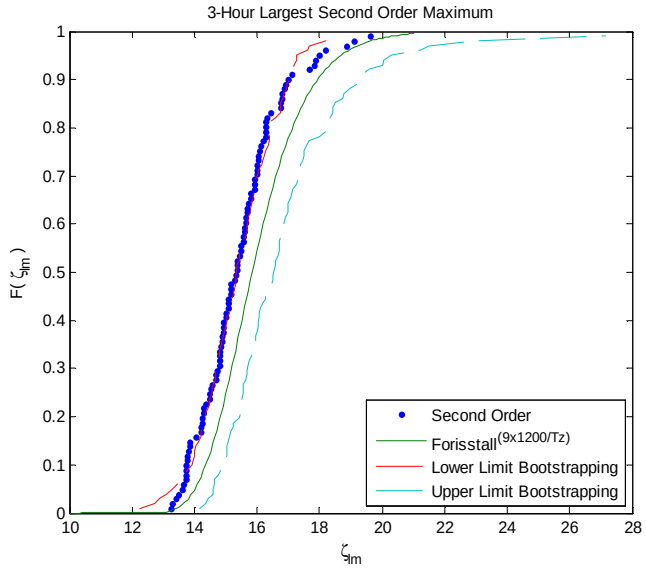
3-Hour Largest Second Order Maximum
F(ζlm)
ζlm
Second Order
Forisstall(9x1200/Tz)
Lower Limit Bootstrapping
Upper Limit Bootstrapping

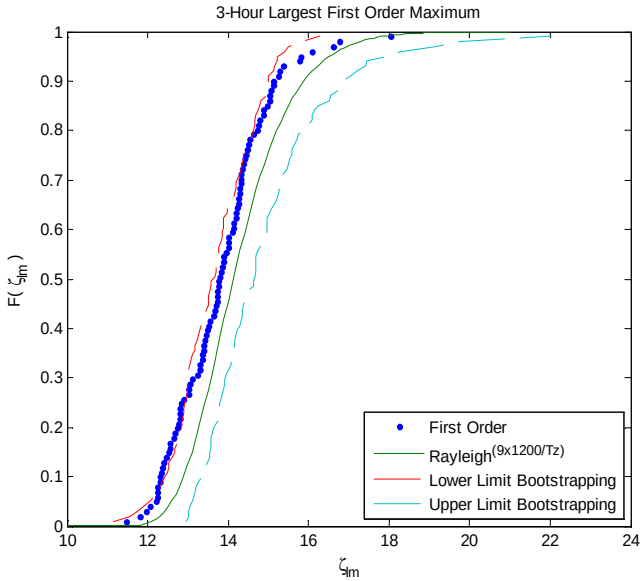
3-Hour Largest First Order Maximum
F(ζlm)
ζlm
First Order
Rayleigh(9x1200/Tz)
Lower Limit Bootstrapping
Upper Limit Bootstrapping

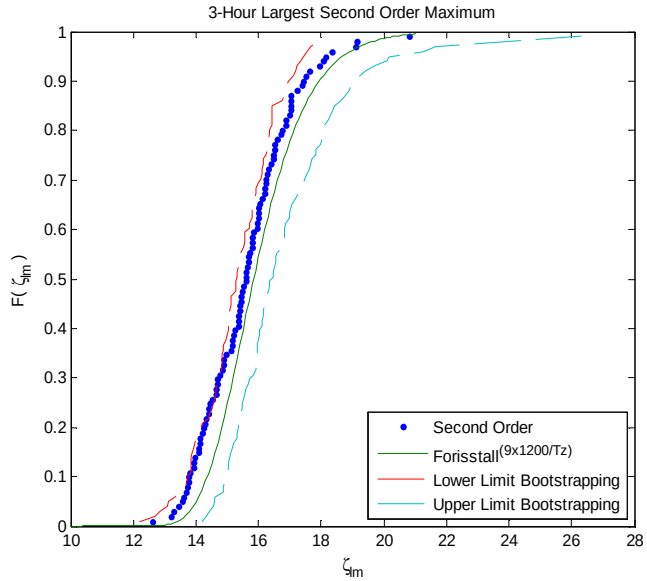
3-Hour Largest Second Order Maximum
F(ζlm)
ζlm
Second Order
Forisstall(9x1200/Tz)
Lower Limit Bootstrapping
Upper Limit Bootstrapping

APPENDIX 22- Horizontal Velocity: Second Order Model vs 5TH Stokes

Partition Time Series, Deterministic Amplitude

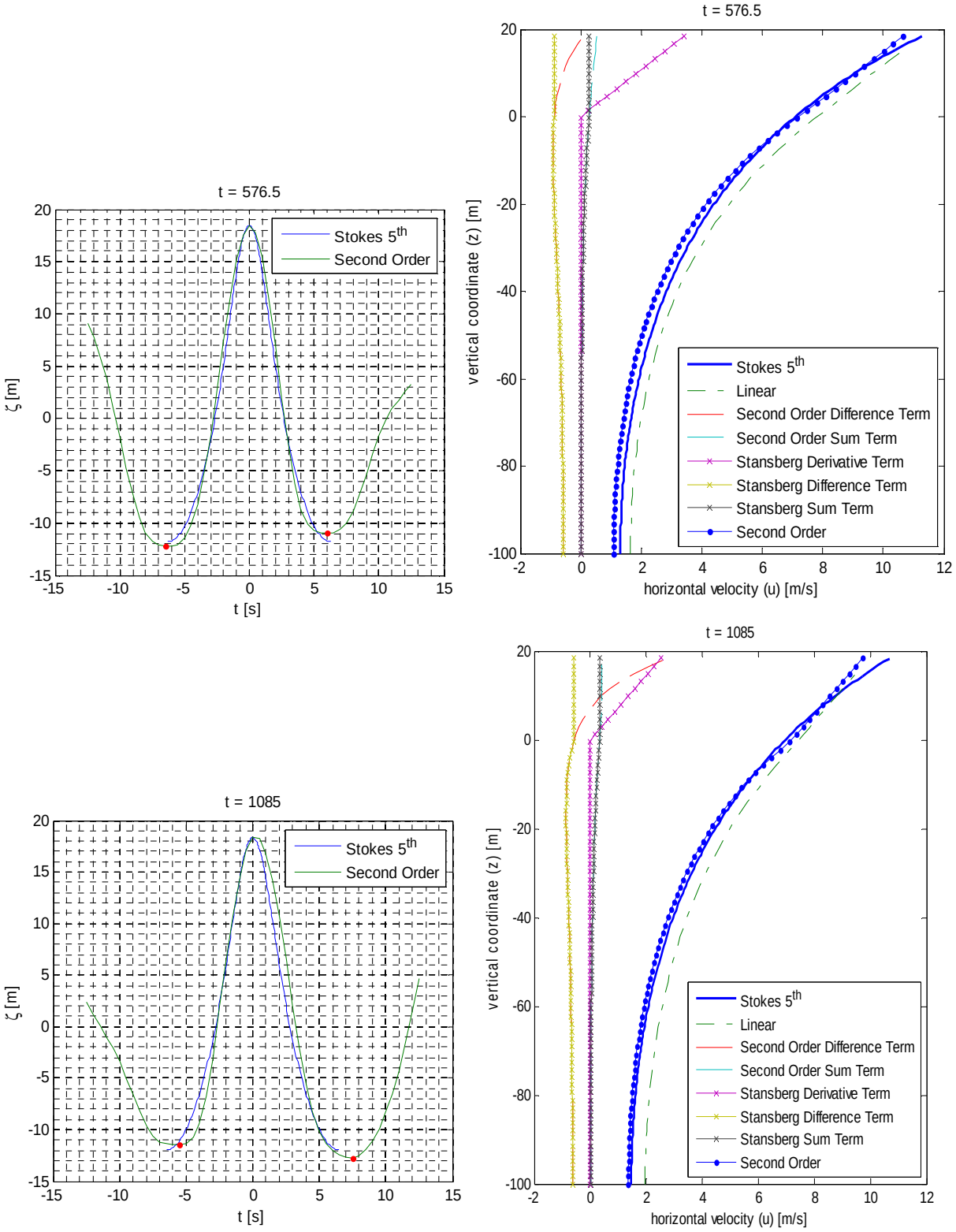

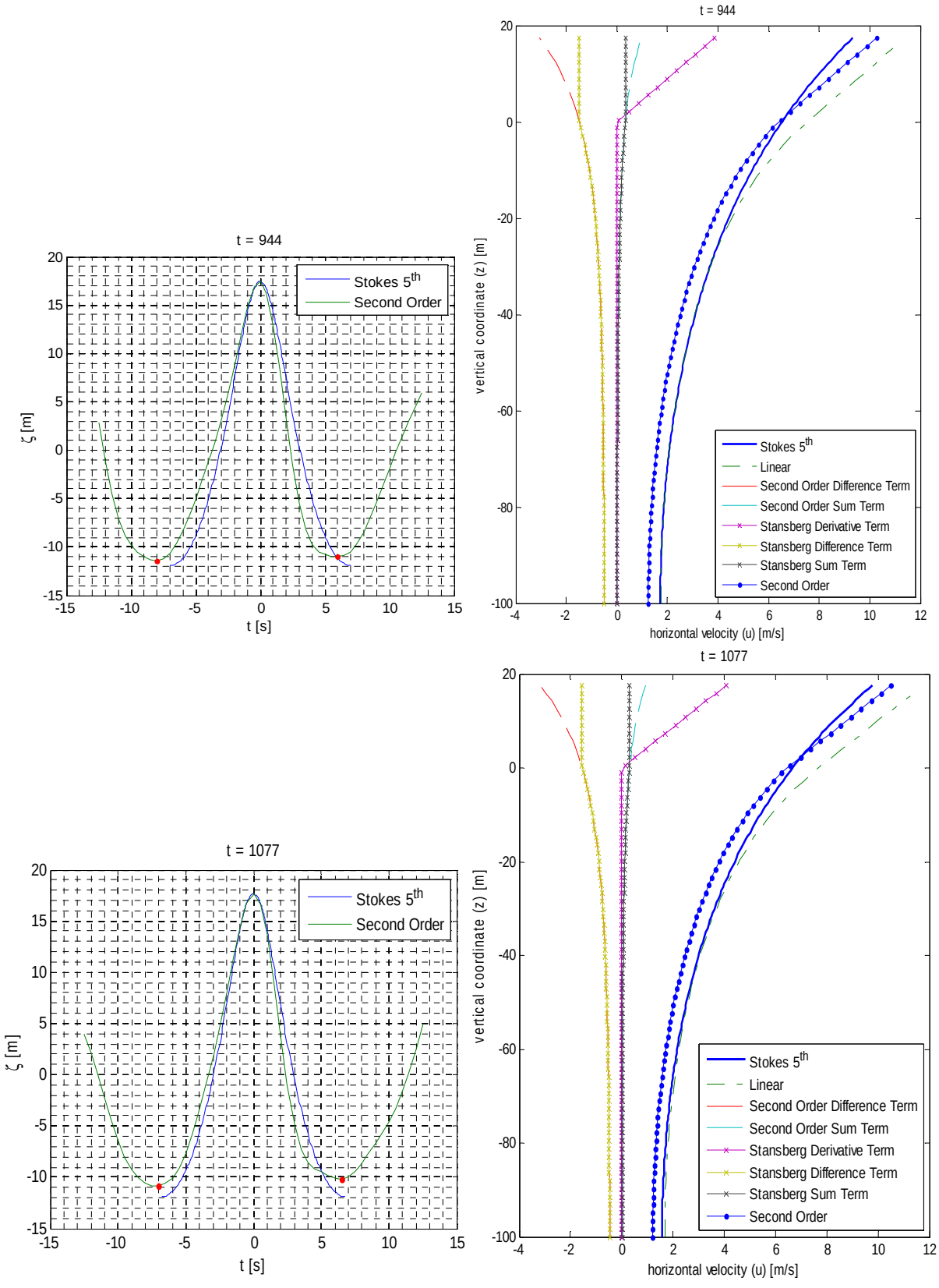
t = 944
ζ [m]
t [s]
Stokes 5th
Second Order
t = 944
vertical coordinate (z) [m]
horizontal velocity (u) [m/s]
Stokes 5th
Linear
Second Order Difference Term
Second Order Sum Term
Stansberg Derivative Term
Stansberg Difference Term
Stansberg Sum Term
Second Order
t = 1077
ζ [m]
t [s]
Stokes 5th
Second Order
t = 1077
vertical coordinate (z) [m]
horizontal velocity (u) [m/s]
Stokes 5th
Linear
Second Order Difference Term
Second Order Sum Term
Stansberg Derivative Term
Stansberg Difference Term
Stansberg Sum Term
Second Order

APPENDIX 23- Horizontal Velocity: Second Order Model vs 5TH Stokes

Partition Time Series, Random Amplitude

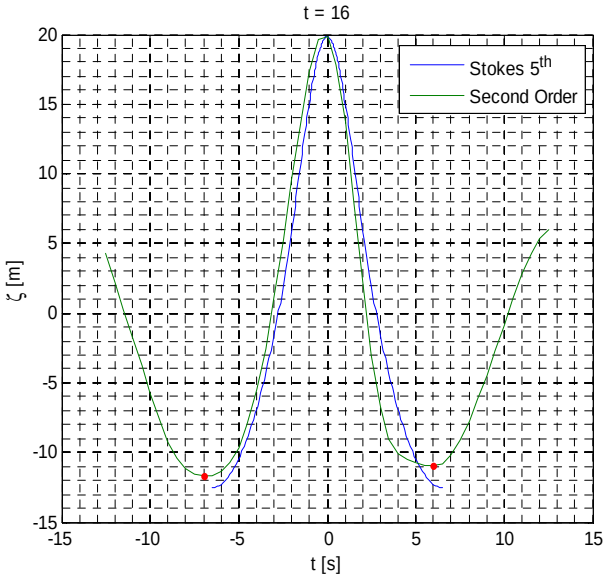

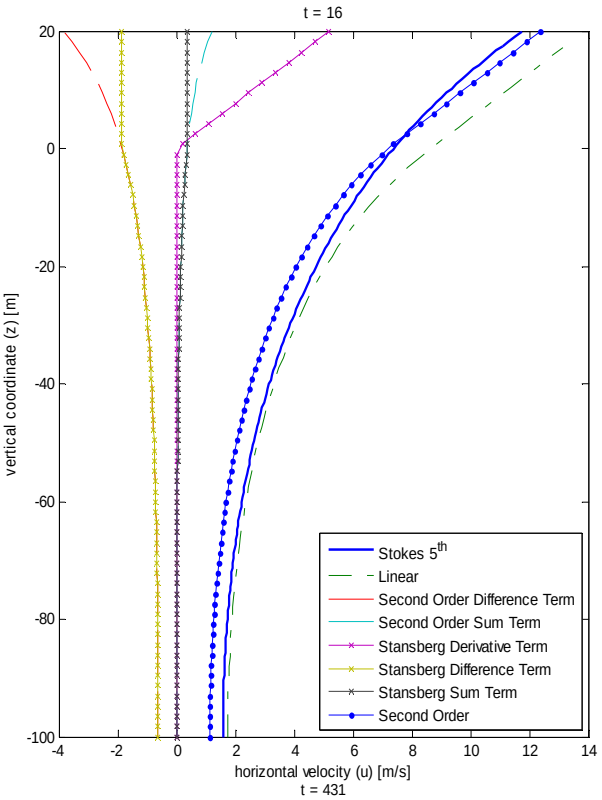

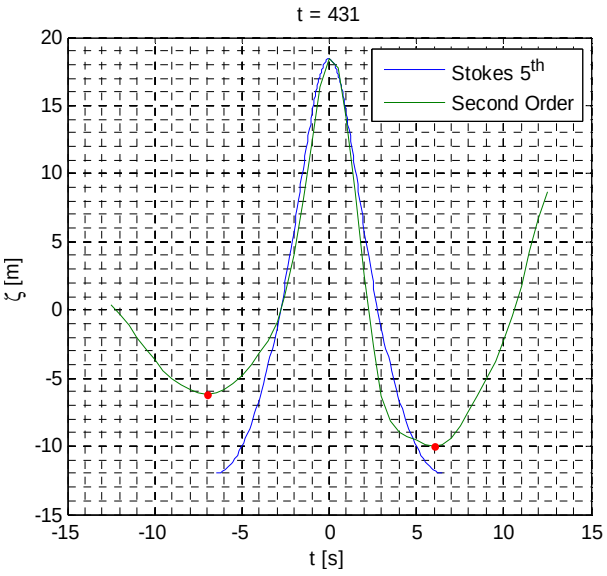

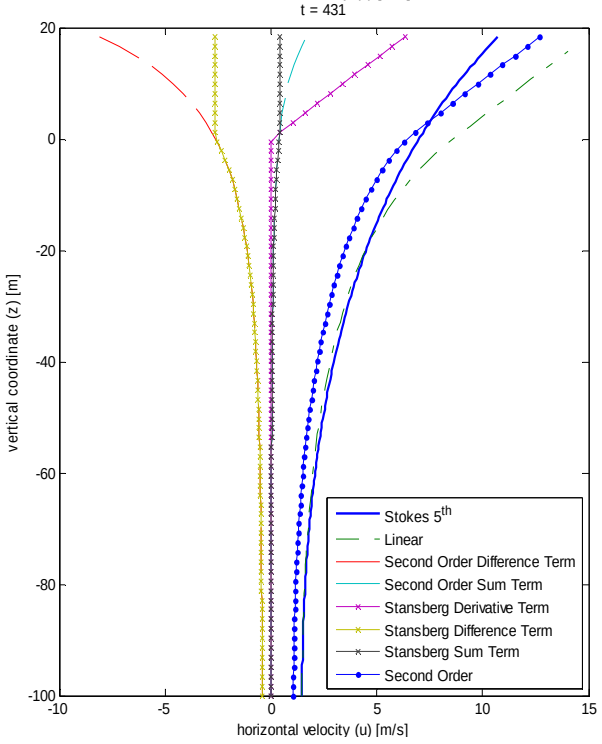

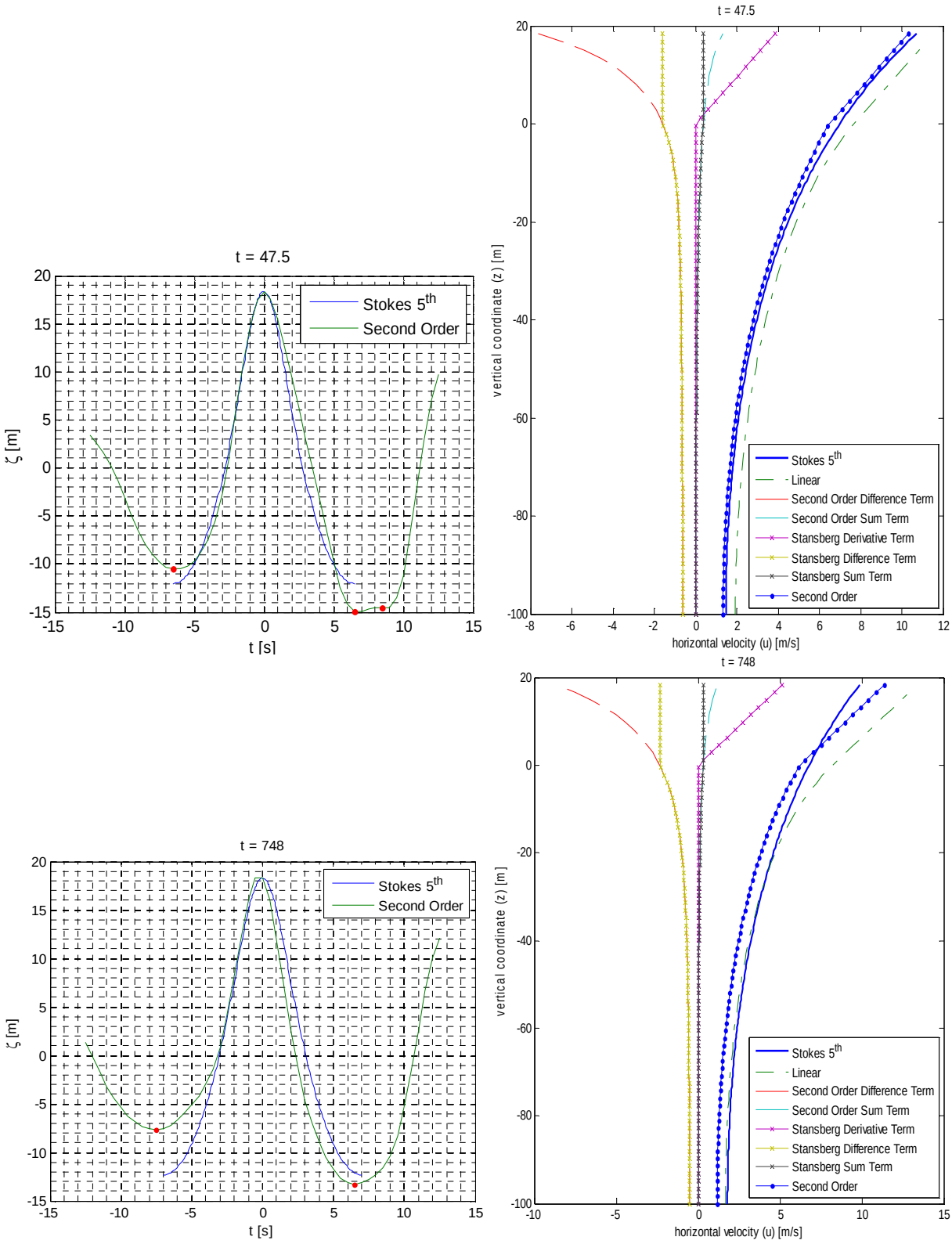
t = 47.5
Stokes 5th
Second Order
ζ [m]
t [s]
t = 47.5
vertical coordinate (z) [m]
horizontal velocity (u) [m/s]
Stokes 5th
Linear
Second Order Difference Term
Second Order Sum Term
Stansberg Derivative Term
Stansberg Difference Term
Stansberg Sum Term
Second Order
t = 748
Stokes 5th
Second Order
ζ [m]
t [s]
t = 748
vertical coordinate (z) [m]
horizontal velocity (u) [m/s]
Stokes 5th
Linear
Second Order Difference Term
Second Order Sum Term
Stansberg Derivative Term
Stansberg Difference Term
Stansberg Sum Term
Second Order

APPENDIX 24- Horizontal Velocity: Second Order Model vs 5TH Stokes

Random Frequency

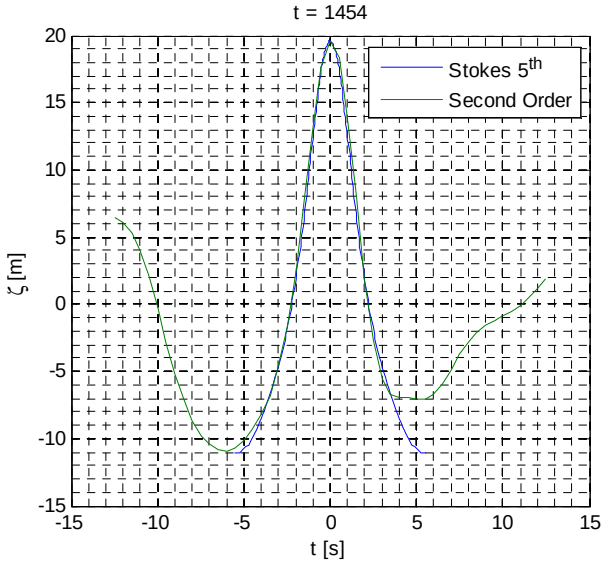

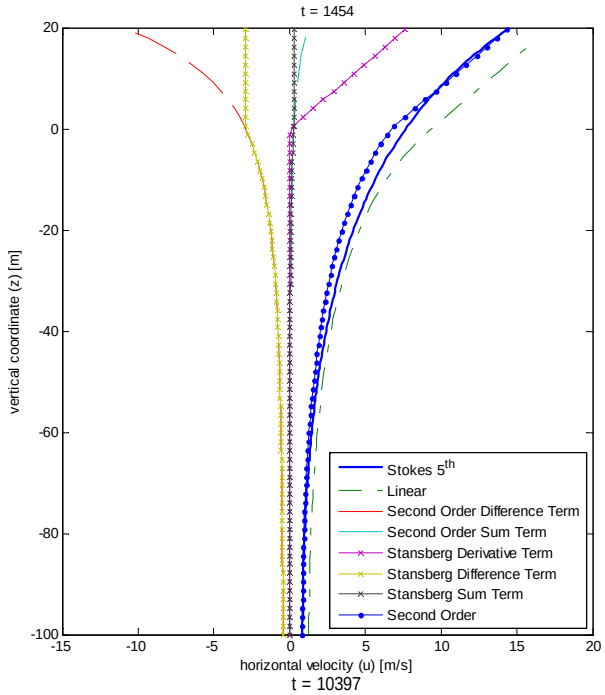

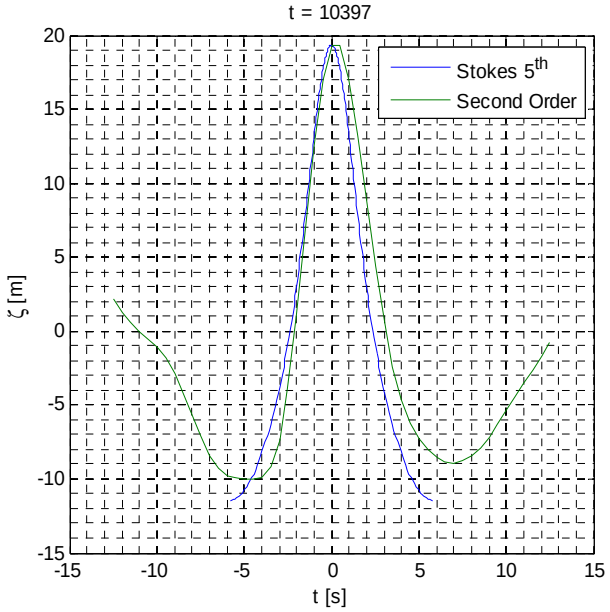

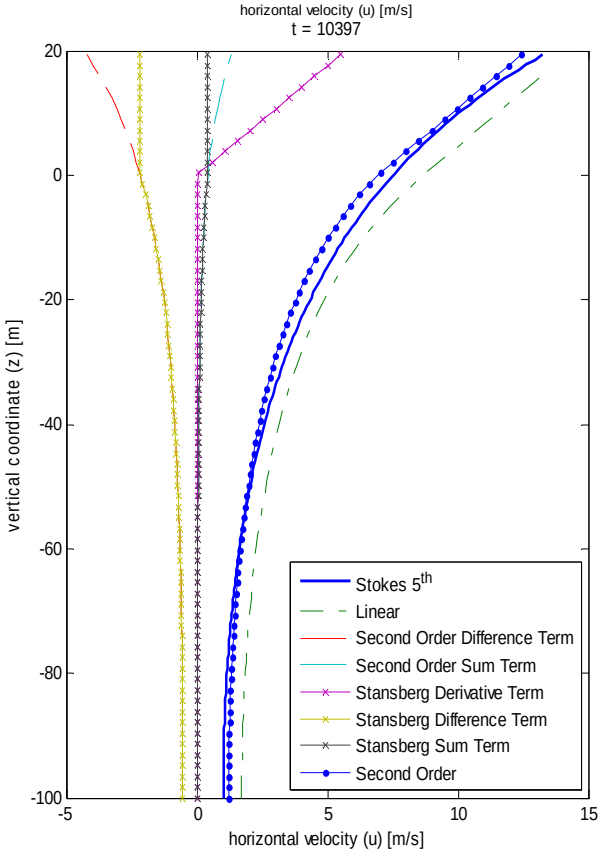

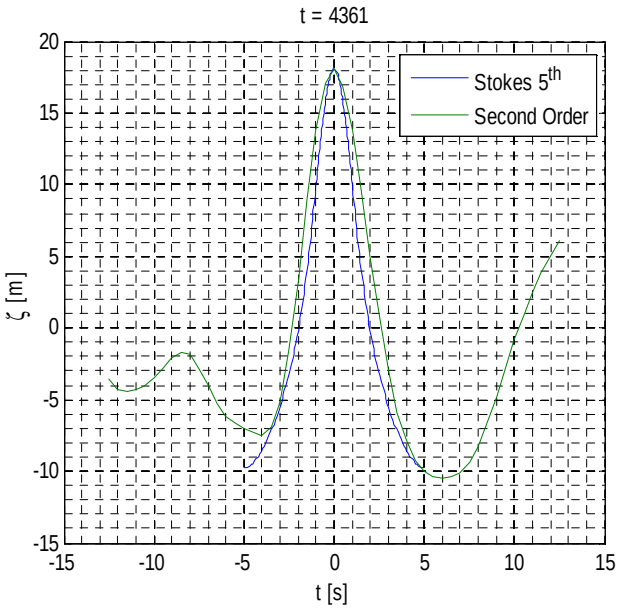
t = 4361
Stokes 5th
Second Order
ζ [m]
t [s]

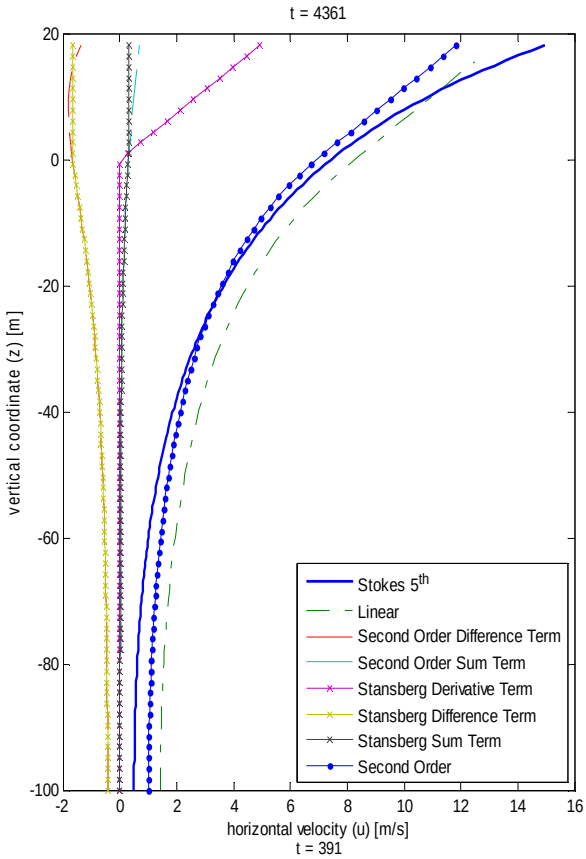
t = 4361
vertical coordinate (z) [m]
horizontal velocity (u) [m/s]
Stokes 5th
Linear
Second Order Difference Term
Second Order Sum Term
Stansberg Derivative Term
Stansberg Difference Term
Stansberg Sum Term
Second Order

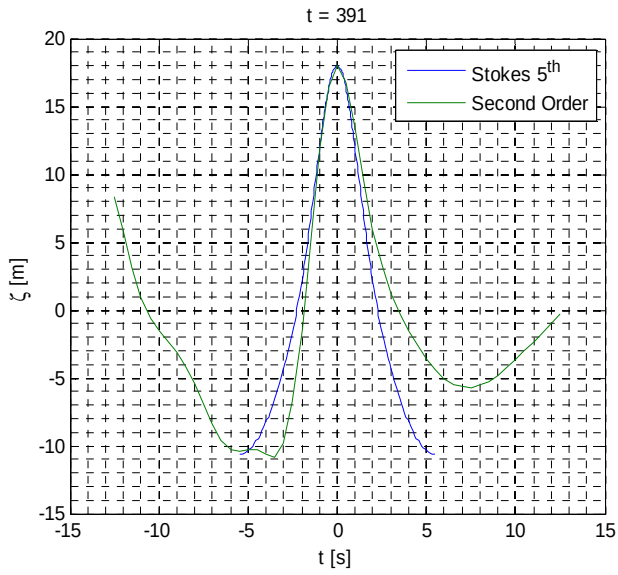
t = 391
Stokes 5th
Second Order
ζ [m]
t [s]

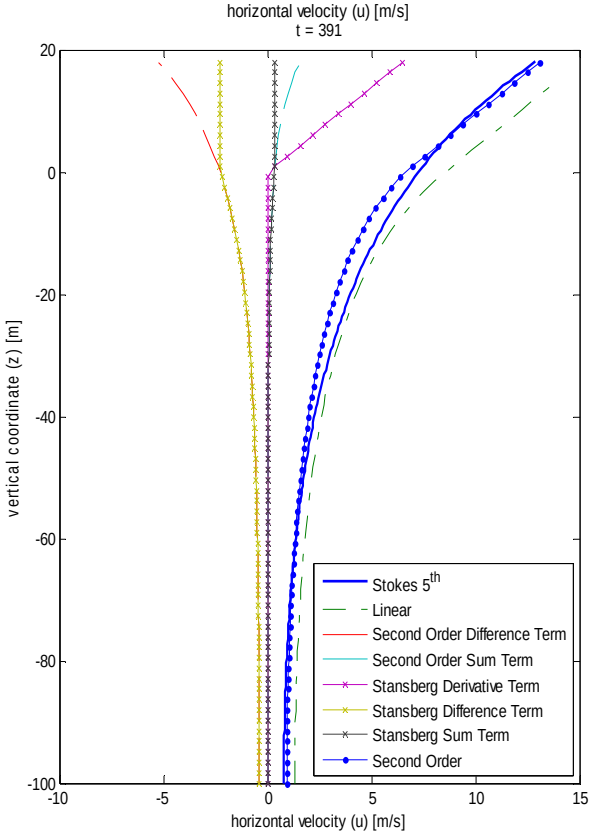
t = 391
vertical coordinate (z) [m]
horizontal velocity (u) [m/s]
Stokes 5th
Linear
Second Order Difference Term
Second Order Sum Term
Stansberg Derivative Term
Stansberg Difference Term
Stansberg Sum Term
Second Order

APPENDIX 25- Horizontal Velocity: Second Order Model vs 5TH Stokes

Equal Area, Deterministic Amplitude

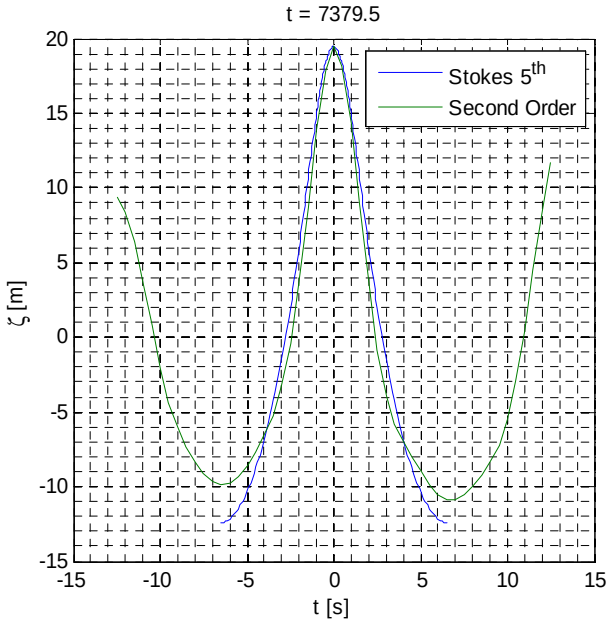

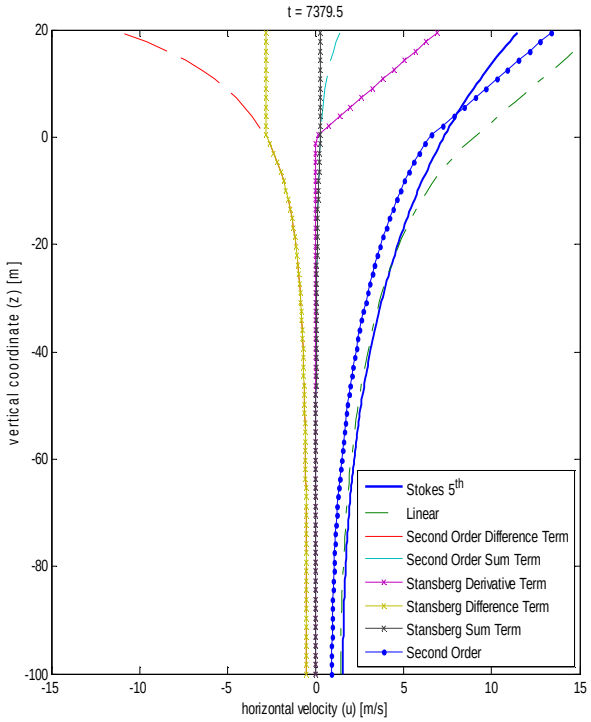

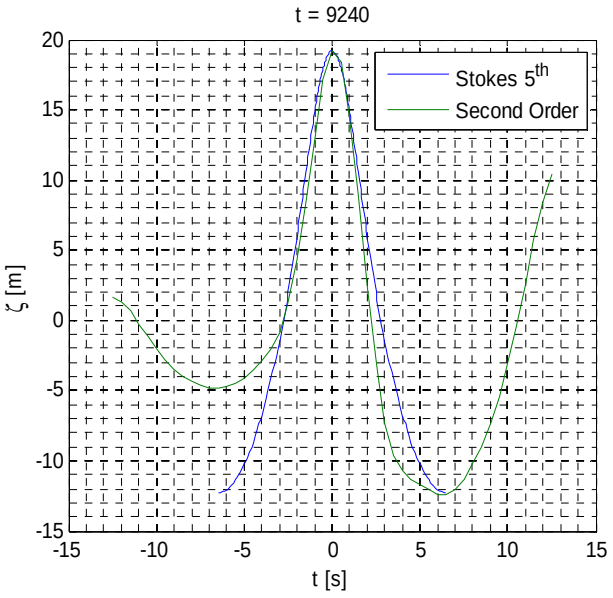

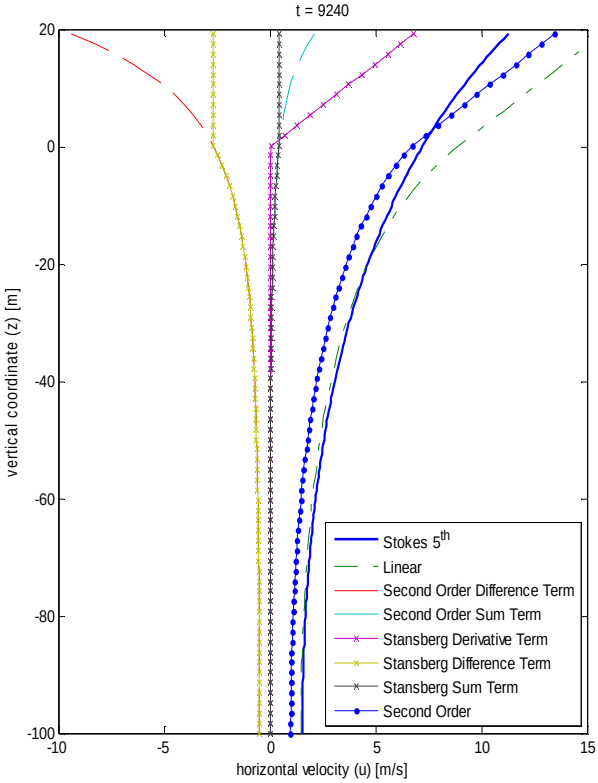

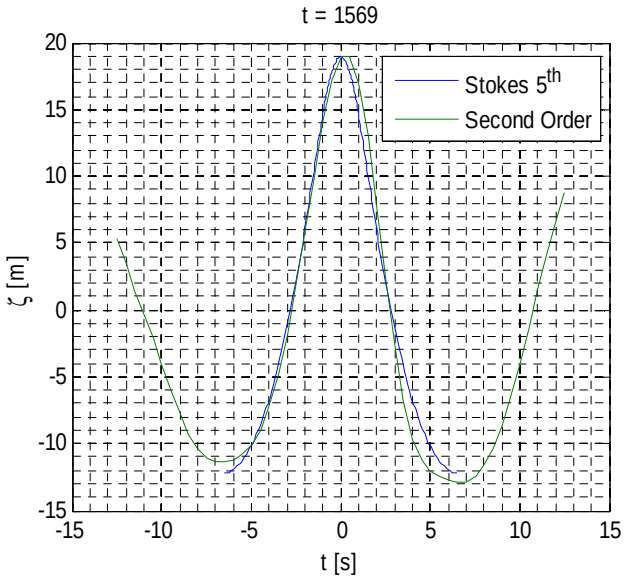
t = 1569
Stokes 5th
Second Order
ζ [m]
t [s]

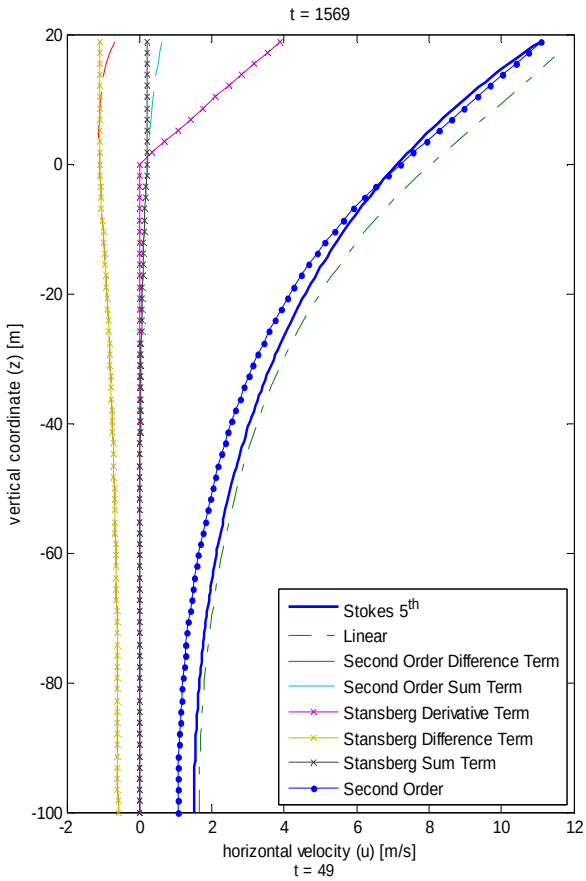
t = 1569
Stokes 5th
Linear
Second Order Difference Term
Second Order Sum Term
Stansberg Derivative Term
Stansberg Difference Term
Stansberg Sum Term
Second Order
vertical coordinate (z) [m]
horizontal velocity (u) [m/s]

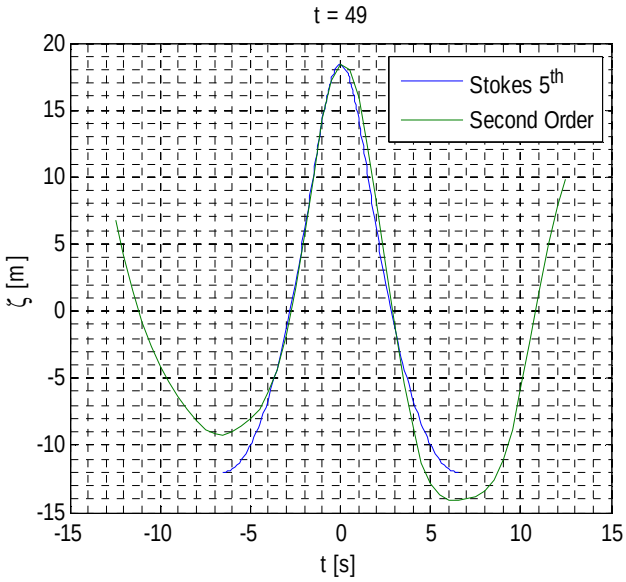
t = 49
Stokes 5th
Second Order
ζ [m]
t [s]

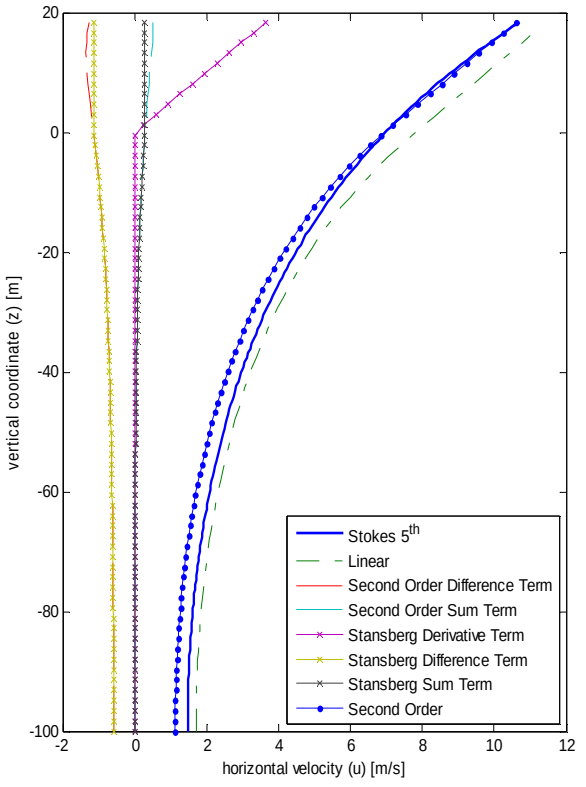
t = 49
Stokes 5th
Linear
Second Order Difference Term
Second Order Sum Term
Stansberg Derivative Term
Stansberg Difference Term
Stansberg Sum Term
Second Order
vertical coordinate (z) [m]
horizontal velocity (u) [m/s]

APPENDIX 26- Horizontal Velocity: Second Order Model vs 5TH Stokes

Equal Area, Random Amplitude

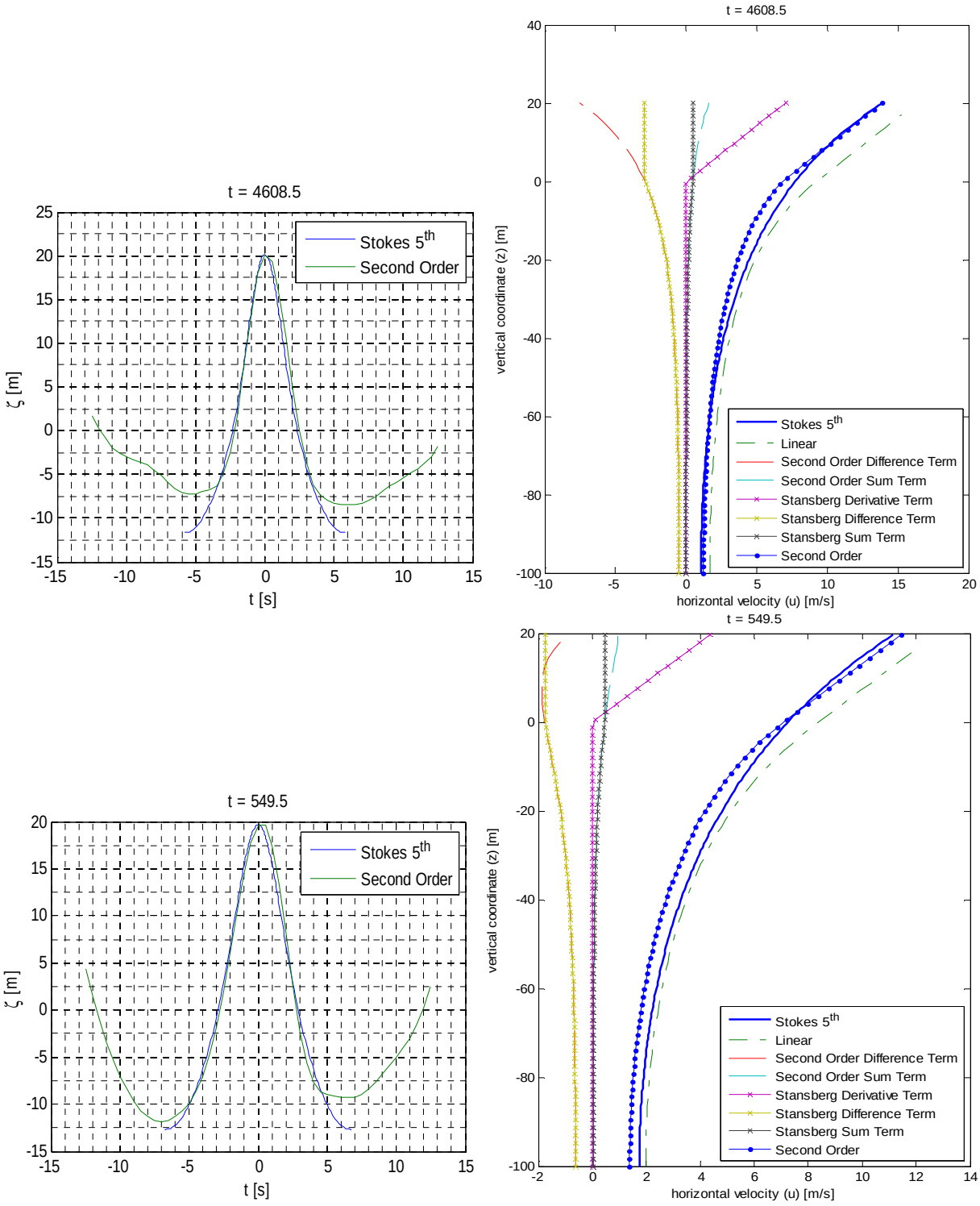

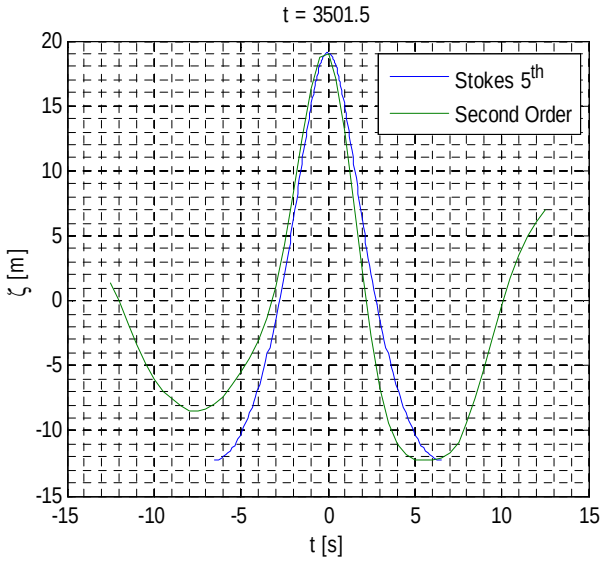
t = 3501.5
Stokes 5th
Second Order
ζ [m]
t [s]

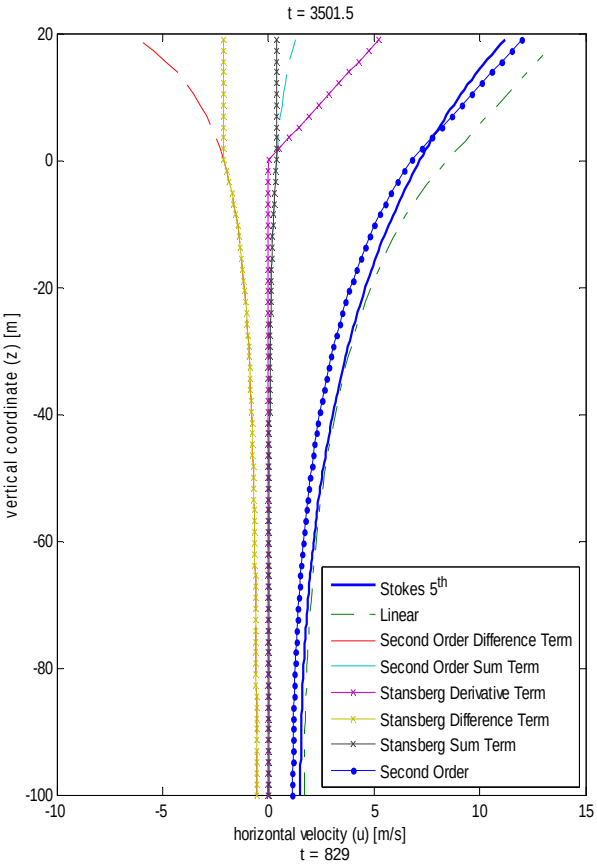
t = 3501.5
vertical coordinate (z) [m]
horizontal velocity (u) [m/s]
Stokes 5th
Linear
Second Order Difference Term
Second Order Sum Term
Stansberg Derivative Term
Stansberg Difference Term
Stansberg Sum Term
Second Order

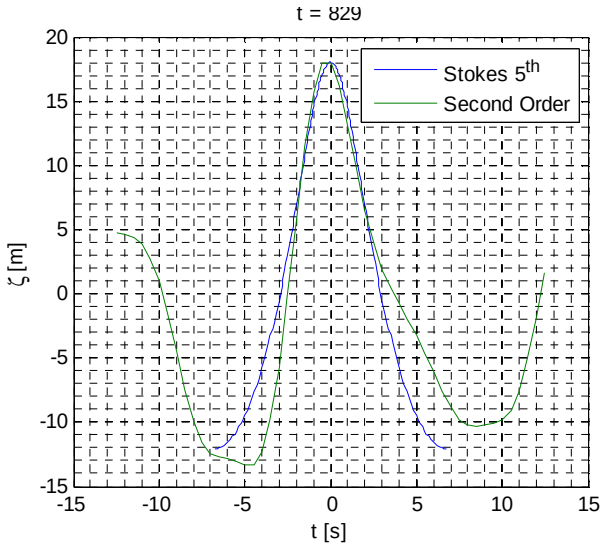
t = 829
Stokes 5th
Second Order
ζ [m]
t [s]

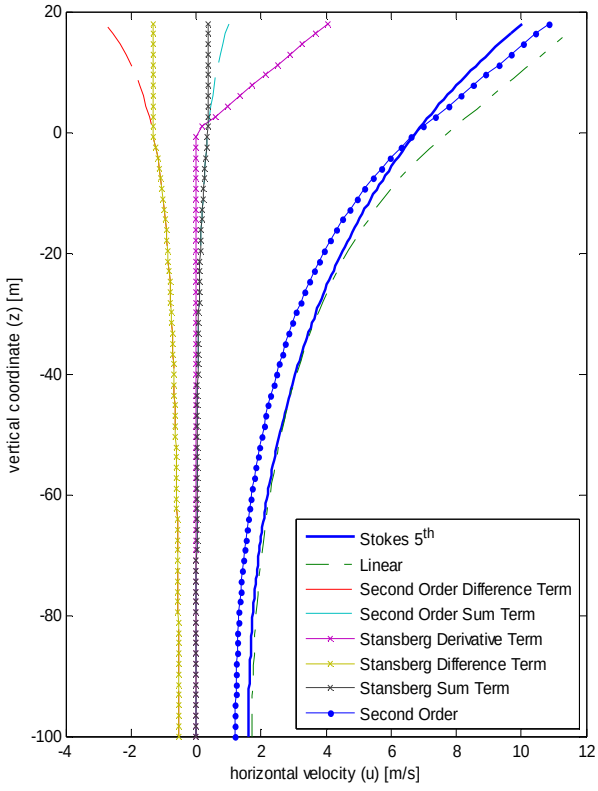
t = 829
vertical coordinate (z) [m]
horizontal velocity (u) [m/s]
Stokes 5th
Linear
Second Order Difference Term
Second Order Sum Term
Stansberg Derivative Term
Stansberg Difference Term
Stansberg Sum Term
Second Order

APPENDIX 27- Single Cyllinder Static Base Shear CDF

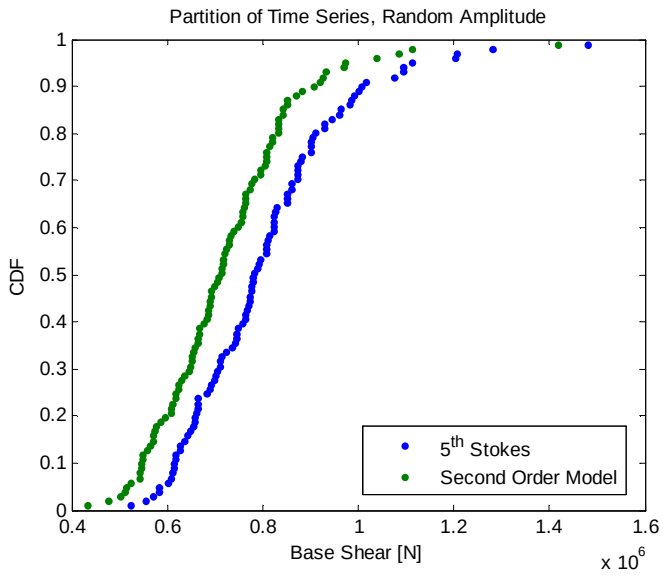

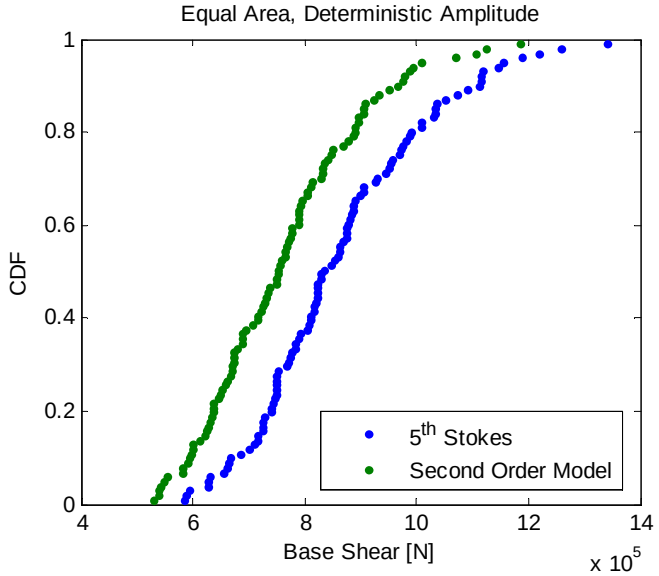

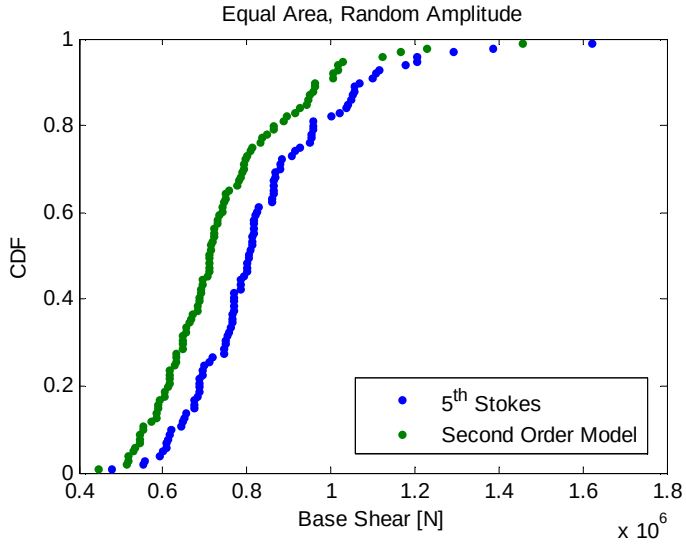

APPENDIX 28- Single Cyllinder Static Overturning Moment CDF

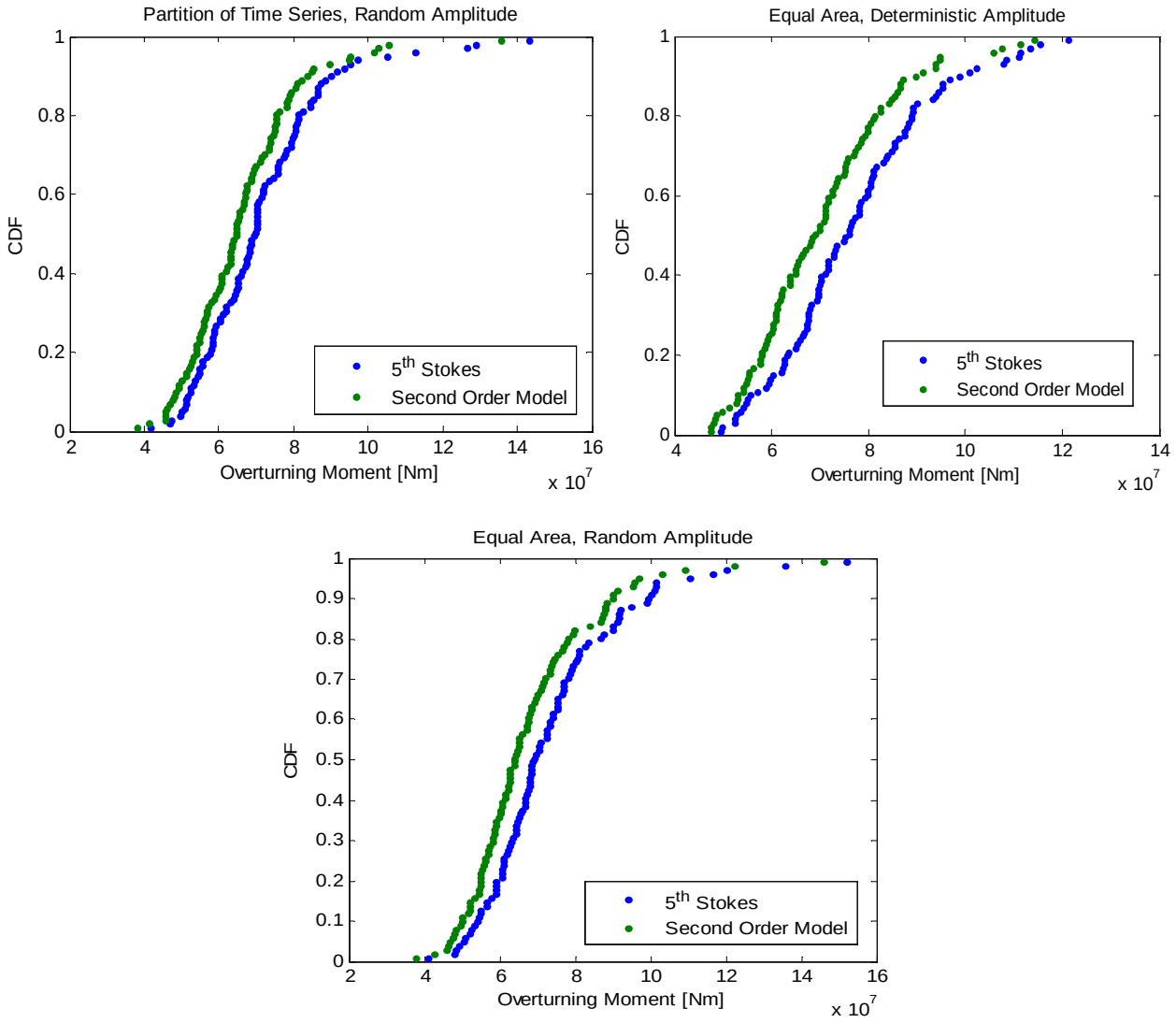

APPENDIX 29- Surface Profile at Jack-Up Lergest Response